SPECTRUM MANAGEMENT IN MULTI-HOP COGNITIVE RADIO NETWORKS: ARCHITECTURE, MODELING AND DESIGN

By

MIAO PAN

A DISSERTATION PRESENTED TO THE GRADUATE SCHOOL
OF THE UNIVERSITY OF FLORIDA IN PARTIAL FULFILLMENT
OF THE REQUIREMENTS FOR THE DEGREE OF
DOCTOR OF PHILOSOPHY

UNIVERSITY OF FLORIDA

2012

To all who nurtured my intellectual curiosity, academic interests, and sense of scholarship throughout my lifetime, making this milestone possible

ACKNOWLEDGMENTS

First and foremost, I would like to express my sincere gratitude to my advisor, Prof. Yuguang Fang, for his invaluable guidance, encouragement and support with my years in Wireless Networks Laboratory (WINET). He convinced me to join the Ph.D. program at UFL seven years ago, and encouraged me in my pursuit of an academic career after graduation. I am looking forward to our collaboration in the future.

I also would like to thank Professor Pramod Khargonekar, Professor Sartaj Sahni, and Professor Shigang Chen for serving on my supervisory committee and for their great help in various stages of my work and career.

I would not be a sane graduate student without a group of great friends. I would like to extend my thanks to all my colleagues in WINET for providing me a warm, family-like environment and for their collaboration and insightful advice. I specially thank Dr. Younggoo Kwon, Dr. Wenjing Lou, Dr. Wenchao Ma, Dr. Byung-Seo Kim, Dr. Wei Liu, Dr. Xiang Chen, Dr. Jing Zhao, Dr. Hongqiang Zhai, Dr. Yanchao Zhang, Dr. Shushan Wen, Dr. Jianfeng Wang, Dr. Yun Zhou, Dr. Xiaoxia Huang, Dr. Pan Li, Dr. Feng Chen, Dr. Jinyuan Sun, Dr. Yang Song, Dr. Rongsheng Huang, Hao Yue, Linke Guo, Huang Lin, Yuanxiong Guo, Zongrui Ding, Xinxin Liu, Han zhao, Huai-lei Fu, Yan Long, Junji Nakamoto, Dr. Sunmyeng Kim, Dr. Nicola Scalabrino, Dr. Roberto Riggio, Dr. Qiang Shen, Dr. Xiaoyan Yin, Dr. Leifang Hui, Dr. Xiaobin Tan, Dr. Jianwei Liu, Dr. Xiaoyan Zhu and Dr. Guoliang Yao for many valuable discussions and all the good memories.

Special thanks are due to the Fang family: my advisor Yuguang Fang and his wife Jennifer Lu, who not only constantly encouraged me and helped me in many ways, but also shared their view of life with me.

Finally, I owe a special debt of gratitude to my beloved parents. Without their love and unwavering support, I would never imagine what I have achieved.

TABLE OF CONTENTS

LIST OF TABLES

LIST OF FIGURES

Abstract of Dissertation Presented to the Graduate School
of the University of Florida in Partial Fulfillment of the
Requirements for the Degree of Doctor of Philosophy

SPECTRUM MANAGEMENT IN MULTI-HOP COGNITIVE RADIO NETWORKS:
ARCHITECTURE, MODELING AND DESIGN

By

Miao Pan

August 2012

Chair: Yuguang Fang
Major: Electrical and Computer Engineering

Cognitive radio technology is a promising solution to the dilemma between the ever-increasing spectrum demand brought by the booming growth of wireless services and the exhaustion of available spectrum. Multi-hop cognitive radio networks have also been widely accepted as an indispensable component of next-generation communication systems to improve spectrum utilization and to facilitate ubiquitous network access from anywhere at any time. Although offering significant benefits, they also provide unique research challenges over other wireless networks. Of note are the issues associated with the architecture, modeling and design of spectrum management in multi-hop cognitive radio networks.

In this dissertation, we aim to address these challenging and fundamental issues in multi-hop cognitive radio networks, cognitive vehicular ad hoc networks, spectrum auction mechanisms, and spectrum trading systems. Our contributions are mainly sixfold. First, due to the unpredictable activities of the primary users, we propose metrics to evaluate the potential loss for opportunistic spectrum accessing. Second, considering uncertain spectrum supply, we propose a novel architecture of CRNs for spectrum harvesting and sharing, and presented a theoretical study on the joint frequency scheduling and routing problem in multi-hop CRNs. Third, we have a comprehensive study on the path selection problem considering multiple factors including the price of the bands, budget constraints of CR source, link scheduling constraints, flow

routing constraints, and activities of primary services. Fourth, under the proposed network architecture, we extend the per-user based spectrum trading into session based spectrum trading, which effectively simplifies the design of spectrum trading systems. Fifth, with a joint consideration of cooperative communications, we propose a cooperative communication aware link scheduling scheme to maximize the throughput for a session in cognitive vehicular ad hoc networks. Last, we incorporate cryptographic technique into the spectrum auction design, and propose a secure spectrum auction scheme leveraging Paillier cryptosystem to purge all the back-room dealings.

CHAPTER 1
INTRODUCTION

1.1 Cognitive Radio Networks: An Overview

Due to the popularity of smart mobile devices such as iPhones, people nowadays could conduct their business or access information superhighway via their mobile devices. Many people just could not live without their mobile toys! This leads to tremendous traffic increase over the wireless access networks and a dramatic increase in the demand for radio spectrum. In parallel with that, current static spectrum allocation policy of Federal Communications Commission (FCC) [3, 20, 73] results in the exhaustion of available spectrum, while a lot of licensed spectrum bands are extremely under-utilized. Experimental tests in academia [9, 72] and measurements conducted in industries [70, 71] both show that even in the most crowed region of big cities (e.g., Washington, DC, Chicago, New York City, etc.), many licensed spectrum bands are not used in certain geographical areas and are idle most of the time.

Observing such unbalanced spectrum utilization, FCC revisited its spectrum policy and looked into new spectrum management policy to allow others to utilize the unused licensed bands as long as it does not cause interference to the services offered to the primary users (e.g., unlicensed users is allowed to use the unoccupied licensed band, but must vacant the licensed band immediately when the licensed users return to use this band). Cognitive radios are designed to address such opportunistic use of unoccupied spectrum bands for unlicensed users (secondary users).

Compared with other traditional multi-hop wireless networks (e.g., Ad hoc networks), multi-hop cognitive radio networks (CRNs) release the spectrum from shackles of authorized licenses, and allow opportunistic usage of the vacant licensed spectrum bands in either temporal or spatial domain. Due to the great potential of improving the spectrum utilization, CRNs have attracted tremendous interest in the last few years, and promote numerous possible applications in battle communications,

public safety, disaster relief, search and rescue, environment monitoring, and many other military and civilian areas.

1.2 Research Challenges

While offering significant benefits, multi-hop CRNs also provide unique research challenges over other wireless networks. This subsection outlines the major problems that ought to be addressed.

First of all, the design of cognitive radios with wide dynamic frequency range may be hard. In most of research activities, it seems to assume that a cognitive radio can be operated across multiple frequency bands, say, ranging from MHz bands such as TV white spaces to GHz bands such as 2 GHz PCS bands or 5 GHz unlicensed band [14, 73, 97, 110]. In theory, this may be possible, but it is hard to implement in light weight radios, which may be the likely scenarios for any business push. Although some of the desired features may be realized in the near future, enormous amount of time and efforts must be spent in hardware designs and signal processing in order to implement these harsh frequency-agile requirements in light weight radios [73, 97, 110, 122].

Second, spectrum licensed holders may not be willing to let others utilize their bands without compensation even though FCC allows secondary market to utilize such unused resource and they may try every way to meddle with the usage of secondary users [11, 86]. Thus, the more feasible economical model may be to let primary spectrum holders to participate in the business through the spectrum trading process (e.g., spectrum auction). This is why there are many research papers focusing on the design of spectrum trading systems/mechanisms [48, 100, 124, 135, 136]. Unfortunately, many proposed spectrum trading schemes assume the existence of spectrum traders/auctioneers without specifying who they are in CRNs [48, 124, 135, 136]. Some of papers assume that the primary users act as the traders/auctioneers, which would compromise the impartiality of the spectrum traders/auctioneers and make

some spectrum trading schemes, such as the VCG, impractical because of the partiality of the primary users and lack of trusted monitoring impartial party.

Third, most research work assumes per-user based spectrum trading, i.e., each cognitive radio bids and uses the purchased spectrum for communications [48, 100, 124, 135, 136]. There are two problems: (1) it is not really clear whom a winning radio communicates with (the receiver is not clearly specified) and what kinds of quality of service (QoS) it would get except that it can use the purchased spectrum to transmit; (2) it is not clear how to enforce the FCC rule for the usage of the spectrum (it should not impact the service of the primary user) and how to collect the revenue, which is particularly difficult when online spectrum trading is on the scale of minutes or even hours [3, 31]. Thus, although some of online spectrum trading/auction techniques are theoretically interesting, they may not be practical.

Fourth, user traffic tends to be location-based and time-varying, and most traffic may target at Internet services, while the current spectrum management approaches tend to mostly favor the one-hop traffic services, and thus it is not clear what kinds of communications CRNs are designed to support. Although group-based spectrum management schemes intend to consider the spectrum reuse and interference mitigation with certain efficiency optimization, it mostly considers how to optimally utilize the purchased or harvested spectrum for the communications among the cognitive radios themselves in the region that the spectrum can be used in the ad hoc networking. This application scenario may not be truly interesting in practice (which can be observed in most hotspots).

Fifth, since the returns of primary users are unpredictable, thus the spectrum bands harvested from the licensed users is stochastic in nature [51, 88], we may have to take advantage of the stochastic multiplexing in order to maximize the spectrum efficiency. This can be done only when multiple users can collectively share the harvested

resource, while the current spectrum management in cognitive radio networks may not be enough.

Finally, to attract customers for any new technologies, it is always good idea to minimize the complexity on the customers side. For multi-hop CRNs, it is always a great idea to minimize the changes on the users' devices while harvesting the unused resource (the white spaces). Thus, it may be more viable to develop technologies to maximize the spectral efficiency while minimizing the users' side complexity.

1.3 Scope and Organization of the Dissertation

This dissertation contributes to the development of novel solutions to a number of challenging and fundamental issues of spectrum management in multi-hop cognitive radio networks, which are either ignored or not well addressed in previous research. The rest of the dissertation is organized as follows.

Considering the uncertain licensed spectrum availability, in 2, we first introduce an intuitive method, the X loss, to quantify the risk for secondary users at a given confident level. Since the X loss theoretically underestimates the potential risk for opportunistic spectrum accessing and mathematically lacks of subadditivity, we further propose the expected X loss, a more suitable risk measurement for opportunistic spectrum accessing with desired properties.

Based on the proposed metrics characterizing the spectrum availability, in Chapter 3, we propose a novel architecture of CRNs for spectrum harvesting and sharing, and presented a theoretical study on the joint frequency scheduling and routing problem in multi-hop CRNs under uncertain spectrum supply. We first introduce a new service provider, SSP, and let the SSP provide coverage in CRNs with low-cost CR mesh routers in order to facilitate the accessing of SUs without CR capability. We characterize the network with a pair of (α, β) parameters, present a mathematical formulation with the goal of minimizing the required network-wide spectrum resource at a (α, β) level for a set of CR sessions with rate requirements, provide feasible solutions

to the formulated optimization problem, and show the (α, β) based approach is better than expected bandwidth based one in terms of blocking ratio and spectrum utilization.

Under the proposed network architecture in Chapter 3, Chapter 4 studies the path selection problem in multi-hop CRNs under flow routing, link scheduling and CR source's budget constraints. Considering the inherent single radio constraint of CR devices and the features of spectrum trading, we propose a 4-D conflict graph to describe the conflict relations among CR links, mathematically formulate the path selection problem under multiple constraints into an optimization problem with the objective of maximizing the end-to-end throughput for a certain CR session, and solve it by linear programming.

As a follow-up investigation in Chapter 4, in Chapter 5, we further extend the per-user based spectrum trading into the per-session based one, where multiple sessions exist in the network, and propose a novel spectrum trading system, i.e., spectrum clouds. Given the rate requirements and bidding values of candidate trading sessions, we formulate the optimal spectrum trading into the SSP's revenue maximization problem under the availability of spectrum, link scheduling and flow routing constraints in multi-hop CRNs. Since the formulated problem is NP-hard to solve, we derive an upper bound for the optimization by relaxing the integer variables, propose heuristic algorithms for low bounds, and show that the proposed session based spectrum trading has superior advantages over the per-user based one in multi-hop CRNs.

Chapter 6 studies the throughput maximization problem in cognitive vehicular Ad hoc networks under multiple constraints (i.e., CR devices' inherent single-radio constraint, the availability of licensed spectrum, transmission mode selection and link scheduling). Considering the special features of cooperative communications, we extend the links and classify them into cooperative links/general links. Depending on the available bands at different extended links, we conduct cooperative communication aware link scheduling to choose the optimal route in terms of end-to-end throughput.

Security issues are important is the design of spectrum management in multi-hop CRNs as well. In Chapter 7, against the untrustworthy spectrum trader, we incorporate cryptographic technique into the spectrum auction design and propose a secure spectrum auction scheme leveraging Paillier cryptosystem to purge the back-room dealing.

Finally, Chapter 8 summarizes this dissertation.

CHAPTER 2
THE X LOSS: BAND-MIX SELECTION FOR OPPORTUNISTIC SPECTRUM ACCESSING

2.1 Chapter Overview

Booming growth of wireless networks and flourish of various wireless services have been witnessed in the past decade. In parallel with that, current static spectrum allocation policy of Federal Communications Commission (FCC) [3, 21, 73] results in the exhaustion of available spectrum, while many licensed spectrum bands are extremely under-utilized (so called "white space"). As one of the most promising solutions to improve spectrum utilization, cognitive radio technology allows the secondary users (SUs) to opportunistically access to vacant bands belonging to primary users (PUs) in either temporal or spatial domain [3, 21, 73].

The idea of opening up the licensed spectrum bands in cognitive radio networks initiates the market of spectrum trading, and promotes a batch of interesting research on related topics. Specifically, in [35], Grandblaise et al. generally describe the possible scenarios and introduce some microeconomics inspired mechanisms for opportunistic spectrum accessing (OSA), and in [100], Sengupta and Chatterjee propose an economic framework for OSA and service pricing to guide the design of dynamic spectrum allocation algorithms as well as service pricing mechanisms that the service providers can possibly use. From the view of system design, models in game theory, by Wang et al. in [119, 120], Pan et al. in [84] and Zhang et al. in [132], and auction designs in microeconomics, by Zhou et al. in [135, 136], Jia et al. in [48] and Wu et al. in [124], are exploited to construct the spectrum trading mechanisms with desired properties, such as power efficiency, allocation fairness, incentive compatibility, Pareto efficiency, etc. From the view of the primary service provider (PSP), Xing et al. in [125] and Niyato et al. in [75, 76] have well investigated the spectrum pricing issues in the spectrum market, where multiple PSPs, whose goal is to maximize the monetary gains with their vacant spectrum, compete with each other to offer spectrum access to the

secondary service provider (SSP). From the view of the SSP, people are interested in how the SSP optimally distributes SUs' traffic demands over the spectrum bands when there is more than one unoccupied licensed band. Motamedi and Bahai in [74] have formulated this problem as a multi-armed bandit problem and propose a reinforce learning algorithm to consistently track the best band in terms of band conditions.

However, the concept of the best band for OSA tends to be ambiguous considering the characteristics of different bands. As described in [75, 125], the spectrum bands from PSPs may be evaluated unequally by the SSP from different perspectives, such as the frequency of the available band, the segment type of the band (i.e., contiguous segment or discontinuous one), the price of the band, the location of the PSP, etc. Among all these factors, the PUs' activities on the band are the most crucial one for the SSP, because the unexpected returning of primary services may terminate the SSP's spectrum provision to the SUs and incur enormous monetary risk for the SSP on its spectrum purchasing. Therefore, it is necessary for the SSP to find a metric to quantify the potential risk for OSA due to the PSPs' uncertain spectrum supply.

State-of-the-art work on investigating the unpredictable activities of primary services can generally be classified into two categories: i) spectrum sensing [12, 26, 27, 51, 65, 134] and ii) statistical analysis of the collected/historical spectrum vacancy/occupancy data [9, 70, 71]. In spite of the overwhelming waste of sensing time which can be used for more traffic delivery, individual sensing is trapped by sensing accuracy since both false alarm probability and missing detection probability are really high [12, 26, 51]. To overcome the weakness of individual sensing, cooperative sensing is proposed to improve the sensing accuracy by grouping SUs to sense together and share information among the group [26, 27]. But the trouble is that it is too difficult to synchronize/schedule the SUs in the group sensing simultaneously/sequentially. In addition, cooperative sensing has to set up a common channel for information exchange, which will incur enormous communication overhead. On the other hand,

in [9, 21, 34, 70, 71][1] , researchers in academia as well as engineers in industry try to identify the spectrum supply for OSA with the statistics of licensed spectrum utilization rather than attempting to detect the activities of primary services. They have carried out spectrum measurements, collected and analyzed the data about spectrum utilization, summarized the statistical characteristics of the band vacancy/occupancy, and stored these statistics into the database. This database architecture is adopted by FCC in its latest released rule for the opportunistic usage of white space [21], and many companies including Spectrum Bridge, Microsoft, Google [34], etc. have proposed their solutions and experimental prototypes based on this architecture. In addition, authors in [2, 19] integrate the historical data with the sensing results to provide better statistics or give better prediction for the activities of primary services. These statistical results contain abundant information about the uncertain spectrum supply and provide a nice guide to the band selection and purchase of the SSP for the SUs' OSA.

Inspired by the statistical characteristics of spectrum bands obtained on observation and experiments in [9, 21, 34, 70, 71], in this chapter, we novelly model the unpredictable activities of primary services on the licensed bands as a vector of random variables and propose metrics to evaluate the risk for OSA. Due to the uncertain spectrum supply, heaping all the traffic on one band makes the secondary services vulnerable to the activities of the primary services. Therefore, based on the proposed loss metrics, we illustrate how the SSP optimally splits the traffic demands of the SUs on a band-mix, when there are multiple available licensed bands. Our major contributions are summarized as follows.

[1] Chen et al. in [9] carried out a set of spectrum measurements in the 20MHz to 3GHz spectrum bands at 4 locations concurrently in Guangdong province of China. They used these data sets to conduct a set of detailed analysis of the first and second order statistics of the collected data, including channel occupancy/vacancy statistics, channel utilization, also spectral and spatial correlation of these measures.

- We first introduce the X loss to intuitively answer the question: what is the risk for OSA at a specified confidence level with uncertain spectrum supply from the PSPs. Despite the simplicity of the X loss in definition, it in fact underestimates the potential risk of the SSP and mathematically lacks of subadditivity (i.e., the X loss of a mix with two bands may be larger than the sum of individual X losses of the two bands.), which makes the X loss unable to support the traffic splitting over different bands.

- Beyond the X loss, we formally define the expected X loss, a measurement with desirable properties including subadditivity and convexity, to quantify the risk for OSA. Besides, the expected X loss can support the traffic splitting without any limitation on the distribution of primary services on the bands. Due to the difficulty in calculation of the expected X loss, we simplify it with a characteristic function into a discritized version, which is feasible to be used in evaluating the risk for OSA.

- To reduce the risk of the SUs for OSA, we put eggs into different baskets [69], i.e., we make the SSP split the traffic demands from SUs on a mix of bands instead of swarming all the traffic over one band. The reason is that it is generally impossible for bands with different frequencies to perform poorly at the same time. Moreover, we introduce the SSP's band-mix selection criterion, i.e., selecting the band-mix for traffic splitting with maximum expected reward for given risk for OSA, or with minimum risk for given reward, as well as other concepts related to the spectrum band-mix selection for OSA, such as efficient OSA curves and utility functions of the SSP.

- Based on the expected X loss, we specifically illustrate how the SSP optimally selects the proportional composition of the mix of bands owned by the PSPs for traffic splitting with the risk for OSA at a given confidence level[2] . Furthermore, we formulate the band-mix selection for OSA into a non-linear revenue maximization problem. By replacing the expected X loss with its discritized version for risk estimation, we prove that the two problems achieve the same results in terms of the optimal band-mix selection for OSA, and we solve the latter optimization problem by linear programming.

[2] Actually, the process of selecting the band-mix for OSA can be divided into two stages. The first stage starts with sampling and observation, and ends with statistical values about the future performance of available spectrum bands from PSPs. Chen et al. in [9] have accomplished the first stage work of band-mix selection for OSA; the second stage starts with the latest statistical values related to future spectrum supply from PSPs, and ends with the SSP's risk quantification and band-mix selection for OSA. In this chapter, we are only concerned with the second stage.

- By carrying out numerical simulations, we provide the efficient OSA curves with risk for OSA at different confidence levels, and show that with the designated utility function of the SSP, the proposed spectrum band-mix selection scheme is effective in improving the spectrum utilization, the satisfaction degree of SUs and the SSP's profit.

The rest of this chapter is organized as follows. In Section 2.2, we describe the roles of the PSPs and the SSP in the spectrum trading and define the reward function for the SUs as well as the risk function for OSA. We introduce related concepts to band-mix selection including band-mix selection rule, efficient OSA curves and the SSP's utility function in Section 2.3. We elaborate on the two proposed risk metrics for OSA: the X loss and the expected X loss in Section 2.4. With the discritized version of the expected X loss, we illustrate the optimal band-mix selection of the SSP for OSA in Section 2.5. Finally, we conduct numerical simulations and analyze the performance results in Section 2.6, and draw the concluding remarks in Section 6.8.

2.2 System Model

2.2.1 Spectrum Market

We consider a spectrum market in cognitive radio networks [75] with multiple PSPs operating on different spectrum bands and a SSP who serves a group of SUs as shown in Fig. 2-1A. The SUs can take opportunistic use of these licensed spectrum bands when the primary services are not on, but must evacuate from these bands immediately when primary services become active. In addition, we assume all the spectrum transactions take place at starting time of each period[3] as shown in Fig. 2-1B, and the payment for spectrum trading is non-refundable.

[3] The selling/buying period $\triangle t$ should not be too long (e.g., days, months or years) to make dynamic spectrum access infeasible, and it should not be too short (e.g., milliseconds or seconds) to incur overwhelming overhead in spectrum trading. The typical duration is minutes or hours as shown in [31]. In the rest of this chapter, we assume that all the spectrum transactions are of fixed duration, so that the time parameter is not included in our formulation.

In this case, PSPs will set reasonable prices for the unoccupied bands considering the quality of the bands as well as competition among the PSPs in the spectrum market [48, 75, 125], and sell those bands periodically for monetary gains. Correspondingly, if the SSP (e.g., the base station (BS) or the access point (AP)) realizes there is not enough radio resource for the traffic demands of its SUs, the SSP will play the role of trading agent for the SUs [100]. Specifically, the SSP will try to select a mix of currently vacant licensed bands, buy those bands from the PSPs, charge the SUs with the prices set by PSPs and share the bands purchased among multiple SUs in a time-division multiple access (TDMA) manner.

2.2.2 SSP's Revenue and Risk Function

Assume there are n available spectrum bands owned by different PSPs with identical bandwidth, which equals to 1, within the sensing range of the SSP. Considering the unpredictable activities of primary services, the uncertain spectrum supply of different bands for a given period is represented by $\mathbf{s} = (s_1, s_2, \cdots, s_n)$, where s_i is a random variable[4] within the domain of $[0, 1]$. Suppose the total traffic demand from the SUs is 1, and the proportional composition of the band-mix that the SSP picks up is $\boldsymbol{\omega} = (\omega_1, \omega_2, \cdots, \omega_n)$, $\boldsymbol{\omega} \in \mathcal{W}$, where $\sum_{i=1}^{n} \omega_i = 1$. Then, the total spectrum resources the SSP can obtain is $\sum_{i=1}^{n} s_i \omega_i$, and the expected reward for the SSP can be written as

$$\Pi(\boldsymbol{\omega}) = r \sum_{i=1}^{n} \mathbb{E}[s_i]\omega_i. \tag{2–1}$$

[4] Here, s_i can be interpreted as unoccupied time or unoccupied bandwidth by primary services for band i during one time period.

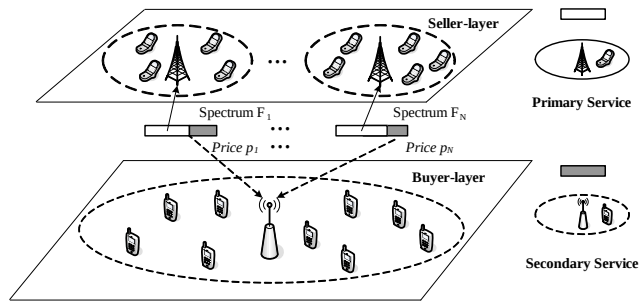

A The architecture of spectrum market

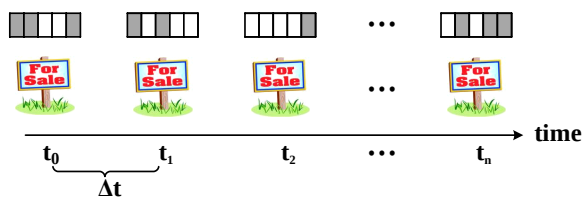

B Periodical spectrum selling

Figure 2-1. System model for spectrum trading

where r is a constant, representing the SSP's reward for satisfying one unit of traffic[5] . Correspondingly, the risk function of the SSP can be expressed as

$$\ell(\boldsymbol{\omega}, \mathbf{s}) = \mathbf{p}^T \boldsymbol{\omega} - r\mathbf{s}^T \boldsymbol{\omega}, \tag{2–2}$$

where $\mathbf{p} = (p_1, p_2, \cdots, p_n)$ is the charging price vector set by the PSPs for OSA per period, and p_i is a constant during a spectrum trading period. Note that $p_i \geq p_j$, if $\mathbb{E}(s_i) \geq \mathbb{E}(s_j)$. Since r is a fixed number and $\mathbf{s}$ is a random vector, the risk for OSA depends on both the statistical characteristics of $\mathbf{s}$ and the SSP's selection of bands belonging to the PSPs.

[5] With the assumption that r is fixed, $\Pi(\boldsymbol{\omega})$ can also be interpreted as the expected traffic demands that the SSP is able to support.

2.3 Primary Concepts for Band-Mix Selection

2.3.1 Band-Mix Selection Principle

Intuitively, the SSP is able to maximize his revenue by pouring all the traffic of secondary users over a particular band with the maximal expected reward. However, the risk of using that band may be quite high. A rational or risk-averse SSP is not likely to gamble all the traffic on one band since the reward may be extraordinarily low considering the activities of primary services.

Therefore, the expected reward should not be the only criterion in choosing the spectrum bands to access; instead, the risk of the reward must be considered by the SSP. It is reasonable to believe that if any two band-mixes have the same expected reward, the SSP will prefer the one having the smaller risk for OSA, and if any two band-mixes have the same risk, the SSP will prefer the one having the greater expected reward. So, the criterion for band-mix selection is as the follows.

Reward-Risk (Dual-R) Rule: The SSP should choose a mix of licensed bands with maximum expected reward for given risk for OSA, or with minimum risk for given expected reward for OSA, with respect to the uncertain spectrum supply from the PSPs.

2.3.2 The Efficient OSA Curve

With all band-mixes that can be constructed from the set of vacant spectrum bands from PSPs, it is obvious that the *Dual-R rule* produces not an optimal OSA point but an efficient OSA curve for the SSP's band-mix selection, if we consider the SSP may tolerate different levels of risk for OSA. Given a fixed risk, the corresponding band-mix on the efficient OSA curve always provides the highest reward. Or, given a fixed expected reward, the corresponding band-mix on the efficient OSA curve always provides the lowest risk for OSA, i.e., the efficient OSA curve is the set of all the band-mixes with the reward-risk pairs which are not dominated by any other band-mixes for OSA.

2.3.3 Utility Function of the SSP

To determine a specific band-mix selection for OSA on the efficient OSA curve, the SSP needs to specify his utility function, which can jointly measure the SSP's satisfaction of receiving a certain amount of reward and the risk-aversion associated with that reward. A rational SSP's goal is to find the optimal band-mix for OSA to maximize the expected utility with respect to all expected reward-risk pairs of possible band-mixes for OSA. In this chapter, the SSP's utility function is assumed to be an increasing and concave function, which may be polynomial, exponential, etc., e.g., the utility function of the SSP can be defined as the difference between the value of its expected reward and the value of its risk for monetary loss [69, 106, 107] during the opportunistic accessing process.

2.4 The Risk Measurement for OSA

In this section, we begin with an intuitive way, the X loss, to quantify the risk of the SSP for OSA at a given confidence level. Then, we dwell on the expected X loss, a more reasonable and effective metric with desirable properties for risk evaluation.

2.4.1 The X Loss for OSA

For convenience, we assume the random vector $\mathbf{s}$, which represents the uncertain spectrum supply from PSPs, has a probability density function $f(\mathbf{s})$[6] . From Equation (2–2), we find that the risk, $\ell(\boldsymbol{\omega}, \mathbf{s})$, is a random variable having a distribution depending on that of $\mathbf{s}$. The probability of the risk, $\ell(\boldsymbol{\omega}, \mathbf{s})$, not exceeding a threshold $\alpha \in \mathcal{R}$ is then given by

$$F(\boldsymbol{\omega}, \alpha) = \int_{\ell(\boldsymbol{\omega}, \mathbf{s}) \leq \alpha} f(\mathbf{s}) \, \mathrm{d}\, \mathbf{s}. \tag{2–3}$$

[6] This assumption is not essential for the expected X loss and can be relaxed.

As a function of α for fixed $\boldsymbol{\omega}$, $F(\boldsymbol{\omega}, \alpha)$ [7] is the cumulative distribution function for the risk caused by the unpredictable activities of primary services.

Given any specified confidence level $\beta \in (0, 1)$, the X loss for OSA associated with $\boldsymbol{\omega}$ is denoted as

$$X_\beta(\boldsymbol{\omega}) = \inf\{\alpha \in \mathcal{R} : F(\boldsymbol{\omega}, \alpha) \geq \beta\}. \tag{2–4}$$

According to Equation (2–4), the X loss[8] represents the potential risk that the SSP needs to take for OSA with a specified band-mix $\boldsymbol{\omega}$ at the confidence level β.

Ex. 1: Let β be equal to 0.9. With a given $\boldsymbol{\omega}$, the probability distribution of the risk for OSA is supposed to be like that shown in Fig. 2-2A. Then, the area in shade is equal to $(1 - \beta) = 0.1$, and $X_\beta(\boldsymbol{\omega}) = 0.57$.

Although the X loss seems simple to follow, its inherent weakness makes this measurement difficult to be applied in band-mix selection and traffic splitting for OSA in our setting. The shortcomings of the X loss are as follows:

- The X loss underestimates the risk for OSA. From Equation (2–4) and **Ex. 1**, we find the X loss denotes the risk that the SSP suffers in the β best cases in terms of the uncertain spectrum supply from PSPs. Actually, with the given $\boldsymbol{\omega}$, the SSP is not interested in the loss in the least β cases of risk irrespectively of how serious the risk in all the other cases is.

- The X loss is not valid when $\mathbf{s}$ has a fat-tailed (a.k.a., heavy-tailed) distribution. However, recent works on traffic measurements [9, 46] show that the traffic of the

[7] The function $F(\boldsymbol{\omega}, \alpha)$ is nondecreasing w.r.t. α and we assume that $F(\boldsymbol{\omega}, \alpha)$ is everywhere continuous w.r.t. α. This assumption is also made for simplicity.

[8] Compared with the classical risk metric (i.e., the variance of the reward) in portfolio theory [69], the proposed X loss and the expected X loss exclude the negative effects of the variance approach [38] and take full use of the inherent information contained in the statistics of band vacancy [88].

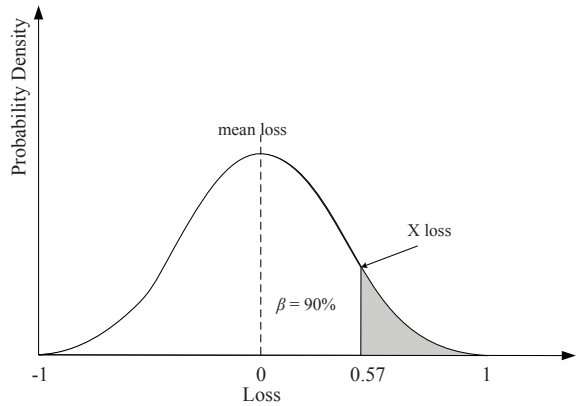

A The X loss for OSA.

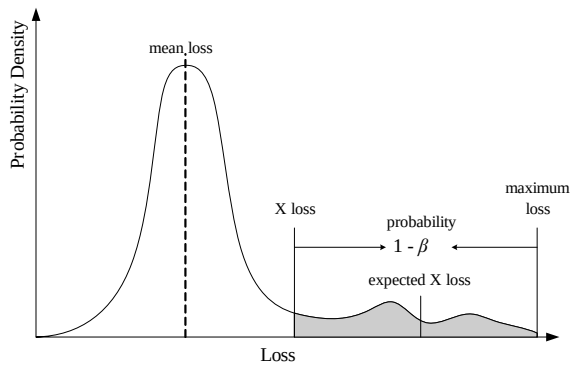

B The expected X loss for OSA.

Figure 2-2. The loss metrics for OSA.

primary services may statistically exhibit not only a thin-tailed (a.k.a., light-tailed) distribution but also a fat-tailed distribution[9] .

- The X loss lacks subadditivity [10] and is non-convex as a function of ω, which make it difficult to optimize as well as to apply in band-mix selection for traffic splitting.

2.4.2 The Expected X Loss for OSA

The weakness of the X loss gives us the impetus to seek another measurement for the risk incurred by the uncertain spectrum supply. So, we define an alternative risk

[9] To be specific, the distribution of voice services in GSM measured in [9] is said to have a thin tail, and the distribution of data packet services measured in [46] is said to have a fat tail.

[10] Please refer to **Ex. 2** for better understanding.

Table 2-1. Spectrum vacancy from the primary service providers.

Band A	Band B	B-mix (A+B)	Probability
0.5	1	0.75	6%
0.8	1	0.9	4%
1	0.5	0.75	6%
1	0.8	0.9	4%
1	1	1	80%

metric, the expected X loss, as

$$EX_\beta(\boldsymbol{\omega}) = \frac{1}{1-\beta}\int_{\ell(\boldsymbol{\omega},\mathbf{s})\geq X_\beta(\boldsymbol{\omega})} \ell(\boldsymbol{\omega},\mathbf{s}) f(\mathbf{s})\,\mathrm{d}\,\mathbf{s}. \tag{2–5}$$

In Equation (2–5), the probability that $\ell(\boldsymbol{\omega},\mathbf{s}) \geq X_\beta(\boldsymbol{\omega})$ is equal to $(1-\beta)$. Therefore, $EX_\beta(\boldsymbol{\omega})$ comes out as the expectation of the risk being $X_\beta(\boldsymbol{\omega})$ or greater.

As the comparison shown in Fig. 2-2, the expected X loss considers the risk for OSA in general cases, but the X loss only considers the risk for OSA in the β best cases. Moreover, the expected X loss is subadditive but the X loss is not. To be simple, we illustrate this property in the following example.

Ex. 2: Assume the SSP selects a band-mix consisting of band A and B, where $\boldsymbol{\omega}_\mathrm{A} = (1,0)$, $\boldsymbol{\omega}_\mathrm{B} = (0,1)$ and $\boldsymbol{\omega}_\mathrm{mix} = (0.5, 0.5)$. The availability of band A and B for OSA is given in Tab. 2-1. Given $\mathbf{p} = (p_1, p_2) = (1,1)$, $r = 1$, and $\beta = 0.9$, the X loss and the expected X loss for band A, band B and the band-mix are calculated and listed in Tab. 2-2. Observation shows that $X_\beta(\boldsymbol{\omega}_\mathrm{A}) = X_\beta(\boldsymbol{\omega}_\mathrm{B}) = 0.2 < X_\beta(\boldsymbol{\omega}_\mathrm{mix}) = 0.25$, but $EX_\beta(\boldsymbol{\omega}_\mathrm{A}) = EX_\beta(\boldsymbol{\omega}_\mathrm{B}) = 0.38 > EX_\beta(\boldsymbol{\omega}_\mathrm{mix}) = 0.25$, which indicates the expected X loss is subadditive but the X loss is not.

2.4.3 Characterization and Discretization of the Expected X Loss

With the definition of the expected X loss, we still find it difficult to handle because $X_\beta(\boldsymbol{\omega})$ is involved in the calculation of $EX_\beta(\boldsymbol{\omega})$. Thus, we simplify $EX_\beta(\boldsymbol{\omega})$ by characterizing it with the function Γ_β on $\mathcal{W}\times\mathcal{R}$, which can be denoted as

$$\Gamma_\beta(\boldsymbol{\omega},\alpha) = \alpha + \frac{1}{1-\beta}\int_{\mathbf{s}\in\mathcal{R}^n} [\ell(\boldsymbol{\omega},\mathbf{s}) - \alpha]^+ f(\mathbf{s})\,\mathrm{d}\,\mathbf{s}, \tag{2–6}$$

where $[t]^+ = \max\{0, t\}$. The critical features of Γ_β are as follows.

Theorem 2.1. *As a function of α, $\Gamma_\beta(\boldsymbol{\omega}, \alpha)$ is convex and continuously differentiable. The expected X loss associated with any $\boldsymbol{\omega} \in \mathcal{W}$ can be determined from the formula*

$$EX_\beta(\boldsymbol{\omega}) = \min_{\alpha \in \mathcal{R}} \Gamma_\beta(\boldsymbol{\omega}, \alpha). \tag{2–7}$$

In this formula, the set consisting of the values of α, for which the minimum is attained, is a nonempty, closed, bounded interval (perhaps reducing to a single point), and in particular, we obtain

$$\begin{cases} X_\beta(\boldsymbol{\omega}) \in \operatorname*{argmin}_{\alpha \in \mathcal{R}} \Gamma_\beta(\boldsymbol{\omega}, \alpha) \\ EX_\beta(\boldsymbol{\omega}) = \Gamma_\beta(\boldsymbol{\omega}, X_\beta(\boldsymbol{\omega})). \end{cases} \tag{2–8}$$

Proof. The following lemma is essential for establishing Theorem 2.1 and Theorem 2.2 with respect to α of the integral expression in the definition of $\Gamma_\beta(\boldsymbol{\omega}, \alpha)$. Here, we rely on the assumption that $F(\boldsymbol{\omega}, \alpha)$ is continuous with respect to α, which is equivalent to saying that regardless of the choice of $\boldsymbol{\omega}$, the set of $\mathbf{s}$ with $\ell(\boldsymbol{\omega}, \mathbf{s}) = \alpha$ has probability zero, i.e.,

$$\int_{\ell(\boldsymbol{\omega}, \mathbf{s}) = \alpha} f(\mathbf{s}) \, \mathrm{d}\, \mathbf{s} = 0.$$

Lemma 1. *With $\boldsymbol{\omega}$ fixed, let $G(\alpha) = \int_{\mathbf{s} \in \mathcal{R}^n} g(\alpha, \mathbf{s}) f(\mathbf{s}) \mathrm{d}\, \mathbf{s}$, where $g(\alpha, \mathbf{s}) = [\ell(\boldsymbol{\omega}, \mathbf{s}) - \alpha]^+$. Then, G is a convex, continuously differentiable function with derivative*

$$\frac{\partial}{\partial \alpha} G(\alpha) = F(\boldsymbol{\omega}, \alpha) - 1.$$

Table 2-2. X_β vs EX_β with $\beta = 0.9$.

$\beta = 90\%$	Band A	Band B	B-mix (A+B)
X_β	0.2	0.2	0.25
EX_β	0.38	0.38	0.25

Proof. The lemma above is from Proposition 2.1 in [102], where the following equations are proved, i.e.,

$$\begin{aligned}\frac{\partial}{\partial\alpha}G(\alpha) &= \mathbb{E}[\frac{\partial}{\partial\alpha}g(\alpha,\mathbf{s})] \\ &= \int_{\mathbf{s}\in\mathcal{R}^n}\frac{\partial}{\partial\alpha}g(\alpha,\mathbf{s})f(\mathbf{s})\,\mathrm{d}\,\mathbf{s} \\ &= \int_{\ell(\boldsymbol{\omega},\mathbf{s})\geq\alpha}\frac{\partial}{\partial\alpha}[\ell(\boldsymbol{\omega},\mathbf{s})-\alpha]f(\mathbf{s})\,\mathrm{d}\,\mathbf{s} \\ &= F(\boldsymbol{\omega},\alpha)-1.\end{aligned}$$

□

In view of the defining formula for $\Gamma(\boldsymbol{\omega},\alpha)$, it can easily be deduced from the lemma that $\Gamma(\boldsymbol{\omega},\alpha)$ is convex and continuously differentiable with derivative

$$\begin{aligned}\frac{\partial}{\partial\alpha}\Gamma(\boldsymbol{\omega},\alpha) &= 1+\frac{1}{(1-\beta)}[F(\boldsymbol{\omega},\alpha)-1] \\ &= \frac{1}{(1-\beta)}[F(\boldsymbol{\omega},\alpha)-\beta].\end{aligned}$$

Therefore, the values of α that minimize $\Gamma(\boldsymbol{\omega},\alpha)$ are exactly those for which $F(\boldsymbol{\omega},\alpha)-\beta = 0$. They form a nonempty closed interval, in as much as $F(\boldsymbol{\omega},\alpha)$ is continuous and nondecreasing in α with limit 1 as $\alpha\to-\infty$. This further demonstrates the validity of the X_β formula. So, we have

$$\begin{aligned}&\min_{\alpha\in\mathcal{R}}\Gamma_\beta(\boldsymbol{\omega},\alpha) = \Gamma_\beta(\boldsymbol{\omega},X_\beta(\boldsymbol{\omega})) \\ &= X_\beta(\boldsymbol{\omega})+\frac{1}{1-\beta}\int_{\mathbf{s}\in\mathcal{R}^n}[\ell(\boldsymbol{\omega},\mathbf{s})-X_\beta(\boldsymbol{\omega})]^+f(\mathbf{s})\,\mathrm{d}\,\mathbf{s}.\end{aligned}$$

But the integral here equals

$$\int_{\ell(\boldsymbol{\omega},\mathbf{s})\geq X_\beta(\boldsymbol{\omega})}[\ell(\boldsymbol{\omega},\mathbf{s})-X_\beta(\boldsymbol{\omega})]f(\mathbf{s})\,\mathrm{d}\,\mathbf{s}=$$
$$\int_{\ell(\boldsymbol{\omega},\mathbf{s})\geq X_\beta(\boldsymbol{\omega})}\ell(\boldsymbol{\omega},\mathbf{s})f(\mathbf{s})\,\mathrm{d}\,\mathbf{s}-X_\beta(\boldsymbol{\omega})\int_{\ell(\boldsymbol{\omega},\mathbf{s})\geq X_\beta(\boldsymbol{\omega})}f(\mathbf{s})\,\mathrm{d}\,\mathbf{s},$$

where the first integral on the right is by definition $(1-\beta)EX_\beta(\boldsymbol{\omega})$ and the second is $1-F(\boldsymbol{\omega},X_\beta(\boldsymbol{\omega}))$. Moreover, $F(\boldsymbol{\omega},X_\beta(\boldsymbol{\omega}))=\beta$. Thus,

$$\begin{aligned}\min_{\alpha\in\mathcal{R}}\Gamma_\beta(\boldsymbol{\omega},\alpha)&=X_\beta(\boldsymbol{\omega})+\frac{1}{1-\beta}[(1-\beta)EX_\beta(\boldsymbol{\omega})-X_\beta(\boldsymbol{\omega})(1-\beta)]\\&=EX_\beta(\boldsymbol{\omega}).\end{aligned}$$

The proof is finished. □

Theorem 2.2. *Minimizing the expected X loss with $\boldsymbol{\omega}$ over all $\boldsymbol{\omega}\in\mathcal{W}$ is equivalent to minimizing $\Gamma_\beta(\boldsymbol{\omega},\alpha)$ over all $(\boldsymbol{\omega},\alpha)\in\mathcal{W}\times\mathcal{R}$, i.e.,*

$$\min_{\boldsymbol{\omega}\in\mathcal{W}}EX_\beta(\boldsymbol{\omega})=\min_{(\boldsymbol{\omega},\alpha)\in\mathcal{W}\times\mathcal{R}}\Gamma_\beta(\boldsymbol{\omega},\alpha),\tag{2–9}$$

Proof. The claims in Theorem 2.2 are simple results of the expected X loss formula in Theorem 2.1 and the fact that the minimization of $\Gamma_\beta(\boldsymbol{\omega},\alpha)$ with respect to $(\boldsymbol{\omega},\alpha)\in\mathcal{W}\times\mathcal{R}$ can be carried out by sequential fixing minimization [41], i.e., first minimizing over $\alpha\in\mathcal{R}$ for fixed $\boldsymbol{\omega}$ and then minimizing the result over $\boldsymbol{\omega}\in\mathcal{W}$.

The convexity claim starts with the observation that $\Gamma_\beta(\boldsymbol{\omega},\alpha)$ is convex with respect to $(\boldsymbol{\omega},\alpha)$ whenever the integrand $[\ell(\boldsymbol{\omega},\mathbf{s})-\alpha]^+$, in the equation: $\Gamma_\beta(\boldsymbol{\omega},\alpha)=\alpha+\frac{1}{1-\beta}\int_{\mathbf{s}\in\mathcal{R}^n}[\ell(\boldsymbol{\omega},\mathbf{s})-\alpha]^+f(\mathbf{s})\,\mathrm{d}\,\mathbf{s}$ for $\Gamma_\beta(\boldsymbol{\omega},\alpha)$, is itself convex with respect to $(\boldsymbol{\omega},\alpha)$. For each $\mathbf{s}$, this integrand is the composition of the function $(\boldsymbol{\omega},\alpha)\mapsto\ell(\boldsymbol{\omega},\mathbf{s})-\alpha$ with the nondecreasing convex function $t\mapsto[t]^+$, so by the rules in Theorem 5.1 in [98], it is convex as long as the function $(\boldsymbol{\omega},\alpha)\mapsto\ell(\boldsymbol{\omega},\mathbf{s})-\alpha$ is convex. The latter is true when $\ell(\boldsymbol{\omega},\mathbf{s})$ is convex with respect to $\boldsymbol{\omega}$. The convexity of the function $EX_\beta(\boldsymbol{\omega})$ can be illustrated from the fact that minimizing of an extended real-valued convex function of

two vector variables with respect to one of these variables, results in a convex function of the remaining variable [98]. □

According to Theorem 2.1 and 2.2, the SSP is not necessary, for the purpose of determining $\boldsymbol{\omega}^*$ that yields the minimum expected X loss for the given reward, to work directly with the function $EX_\beta(\boldsymbol{\omega})$, which may be too difficult to do because its definition contains $X_\beta(\boldsymbol{\omega})$, a value with troublesome mathematical properties. Instead, the SSP can operate on the much simpler expression $\Gamma_\beta(\boldsymbol{\omega}, \alpha)$ with its convexity in the variable α and even with respect to $(\boldsymbol{\omega}, \alpha)$.

Moreover, the integral in $\Gamma_\beta(\boldsymbol{\omega}, \alpha)$ can be approximated by sampling the probability distribution of $\mathbf{s}$ according to its density $f(\mathbf{s})$ or by directly using the data collected by Yin et al. in [9]. Assuming this procedure generates a collection of vectors $(\mathbf{s}_1, \mathbf{s}_2, \cdots, \mathbf{s}_m)$, then the corresponding approximation to $\Gamma_\beta(\boldsymbol{\omega}, \alpha)$ can be written as

$$\tilde{\Gamma}_\beta(\boldsymbol{\omega}, \alpha) = \alpha + \frac{1}{m(1-\beta)} \sum_{k=1}^{m} [\ell(\boldsymbol{\omega}, \mathbf{s}_k) - \alpha]^+. \tag{2–10}$$

Since $\ell(\boldsymbol{\omega}, \mathbf{s})$ is linear $w.r.t.$ $\boldsymbol{\omega}$ and $\Gamma_\beta(\boldsymbol{\omega}, \alpha)$ is convex, the function $\tilde{\Gamma}_\beta(\boldsymbol{\omega}, \alpha)$ is convex and piecewise linear.

2.5 Optimal Band-Mix Selection Based on the Expected X Loss

Based on the concept of the efficient OSA curve, the SSP will choose the proportional composition of the band-mix, $\boldsymbol{\omega}$, to maximize the expected reward for SUs with an expected X loss constraint, or to minimize the expected X loss with an expected reward constraint, i.e.,

$$\max_{\boldsymbol{\omega} \in \mathcal{W}} \Pi(\boldsymbol{\omega}), \quad EX_\beta(\boldsymbol{\omega}) \leq \tau, \quad \boldsymbol{\omega} \in \mathcal{W} \tag{2–11}$$

and

$$\min_{\boldsymbol{\omega} \in \mathcal{W}} EX_\beta(\boldsymbol{\omega}), \quad \Pi(\boldsymbol{\omega}) \geq \nu, \quad \boldsymbol{\omega} \in \mathcal{W} \tag{2–12}$$

Varying the parameters τ and ν, the two problems above are equivalent in the sense that they produce the same efficient OSA curves. Thus, we can only work on Equation (2–11). Furthermore, we demonstrate that the function $\Gamma_\beta(\boldsymbol{\omega}, \alpha)$ can be used instead of $EX_\beta(\boldsymbol{\omega})$ in this problem.

Theorem 2.3. *The two reward maximization problems below*

$$\max_{\boldsymbol{\omega}\in\mathcal{W}} \Pi(\boldsymbol{\omega}), \quad EX_\beta(\boldsymbol{\omega}) \leq \tau, \quad \boldsymbol{\omega} \in \mathcal{W} \tag{2–13}$$

and

$$\max_{(\alpha,\boldsymbol{\omega})\in\mathcal{W}\times\mathcal{R}} \Pi(\boldsymbol{\omega}), \quad \Gamma_\beta(\boldsymbol{\omega}, \alpha) \leq \tau, \quad \boldsymbol{\omega} \in \mathcal{W} \tag{2–14}$$

are equivalent in the sense that their objectives achieve the same maximum values.

Proof. The maximization problem

$$\max_{\boldsymbol{\omega}\in\mathcal{W}} \Pi(\boldsymbol{\omega}), \quad EX_\beta(\boldsymbol{\omega}) \leq \tau, \quad \boldsymbol{\omega} \in \mathcal{W}$$

is the same as the minimization problem

$$\min_{\boldsymbol{\omega}\in\mathcal{W}} -\Pi(\boldsymbol{\omega}), \quad EX_\beta(\boldsymbol{\omega}) \leq \tau, \quad \boldsymbol{\omega} \in \mathcal{W}$$

Meanwhile, the maximization problem

$$\max_{(\alpha,\boldsymbol{\omega})\in\mathcal{W}\times\mathcal{R}} \Pi(\boldsymbol{\omega}), \quad \Gamma_\beta(\boldsymbol{\omega}, \alpha) \leq \tau, \quad \boldsymbol{\omega} \in \mathcal{W}$$

is the same as the minimization problem

$$\min_{(\alpha,\boldsymbol{\omega})\in\mathcal{W}\times\mathcal{R}} -\Pi(\boldsymbol{\omega}), \quad \Gamma_\beta(\boldsymbol{\omega}, \alpha) \leq \tau, \quad \boldsymbol{\omega} \in \mathcal{W}$$

Therefore, to prove Theorem 2.3 is the same as proving the two minimization problems below

$$\min_{\boldsymbol{\omega}\in\mathcal{W}} -\Pi(\boldsymbol{\omega}), \quad EX_\beta(\boldsymbol{\omega}) \leq \tau, \quad \boldsymbol{\omega} \in \mathcal{W} \tag{2–15}$$

and

$$\min_{(\alpha,\boldsymbol{\omega})\in\mathcal{W}\times\mathcal{R}} -\Pi(\boldsymbol{\omega}), \quad \Gamma_\beta(\boldsymbol{\omega},\alpha)\leq\tau, \quad \boldsymbol{\omega}\in\mathcal{W} \tag{2–16}$$

are equivalent in the sense that their objectives achieve the same minimum values.

With Kuhn-Tacker (K-T) conditions[11] , the necessary and sufficient conditions for the problem are stated as follows

$$-\Pi(\boldsymbol{\omega}^*)+\mu\Gamma_\beta(\boldsymbol{\omega}^*,\alpha^*)\leq-\Pi(\boldsymbol{\omega})+\mu\Gamma_\beta(\boldsymbol{\omega},\alpha),$$
$$\mu(\Gamma_\beta(\boldsymbol{\omega},\alpha)-\tau)=0, \quad \mu\geq 0, \quad \boldsymbol{\omega}\in\mathcal{W}$$

First, suppose that $\boldsymbol{\omega}^*$ is a solution to the problem in Equation (2–15). Let us show that $(\boldsymbol{\omega}^*,\alpha^*)$ is a solution to the problem in Equation (2–16). Using necessary and sufficient conditions (K-T conditions) and Theorem 2.1, we have

$$\begin{aligned}&-\Pi(\boldsymbol{\omega}^*)+\mu\Gamma_\beta(\boldsymbol{\omega}^*,\alpha^*)=-\Pi(\boldsymbol{\omega}^*)+\mu EX_\beta(\boldsymbol{\omega}^*)\\&\leq-\Pi(\boldsymbol{\omega})+\mu EX_\beta(\boldsymbol{\omega})=-\Pi(\boldsymbol{\omega})+\mu\min_{\alpha\in\mathcal{R}}\Gamma_\beta(\boldsymbol{\omega},\alpha)\\&\leq-\Pi(\boldsymbol{\omega})+\mu\Gamma_\beta(\boldsymbol{\omega},\alpha),\end{aligned}$$

and

$$\mu(\Gamma_\beta(\boldsymbol{\omega}^*,\alpha^*)-\tau)=\mu(EX_\beta(\boldsymbol{\omega}^*)-\tau)=0,\ \mu\geq 0,\ \boldsymbol{\omega}\in\mathcal{W}.$$

Thus, K-T conditions are satisfied and $(\boldsymbol{\omega}^*,\alpha^*)$ is a solution to the problem in Equation (2–16).

Now, let us suppose that $(\boldsymbol{\omega}^*,\alpha^*)$ achieves the minimum of $-\Pi(\boldsymbol{\omega})$ in Equation (2–16) and $\mu>0$. For fixed $\boldsymbol{\omega}^*$, the point α^* minimizes the function $-\Pi(\boldsymbol{\omega}^*)+\mu\Gamma_\beta(\boldsymbol{\omega}^*,\alpha)$, and, consequently, the function $\Gamma_\beta(\boldsymbol{\omega}^*,\alpha)$. Since $(\boldsymbol{\omega}^*,\alpha^*)$ is a solution to the problem in

[11] See details in Theorem 2.5 in [95].

Equation (2–16), K-T conditions and Theorem 2.1 imply that

$$-\Pi(\boldsymbol{\omega}^*) + \mu EX_\beta(\boldsymbol{\omega}^*) = -\Pi(\boldsymbol{\omega}^*) + \mu\Gamma_\beta(\boldsymbol{\omega}^*, \alpha^*)$$
$$\leq -\Pi(\boldsymbol{\omega}) + \mu\Gamma_\beta(\boldsymbol{\omega}, X_\alpha(\boldsymbol{\omega})) = -\Pi(\boldsymbol{\omega}) + \mu EX_\beta(\boldsymbol{\omega}),$$

and

$$\mu(EX_\beta(\boldsymbol{\omega}^*) - \tau) = \mu(\Gamma_\beta(\boldsymbol{\omega}^*, \alpha^*) - \tau) = 0,\ \mu \geq 0,\ \boldsymbol{\omega} \in \mathcal{W}.$$

We proved that K-T conditions are satisfied, i.e., $\boldsymbol{\omega}^*$ is a solution to the problem in Equation (2–15). Theorem 2.3 is proved. □

As illustrated in Sec. 2.4.3, the function $\Gamma_\beta(\boldsymbol{\omega}, \alpha)$ can be approximated by the function $\tilde{\Gamma}_\beta(\boldsymbol{\omega}, \alpha)$. By using dummy variables z_k, where $k = 1, 2, \cdots, m$, the function $\tilde{\Gamma}_\beta(\boldsymbol{\omega}, \alpha)$ can be replaced by the linear function $\alpha + \frac{1}{m(1-\beta)}\sum_{k=1}^{m} z_k$ and the set of linear constraints

$$z_k \geq \ell(\boldsymbol{\omega}, \mathbf{s}_k) - \alpha, \quad z_k \geq 0, \quad k = 1, 2, \cdots, m. \tag{2–17}$$

Below we summarize the optimal band-mix selection problem for OSA described in this section.

$$\max_{(\alpha,\boldsymbol{\omega})\in\mathcal{W}\times\mathcal{R}} r\sum_{i=1}^{n}\mathbb{E}[s_i]\omega_i, \tag{2–18}$$

s.t.

$$\alpha + \frac{1}{m(1-\beta)}\sum_{k=1}^{m} z_k \leq \tau,$$
$$z_k \geq \ell(\boldsymbol{\omega}, \mathbf{s}_k) - \alpha, \quad z_k \geq 0, \quad k = 1, 2, \cdots, m,$$
$$\omega_i \leq \rho_i, \quad i = 1, \cdots, n,$$

where $\omega_i \leq \rho_i$ indicates that the SSP would not distribute traffic on a band s_i more than a given percent ρ_i of the overall traffic demands from SUs. This constraint can be relaxed by setting $\rho_i = 1$ if there is no limitation for the proportional composition of the band-mix selected for OSA.

By solving problem in Equation (2–18) with linear programming, the SSP attains the optimal vector $\boldsymbol{\omega}^*$ and the corresponding maximum expected reward for SUs, which equals $\mathbb{E}[\mathbf{s}]\boldsymbol{\omega}^*$. By solving problem above for the different levels of the expected X loss that the SSP can suffer, τ, the SSP obtains the efficient OSA curve for the band-mix selection.

2.6 Performance Analysis

By carrying out numerical simulations, in this section, we further demonstrate the band-mix selection problem with the risk at different confidence levels for OSA, where the risk is evaluated by the X loss or the expected X loss. Without the specific utility function of the SSP, we build up the efficient OSA curves on the *Reward-Risk* plane, and analyze the differences between efficient OSA curves based on the X loss and those based on the expected X loss. Moreover, with the SSP's specified utility functions, we compare the expected X loss based band-mix selection with the X loss based band-mix selection and the maximum expected reward based band-mix selection [85, 88, 126] in terms of the spectrum utilization, the SUs' satisfaction as well as the profit of the SSP.

2.6.1 Simulation Setup

We set up the simulation with a similar setting to that shown in Fig. 2-1, where the number of spectrum bands from PSPs within the range of the SSP is 6, and the SSP, operating as the trading agent for SUs, selects the mix of bands for traffic delivering. For illustrative purpose, we assume the overall traffic demand from SUs is equal to 1, and the SSP's reward for satisfying one unit of traffic, r, is equal to 120. As for the uncertain spectrum supply from PSPs, we represent it by a random vector $\mathbf{s} = (s_1, s_2, \cdots, s_n)$, where $s_i \in [0, 1]$ is a random variable. Moreover, we assume the price of the band i from PSPs, p_i, which is ascending as $\mathbb{E}(s_i)$ increases, is in the range of $[80, 130]$, for $i = (1, 2, \cdots, 6)$. Based on the two risk metrics in this chapter, i.e., the X loss and the

expected X loss, we carry out the band-mix selection optimization with confidence level β = 0.7, 0.8 and 0.9, respectively[12] .

Meanwhile, according to the analysis in [9, 46], the distribution of the unpredictable primary services, s_i, is either thin-tailed or fat-tailed. As we know, many types of distribution can be categorized as thin-tailed distribution, e.g., normal distribution, exponential distribution, etc., and several types of distribution can be regarded as fat-tailed distribution, e.g., log-normal distribution, Cauchy distribution, etc. [5, 24]. Without loss of generality, we let s_i be normally distributed to represent the unpredictable primary traffic with a thin tail in the first simulation scenario, and let s_i be log-normally distributed to represent the unpredictable primary traffic with a fat tail in the second one[13] , while the other parameters are the same in the two simulation scenarios.

2.6.2 Construction of Efficient OSA Curves

In Fig. 2-3A, the X loss based efficient OSA curves for band-mix selection and the expected X loss based ones overlap at different confidence levels, which is not surprising to see because s_i is normally distributed. A little more thought is enough to understand that in the Gaussian world everything is proportional to the standard deviation, which in turn is subadditive. Therefore, when s_i has normal distribution, the X loss is subadditive, and there is no difference between the efficient OSA curves with X loss and those with the expected X loss. In addition, it should be noted that the risk for OSA becomes larger with the increasing of the SSP's confidence levels in a general sense.

[12] It does not make sense for simulations with $\beta \leq 0.5$, because it is the same as guessing.

[13] By Monte Carlo simulations, the distribution of the primary services can be fitted from the data collected/sampled, as conducted in [9].

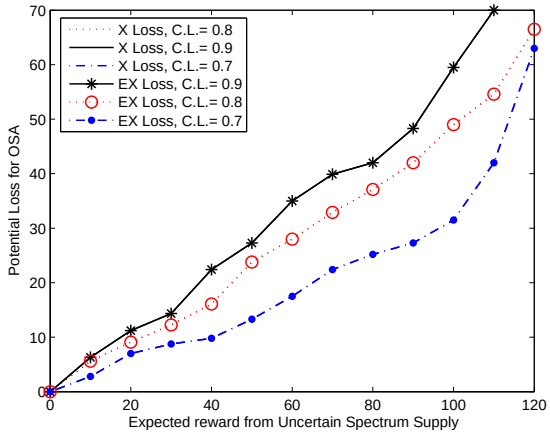

A Efficient OSA curves with different confidence levels (s_i is normally distributed, and $n = 6$.).

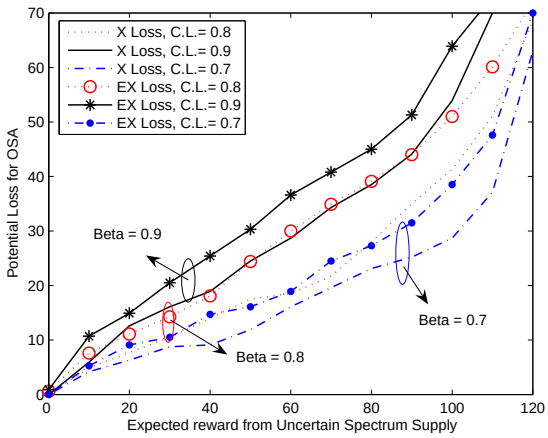

B Efficient OSA curves with different confidence levels (s_i is log-normally distributed, and $n = 6$.).

Figure 2-3. Optimal band-mix selection for OSA based on the X loss and the expected X loss.

With the assumption that the probability distribution of the uncertain spectrum supply is log-normal, the X loss based efficient OSA curves and the expected X loss based ones are compared at different confidence levels as depicted in Fig. 2-3B. We find that with a given β, the X loss based efficient OSA curves for band-mix selection severely underestimate the potential risk for OSA, and make the SUs more liable to be affected by the unpredictable activities of primary services. On the contrary, the

Table 2-3. Utility functions with risk at different confidence levels.

Index	Utility Function	Risk Metric	Confidence Level
1	$\Pi(\boldsymbol{\omega}) + \theta \cdot X_\beta(\boldsymbol{\omega})$	$X_\beta(\boldsymbol{\omega})$	β = 0.70
2	$\Pi(\boldsymbol{\omega}) + \theta \cdot EX_\beta(\boldsymbol{\omega})$	$EX_\beta(\boldsymbol{\omega})$	β = 0.70
3	$\Pi(\boldsymbol{\omega}) + \theta \cdot X_\beta(\boldsymbol{\omega})$	$X_\beta(\boldsymbol{\omega})$	β = 0.80
4	$\Pi(\boldsymbol{\omega}) + \theta \cdot EX_\beta(\boldsymbol{\omega})$	$EX_\beta(\boldsymbol{\omega})$	β = 0.80
5	$\Pi(\boldsymbol{\omega}) + \theta \cdot X_\beta(\boldsymbol{\omega})$	$X_\beta(\boldsymbol{\omega})$	β = 0.90
6	$\Pi(\boldsymbol{\omega}) + \theta \cdot EX_\beta(\boldsymbol{\omega})$	$EX_\beta(\boldsymbol{\omega})$	β = 0.90

expected X loss based efficient OSA curves perform better in evaluating the risk for OSA, and provide more accurate guide for the SSP with various levels of risk tolerance.

2.6.3 Performance Comparison

In order to select a particular band-mix for OSA based on the X loss or the expected X loss, it is necessary to present the utility function of the SSP as a bond between the expected reward of the SSP and the potential risk for OSA, otherwise it will be difficult for the SSP to make a choice among the band-mixes on the efficient OSA curves. Thus, we adopt a widely used utility function [49, 106, 107] and list a few of its variations with the two risk metrics at different confidence levels in Tab. 2-3. Here, θ represents the risk tolerance levels of the SSP for the OSA. The value of θ is assumed to be within the range of $[-\infty, 0]$, where $\theta = -\infty$ indicates that the SSP is extremely risk-averse and the SSP will never buy the spectrum band from PSPs, and $\theta = 0$ indicates that the SSP has no concern about the risk for OSA and only cares about the maximum expected reward. Using these utility functions, we let the number of available spectrum bands of PSPs increase[14] from 1 to 6, and compare the X loss based band-mix selection scheme with the expected X loss based one for opportunistic accessing in terms of spectrum utilization, SUs' satisfaction and the SSP's profit.

[14] In the simulation, we assume that the price of the band and the corresponding risk for OSA increase with the index of the bands, e.g., Band 1 is the cheapest band, and Band 6 is the most expensive one.

Since the X loss based efficient OSA curves and the expected X loss based efficient OSA curves overlap for the normally distributed traffic of the primary services, it is obvious that the X loss based band-mix selection scheme and the expected X loss based one will produce the same performance, provided that their utility functions have the same parameters in the first scenario. Therefore, we just need to compare the performance of the X loss based band-mix selection scheme and the expected X loss based one in the second scenario, where the distribution of the primary services has a fat tail. For illustrative purposes, we carry out the performance comparison with $\theta = -0.6$ and $\theta = -1.4$, respectively.

In Fig. 2-4A and Fig. 2-5A, we evaluate the performance of spectrum utilization with the X loss based band-mix selection and the expected X loss based band-mix selection. Note that spectrum utilization is calculated as the ratio of the utilized bands to the total bands. No matter the portion of a band is used by the primary services or used by the secondary services, this portion of spectrum band should be considered as utilized. It is not surprising to see that the performance of the maximum expected reward based band selection is worst since it has no consideration about the risk and always makes the SSP swarm all the traffic on the most risky band from the PSPs for OSA. On the other hand, all the band-mix selection schemes support traffic splitting on a mix of bands to reduce the risk for OSA, so that they are superior to the maximum expected reward based one.

Among the band-mix selection schemes, we find that the expected X loss based band-mix selection outperforms the X loss based band-mix selection. The reason is that when the primary traffic has a fat-tailed distribution, the X loss based band-mix selection often underestimates the risk for OSA and causes the SSP more liable to be affected by the returning of the primary services; on the other hand, the expected X loss based band-mix selection makes much more accurate estimation for the potential risk for OSA and helps the SSP to take better use of the unoccupied spectrum bands from PSPs.

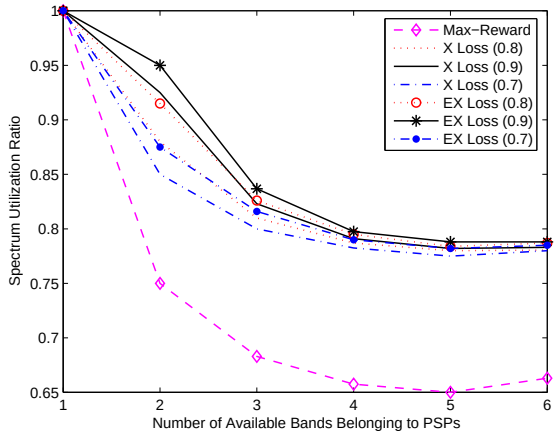

A Spectrum utilization ($\theta = -0.6$)

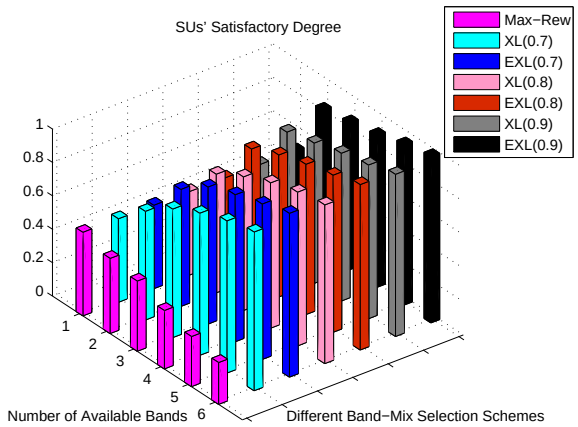

B SUs' satisfaction ($\theta = -0.6$)

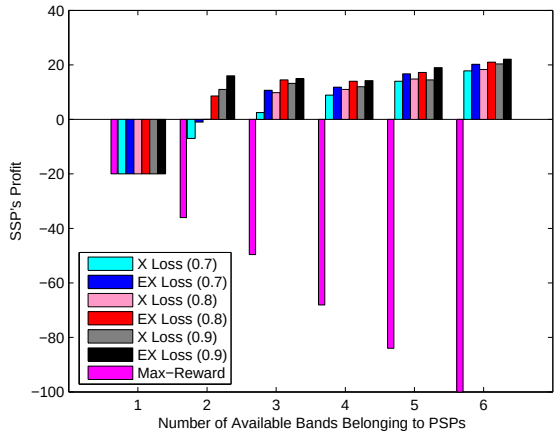

C The SSP's profit ($\theta = -0.6$)

Figure 2-4. Performance comparison of band-mix selection schemes with two risk metrics at different confidence levels ($\theta = -0.6$)

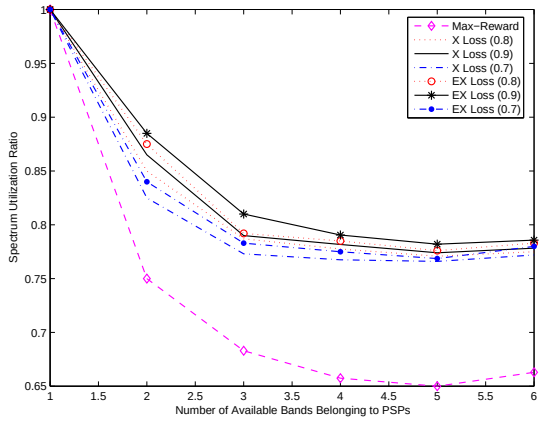

A Spectrum utilization ($\theta = -1.4$)

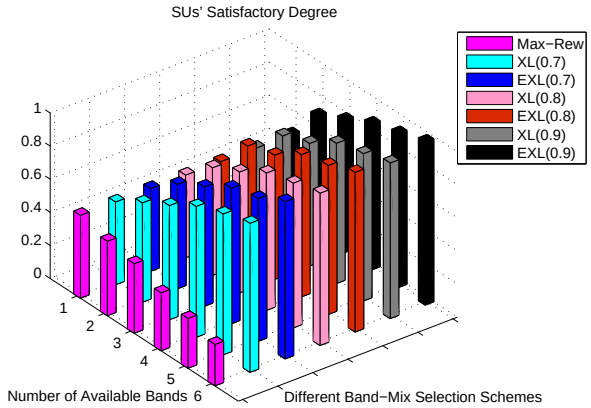

B SUs' satisfaction ($\theta = -1.4$)

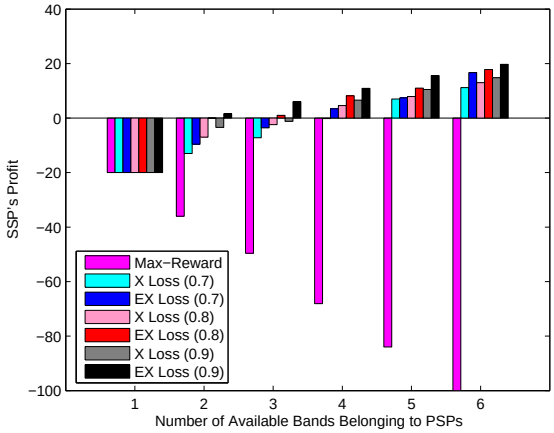

C The SSP's profit ($\theta = -1.4$)

Figure 2-5. Performance comparison of band-mix selection schemes with two risk metrics at different confidence levels ($\theta = -1.4$)

Besides, the spectrum utilization ratio of the band-mix selection with risk for OSA at higher confidence levels is generally better than that of the band-mix selection with risk for OSA at lower confidence levels. However, sometimes the difference is not so distinct, because if the confidence level is high, that band-mix selection scheme may be conservative for the estimation of risk for OSA, e.g., the spectrum utilization ratio of the band-mix selection with $\beta = 0.8$ and that of the band-mix selection with $\beta = 0.9$ are close as shown in Fig. 2-4A and Fig. 2-5A.

Similar analysis also applies to the SUs' satisfaction as well as the SSP's profit. SUs' satisfaction is defined to be the ratio of satisfied traffic demands to overall traffic demands of the SUs. Compared with band-mix based selection for OSA, the maximum expected reward based band selection is not good enough. With the increasing of the number of bands available from PSPs, its performance even degrades to some extent, since there emerge more risky bands when there are more bands for selection. The SUs' satisfactory degree of the X loss based band-mix selection is lower than that of the expected X loss based band-mix selection due to the distribution type of the primary services, especially when the spectrum supply from PSPs is limited for the traffic demands of secondary services as shown in Fig. 2-4B and Fig. 2-5B.

Fig. 2-4C and Fig. 2-5C describe the performance comparison of different band selection schemes in terms of the SSP's profit, which is defined as the difference between the SSP's reward and its payment for spectrum purchasing from the PSPs. If the SSP adopts the maximum expected reward based band selection, it always has negative profit for the traffic distributed on that band because of the unexpected returning of primary services. Although the SSP play the role of trading agent for SUs with the goal of satisfying as much demands of the SUs as possible rather than maximizing his profit as illustrated in Sec. 2.2.1, negative profit will discourage the SSP and reduce the SSP's incentive for trading spectrum with the PSPs. By contrast, as shown in Fig. 2-4C and Fig. 2-5C, the SSP's profit is generally better when the

SSP takes the band-mix selection schemes, among which the expected X loss based band-mix selection has the best performance in view of its accurate risk estimation for OSA.

2.7 Chapter Summary

Considering the uncertain spectrum supply from the PSPs, in this chapter, we first introduce an intuitive method, the X loss, to quantify the risk for SUs at a given confident level. Since the X loss theoretically underestimates the potential risk for OSA and mathematically lacks of subadditivity, we further propose the expected X loss, a more suitable risk measurement for OSA with desired properties. Based on the simplified expected X loss, we formulate the SSP's band-mix selection for traffic splitting into an optimization problem and solve it by linear programming. By numerical simulations, we show that compared with the X loss based band-mix selection for OSA, the expected X loss based selection not only provides much more accurate efficient OSA curves at different confidence levels, but also gives much better performance in terms of spectrum utilization, SUs' satisfaction and the SSP's profit, especially when the distribution of the primary services has a fat tail.

CHAPTER 3
SPECTRUM HARVESTING AND SHARING IN MULTI-HOP CRNS UNDER UNCERTAIN SPECTRUM SUPPLY

3.1 Chapter Overview

Recent years has witnessed the boosting growth of wireless networks and flourish of various wireless services. In parallel with that, current static spectrum allocation policy of Federal Communications Commission (FCC) [3, 20, 73] results in the exhaustion of available spectrum, while a lot of licensed spectrum bands are extremely under-utilized. Experimental tests in academia [9, 72] and measurements conducted in industries [70, 71] both show that many licensed spectrum blocks are not used in certain geographical areas and are idle most of the time. Even in the most crowded area near downtown Washington, DC, where both government and commercial spectrum use is intensive, only 38% of the licensed spectrum remains occupied and the rest of spectrum resource (a.k.a., "white space/spectrum hole") is wasted. These statistics and studies spur the FCC to open up licensed spectrum bands and pursue new innovative technologies to encourage dynamic use of the under-utilized spectrum [20].

As one of the most promising solutions, cognitive radio (CR) technology releases the spectrum from shackles of authorized licenses, and allows opportunistic usage of the vacant licensed spectrum bands in either temporal or spatial domain. Due to the potential of greatly improving the spectrum utilization, CR technology promotes numerous possible applications in various areas, e.g., military communications, public safety, disaster relief, search and rescue, environment monitoring, etc.

However, to opportunistically access to the licensed bands, CR devices have to be frequency-agile [73, 97]. It is imperative for the CR devices to have the capability of exploring licensed spectrum bands, reconfiguring RF, switching frequencies across a wide spectrum range (i.e., from 20 MHz to 2.5 GHz [14, 97, 110]), sending and receiving packets over non-contiguous spectrum bands, etc. Although some of the desired features may be realized in future, enormous amount of time and efforts must be

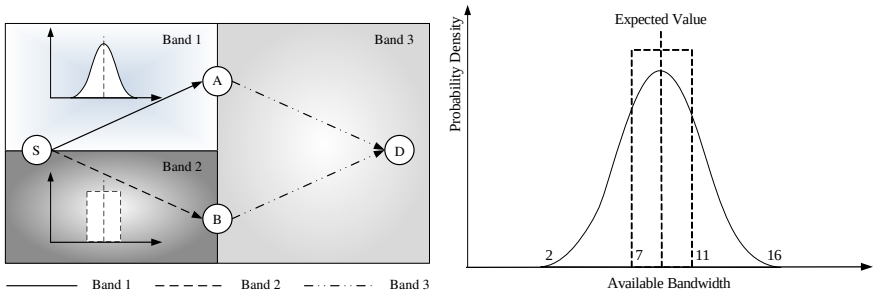

A Toy topology with one session.

B The probability density functions of available bandwidth for band 1 and band 2.

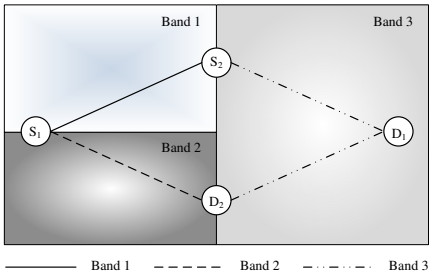

C Toy topology with two sessions.

Figure 3-1. Simple examples for CR sessions under uncertain spectrum supply in CRNs.

spent in hardware designs and signal processing in order to implement these features in light weight radios [73, 97, 110, 122]. In addition, to attract customers for any new technologies, there is no reason to enforce the users to replace their communication devices or to increase the complexity on the customers' side. For cognitive radio networks (CRNs), it is always a good idea to minimize the changes on the handsets of secondary users (SUs) while maximizing the spectral efficiency. Thus, it may be more viable to design a new architecture of networks to effectively harvest white space while minimizing the complexity of SUs.

Another key obstacle to the employment of multi-hop CRNs lies in the uncertain licensed spectrum supply [3, 19, 73]. Since the CR services must evacuate the licensed bands when primary services are active, the returning of primary services has significant impact on how to perform opportunistic spectrum accessing (OSA), scheduling and interference avoidance, and multi-hop multi-path routing in CRNs.

State-of-the-art work on investigating the unpredictable activities of primary services can generally be classified into two categories: i) spectrum sensing and ii) statistical analysis of the collected/historical spectrum vacancy/occupancy data.

In spite of the overwhelming waste of sensing time which can be used for more traffic delivery, individual sensing is trapped by sensing accuracy since both false alarm probability and missing detection probability are really high. To overcome the weakness of individual sensing, cooperative sensing is proposed to improve the sensing accuracy by grouping CR devices to sense together and share information among the group. But the trouble is that it is too difficult to synchronize the CR devices in the group sensing simultaneously. In addition, cooperative sensing has to set up a common channel for information exchange, which will incur enormous communication overhead. On the other hand, in [9, 70, 71], researchers as well as engineers try to identify the spectrum supply for OSA with the statistics of licensed spectrum utilization rather than attempting to detect the activities of primary services. They have carried out spectrum measurements, collected and analyzed the data about spectrum utilization, and summarized the statistical characteristics of the band vacancy/occupancy in details. These statistical results contain abundant information about the activities of primary services and provide a nice guide to the CR devices for OSA.

Resorting to the latter approach dealing with the unpredictable returning of primary services, in this chapter, we study the spectrum harvesting and sharing problem for multi-hop CRNs under uncertain spectrum supply. To effectively harvest and share the under-utilized licensed spectrum, we introduce a new emerging service provider, called *Secondary Service Provider* (SSP). Suppose that the SSP has its own bands (i.e., basic bands) and is able to collectively harvest the available licensed bands. In order to facilitate the accessing of SUs without CR capability, we assume the SSP has

already established some partial infrastructure with CR mesh routers[1] at low cost to provide coverage in the area of interest. Those CR mesh routers have CR capability and are equipped with multiple CR radios. SUs can cooperate with CR routers for packet delivery. Under the guidance of the SSP, SUs access their nearby CR mesh routers using basic bands and deliver packets via CR mesh routers using both basic bands and harvested bands. In such a CRN, more spectrum reuse opportunities can be created and the network capacity can be increased.

As for spectrum sharing, we focus on the joint frequency scheduling and routing problem among CR mesh routers in multi-hop CRNs. Suppose that CR mesh routers collect traffic from end users/SUs and form a set of CR sessions, each of which is characterized by a pair of source and destination CR routers and has a certain rate requirement. The SSP may ask an interesting question: how much bandwidth is at least required to maintain these CR sessions considering the availability of spectrum resources at a certain confidence level w.r.t. all the constraints from multiple layers in CRNs. To put it in another way, in this chapter, we are trying to address how the SSP performs OSA, frequency scheduling and multi-hop multi-path routing so that the required network-wide spectrum resource is minimized[2] , given the fact that the licensed spectrum supply cannot be guaranteed.

Inspired by the statistics of spectrum bands obtained on observation and experiments in [9][3] ,[70, 71], we novelly model the uncertain spectrum vacancy of a licensed band

[1] In the rest of this chapter, we use the words CR router/CR mesh router/router interchangeably.

[2] We follow the same objective as that in [42, 43], where the so-called space-bandwidth product defined in [68] is adopted as the performance metric in the setting of multi-hop CRNs.

[3] Chen et al. in [9] carried out a set of spectrum measurements in the 20MHz to 3GHz spectrum bands at 4 locations concurrently in Guangdong province of China. They used these data sets to conduct a set of detailed analysis about the statistics of the collected

(i.e., available bandwidth for OSA) as a random variable satisfying certain distribution. This modeling explicitly distinguishes the joint routing and frequency scheduling problem in CRNs from that in single-channel single-radio networks [10, 63, 64, 131] or multi-channel multi-radio networks [4, 18, 45, 53, 57, 61, 115]. The reason is that in those networks, the bandwidth is always regarded as a constant value. Even compared with prior work in the literature of multi-hop CRNs [23, 42, 43, 114], the unique feature of uncertain spectrum supply makes the route selection and scheduling in this chapter much more challenging as well.

For example, suppose there is a toy CRN consisting of 4 CR mesh routers and 3 bands available for OSA. The source CR router can choose either the route S-A-D or the route S-B-D to deliver traffic as shown in Fig. 3-1A. Moreover, assume the available bandwidth of Band 1 is normally distributed with $\mathcal{N}(9, 6)$, the available bandwidth of Band 2 is uniformly distributed with $\mathcal{U}(7, 11)$, and Band 3 is not the bottleneck for traffic delivery. An interesting question for the source CR router is which route is better. The answer is not straight-forward when the vacant bandwidth of Band 1 and that of Band 2 are represented by random variables. An intuitive solution is to evaluate the expected value of the available bandwidth, i.e., to measure which band can support larger flow rate or accommodate more flows on average[4] . In this case, consider the probability density functions (PDF) of bandwidth for the two bands, each random variable has an expected value of 9 as shown in Fig. 3-1B, which makes the first order statistics based route selection implausible. Furthermore, consider the toy topology with two sessions in Fig. 3-1C. Provided that all those licensed bands offer uncertain spectrum supply to CR

data, including channel occupancy/vacancy statistics, channel utilization, also spectral and spatial correlation of these measures.

[4] The available bandwidth for OSA can directly be interpreted into link capacity using Shannon-Hartley theorem as illustrated in Sec. 5.3.3.2.

routers, we must identify how to calculate the sum of random variable for the scheduling and routing, which makes this problem in CRNs even more complex.

Although we have devoted some efforts to analyzing this problem in [88], there is a lack of a solid system architecture to support our theoretical study. Meanwhile, requirements of CR capability are imposed on SUs' handsets, since there is no cooperation between SUs and CR routers for packet delivery.

Within the proposed architecture of CRNs, we exploit a pair of (α, β) parameters to characterize the SSP's concerns about the CRNs and mathematically formulate the joint frequency scheduling and routing problem. Specifically, α denotes the targeted confidence level for the availability of the required network-wide spectrum resource, and β denotes the targeted quality of CR communications. Besides, we demonstrate constraints from multiple layers under the situation that spectrum supply is uncertain. In particular, we pay special attention to modeling the unpredictable activities of primary services, scheduling and interference models, and multi-path routing constraints. We also dwell on how to integrate the bandwidth of different bands and calculate the sum of link capacity, when the vacant bandwidth of every licensed band is a random variable. We formulate an optimization problem with the objective of minimizing the required network-wide spectrum resource at an (α, β) level.

For a fixed pair of (α, β), the formulated optimization problem falls into a mixed integer non-linear programming and is proved to be NP-hard [29]. Aiming to derive a feasible solution, we present a sub-optimal algorithm for the NP-hard optimization. We first find a lower bound for the objective by relaxing the integer variables in scheduling and interference constraints. Then, we propose a coarse-grained fixing algorithm to iteratively determine binary integer variables exploiting a threshold, where the bandwidth integration and the sum of link capacity from different bands are computed using discrete Fourier transform (DFT) and inverse discrete Fourier transform (IDFT). As long as fixing all the integer variables, we can determine flow routing variables and solve the

optimization problem. Since the solutions attained by the coarse-grained fixing algorithm is an upper bound for the optimization objective, we compare it with the lower bound we have developed earlier. Simulation results show that (i) the proposed coarse-grained fixing algorithm is near-optimal for any (α, β) level; (ii) compared with the expected bandwidth based solution, the (α, β) based one has better performance in the sense that it lowers down the blocking ratio of CR sessions and improves the spectrum utilization.

The rest of this chapter is organized as follows. In Section 6.3, we propose a novel architecture for spectrum harvesting and sharing, introduce the model of spectrum uncertainty and present other related models in CRNs. In Section 3.3, we mathematically describe scheduling and interference constraints and multi-hop multi-path routing in CRNs. In Section 3.4, We illustrate the bandwidth integration, define bandwidth required at α, and formulate joint routing and scheduling as an NP-hard optimization problem. Besides, we find a lower bound for this optimization problem. In Section 3.5, we develop a coarse-grained algorithm for a sub-optimal solution. Finally, we conduct simulations and analyze the performance results in Section 6.7, and draw concluding remarks in Section 6.8.

3.2 Network Model

3.2.1 Spectrum Harvesting and Opportunistic Spectrum Accessing

We consider a novel multi-hop CRN consisting of the SSP, a group of SUs, $\mathcal{N} = \{1, 2, \cdots, n, \cdots, N\}$ CR mesh routers and a set of available licensed spectrum bands[5] with unequal size of bandwidths as shown in Fig. 5-1A. The SSP is an independent wireless service provider with its own spectrum, i.e., the SSP's basic bands (potentially congested already), and is able to collectively harvest the available licensed

[5] Taking the least-utilized spectrum bands introduced in [43] [19] for example, we found that the bandwidth between [1240, 1300] MHz (allocated to amateur radio) is 60 MHz, while bandwidth between [1525, 1710] MHz (allocated to mobile satellites, GPS systems, and meteorological applications) is 185 MHz.

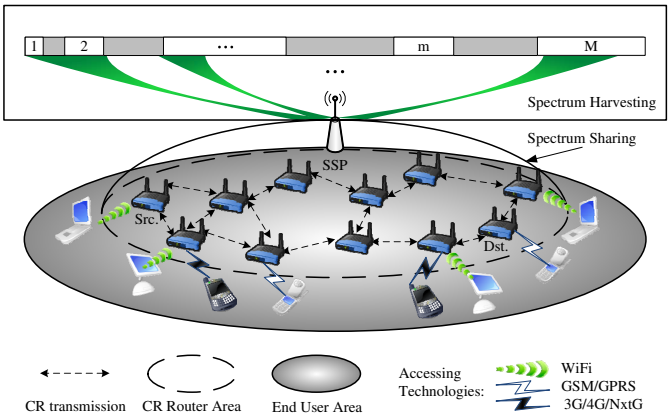

Figure 3-2. A novel architecture for spectrum harvesting and sharing under uncertain spectrum supply in multi-hop CRNs.

bands. The SSP has also deployed some CR mesh routers at low cost to facilitate the accessing of SUs. SUs are just end-users not subscribed to primary services. No specific requirements are imposed on the SUs' communication devices. They could be any devices using any accessing technologies (e.g. laptops or desktop computers using Wi-Fi, cell phones using GSM/GPRS, smart phones using 3G/4G/NxtG accessing technology, etc.). SUs can access to the basic bands owned by the SSP, but they cannot be tuned to the harvested licensed frequency. The CR mesh routers deployed by the SSP have CR capability and are equipped with multiple CR radios.

Under the guidance of the SSP, SUs and CR mesh routers cooperate with each other for packet delivery. Specifically, the mobile SUs report their online traffic requests to their nearby CR mesh routers via basic bands. The fixed CR mesh routers collect traffic demands from different end-users, form uni-cast CR communication sessions, and deliver packets using both the leftover basic bands and harvested bands. For better network capacity, reuse of the SSP's basic spectrum and sharing of the harvested spectrum, the SSP coordinates those CR mesh routers and jointly conducts frequency scheduling and flow routing among them as shown in Fig. 5-1A.

Suppose there are a set of $\mathcal{L}$ uni-cast communication sessions among these CR mesh routers. Let $s(l)/d(l)$ denote the source/destination CR router of session

$l \in \mathcal{L}$, and $r(l)$ be the rate requirement of session l. Assume the SUs' usage of basic bands in the multi-hop CRNs is a *priori* information. The CR routers are able to use the rest of basic spectrum owned by the SSP. The CR routers are also allowed to communicate with each other by opportunistically accessing to the licensed bands when the primary services are not active, but they must evacuate from these bands immediately when primary services become active. Considering the geographical location of the CR routers, the available spectrum bands at one CR router may be different from another one in the network. To put it in a mathematical way, let $\mathcal{M} = \{1, 2, \cdots, m \cdots, M\}$ be the band set including the available basic bands and licensed bands for CR communications, and $\mathcal{M}_i \subseteq \mathcal{M}$ represent the set of available bands at CR mesh router $i \in \mathcal{N}$. $\mathcal{M}_i$ may be different from $\mathcal{M}_j$, where j is not equal to i, and $j \in \mathcal{N}$, i.e., possibly $\mathcal{M}_i \neq \mathcal{M}_j$.

3.2.2 Modeling of Uncertain Spectrum Supply

The unique feature of CRNs is the uncertain spectrum supply from licensed bands, or say, the unpredictable bandwidth occupancy of primary services. To model this key feature of CRNs, we make W^m denote the unoccupied bandwidth of the available band $m \in \mathcal{M}$, where W^m is a random variable considering the unpredictable activities of primary services. Note that for an available basic band, the unoccupied bandwidth is a constant and the transmissions of CR routers over this band are not affected by primary services because the basic band belongs to the SSP. However, in probability theory, a constant can be regarded as a special random variable that takes a constant value, regardless of any event that occurs [22, 89]. Therefore, the modeling of W^m as a random variable is applicable not only to the available licensed bands but also to the available basic bands for CR communications.

Generally speaking, people [85, 111] would like to use $\boldsymbol{E}(W^m)$, the first order statistics of W^m [9] to predict the white space as shown in Fig. 6-2. Although this measurement is intuitive and easy to quantify, it ignores so much significant information

w.r.t. the activities of primary services that it may lead to the failure of traffic delivery between CR routers as depicted in the zoomed-in picture of Fig. 6-2. It should be noted that the statistical characteristics of W^m contain abundant knowledge about the available bandwidth of band m for CR routers' opportunistic accessing. For example, assume W^m is normally distributed with $\boldsymbol{E}(W^m) = 2$ and $\sigma_{W^m} = 1$, i.e., $W^m \sim \mathcal{N}(2, 1^2)$. Then, the probability that $W^m \leq 3$ is equal to 84.1%.

3.2.3 Other Related Models

3.2.3.1 Transmission Range and Interference Range

Suppose all CR mesh routers use the same power for transmission, and the power spectral density from the transmitter is Q. A widely used model [23, 33, 43] for power propagation gain is

$$g_{ij} = \gamma \cdot d_{ij}^{-n}, \tag{3–1}$$

where n is the path loss factor, γ is an antenna related constant, and d_{ij} is the distance between CR routers i and j. We assume that the data transmission is successful only if the received power spectral density at the receiver exceeds a threshold Q_T. Meanwhile, we assume interference becomes non-negligible only if it produces a power spectral density over a threshold of Q_I at the receiver. Thus, the transmission range for a CR router is $R_T = (Q/Q_T)^{1/n}$, which comes from $(R_T)^{-n} \cdot Q = Q_T$. Similarly, based on the interference threshold $Q_I (Q_I < Q_T)$, the interference range for a CR router is $R_I = (Q/Q_I)^{1/n}$. It is obvious that $R_I > R_T$ since $Q_I < Q_T$.

3.2.3.2 Link Capacity

According to Shannon-Hartley theorem, if CR router i sends data to CR router j on link (i, j) with band m, the capacity of link (i, j) with band m is

$$c_{ij}^m = W^m \log_2 \left(1 + \frac{g_{ij} Q}{\eta}\right), \tag{3–2}$$

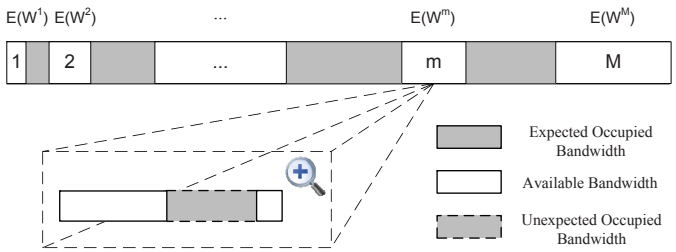

Figure 3-3. A schematic illustrating available bandwidth for OSA and unpredictable occupation of primary services in CRNs.

where η is the ambient Gaussian noise density. As we know, to mathematically model the link capacity is imperative in the sense that the aggregate flow rates on each radio link can never exceed this link's capacity, which is an important constraint for routing. Different from modeling of link capacity in the other wireless networks [64, 111] or in existing literature [43, 108], we are also aware that c_{ij}^m is not a fixed number but a random variable since the available bandwidth W^m is uncertain in CRNs. Besides, note that the denominator inside the log function contains only η. This is because of one of our interference constraints, i.e., when CR router i is transmitting to CR router j on band m, then all the other neighbors of router j within its interference range are prohibited from using this band. We will address the interference constraints in details in the following section.

3.3 Frequency Scheduling and Routing Constraints for Opportunistic Accessing

3.3.1 Scheduling and Interference Constraints

Scheduling can be conducted in time domain, in frequency domain, or in both of them. In this chapter, we only focus on frequency based band assignment, i.e., how to assign bands at a CR mesh router for transmission and reception. A plausible scheduling on frequency bands must consider the limitations at the transmitter side and guarantee no interference at the receiver side.

Assume band m is available at both router i and router j, i.e., $m \in \mathcal{M}_i \bigcap \mathcal{M}_j$. We denote

$$s_{ij}^m = \begin{cases} 1 & \text{If router } i \text{ transmits data to router } j \text{ on} \\ & \text{band } m, \\ 0 & \text{otherwise.} \end{cases} \tag{3–3}$$

For a router $i \in \mathcal{N}$ and a band $m \in \mathcal{M}_i$, denote $\mathcal{T}_i^m$ the set of CR routers that can also opportunistically access to band m and are within the transmission range to router i, i.e.,

$$\mathcal{T}_i^m = \{j : d_{ij} \leq R_T, j \neq i, m \in \mathcal{M}_j\}. \tag{3–4}$$

From the view of the transmitter, CR router i is not able to transmit to multiple routers on the same frequency band. Thus, we have

$$\sum_{q \in \mathcal{T}_i^m} s_{iq}^m \leq 1. \tag{3–5}$$

From the view of the receiver, a CR router cannot use the same frequency band for transmission and reception[6] , due to "self-interference" at the physical layer. That is, if $s_{ij}^m = 1$, then for any $q \in \mathcal{T}_j^m$, s_{jq}^m must be 0, i.e.,

$$s_{ij}^m + \sum_{q \in \mathcal{T}_j^m} s_{jq}^m \leq 1. \tag{3–6}$$

Note that in (3–6), we are referring to a specific router j to which router i is transmitting. If $s_{ij}^m = 1$, then $\sum_{q \in \mathcal{T}_j^m} s_{jq}^m = 0$, i.e., CR router j is not able to use the same frequency band m for transmission. On the other hand, if $s_{ij}^m = 0$, then $\sum_{q \in \mathcal{T}_j^m} s_{jq}^m \leq 1$, i.e., router

[6] This limitation applies to both the transmitter and receiver. The reason to categorize it into the constraints of the receiver is for the ease of writing in the rest of this chapter. Also, as for this constraint, the roles of transmitter and receiver are symmetric and interchangeable.

j may use band m for transmission, but can only use it for one receiving router $q \in \mathcal{T}_j^m$, which is the same as in (3–5).

Beyond the constraints above at the receiver, there are also interference constraints from the other CR routers in CRNs. To be specific, for a frequency band m, if CR router i uses this band for transmitting data to a CR router $j \in \mathcal{T}_i^m$, then any other routers that may produce interference on CR router j should not use this band[7] . To model this constraint, we let $\mathcal{P}_j^m$ represent the set of routers that can produce interference at CR router j on band m, i.e.,

$$\mathcal{P}_j^m = \{p : d_{pj} \leq R_I, p \neq j, \mathcal{T}_p^m \neq \emptyset\}. \tag{3–7}$$

The physical interpretation of $\mathcal{T}_p^m \neq \emptyset$ in the above formula is that CR router p may use band m for a valid transmission to a CR router in $\mathcal{T}_p^m$ and then may cause interference to router j. Based on the definition of $\mathcal{P}_j^m$, we have

$$s_{ij}^m + \sum_{q \in \mathcal{T}_p^m} s_{pq}^m \leq 1 \quad (p \in \mathcal{P}_j^m, p \neq i). \tag{3–8}$$

In (3–8), if $s_{ij}^m = 1$, i.e., router i uses band m to transmit to router j, then any CR router p that may interfere with CR router j should not transmit on this band, i.e., $\sum_{q \in \mathcal{T}_p^m} s_{pq}^m = 0$. Likewise, if $s_{ij}^m = 0$, (3–8) reduces into (3–5), i.e., router p may transmit on band m to one router $q \in \mathcal{T}_p^m$, i.e., $\sum_{q \in \mathcal{T}_p^m} s_{pq}^m \leq 1$.

Now, we integrate the constraints in (3–6) and (3–8) into a general constraint at the receiver side. We define

$$\mathcal{I}_j^m = \{p : d_{pj} \leq R_I, \mathcal{T}_p^m \neq \emptyset\}, \tag{3–9}$$

[7] "Hidden terminal" problem is a special case under this constraint.

which is equivalent to

$$\mathcal{I}_j^m = \begin{cases} \mathcal{P}_j^m \bigcup \{j\} & \text{If } \mathcal{T}_j^m \neq \emptyset, \\ \mathcal{P}_j^m & \text{otherwise.} \end{cases} \tag{3–10}$$

In this way, both (3–6) and (3–8) can be described by the following generalized constraint.

$$s_{ij}^m + \sum_{q \in \mathcal{T}_p^m} s_{pq}^m \leq 1 \quad (p \in \mathcal{I}_j^m, p \neq i) \tag{3–11}$$

3.3.2 Routing Constraints

As for routing, a source CR router may employ a number of relay CR routers to forward data packets toward its destination CR router. Obviously, there should be more than one path involved in data delivery since multi-path routing[8] is more flexible to route the traffic from a source router to its destination. Following the routing model in [43, 108], we mathematically present the constraints at network layer as follows.

Let $f_{ij}(l)$ denote the data rate on link (i, j) that is attributed to session l, where $i \in \mathcal{N}$, $j \in \bigcup_{m \in \mathcal{M}_i} \mathcal{T}_i^m$, and $l \in \mathcal{L}$. To simplify the notation, let $\mathcal{T}_i = \bigcup_{m \in \mathcal{M}_i} \mathcal{T}_i^m$.

If CR router i is the source router of session l, i.e., $i = s(l)$, then

$$\sum_{j \in \mathcal{T}_i} f_{ij}(l) = r(l). \tag{3–12}$$

If CR router i is an intermediate relay router for session l, i.e., $i \neq s(l)$ and $i \neq d(l)$, then

$$\sum_{j \in \mathcal{T}_i}^{j \neq s(l)} f_{ij}(l) = \sum_{p \in \mathcal{T}_i}^{p \neq d(l)} f_{pi}(l). \tag{3–13}$$

[8] The multiple radios of CR routers allow for multi-path routing.

If CR router i is the destination router of session l, i.e., $i = d(l)$, then

$$\sum_{p \in \mathcal{T}_i} f_{pi}(l) = r(l). \tag{3–14}$$

If (6–12) and (6–14) are satisfied, it can be easily verified that (6–15) must be satisfied. As a result, it is sufficient to list only (6–12) and (6–14) as routing constraints in the problem formulation.

In addition to the above flow balance equations at each router i for each session l, the aggregate flow rates on each radio link cannot exceed this link's capacity, which is defined in (5–2). Taking interference constraints into consideration, the calculation of the link capacity c_{ij}^m can be further simplified. When $s_{ij}^m = 0$, we have $c_{ij}^m = 0$. Thus, c_{ij}^m should be written as

$$c_{ij}^m = s_{ij}^m \cdot W^m \log_2 \left(1 + \frac{g_{ij} Q}{\eta}\right). \tag{3–15}$$

Therefore, for the requirement that the aggregate data rates on each link (i, j) cannot exceed the link's capacity, we obtain

$$\begin{aligned} \sum_{l \in \mathcal{L}}^{s(l) \neq j, d(l) \neq i} f_{ij}(l) &\leq \sum_{m \in \mathcal{M}_i \bigcap \mathcal{M}_j} c_{ij}^m \\ &= \sum_{m \in \mathcal{M}_i \bigcap \mathcal{M}_j} s_{ij}^m \cdot W^m \log_2 \left(1 + \frac{g_{ij} Q}{\eta}\right). \end{aligned} \tag{3–16}$$

3.4 Problem Formulation and a Lower Bound for the Cross-layer Optimization

The essential objective of CRNs is to avoid the waste of "white space" and to improve the spectrum utilization. To put it in another word, for the given amount of radio resource, we try to use it to support as many CR routers' sessions as possible; correspondingly, for the given number of CR routers' sessions, we try to use as little radio resource as possible to support them. In this chapter, we measure the radio resource in terms of the total bandwidth required by the SSP to support a set of

CR sessions, which is the simplified form of the so called space-bandwidth product proposed in [68] with fixed transmission power.

As introduced in Sec. 6.3, there is a set of source and destination pairs (CR routers' sessions) in the network, each with a certain rate requirement. Each CR router is entitled to opportunistically access to a set of spectrum bands with uncertain supply for communications. We seek for a feasible solution to assigning the available frequency bands to each router, scheduling bands for transmission and reception, and routing the flows so that the total radio bandwidth required in the multi-hop CRNs is minimized.

Intuitively, the optimization problem can be formulated as follows [42, 43].

$$\textbf{Min} \qquad \sum_{i\in\mathcal{N}}\sum_{m\in\mathcal{M}_i}\sum_{j\in\mathcal{T}_i^m} W^m s_{ij}^m \tag{3–17}$$

$$\begin{aligned}
\textbf{s.t.} \qquad & \sum_{q\in\mathcal{T}_i^m} s_{iq}^m \le 1 \quad (i\in\mathcal{N}, m\in\mathcal{M}_i) \\
& s_{ij}^m + \sum_{q\in\mathcal{T}_p^m} s_{pq}^m \le 1 \; (i\in\mathcal{N}, m\in\mathcal{M}_i, j\in\mathcal{T}_i^m, p\in\mathcal{I}_j^m, p\neq i) \\
& \sum_{l\in\mathcal{L}}^{s(l)\neq j, d(l)\neq i} f_{ij}(l) - \sum_{m\in\mathcal{M}_i\bigcap\mathcal{M}_j} W^m \log_2\left(1+\frac{g_{ij}Q}{\eta}\right) s_{ij}^m \;\le\; 0 \\
& \qquad\qquad\qquad\qquad\qquad\qquad\qquad\qquad (i\in\mathcal{N}, j\in\mathcal{T}_i) \\
& \sum_{j\in\mathcal{T}_i} f_{ij}(l) = r(l) \qquad\qquad\qquad\qquad (l\in\mathcal{L}, i=s(l)) \\
& \sum_{j\in\mathcal{T}_i}^{j\neq s(l)} f_{ij}(l) - \sum_{p\in\mathcal{T}_i}^{p\neq d(l)} f_{pi}(l) = 0 \quad (l\in\mathcal{L}, i\in\mathcal{N}, i\neq s(l), d(l)) \\
& s_{ij}^m = 0 \text{ or } 1, f_{ij}(l)\ge 0 \; (l\in\mathcal{L}, i\in\mathcal{N}, i\neq d(l), j\in\mathcal{T}_i, j\neq s(l)),
\end{aligned} \tag{3–18}$$

where s_{ij}^m and $f_{ij}(l)$ are optimization variables, and g_{ij}, Q, η and $r(l)$ are all constants.

Note that due to the unpredictable returning of primary services, W^m is not modeled as a constant but modeled as a random variable in CRNs as illustrated in Sec. 3.2.3. This feature makes the spectrum resource minimization problem in this chapter

far different from that with guaranteed spectrum supply in existing works [43, 108]. Therefore, two critical issues need to be addressed in the intuitive formulation above.

First, bandwidth integration in (3–17) and (3–18) is the sum of a series of random variables in CRNs rather than the sum of a series of deterministic quantities in other kinds of wireless networks.

Second, with different choices of s_{ij}^m and $f_{ij}(l)$, we have difficulty in comparing results of the optimization, i.e., $\sum_{i\in\mathcal{N}}\sum_{m\in\mathcal{M}_i}\sum_{j\in\mathcal{T}_i^m} W^m s_{ij}^m$, because they are random variables with different kinds of distribution.

3.4.1 Problem Formulation

3.4.1.1 Bandwidth integration

We take a simple example to illustrate how to integrate the bandwidth of different bands. We let $W^c = W^a + W^b$, where W^a and W^b are independent[9] , and bands $a, b \in \mathcal{M}$. Furthermore, we assume the probability density function (PDF) and cumulative distribution function (CDF) of W^a and W^b are $h_{W^a}(w^a)$, $h_{W^b}(w^b)$, $H_{W^a}(w^a)$ and $H_{W^b}(w^b)$, respectively. Then, the CDF and PDF of W^c are derived as follows.

$$\begin{aligned} H_{W^c}(w^c) &= \Pr(W^c \le w^c) \\ &= \Pr(W^a + W^b \le w^c) \\ &= \int_{-\infty}^{\infty}\int_{-\infty}^{w^c - w^a} h_{W^a,W^b}(w^a, w^b)\,dw^b dw^a. \end{aligned} \tag{3–19}$$

Given W^a and W^b are independent, we further calculate

$$\begin{aligned} H_{W^c}(w^c) &= \int_{-\infty}^{\infty}\int_{-\infty}^{w^c - w^a} h_{W^a}(w^a) h_{W^b}(w^b)\,dw^b dw^a \\ &= \int_{-\infty}^{\infty} h_{W^a}(w^a) H_{W^b}\big(w^c - w^a\big)\,dw^a. \end{aligned} \tag{3–20}$$

[9] This assumption is held for any two bands in CRNs for the whole chapter.

Moreover, the probability density of W^c is expressed as

$$\begin{aligned} h_{W^c}(w^c) &= \int_{-\infty}^{\infty} h_{W^a}(w^a) \frac{\partial H_{W^b}(w^c - w^a)}{\partial w^c} dw^a \\ &= \int_{-\infty}^{\infty} h_{W^a}(w^a) h_{W^b}(w^c - w^a) dw^a. \end{aligned} \tag{3–21}$$

Thus, $h_{W^c}(w^c)$ is the convolution of $h_{W^a}(w^a)$ and $h_{W^b}(w^b)$ [89]. It can be written as

$$h_{W^c}(w^c) = h_{W^a}(w^a) * h_{W^b}(w^b) = \bigotimes_{m \in \{a,b\}} h_{W^m}(w^m), \tag{3–22}$$

where $\bigotimes$ denotes the operator for the convolution of a sequence, which is analogy to the use of $\prod$ as the product operator or $\sum$ as the summation symbol. From the calculation of $h_{W^c}(w^c)$, we find that the sum of two independent random variables is associative and commutative. Using the same approach as in (3–19), (3–20) and (3–21), this property can easily be extended to the sum of a finite number of random variables. For example, for the bandwidth integration of link (i, j), the PDF of $W = \sum_{m \in \mathcal{M}_i \bigcap \mathcal{M}_j} W^m s_{ij}^m$ is

$$h_W(w) = \bigotimes_{m \in \mathcal{M}_i \bigcap \mathcal{M}_j} h_{W^m}(w^m) s_{ij}^m. \tag{3–23}$$

3.4.1.2 Bandwidth required at α

Before we re-formulate the problem, we must quantify the bandwidth required for OSA when the vacancy of the licensed band is uncertain and modeled as a random variable. Thus, we leverage parameter α to define bandwidth required at α for OSA. Inspired by the mathematical expression of value at risk (VaR) in [39], we use $X_\alpha(w)$ to denote bandwidth required at α and define it as follows.

$$\begin{cases} H_W(\tau) = \int_{-\infty}^{\tau} h_W(w) dw, & \tau \in \mathcal{R} \\ X_\alpha(W) = \inf\{\tau : H_W(\tau) \geq \alpha\}, & \alpha \in [0, 1]. \end{cases} \tag{3–24}$$

From (5–7), we find that the available bandwidth of the bandwidth integration for OSA is less than $X_\alpha(W)$ at confidence level α as shown in Fig. 3-4A.

3.4.1.3 Formal formulation

Based on the description of bandwidth integration and definition of bandwidth required at α, the optimization problem can be reformulated as follows.

$$\textbf{Min} \quad X_\alpha\Big(\sum_{i\in\mathcal{N}}\sum_{m\in\mathcal{M}_i}\sum_{j\in\mathcal{T}_i^m} W^m s_{ij}^m\Big)$$

$$\textbf{s.t.} \quad \sum_{q\in\mathcal{T}_i^m} s_{iq}^m \le 1 \quad (i\in\mathcal{N}, m\in\mathcal{M}_i) \tag{3–25}$$

$$s_{ij}^m + \sum_{q\in\mathcal{T}_p^m} s_{pq}^m \le 1 \quad (i\in\mathcal{N}, m\in\mathcal{M}_i, j\in\mathcal{T}_i^m, p\in\mathcal{I}_j^m, p\neq i) \tag{3–26}$$

$$\Pr\Big(\sum_{l\in\mathcal{L}}^{s(l)\neq j, d(l)\neq i} f_{ij}(l) \le \sum_{m\in\mathcal{M}_i\bigcap\mathcal{M}_j} W^m \log_2\Big(1+\frac{g_{ij}Q}{\eta}\Big)s_{ij}^m\Big) \ge \beta \quad (i\in\mathcal{N}, j\in\mathcal{T}_i) \tag{3–27}$$

$$\sum_{j\in\mathcal{T}_i} f_{ij}(l) = r(l) \quad (l\in\mathcal{L}, i=s(l))$$

$$\sum_{j\in\mathcal{T}_i}^{j\neq s(l)} f_{ij}(l) - \sum_{p\in\mathcal{T}_i}^{p\neq d(l)} f_{pi}(l) = 0 \quad (l\in\mathcal{L}, i\in\mathcal{N}, i\neq s(l), d(l))$$

$$s_{ij}^m = 0 \text{ or } 1,\ f_{ij}(l)\ge 0\ (l\in\mathcal{L}, i\in\mathcal{N}, i\neq d(l), j\in\mathcal{T}_i, j\neq s(l)).$$

Compared with the intuitive formulation, the reformulated problem mathematically solves the sum of random variables by using bandwidth integration and incorporates the other parameter β to represent the SSP's requirements about quality of CR communications as presented in (3–27).

In addition, the objective of the optimization is clarified, i.e., to minimize bandwidth required at α to support the CR sessions with rate requirements, when joint scheduling and routing constraints are satisfied. Take W and $W^{''}$ in Fig. 3-4B for example, assume they are both integrated bandwidths which satisfy all the constraints listed above. We

can choose either W or $W^{''}$ for OSA. We compare $X_{0.9}(W)$ and $X_{0.9}(W^{''})$ as shown in Fig. 3-4B, and decide to use W for OSA. The reason is that if we choose W, the available bandwidth of bandwidth integration is less than $X_{0.9}(W)$=9 at confidence level of 90%; but if we choose $W^{''}$, the available bandwidth of bandwidth integration is less than $X_{0.9}(W^{''})$=90 at confidence level of 90%. At an (α, β) level, the smaller $X_{\alpha}(W)$ is, the less spectrum required to maintain the set of CR sessions. The less spectrum required, the less CR sessions are affected by the activities of primary services.

Nevertheless, the above optimization problem itself is a mixed-integer nonlinear programming problem, which is proved to be NP-hard [29].

3.4.2 The Lower Bound for the Cross-layer Optimization

For an arbitrary pair of (α, β), the complexity of the problem formulated in Sec. 3.4.1 arises from the binary s_{ij}^{m} variables. To reduce the complexity and pursue a lower bound for the cross-layer optimization, we relax the binary requirement on s_{ij}^{m} and replace it with $0 \leq s_{ij}^{m} \leq 1$. Due to the enlarged optimization space (caused by relaxation on s_{ij}^{m}), the solution to this relaxed optimization problem yields a lower bound for the minimization of bandwidth required at α problem in Sec. 3.4.1. Although the lower bound may not be achieved by a feasible solution, it offers a benchmark to measure the quality of feasible solutions.

3.5 A Fast Fixing Algorithm for Sub-optimal Solutions Using DFT-IDFT

Whereas we have the lower bound as the benchmark, we still seek for an effective and efficient solution to the proposed problem since the s_{ij}^{m} variables are binary values rather than real numbers within 0 and 1. Given the values of the (α, β) pair, in this section, we first investigate how to reduce the complexity of computing the PDF convolution involved in the bandwidth integration. Then, with the knowledge of bandwidth integration computation, we present a coarse-grained fixing procedure to produce a feasible solution to the cross-layer optimization problem [42, 43].

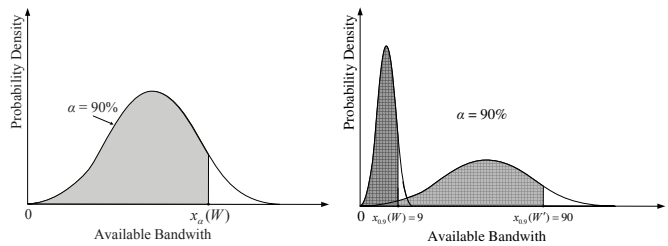

A The geometrical illustration of $X_\alpha(w)$.

B The geometrical illustration of optimization objective.

Figure 3-4. Bandwidth required at α and optimization objective.

3.5.1 Fast Computation of the Bandwidth Integration

Following the typical way to efficiently calculate the linear convolution in [78], we implement the PDF convolution of bandwidth integration in Sec. 3.4.1 in four steps.

Briefly speaking, we firstly convert the continuous PDF of W^m into a discrete sequence by periodic sampling. Then, we zero-pad all the sequences, and compute the DFT of each sequence using the fast Fourier transform (FFT) algorithm (e.g., Cooley-Tukey algorithm). After that, we point-by-point multiply the DFTs of all the sequences, where the product represents the DFT of the PDF convolution of W^m. Finally, we compute the IDFT of the product, and convert the discrete result into continuous one to reconstruct the PDF convolution of the bandwidth integration.

3.5.2 The Coarse-grained Fixing Procedure

Now, the left problem is how to determine the s_{ij}^m variables and fix flow routing in the problem formulation in Sec. 3.4.1. The key to simplifying the NP-hard optimization, fixing $f_{ij}(l)$-variables, and attaining an effective solution is the determination of the binary values for the s_{ij}^m variables [42, 43].

To determine the values of all the s_{ij}^m-variables, we iteratively solve a sequence of relaxed optimization problems. Considering interference constraints, in each iteration, we can fix at least one binary value for some s_{ij}^m. Specifically, for the first iteration, we relax all binary variables s_{ij}^m to $0 \leq s_{ij}^m \leq 1$ as in Sec. 3.4.2 to obtain a new optimization

problem. We integrate the bandwidth with the PDF convolution and solve this new problem, so that we have a solution with each s_{ij}^m being a value between 0 and 1. Then, we select the s_{ij}^m with the largest value among all the s_{ij}^m-values, and set this particular s_{ij}^m to be 1. In parallel with this fixing, by (3–25), we should set $s_{iq}^m = 0$ for $(q \in \mathcal{T}_i^m, q \neq j)$. Meanwhile, by (3–26), we should set s_{pq}^m to 0 for $(p \in \mathcal{I}_j^m, p \neq i, q \in \mathcal{T}_p^m)$. In particular, if the result includes more than one s_{ij}^m-variables with the value of 1, we can set those s_{ij}^m-variables to 1 and perform an additional fixing for the largest fractional variable in the current iteration as illustrated above.

Having fixed some s_{ij}^m-variables in the first iteration, we remove all the terms associated with those already fixed s_{ij}^m-variables, eliminate the related constraints in (3–25) and (3–26), and update the problem to a new one for the second iteration. In the second iteration, we solve the new optimization and then determine the values of some other unfixed s_{ij}^m-variables based on the same process[10] . The iteration continues until we fix all s_{ij}^m-variables to be either 0 and 1. The overall grained fixing procedure is summarized in Alg. 1.

Considering the number of bands with different frequencies and the spatial reuse in multi-hop CRNs, we may further reduce the complexity of the algorithm and speed up the procedure by fixing more s_{ij}^m-variables in a coarse-grained manner during each iteration. Firstly, the transmission in one band has no interference impact on the transmission in any other bands with different frequencies. Thus, for a link (i, j), we may fix multiple bands within a single iteration in the coarse-grained fixing algorithm. Then, from the view of spatial reuse, a band can be used by the links far apart from one another (i.e., beyond the interference range of the routers in communications with a link).

[10] Provided that some s_{ij}^m-variables are fixed in the first iteration, the computation complexity in the second iteration is lower than that in the first iteration because we only need to deal with the remaining un-fixed s_{ij}^m-variables

Thus, for a band m, we may fix multiple links that have no mutual interference within a single iteration in the coarse-grained fixing algorithm.

To be specific, we employ a threshold $\theta > 0.5$ in the coarse-grained fixing process and fix all the s_{ij}^m-variables exceeding θ to 1 in a single iteration. To make sure that the constraints in (3–25) and (3–26) are held in the relaxed problem, we find that at most one variable s_{ij}^m is allowed to be larger than θ in the local area in CRNs. Therefore, $\theta > 0.5$ is suitable for determining the binary values of s_{ij}^m-values. In the case that none of the s_{ij}^m-variables exceed θ, we will resort to the procedure listed in Alg. 1 for the current iteration and set the largest valued s_{ij}^m-variable to 1.

Different from the lower bound obtained in Sec. 3.4.2, the proposed fast algorithm yields an upper bound to the problem formulated in Sec. 3.4.1. The quality of our sub-optimal approach can be assessed by comparing its solution to the lower bound at various (α, β) levels.

Algorithm 1 The Grained Fixing Procedure

1: Initialize the procedure by relaxing all binary s_{ij}^m-variables with $0 \leq s_{ij}^m \leq 1$.
2: Calculate the PDF convolution of bandwidth integration by DFT and IDFT.
3: With a pair of (α, β) determined by the network planner/operator, solve the relaxed optimization problem.
4: Search for the s_{ij}^m with the largest value among all the s_{ij}^m-variables not fixed yet.
5: Set the found $s_{ij}^m = 1$; besides, set $s_{iq}^m = 0$ for $(q \in \mathcal{T}_i^m, q \neq j)$ and s_{pq}^m to 0 for $(p \in \mathcal{I}_j^m, p \neq i, q \in \mathcal{T}_p^m)$.
6: **if** all the s_{ij}^m-variables are fixed **then**
7: Step to ***Line 12***.
8: **else**
9: Reformulate a updated relaxed optimization problem with the latest fixed s_{ij}^m-variables.
10: Step to ***Line 2***.
11: **end if**
12: With all fixed s_{ij}^m-variables, solve the optimization problem and settle all flow routing, i.e., the $f_{ij}(l)$-variables.

3.6 Performance Analysis

3.6.1 Simulation Setup

We conduct simulations with a CRN consisting of $|\mathcal{N}| = 25$ CR routers in a $50 * 50$ m^2 area. Among these CR routers, there are $|\mathcal{L}| = 6$ active CR sessions, each session with a random rate requirement within $[10, 100]$ Mb/s. We assume that the transmission range of each router is 20 m, that the interference range is 30 m, and that the path loss index n is 4. For the simplicity of computation [42, 43], we assume the threshold Q_T is equal to the ambient Gaussian noise density, i.e., η. Thus, we have $Q_I = (\frac{20}{30})^n Q_T$ and the transmission power spectral density $Q = (20)^n Q_T = 1.6 \cdot 10^5 \eta$ according to the analysis in Sec. 3.2.3. We also assume the basic bands of the SSP are fully utilized by the SUs without CR capability.

As for the uncertain spectrum supply, we assume that there are $|\mathcal{M}| = 20$ licensed bands that can be opportunistically used by CR routers in the whole network. The vacant bandwidths of these bands are represented by a series of random variables. Based on data collected and the statistical analysis on spectrum utilization in [9], those random variables are exponentially distributed[11] , i.e., $h_{W^m}(w^m, \lambda^m) = \lambda^m e^{-\lambda^m w^m}$, where $\lambda^m \in (0, 3]$. As we know, available bands for each CR router are a subset of these 20 bands based on its location, and the available bands for any two CR routers in the network may not be the same. Therefore, we randomly select a subset of bands from the spectrum pool of 20 bands for each router in the simulations. Due to different λ^m-values and random selection process, the size of available bandwidth in each band may be unequal, which truthfully mirrors the practical scenario.

[11] The results and analysis can easily be extended to other distributions (e.g., normal distribution, uniform distribution, etc.), even for the case that W^m from different spectrum bands satisfies different distributions.

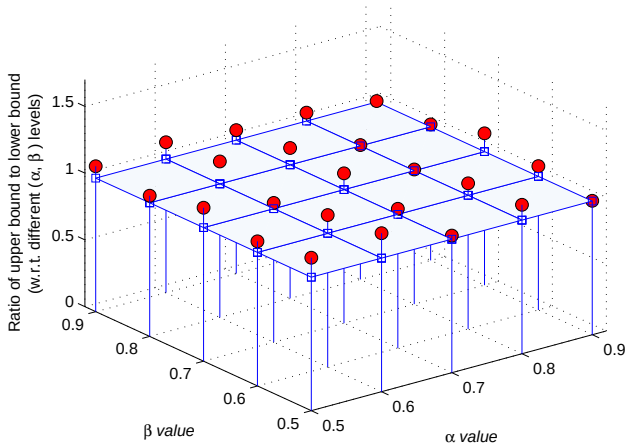

Figure 3-5. Ratio of the upper bound to the lower bound at various (α, β) levels.

It is not surprising that there may exist no feasible solution for some specific data set, because of dis-connectivity, inherent resource bottleneck in a hot spot, etc. In this chapter, we only focus on the data sets with feasible solutions and analyze the corresponding results as shown in the next subsection.

3.6.2 Results and Analysis

In Fig. 3-5, we evaluate the proposed coarse-grained fixing algorithm. We set θ = 0.75 (i.e., the threshold for the coarse-grained fixing), and compare the upper bound determined by the coarse-grained fixing algorithm with the lower bound developed in Sec. 3.4.2 at different (α, β) levels. The range of (α, β) values is from $(50\%, 50\%)$ to $(90\%, 90\%)$, and simulations for the comparison of bounds are conducted for every 10% increase in either α or β value. For each pair of (α, β), we employ 50 data sets that can produce feasible solutions and take the average value as a result. For each data set, we re-generate the network topology, source/destination pair and bit rate of each session, and available frequency bands for each CR router, which follows the guideline of simulation setup. As shown in Fig. 3-5 (the ratio is denoted by balls in shade; the benchmark of value 1 is denoted by the contour area intercepted and by the hollow squares at the sampled (α, β) pairs), the ratio of the upper bound to the lower bound via

integer relaxation is equal to or slightly above to 1 in almost all the area. The average ratio of the upper bound to the lower bound for all the sampled data sets is 1.0506, and the standard deviation is 0.0867. It indicates that since the ratio of the upper bound to the lower bound is close to 1 at any (α, β) level, and the optimal bandwidth required at α is between those bounds, the solution found by the coarse-grained fixing algorithm must be close to the optimum.

Figure 3-6 shows the comparison between the proposed (α, β) based approach and the expected bandwidth based approach in which the expected value of bandwidth is used to characterize both the objective of the optimization and corresponding constraints [85]. For illustrative purposes, we compare the solution of the expected bandwidth based approach with the solutions obtained by the coarse-grained fixing algorithm at $(\alpha, \beta) = (80\%, 80\%)$, $(\alpha, \beta) = (90\%, 90\%)$ and $\beta = 80\%$ with the expected value of required bandwidth as the objective, respectively. We take the blocking ratio of CR sessions as the evaluation metric and present simulation results for 50 data sets. From the results shown in Fig. 3-6, three observations can be made in order. First, the performance of the expected bandwidth based approach is worst of all because it ignores both the uncertainty of spectrum supply and the quality of CR communications when it selects the subset of licensed bands satisfying scheduling and routing constraints for OSA. The expected bandwidth with $\beta = 80\%$ approach is worse than the (α, β) based one because it also neglects the uncertain spectrum supply, i.e., the availability of required spectrum, as illustrated in Sec. 3.4.1.3. By contrast, taking both factors into consideration, the (α, β) based approach performs the best. Second, for the (α, β) based approach, the blocking ratio decreases as the (α, β) level increases. Third, since the blocking ratio of CR sessions is closely associated with the spectrum utilization ratio in CRNs, i.e., low blocking ratio is equivalent to high spectrum utilization ratio for a given set of CR sessions. We can claim that the (α, β) based approach is better than the expected bandwidth based one in terms of spectrum utilization as well.

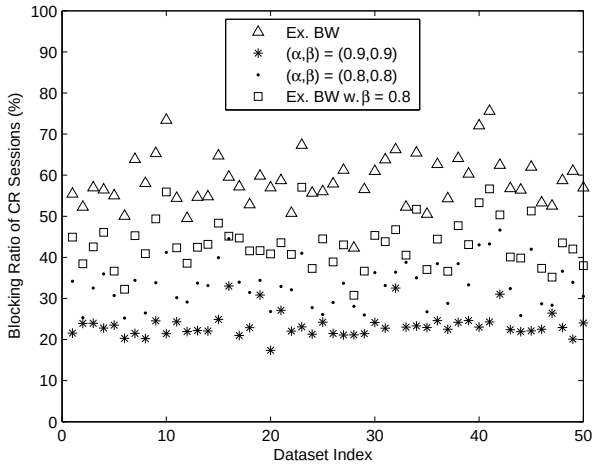

Figure 3-6. The blocking ratio of different approaches.

With a specific set of CR sessions (i.e., the network topology, the source/destination pair and the rate requirement of each session are fixed), Table 3-1 presents a general trend of change in terms of the bandwidth required at α in CRNs at different (α, β) levels. It is obvious that as α-value increases, both the lower bound and the upper bound of the bandwidth required at α increase. Similarly, as β-value increases, both the bounds of the bandwidth required at α increase as well. The reason is from two aspects: i) From the optimization objective's point of view, the larger α, the higher confidence level the network operator requests for the availability of required spectrum. The higher confidence level, the more bandwidth required at α is needed. ii) From the constraint's point of view, the larger β, the better quality of communications in CRNs. The better quality of CR communications, the more bandwidth required at α is needed, provided that the set of CR sessions is identified.

3.7 Chapter Summary

In this chapter, we have proposed a novel architecture of CRNs for spectrum harvesting and sharing, and presented a theoretical study on the joint frequency scheduling and routing problem in multi-hop CRNs under uncertain spectrum supply. We first introduce a new service provider, SSP, and let the SSP provide coverage in

Table 3-1. Lower and upper bounds of the bandwidth required at α for a given set of CR sessions at different (α, β) levels.

Index	α (%)	β (%)	Lower-Bs	Upper-Bs
1	70	80	481.88	496.09
2	75	80	517.29	517.29
3	80	80	566.39	594.37
4	85	80	628.71	631.15
5	90	80	669.76	690.05
6	70	85	490.28	493.25
7	75	85	562.89	573.30
8	80	85	589.02	595.13
9	85	85	662.54	664.74
10	90	85	714.15	725.87
11	70	90	503.32	506.09
12	75	90	602.34	606.50
13	80	90	613.90	631.76
14	85	90	681.88	696.09
15	90	90	735.07	741.68

CRNs with low-cost CR mesh routers in order to facilitate the accessing of SUs without CR capability. Enlightened by the statistics of spectrum utilization, we then model the vacancy of an available band with a random variable satisfying certain statistical distribution. After that, we elaborate on scheduling and interference constraints as well as routing constraints w.r.t. the unpredictable activities of primary services. Furthermore, we characterize the network with a pair of (α, β) parameters, and present a mathematical formulation with the goal of minimizing the required network-wide spectrum resource at a (α, β) level for a set of CR sessions with rate requirements. Since the formulated optimization problem is NP-hard, we derive a lower bound for the objective by relaxing the integer variables. Furthermore, we propose a coarse-grained fixing algorithm for a feasible solution. Through simulations, we show that the solution attained by the proposed algorithm is near-optimal to the formulated NP-hard problem at any (α, β) level; meanwhile, the (α, β) based solution is better than expected bandwidth based one in terms of blocking ratio and spectrum utilization.

CHAPTER 4
PATH SELECTION UNDER BUDGET CONSTRAINTS IN MULTI-HOP CRNS

4.1 Chapter Overview

Nowadays, more and more people, families and companies rely on wireless services for their daily life and business, which leads to a booming growth of various wireless networks and a dramatic increase in the demand for radio spectrum. In parallel with that, current static spectrum allocation policy of Federal Communications Commission (FCC) [3, 20, 73] results in the exhaustion of available spectrum, while a lot of licensed spectrum bands are extremely under-utilized. Experimental tests in academia [9, 72] and measurements conducted in industries [70, 71] both show that even in the most crowed region of big cities (e.g., Washington, DC, Chicago, New York City, etc.), many licensed spectrum bands are not used in certain geographical areas and are idle most of the time. Those studies spur the FCC to open up licensed spectrum bands and pursue new innovative technologies to encourage dynamic use of the under-utilized spectrum [20]. As one of the most promising solutions, cognitive radio (CR) technology releases the spectrum from shackles of authorized licenses, and enables the CR users to opportunistically utilize the vacant licensed spectrum bands in either temporal or spatial domain.

The idea of opportunistic using licensed spectrum in multi-hop cognitive radio networks (CRNs) has initiated the market of spectrum trading and promoted a bunch of interesting research on related topics. Specifically, in [35], Grandblaise et al. generally describe the potential scenarios and introduce some microeconomics inspired mechanisms for opportunistic spectrum accessing, and in [100], Sengupta and Chatterjee propose an economic framework for opportunistic spectrum accessing to guide the design of dynamic spectrum allocation algorithms as well as service pricing mechanisms. From the view of system design, models in game theory, by Wang et al. in [119, 120], Pan et al. in [84] and Zhang et al. in [132], and auction designs in

microeconomics, by Zhou et al. in [135, 136], Jia et al. in [48] and Wu et al. in [124], are exploited to construct the spectrum trading mechanisms with desired properties, such as power efficiency, allocation fairness, incentive compatibility, Pareto efficiency, and so on. From the view of the primary users, Xing et al. in [125] and Niyato et al. in [75, 76] have well investigated the spectrum pricing issues in the spectrum market, where multiple primary users, whose goal is to maximize the monetary gains with their vacant spectrum, compete with each other to offer spectrum access to the CR users. From the view of the CR users, Pan et al. in [85, 87] have addressed how the CR users optimally distribute their traffic demands over the spectrum bands to reduce the risk for monetary loss, when there is more than one unoccupied licensed band.

Unfortunately, most existing work assume per-user based spectrum trading (i.e., each CR user purchases available bands from primary users and uses the purchased spectrum for communications), which confronts those mechanisms with several critical problems when they are deployed in multi-hop CRNs. For instance, it is not clear whom a CR user communicates with (i.e., the CR receiver is not explicitly specified); it is not clear how to find a common band between two CR users to establish communications; it is not clear what kind of quality of service (e.g., throughput, delay, rate or bandwidth requirement, etc.) can be supported. Besides, although some of prior spectrum trading designs consider the impact of frequency reuse [84, 124, 135, 136], they ignore almost all the other factors, e.g., activities of primary services, link scheduling, route selection, etc., which may significantly affect the performance of CR sessions in multi-hop CRNs.

Instead of working on per-user based spectrum trading, in this chapter, we investigate the session-based spectrum trading. Suppose that the CR source has a fixed budget and prices for opportunistic spectrum accessing are different for different licensed bands or for the same band at different locations. Given a CR session and multiple routes between the CR source and destination, we endeavor to find a path with the maximum end-to-end throughput under the CR source's budget in multi-hop

CRNs. To achieve this objective, we have to consider the price of the bands, budget constraints of CR source, link scheduling constraints, flow routing constraints and possible returning of primary services, when selecting the path as well as the licensed bands for opportunistic accessing. In this chapter, we mathematically formulate these concerns into an optimization problem and provide near-optimal solutions using linear programming. We also propose a heuristic algorithm to give feasible solutions to the path selection problem under multiple constraints. Our contributions are summarized as follows.

- We introduce a novel service provider for CR users, called *secondary service provider* (SSP), into the network and employ SSP to help the CR session select the path for packet delivery. On behalf of the CR links, the SSP purchases licensed bands from primary users for CR nodes' opportunistic spectrum accessing w.r.t. the price of the bands as well as the activities of primary services. Meanwhile, the SSP seeks the maximum throughput route for the CR session by conducting link scheduling and path selection under the budget of CR source.

- Inspired by the link conflict graph in single-radio single-channel (SR-SC) networks [10, 131] and the 3-dimensional conflict graph in multi-radio multi-channel (MR-MC) networks [61], we propose a 4-dimensional (4-D) conflict graph to describe the conflict relations among CR links in competing for bands w.r.t. the price of bands and the probability of primary services' returning in multi-hop CRNs. Similar to the methodology used in [61], we interpret each vertex in the graph as a basic resource point for scheduling. Furthermore, we represent each resource point with a *link-band-probability-price* (LBP^2) quadruplet and construct the 4-D conflict graph consisting of LBP^2 quadruplets.

- Based on the 4-D conflict graph, the SSP can mathematically formulate the path selection as a joint routing and link scheduling optimization problem under the CR source's budget constraint. Given all the independent sets in CRNs, the SSP can relax the integer variables in the formulation, solve the optimization problem by linear programming and find the optimal path with the largest end-to-end throughput between CR source and destination.

- It is NP-hard to find all the independent sets in CRNs [30]. It is even too complicated for the SSP to find all independent sets of a given path if the number of links or the available licensed bands is large. Therefore, we develop a heuristic algorithm to deal with the path selection problem using local conflict cliques of LBP^2 quadruplets. We let the SSP layer the 4-D conflict graph by the number of licensed bands, switch LBP^2 quadruplets to mitigate the co-band interference, and

leverage the conflict cliques to find the optimal path with the largest path capacity considering the CR source's budget.

- By carrying out simulations, we demonstrate the impact of the CR source's budget, the number of available bands and the distance between the CR source and destination on the performance of path selection in CRNs. We also compare the path selection algorithms including the optimal path selection, the proposed heuristic path selection and the single-band based path selection proposed in [131], and show that the heuristic algorithm is much better than the single-band based one, and is close to the optimal one in terms of the path capacity.

The rest of this chapter is organized as follows. In Section 6.2, we review related work on cross-layer optimization for SR-SC and MR-MC networks and state-of-the-art on CRNs. In Section 6.3, we introduce the spectrum market and related models in multi-hop CRNs. In Section 6.4, we describe the 4-D conflict graph and present the concept of independent sets and conflict cliques in 4-D conflict graph. In Section 6.5, we mathematically describe scheduling and routing constraints in multi-hop CRNs, formulate the path selection under multiple constraints into an optimization problem and solve it by linear programming. In Section 6.6, we develop a heuristic algorithm for the high throughput path selection. Finally, we conduct simulations and analyze the performance results in Section 6.7, and draw concluding remarks in Section 6.8.

4.2 Related Work

How to find the path with the largest end-to-end throughput under joint link scheduling and routing constraints has been extensively studied in both SR-SC networks and MR-MC networks. Jain et al. in [45] studied the impact of interference on performance of multi-hop wireless network based on an NP-hard optimization problem. Zhai and Fang in [131] investigated the path capacity of a given path considering link scheduling and leveraged the interference clique transmission time to design a routing metric for high throughput path selection in SR-SC networks. In [10], Chen et al. extended this work to multi-rate SR-SC networks, and addressed how to find a path with high available bandwidth considering both the interference from background traffic and that along the path. In MR-MC networks, Li et al. in [61] proposed a 3-dimensional (i.e.,

radio-link-channel) conflict graph and exploited it to efficiently solve the optimal path capacity problem using linear programming.

However, different from the mobile device with a single radio in SR-SC networks or the one with multiple radios in MR-MC networks, the CR device has only one radio but the radio is a software defined one [3, 20, 73], which is supposed to switch frequencies across a wide spectrum range (i.e., from 20 MHz to 2.5 GHz [14, 97, 110]). Besides, the opportunistic spectrum usage of the CR users closely depends on the activities of primary services. The limitations in CR hardware and the impact of primary users make the path selection problem much more complex in CRNs than that in SR-SC networks and MR-MC networks.

In CR research community, there have been some efforts devoted to cross-layer optimization as well. Tang et al. in [114] studied the joint spectrum allocation and link scheduling problems with the objectives of maximizing throughput and achieving certain fairness in CRNs. Hou et al. in [43] investigated the joint frequency scheduling[1] and routing problem with the objective of minimizing the network-wide spectrum resource and presented a centralized algorithm for spectrum sharing in CRNs. In their following work, Shi and Hou in [108] also provided a distributed approach to address this issue. Considering the uncertain spectrum supply, Pan et al. in [88] proposed to model the vacancy of licensed bands as a series of random variables, characterized the multi-hop CRNs with a pair of (α, β) parameters and minimized the usage of licensed spectrum to support CR sessions with rate requirements at certain confidence levels.

In the existing literature of multi-hop CRNs, there remains a lack of study on the path selection problem by jointly considering routing and link scheduling. Meanwhile,

[1] In this chapter, frequency scheduling refers to the scheduling in frequency domain or means frequency band allocation, and link scheduling refers to the scheduling in time domain.

there is a lack of bond to connect the research on spectrum trading and the research on cross-layer optimization in multi-hop CRNs.

Our work bridges the gap between these two active research topics, i.e., spectrum trading mechanism design and cross-layer optimization, in multi-hop CRNs. We have a comprehensive study on the path selection problem considering multiple factors including the price of the bands, budget constraints of CR source, link scheduling constraints, flow routing constraints and activities of primary services. This work extends the per-user based spectrum trading into session based spectrum trading and makes those microeconomics inspired spectrum trading mechanisms practically applicable in multi-hop CRNs.

4.3 Network Model

4.3.1 Spectrum Market and Opportunistic Spectrum Accessing

We consider a spectrum market in multi-hop CRNs [75, 85, 87] consisting of multiple primary users operating on different frequency bands and a SSP (e.g., a base station (BS) or an access point (AP)) who serves a group of CR users $\mathcal{N} = \{1, 2, \cdots, n, \cdots, N\}$. Suppose that the set of licensed spectrum bands $\mathcal{B} = \{1, 2, \cdots, b, \cdots, B\}$ have the identical bandwidth, where the size of the bandwidth is equal to 1. We also assume that a CR user has only one radio, but the radio can be tuned into any available frequency band for packet delivery, i.e., a CR user can only work on one of the available bands at one time. As shown in Fig. 6-2, some spectrum bands at certain geographical locations (the bands fully in shade) may be reserved for the exclusive usage of specific primary services (e.g., restricted areas for military use or public safety, danger areas of emergency or disaster, etc.); some other licensed bands (the bands partially in shade) are opened and the "white space" is available for opportunistic accessing of CR users. To put it in a mathematical way, let $\mathcal{B}_i \subseteq \mathcal{B}$ represent the set of available licensed bands at CR node $i \in \mathcal{N}$. $\mathcal{B}_i$ may be different from $\mathcal{B}_j$, where j is not equal to i, and $j \in \mathcal{N}$, i.e., possibly $\mathcal{B}_i \neq \mathcal{B}_j$.

In this case, primary users will set reasonable prices for the available licensed bands considering the unpredictable activities of the primary services as well as competition among primary users in the spectrum market [48, 75, 125], and sell those bands for monetary gains. Besides, we assume the spectrum trading takes place periodically, where the duration of a trading period is τ, and the payment for spectrum trading is non-refundable[2] . Instead of being the trading proxy for CR users [100], the SSP plays the role of trading proxy for CR sessions. Suppose there is a uni-cast CR session in CRNs. Let s_r/d_t denote the source/destination CR node of this session, and E be the budget of the CR source s_r. To forward packets to the destination, the source CR node[3] must pay for the opportunistic spectrum usage of the CR links along the selected path to primary users via the SSP. Meanwhile, the availability of the purchased bands are not guaranteed. CR links can opportunistically use the purchased licensed bands when the primary services are not on, but have to stop using those bands when primary services become active. Given such a CR session, in this work, the SSP collectively harvests licensed spectral resource, purchases spectrum bands for CR links at different locations, and jointly conduct link scheduling and route selection under the budget constraints with the objective of maximizing the end-to-end throughput[4] .

[2] The trading period τ should not be too long (e.g., months or years) to make dynamic spectrum access infeasible, and it should not be too short (e.g., milliseconds or seconds) to incur overwhelming overhead in spectrum trading. The typical duration is minutes or hours as shown in [31]. In the rest of chapter, we assume that τ is of fixed duration, so that the time parameter is not included in our formulation.

[3] Incentive issues of the relay CR nodes are not considered in this chapter.

[4] By exchanging small-size control messages with the CR users over the dedicated channel (e.g., cognitive pilot channel), the SSP can conduct the spectrum trading and schedule the transmissions of large-size data packets for multihop CR communications.

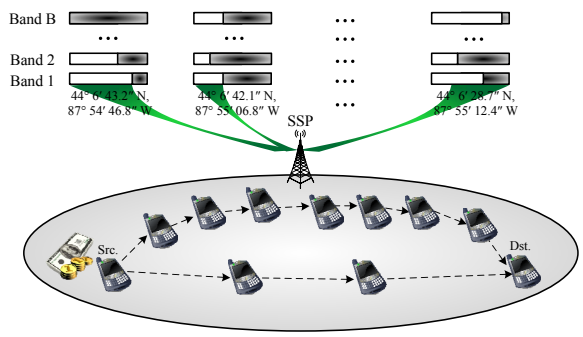

Figure 4-1. Spectrum market and opportunistic spectrum accessing for packet delivery under CR source's budget constraints in multi-hop CRNs.

4.3.2 Other Related Models in CRNs

4.3.2.1 Probability model of primary services

It is necessary to model the activities of primary services because the transmissions of a CR link over band $b \in \mathcal{B}$ closely depend on the availability of band b. As shown in [26, 51, 60], the traffic of primary services can be modeled as a two state ON-OFF process, where an ON state represents the band is occupied by primary services, and an OFF state represents the band is available for CR users' opportunistic accessing. Let q_{ij}^b represent the probability that the band b at link l_{ij} is in OFF state, and $(1 - q_{ij}^b)$ represent the probability that the band b at link l_{ij} is in ON state, where $b \in \mathcal{B}_i \bigcap \mathcal{B}_j$.

4.3.2.2 Transmission range and interference range

The interference in wireless networks can be defined according to the protocol model or the physical model [37]. Suppose all CR nodes use the same power for transmission. Then, in protocol model [37, 131], there will be a fixed transmission range and a fixed interference range, where the interference range is typically 2 or 3 times of the transmission range. These two ranges may vary with the frequency bands. The conflict relationship between two links over the same band can be determined by the specified interference range. The protocol model is adopted by most of the existing work [43, 61, 88, 114, 131], by which the interference over a network can be abstracted into a conflict graph. We also exploit the protocol model to characterize the interference

relationship among CR links in this research, and extend the conflict graph into 4-D conflict graph considering the features of spectrum trading in CRNs, which will be described in the next section. In addition, if we properly set the interference range, we can accurately transform a protocol model into a physical model as illustrated in [109].

4.4 4-Dimensional Conflict Graph, Conflict Cliques and Independent Sets in Multi-hop CRNs

To pursuit high end-to-end throughput or path capacity, it is necessary for the SSP to jointly consider flow routing and link scheduling. To effectively schedule data transmission among different CR links, it is necessary for the SSP to find the independent sets in the conflict graph constructed from CRNs [10, 131]. In this section, we extend the conflict graph to multi-dimension case and establish a 4-dimensional (4-D) conflict graph to characterize the interference relation among CR links. In the background of 4-D conflict graph, we also re-define independent sets and conflict cliques, which can help the SSP make decisions of licensed-band purchasing, spectrum assignment, link scheduling and flow routing under the budget constraints in multi-hop CRNs.

4.4.1 Construction of the 4-D Conflict Graph

Regarding the unpredictable activities of primary services and the features of CR transceivers, we introduce a 4-D conflict graph to characterize the interference relationship among CR links in CRNs. Specifically, we interpret a CRN as a four-dimensional resource space, with dimensions defined by links, bands, the probability that the band is available for OSA and the charging price. In parallel with this, in a 4-D conflict graph $\mathcal{G}(\mathcal{V}, \mathcal{E})$, each vertex corresponds to a link-band-probability-price (LBP^2) quadruplet, where an LBP^2 quadruplet is defined as

$$\text{link-band-probability-price:} \quad (l_{ij}, b, q_{ij}^b, p_{ij}^b).$$

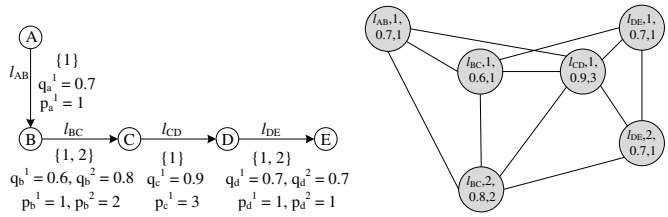

A Toy topology in CRNs. B 4-D conflict graph.

Figure 4-2. Conflict relationship represented by 4-D conflict graph in CRNs.

The LBP^2 quadruplet indicates that the CR link l_{ij} $(i, j \in \mathcal{N})$ operates on band b w.r.t the activities of the primary services over this link. The availability of band b at link l_{ij} is denoted by q_{ij}^b and the price charged for l_{ij}'s opportunistic use of band b is represented by p_{ij}^b. According to the definition of LBP^2 quadruplets, we can enumerate all combinations of CR users, bands, the availability of bands and the price of bands, which can potentially enable a CR communication link.

Obviously, the conflict relationship among LBP^2 quadruplets in CRNs is more complex than that among links in SR-SC networks, and that among link-channel pairs in MR-MC networks. Two quadruplets are said to interfere with each other if either of the following two conditions holds.

- **Condition 1**: Two different LBP^2 quadruplets have one or two CR nodes in common.
- **Condition 2**: If two different LBP^2 quadruplets are using the same band, the receiving CR node of one LBP^2 quadruplet is within the interference range of the transmitting CR node in the other LBP^2 quadruplet.

Based on these conditions, we connect two vertices in $\mathcal{V}$ with an undirected edge in $\mathcal{G}(\mathcal{V}, \mathcal{E})$, if their corresponding LBP^2 quadruplets interfere with each other.

For illustrative purpose, we take a simple example to show how to construct a 4-D conflict graph. In this toy CRNs in Fig. 5-2A, we assume there are five CR users with CR transceivers, i.e., A, B, C, D and E, and two licensed bands, i.e., band 1 and band 2. Depending on the geographic locations, the set of currently available frequency bands at one CR link may not be the same as that at another CR link as mentioned in Sec. 6.3.1.

For example, the currently available band set for link l_{AB} is $\{1\}$ and the band set for link l_{BC} is $\{1, 2\}$. Meanwhile, the CR transmissions are subject to the unpredictable returning of primary services, where the availability of a licensed band at a link is denoted by the probability. For instance, q^1_{AB} = 0.7 for band 1 at link l_{AB}, q^1_{BC} = 0.6 for band 1 at link l_{BC} and q^2_{BC} = 0.8 for the band 2 at link l_{BC} as shown in Fig. 5-2A. Furthermore, we use $d(\cdot)$ to represent Euclidean distance and suppose that $d(A, B) = d(B, C) = d(C, D) = d(D, E) = D_T = \frac{1}{2}D_I$, $d(A, C) = \sqrt{2}D_T$, $d(A, D) = \sqrt{5}D_T$, and $d(A, E) = \sqrt{10}D_T$, where D_T and D_I are the transmission range and interference range of the CR users, respectively.

Given the above assumptions and information about toy CRNs, we can construct the corresponding 4-D conflict graph, which is depicted in Fig. 5-2B. In the figure, each vertex corresponds to an LBP^2 quadruplet, for example, vertex $(l_{AB}, 1, 0.7, 1)$ in the 4-D conflict graph corresponds to LBP^2 quadruplet $(l_{AB}, 1, 0.7, 1)$. Note that there are edges between vertices $(l_{AB}, 1, 0.7, 1)$ and $(l_{BC}, 1, 0.6, 1)$, and $(l_{AB}, 1, 0.7, 1)$ and $(l_{BC}, 2, 0.8, 2)$ because l_{AB} and l_{BC} have a CR node B in common. There are edges between vertices $(l_{AB}, 1, 0.7, 1)$ and $(l_{CD}, 1, 0.9, 3)$ because l_{AB} is incident to l_{CD} over band 1. Moreover, there is an edge between vertices $(l_{BC}, 1, 0.6, 1)$ and $(l_{BC}, 2, 0.8, 2)$ because any CR user has only one radio and can only work on one band at one time. Similar analysis applies to the other vertices in the 4-D conflict graph as well.

4.4.2 Independent Sets and Conflict Cliques

Given a 4-D conflict graph $\mathcal{G} = (\mathcal{V}, \mathcal{E})$ representing CRNs, we describe the impact of vertex $i \in \mathcal{V}$ on vertex $j \in \mathcal{V}$ as follows,

$$w_{ij} = \begin{cases} 1, & \text{if there is an edge connecting vertex } i \text{ and } j \\ 0, & \text{if there is no edge between vertex } i \text{ and } j, \end{cases} \tag{4–1}$$

where the two vertices correspond to two LBP^2 quadruplets, respectively.

Provided that there is a vertex/LBP^2 quadruplet set $\mathcal{I} \subseteq \mathcal{V}$ and an LBP^2 quadruplet $i \in \mathcal{I}$ satisfying $\sum_{j \in \mathcal{I}, i \neq j} w_{ij} < 1$, the transmission at LBP^2 quadruplet i will be successful even if all the other LBP^2 quadruplets belonging to the set $\mathcal{I}$ are transmitting at the same time. If any $i \in \mathcal{I}$ satisfies the condition above, we can schedule the transmissions over all these LBP^2 quadruplets in $\mathcal{I}$ to be active simultaneously. Such a vertex/LBP^2 quadruplet set $\mathcal{I}$ is called an independent set. If adding any one more LBP^2 quadruplet into an independent set $\mathcal{I}$ results in a non-independent one, $\mathcal{I}$ is defined as a maximal independent set. Besides, if there exists a vertex/LBP^2 quadruplet set $\mathcal{Z} \subseteq \mathcal{V}$ in $\mathcal{G}$ and any two LBP^2 quadruplets i and j in $\mathcal{Z}$ satisfying $w_{ij} \neq 0$ (i.e., vertex i and j cannot be scheduled to transmit successfully at the same time.), $\mathcal{Z}$ is called a conflict clique. If $\mathcal{Z}$ is no longer a conflict clique after adding any one more LBP^2 quadruplet, $\mathcal{Z}$ is defined as a maximal conflict clique.

4.5 Optimal Path Selection under Link Scheduling, Routing and Budget Constraints

In this section, we study how the SSP can find the optimal path with the highest throughput under multiple constraints. First, we address how to calculate the path capacity considering link scheduling for a given path. Then, we mathematically describe flow routing constraints for single-radio based CR users. After that, we formulate an integer linear programming optimization problem to find the best possible path to achieve the maximum end-to-end throughput under CR scheduling, routing and budget constraints in multi-hop CRNs.

4.5.1 Path Capacity under CR Link Scheduling Constraints

For a given path $\mathcal{P}$, we can establish the 4-D conflict graph $\mathcal{G}_{\mathcal{P}} = (\mathcal{V}_{\mathcal{P}}, \mathcal{E}_{\mathcal{P}})$ following the same approach illustrated in Sec. 6.4.2. Suppose we can list all independent sets as $\mathfrak{I}_{\mathcal{P}} = \{\mathcal{I}_1, \mathcal{I}_2, \cdots, \mathcal{I}_m, \cdots, \mathcal{I}_M\}$, where M is $|\mathfrak{I}_{\mathcal{P}}|$, and $\mathcal{I}_m \subseteq \mathcal{V}_{\mathcal{P}}$ for $1 \leq m \leq M$. Then, at any time, at most one independent set can be active to transmit packets for all LBP^2 quadruplets in that set. Let $\lambda_m \geq 0$ denote the time share scheduled to independent set

$\mathcal{I}_m$, and

$$\sum_{1 \le m \le M} \lambda_m \le 1, \quad \lambda_m \ge 0 \, (1 \le m \le M). \tag{4–2}$$

Let $r_{ij}^b(\mathcal{I}_m)$ be the data rate for CR link l_{ij} over band b, where $r_{ij}^b(\mathcal{I}_m) = 0$ if LBP[2] quadruplet $(l_{ij}, b, q_{ij}^b, p_{ij}^b) \notin \mathcal{I}_m$; otherwise, $r_{ij}^b(\mathcal{I}_m)$ is the channel rate[5] for l_{ij} over band b. Therefore, by exploiting the independent set $\mathcal{I}_m$, the flow rate that l_{ij} can support over band b in the time share λ_m is $\lambda_m r_{ij}^b(\mathcal{I}_m) q_{ij}^b$, considering the possible returning of primary services in CRNs. Let s represent the flow rate of a given CR session. This CR session is feasible at link l_{ij} if there exists a schedule of the independent sets satisfying

$$s \le s_{ij} = \sum_{m=1}^{M} \lambda_m \sum_{b=1}^{|\mathcal{B}_i \bigcap \mathcal{B}_j|} r_{ij}^b(\mathcal{I}_m) q_{ij}^b. \tag{4–3}$$

To maximize the end-to-end throughput of $\mathcal{P}$, we must consider the traffic traveling through all links along the given path from the CR source to the CR destination, i.e.,

$$C_{\mathcal{P}} = \max \min_{l_{ij} \in \mathcal{P}} s_{ij}. \tag{4–4}$$

Let s_e denote $\min_{l_{ij} \in \mathcal{P}} s_{ij}$, where e is the bottleneck CR link along $\mathcal{P}$ for the end-to-end throughput. As introduced in Sec. 6.3.1, the time is divided into spectrum trading periods with the duration of τ. Each trading period is further partitioned into a set of time slots indexed by $m (1 \le m \le M)$, so that the m-th time slot has a length of $\lambda_m \tau$. In the m-th time slot, all LBP[2] quadruplets in the set $\mathcal{I}_m$ will be scheduled to transmit. The

[5] In this chapter, we assume channel rate is determined by the received power and is equal to the maximum available rate satisfying the requirement of receiver sensitivity. As we know, in most of existing literature [43, 61, 88], the channel rate is approximated by the physical channel capacity obtained from Shannon-Hartley theorem, even though the capacity cannot be achieved. Moreover, the channel rate here can easily be substituted by the more practical effective data rate, which is defined in [131]. Note that all these approximations and substitutions will not affect the theoretical results as well as performance comparison in this work.

end-to-end throughput of $\mathcal{P}$ is determined by the throughput of the bottleneck link, i.e., s_e. So, during each spectrum trading period of length τ, the path capacity of $\mathcal{P}$ is

$$s_e = \frac{1}{\tau}\sum_{m=1}^{M}\lambda_m \tau \sum_{b=1}^{|\mathcal{B}_i \bigcap \mathcal{B}_j|} r_e^b(\mathcal{I}_m) q_e^b = \sum_{m=1}^{M}\lambda_m \sum_{b=1}^{|\mathcal{B}_i \bigcap \mathcal{B}_j|} r_e^b(\mathcal{I}_m) q_e^b, \tag{4–5}$$

where $r_e^b(\mathcal{I}_m)$ and q_e^b represent the data rate and spectrum availability for the bottleneck link e over band b, respectively.

4.5.2 Single-Radio based CR Routing Constraints

As for routing, the SSP will help the source CR node to find the available paths and employ a number of relay CR nodes to forward the data packets toward its destination CR node. Similar to the modeling in [28, 88], we mathematically present the routing constraints as follows.

Let f_{ij} represent the flow rate of the CR session over link l_{ij}, where $i \in \mathcal{N}$ and $j \in \bigcup_{b\in\mathcal{B}_i} \mathcal{T}_i^b$. Here, $\mathcal{T}_i^b$ is the set of CR nodes within CR node i's transmission range, when band $b \in \mathcal{B}_i$ is opportunistically used. To simplify the notation, let $\mathcal{T}_i = \bigcup_{b\in\mathcal{B}_i} \mathcal{T}_i^b$.

If CR node i is the source node of the CR session, i.e., $i = s_r$, then

$$\sum_{j\in\mathcal{T}_i} f_{ij} = s. \tag{4–6}$$

$$\sum_{j\in\mathcal{T}_i} f_{ji} = 0. \tag{4–7}$$

Due to the inherent single-radio constraint of CR devices, we focus on the unicast and single-path routing problem. Thus, we need to modify the routing constraint in (5–9) as follows:

$$\sum_{j\in\mathcal{T}_i} f_{ij}\,\delta_{ij} = s, \tag{4–8}$$

where δ_{ij} = 1 indicates that l_{ij} may have a nonzero flow, i.e.,

$$\sum_{j \in \mathcal{T}_i} \delta_{ij} \leq 1, \quad \delta_{ij} \in \{0, 1\}. \tag{4–9}$$

If CR node i is an intermediate relay node for the CR session, i.e., $i \neq s_r$ and $i \neq d_t$, then

$$\sum_{j \in \mathcal{T}_i} f_{ij}\delta_{ij} = \sum_{j \in \mathcal{T}_i} f_{ji}\delta_{ji}. \tag{4–10}$$

If CR node i is the destination node of the CR session, i.e., $i = d_t$, then

$$\sum_{j \in \mathcal{T}_i} f_{ji}\delta_{ji} = s. \tag{4–11}$$

Note that if (6–11), (6–12), (6–13) and (6–14) are satisfied, it can be easily verified that (6–15) must be satisfied. As a result, it is sufficient to list only (6–11), (6–12), (6–13) and (6–14) as routing constraints in the problem formulation.

4.5.3 Optimal Path Selection under Multiple Constraints

If there is more than one route available for the data delivery from the source CR node to the destination CR node, the SSP will select the optimal path on behalf of the source CR node in terms of the end-to-end throughput. Since the SSP purchases available licensed bands and charges the source CR node for the CR session's opportunistic usage of these bands as mentioned in Sec. 6.3.1, the SSP must consider the budget of the source CR node besides the CR link scheduling and routing constraints. Thus, the SSP seeks for a feasible solution to trading the available frequency bands, assigning these bands to CR nodes, scheduling bands for transmission and reception, and routing the CR flow so that the end-to-end throughput of the CR session is maximized in multi-hop CRNs.

The optimal path selection problem under multiple constraints in multi-hop CRNs can be formulated as follows.

$$\text{Maximize } s$$

$$\text{s.t.:} \quad \sum_{j \in \mathcal{T}_i} f_{ji} = 0 \quad (i = s_r) \tag{4–12}$$

$$\sum_{j \in \mathcal{T}_i} f_{ij}\, \delta_{ij} = s \quad (i = s_r) \tag{4–13}$$

$$\sum_{j \in \mathcal{T}_i} f_{ij} \delta_{ij} = \sum_{j \in \mathcal{T}_i} f_{ji} \delta_{ji} \quad (i \in \mathcal{N} \backslash \{s_r, d_t\}) \tag{4–14}$$

$$\sum_{j \in \mathcal{T}_i} \delta_{ij} \leq 1, \;\; \delta_{ij} \in \{0, 1\}, \quad (i \in \mathcal{N}) \tag{4–15}$$

$$0 \leq f_{ij} \leq \sum_{m=1}^{|\mathfrak{I}|} \lambda_m \sum_{b=1}^{|\mathcal{B}_i \bigcap \mathcal{B}_j|} r_{ij}^b(\mathcal{I}_m) q_{ij}^b \tag{4–16}$$

$$(i \in \mathcal{N}, j \in \mathcal{T}_i, b \in \mathcal{B}_i \bigcap \mathcal{B}_j \text{ and } \mathcal{I}_m \in \mathfrak{I})$$

$$\sum_{m=1}^{|\mathfrak{I}|} \lambda_m \leq 1, \;\; \lambda_m \geq 0 \tag{4–17}$$

$$\sum_{m=1}^{|\mathfrak{I}|} \lambda_m \sum_{(l_{ij}, b, q_{ij}^b, p_{ij}^b) \in \mathcal{I}_m} p_{ij}^b \;\; \leq \;\; E \tag{4–18}$$

$$(i \in \mathcal{N}, j \in \mathcal{T}_i, b \in \mathcal{B}_i \bigcap \mathcal{B}_j \text{ and } \mathcal{I}_m \in \mathfrak{I}),$$

where p_{ij}^b is the price charged for l_{ij}'s usage of band b, if LBP[2] quadruplet $(l_{ij}, b, q_{ij}^b, p_{ij}^b) \in \mathcal{I}_m$. As mentioned in Sec. 6.3.1, E is the budget of the source CR node. Correspondingly, (4–18) means that the overall expense of spectrum purchasing should be within the budget of the source CR node. In addition, (6–16), (6–17), (6–18) and (6–19) specify that there is at most one outgoing link from each CR node with a nonzero flow, and that there is only one path selected by the SSP between the CR source and the CR destination. (6–20)

and (6–21) indicate that the flow rates over l_{ij} cannot exceed the capacity of this CR link, which is obtained from the CR link scheduling as illustrated in Sec. 6.5.2.

Note that $\mathfrak{I}$ includes all independent sets in CRNs. Given all independent sets[6] in the network, we find that the formulated optimization is a mixed-integer linear programming problem since δ_{ij} only has binary values. It can near-optimally be solved in polynomial time by some typical algorithms (e.g., sequential fixing algorithm [88, 108], branch and bound [94], etc.) or softwares (e.g., CPLEX [79]), provided that all the independent sets along different paths can be found in $\mathcal{G}(\mathcal{V}, \mathcal{E})$.

4.6 A Heuristic Path Selection Algorithm for High End-to-End Throughput

As we know, to find all independent sets in $\mathcal{G}(\mathcal{V}, \mathcal{E})$ is NP-hard [10, 45, 61, 115, 131]. Even though a candidate path is given, it is too complex for the SSP to find all the independent sets along the path, if the number of links of the path or the number of available licensed bands for selection in CRNs is large. Therefore, in this section, we propose a 7-step heuristic algorithm for path selection with the objective of maximizing the end-to-end throughput for a CR session. Instead of using independent sets, we classify the edges in the 4-D conflict graph into two types, layer the graph by the number of licensed bands, and leverage conflict cliques to find the path with the highest end-to-end throughput for the CR session under budget constraints.

4.6.1 A Counterexample for the Maximal Clique Approach

In SR-SC networks, authors in [10, 131] leverage the maximal local cliques to approximately select the path with the highest throughput. Unfortunately, this approach cannot be applied in CRNs. We take a toy CR path shown in Fig. 5-2A as a counterexample. Suppose that the packet length is 1 and the transmission time of a

[6] That is a general assumption used in existing literature [10, 61, 114, 115, 131] for obtaining throughput bounds or performance comparison, where both link scheduling and flow routing are considered.

packet over all LBP^2 quadruplets is the same, which is equal to T. According to the local clique approach, $C_{\mathcal{P}} \leq \frac{1}{4T}$ since the maximal local clique contains 4 LBP^2 quadruplets as shown in Fig. 5-2B. However, if we only consider band 1 for CR nodes' usage regardless of primary services' activities, $C_{\mathcal{P}} \leq \frac{1}{3T}$ since the maximal local clique contains 3 LBP^2 quadruplets. Intuitively, if we consider both band 1 and 2 for CR nodes' opportunistic accessing, the throughput of the toy path should be further improved. The paradox above indicates that the maximal local clique based algorithm is no longer suitable for path selection in CRNs.

4.6.2 The Proposed Algorithm for Path Selection in CRNs

The detailed procedure of the proposed heuristic algorithm for path selection in CRNs is presented as follows.

Step 1: *Construction of the 4-D conflict graph*

Given a candidate path $\mathcal{P}$, we first set up a corresponding 4-D conflict graph $\mathcal{G}_{\mathcal{P}}(\mathcal{V}_{\mathcal{P}}, \mathcal{E}_{\mathcal{P}})$ as illustrated in Sec. 6.4.2.

Step 2: *Decoupling the 4-D conflict graph into layers*

With the established 4-D conflict graph of the path, we further divide $\mathcal{G}_{\mathcal{P}}(\mathcal{V}_{\mathcal{P}}, \mathcal{E}_{\mathcal{P}})$ into different layers according to the number of bands, i.e., $|\mathcal{B}|$. To put it in another way, each layer represents a band, and the intercepted conflict graph on layer b describes the interference relationship among the CR links over band b, $b \in \mathcal{B}$.

For example, for a path from CR node A to node E as shown in Fig. 5-2A, we build up the corresponding 4-D conflict graph and divide the graph into two layers because the total number of available bands in CRNs is 2.

Step 3: *Differentiating two types of edges*

Then, we classify the edges on a layer of the 4-D conflict graph into two categories. For layer b in $\mathcal{G}_{\mathcal{P}}$, one kind of edges connect two different LBP^2 quadruplets who have one CR node in common, i.e., LBP^2 quadruplets on layer b satisfying **Condition 1**. We define these edges as *non-reducible edges*. The other kind of edges connect two

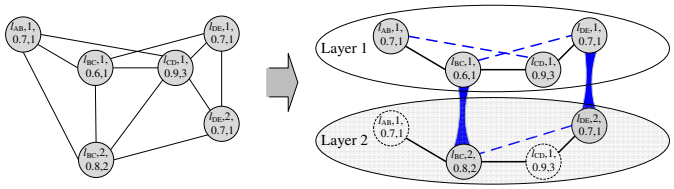

Figure 4-3. An illustrative example for the proposed procedure with a given path.

different LBP^2 quadruplets who have co-band interference, i.e., LBP^2 quadruplets on layer b satisfying **Condition 2**. We define these edges as *reducible edges*.

For example, in Fig. 4-3, edges between LBP^2 quadruplets $(l_{AB}, 1, 0.7, 1)$ and $(l_{BC}, 1, 0.6, 1)$, between $(l_{BC}, 1, 0.6, 1)$ and $(l_{CD}, 1, 0.9, 3)$, and between $(l_{CD}, 1, 0.9, 3)$ and $(l_{DE}, 1, 0.7, 1)$ on layer 1 are non-reducible edges (denoted by solid lines) due to the single-radio constraint; correspondingly, edges between $(l_{AB}, 1, 0.7, 1)$ and $(l_{CD}, 1, 0.9, 3)$ and between $(l_{BC}, 1, 0.6, 1)$ and $(l_{DE}, 1, 0.7, 1)$ on layer 1, and edges between $(l_{BC}, 2, 0.8, 2)$ and $(l_{DE}, 2, 0.7, 1)$ on layer 2 are reducible edges (denoted by dashed lines). The co-band interference between LBP^2 quadruplets represented by reducible edges may be mitigated by switching LBP^2 quadruplets to different layers.

Step 4: *Selecting the benchmark layer*

If there is only one layer in $\mathcal{G}_{\mathcal{P}}$, select it as the benchmark layer; if there is more than one layer in $\mathcal{G}_{\mathcal{P}}$, select the one which has the most edges (either non-reducible edges or reducible ones) because this layer can most effectively show the interference relationship among different links along the path $\mathcal{P}$. For instance, layer 1 is the benchmark layer for the toy CR path from CR node A to node E as shown in Fig. 4-3.

Step 5: *Establishing the benchmark path capacity*

After choosing the benchmark layer, we further estimate the benchmark expense. To calculate the benchmark expense, we need information from two sides: i) the unit price of the band used by a link and ii) the active time of that link along the path $\mathcal{P}$ for one time period τ, under the condition that layer b of $\mathcal{G}_{\mathcal{P}}$ is selected as the benchmark layer.

Let l_{ij} be a CR link along the path $\mathcal{P}$, E_{ij} be the estimated expense of l_{ij}, and $\mathcal{Q}_{ij}$ represent the LBP^2 quadruplet set associated with l_{ij} (e.g., $\mathcal{Q}_{DE} = \{(l_{DE}, 1, 0.7, 1), (l_{DE}, 2, 0.7, 1)\}$ as shown in Fig. 4-3). Given layer b as the benchmark layer, the unit price of the band used by l_{ij} is calculated as the following three cases.

- *Case 1:* If $|\mathcal{Q}_{ij}| = 1$, there is only one LBP^2 quadruplet available for l_{ij}. Thus, the SSP can only choose the LBP^2 quadruplet for l_{ij} and pay the corresponding price for using the band enclosed in that LBP^2 quadruplet.
- *Case 2:* If $|\mathcal{Q}_{ij}| \geq 1$ and $(l_{ij}, b, q_{ij}^b, p_{ij}^b) \in \mathcal{Q}_{ij}$, there are multiple LBP^2 quadruplets available for l_{ij} including $(l_{ij}, b, q_{ij}^b, p_{ij}^b)$. Since layer b is the benchmark layer, the SSP will choose LBP^2 quadruplet $(l_{ij}, b, q_{ij}^b, p_{ij}^b)$ for l_{ij} to calculate the benchmark expense and pay p_{ij}^b for using band b, i.e., $E_{ij} = p_{ij}^b$.
- *Case 3:* If $|\mathcal{Q}_{ij}| \geq 1$ and $(l_{ij}, b, q_{ij}^b, p_{ij}^b) \notin \mathcal{Q}_{ij}$, there are some other LBP^2 quadruplets available for l_{ij} except $(l_{ij}, b, q_{ij}^b, p_{ij}^b)$. In this case, the SSP can randomly choose an LBP^2 quadruplet $(l_{ij}, k, q_{ij}^k, p_{ij}^k)$ in $\mathcal{Q}_{ij}$ for l_{ij} to estimate the benchmark expense and pay the corresponding price for using the band enclosed in that LBP^2 quadruplet, i.e., $E_{ij} = p_{ij}^k$ $(k \neq b)$.

Then, we employ conflict cliques over layer b to estimate the active time of links along the path $\mathcal{P}$ for one time period τ. Similar to the illustration in [10, 131], we define the interference clique transmission time $T_{\mathcal{Z}}$ for one conflict clique $\mathcal{Z}$ over the selected benchmark layer as

$$T_{\mathcal{Z}} = \sum_{(l_{ij}, b, q_{ij}^b, p_{ij}^b) \in \mathcal{Z}} T_{(l_{ij}, b, q_{ij}^b, p_{ij}^b)} \tag{4–19}$$

where $T_{(l_{ij}, b, q_{ij}^b, p_{ij}^b)}$ is the transmission time for a packet over l_{ij} using band b. Assume the packet length is 1, considering the activities of primary services, $T_{(l_{ij}, b, q_{ij}^b, p_{ij}^b)}$ can be written as

$$T_{(l_{ij}, b, q_{ij}^b, p_{ij}^b)} = \frac{1}{r_{ij}^b \cdot q_{ij}^b} \tag{4–20}$$

For the given path $\mathcal{P}$, find the set $\mathfrak{Z}$ of all the maximal interference clique $\mathcal{Z}$ for the LBP^2 quadruplets on the benchmark layer. Let $T_{\mathcal{P}}$ be the maximal value of $T_{\mathcal{Z}}$ for all

cliques over the benchmark layer and

$$T_{\mathcal{P}} = \max_{\mathcal{Z} \in \mathfrak{Z}} T_{\mathcal{Z}} \tag{4–21}$$

Considering the link l_{ij} in $\mathcal{Z}$ and any one packet successfully delivered from the CR source to the CR destination, the packet takes time $T_{\mathcal{P}}$ to travel through all the LBP^2 quadruplets in $\mathcal{Z}$, and l_{ij} cannot be scheduled to do any other transmission during $T_{\mathcal{P}}$. That indicates that a packet takes at least time $T_{\mathcal{P}}$ at link l_{ij} over the benchmark layer, and the throughput at link l_{ij} is less than or equal to $\frac{1}{T_{\mathcal{P}}}$ over the benchmark layer. Since the end-to-end throughput cannot be larger than the throughput of any link along the path, the benchmark path capacity $C_{\mathcal{P}}$ can be approximated as $\frac{1}{T_{\mathcal{P}}}$ [131].

This statement holds if there are no odd cycles [15] in $\mathcal{G}_{\mathcal{P}}$. In fact, the problem can be simplified for the conflict graph constructed from general paths without odd cycles as illustrated in [131]. Instead of finding all the maximal cliques including one LBP^2 quadruplet, the SSP only needs to consider other LBP^2 quadruplets close to this one along the path. We refer to these cliques as the *local interference cliques* of a path. For paths over a certain layer, the maximal value of the interference clique transmission time of all local cliques (i.e., $\hat{T}_{\mathcal{P}}$ over benchmark layer) is equal to that for all cliques (i.e., $T_{\mathcal{P}}$ over benchmark layer)[7] .

Thus, we can further establish the benchmark path capacity[8] using $\hat{T}_{\mathcal{P}}$ as $C_{\mathcal{P}} = \frac{1}{T_{\mathcal{P}}} = \frac{1}{\hat{T}_{\mathcal{P}}}$ [131].

Step 6: *Establishing the benchmark expense*

[7] Some brute-force algorithms can be designed to find all local cliques on a specific layer (i.e., for a specific band) in polynomial time as illustrated in [131], which is omitted in this chapter due to the limited space.

[8] Similar to [10, 131], in this chapter, we only consider the direct routes as defined in [131]. Note that for direct routes, $C_{\mathcal{P}} = \frac{1}{T_{\mathcal{P}}} = \frac{1}{\hat{T}_{\mathcal{P}}}$ holds.

Given the benchmark path capacity $C_{\mathcal{P}}$, the SSP will establish the benchmark expense $\Pi_{\mathcal{P}}$.

For a CR link l_{ij} along the path $\mathcal{P}$, if the LBP^2 quadruplet $(l_{ij}, b, q_{ij}^b, p_{ij}^b) \in \mathcal{Q}_{ij}$, i.e., the LBP^2 quadruplet $(l_{ij}, b, q_{ij}^b, p_{ij}^b)$ is on the benchmark layer b, it takes up t_{ij} for packet delivery during one period τ, where t_{ij} is

$$t_{ij} = \frac{\tau C_{\mathcal{P}}}{r_{ij}^b q_{ij}^b} = \frac{\tau T_{(l_{ij}, b, q_{ij}^b, p_{ij}^b)}}{\hat{T}_{\mathcal{P}}}. \tag{4–22}$$

Correspondingly, the benchmark expense of l_{ij} is

$$\Pi_{ij} = \frac{E_{ij}}{\tau} \frac{\tau T_{(l_{ij}, b, q_{ij}^b, p_{ij}^b)}}{\hat{T}_{\mathcal{P}}} = \frac{E_{ij} T_{(l_{ij}, b, q_{ij}^b, p_{ij}^b)}}{\hat{T}_{\mathcal{P}}}. \tag{4–23}$$

Similarly, for a CR link l_{uv} along the path, where the LBP^2 quadruplet $(l_{uv}, b, q_{uv}^b, p_{uv}^b) \notin \mathcal{Q}_{uv}$ and band k other than band b is exploited by l_{uv} for packet delivery, the benchmark expense is written as

$$\Pi_{uv} = \frac{E_{uv} T_{(l_{uv}, k, q_{uv}^k, p_{uv}^k)}}{\hat{T}_{\mathcal{P}}}. \tag{4–24}$$

Therefore, the benchmark expense of the path $\mathcal{P}$ can be expressed as

$$\Pi_{\mathcal{P}} = \sum_{(l_{ij}, b, q_{ij}^b, p_{ij}^b) \in \mathcal{Q}_{ij}} \frac{T_{(l_{ij}, b, q_{ij}^b, p_{ij}^b)}}{\hat{T}_{\mathcal{P}}} E_{ij} + \sum_{(l_{uv}, b, q_{uv}^b, p_{uv}^b) \notin \mathcal{Q}_{uv}} \frac{T_{(l_{uv}, k, q_{uv}^k, p_{uv}^k)}}{\hat{T}_{\mathcal{P}}} E_{uv}. \tag{4–25}$$

The procedure of **Step 5** and **Step 6** is summarized in Alg. 2.

Step 7: *Switching quadruplets for high throughput*

Depending on the values of $\Pi_{\mathcal{P}}$, $\frac{1}{\hat{T}_{\mathcal{P}}}$ and the budget E, the SSP may apply differen strategies to switch LBP^2 quadruplets.

If $\Pi_{\mathcal{P}}$ is beyond E, i.e., the budget of the CR source, the SSP will switch LBP^2 quadruplets to reduce the overall expense for the given path $\mathcal{P}$. Note that $\Pi_{\mathcal{P}}$ increases when $\hat{T}_{\mathcal{P}}$ decreases as shown in (4–25). Thus, the SSP would switch the LBP^2 quadruplets on other layers (i.e., $(l_{uv}, k, q_{uv}^k, p_{uv}^k)$ in (4–25), where $(l_{uv}, b, q_{uv}^b, p_{uv}^b) \notin \mathcal{Q}_{uv}$) rather than the ones on the benchmark layer (i.e., $(l_{ij}, b, q_{ij}^b, p_{ij}^b)$ in (4–25), where

Algorithm 2 Establishing the benchmark expense

Require: Initialize the procedure after layering $\mathcal{G}_{\mathcal{P}}$ and selecting layer b as the benchmark layer.

for all $l_{ij} \in \mathcal{P}$ **do**
  if $|\mathcal{Q}_{ij}| == 1$ **then**
    The SSP chooses that LBP^2 quadruplet for l_{ij}.
  else if $|\mathcal{Q}_{ij}| \geq 1$ and $(l_{ij}, b, q_{ij}^b, p_{ij}^b) \in \mathcal{Q}_{ij}$ **then**
    The SSP chooses $(l_{ij}, b, q_{ij}^b, p_{ij}^b)$ for l_{ij} and set $E_{ij} = p_{ij}^b$.
  else if $|\mathcal{Q}_{ij}| \geq 1$ and $(l_{ij}, b, q_{ij}^b, p_{ij}^b) \notin \mathcal{Q}_{ij}$ **then**
    The SSP randomly chooses $(l_{ij}, k, q_{ij}^k, p_{ij}^k) \in \mathcal{Q}_{ij}$ for l_{ij} and set $E_{ij} = p_{ij}^k$.
  end if
  Calculate the transmission time for $l_{ij} \in \mathcal{P}$.
end for
Find the maximum value of the local clique's transmission time $\hat{T}_{\mathcal{P}}$ and estimate the benchmark path capacity with $\frac{1}{\hat{T}_{\mathcal{P}}}$.
Given the benchmark path capacity, calculate the transmission time and the corresponding benchmark expense at $l_{ij} \in \mathcal{P}$.
Sum up the benchmark expense of each link along $\mathcal{P}$ and establish the benchmark expense of $\mathcal{P}$.

$(l_{ij}, b, q_{ij}^b, p_{ij}^b) \in \mathcal{Q}_{ij}$) to lower down the expense. The SSP will replace $(l_{uv}, k, q_{uv}^k, p_{uv}^k)$ with $(l_{uv}, h, q_{uv}^h, p_{uv}^h)$, where $p_{uv}^h < p_{uv}^k$ and $(l_{uv}, h, q_{uv}^h, p_{uv}^h) \in \mathcal{Q}_{uv}$. By switching LBP^2 quadruplets, if the overall expense of $\mathcal{P}$ can be reduced to the budget of CR source, the path capacity of $\mathcal{P}$, i.e., $C_{\mathcal{P}}^*$ can be estimated with the benchmark path capacity, i.e., $C_{\mathcal{P}} = \frac{1}{\hat{T}_{\mathcal{P}}}$. Otherwise, path $\mathcal{P}$ is not feasible for the CR session due to budget constraints.

On the other hand, if $\Pi_{\mathcal{P}}$ is below E, the SSP will switch LBP^2 quadruplets to improve the throughput of the path $\mathcal{P}$.

From (4–19), (6–24) and $C_{\mathcal{P}} = \frac{1}{T_{\mathcal{P}}} = \frac{1}{\hat{T}_{\mathcal{P}}}$, we find that if the number of LBP^2 quadruplets in the conflict clique can be reduced, the throughput of the path will increase. Moreover, it is obvious that the co-band interference between LBP^2 quadruplets, which are the vertices of *reducible edges* defined in **Step 3**, can be mitigated by switching LBP^2 quadruplets. Therefore, the SSP will switching LBP^2 quadruplets to increase the path capacity under the budget E as follows.

The SSP first sorts the LBP^2 quadruplets on the benchmark layer. According to the number of *reducible edges* associated with the LBP^2 quadruplets, the SSP indexes the LBP^2 quadruplets in a decreasing manner, i.e., the more *reducible edges* an LBP^2 quadruplet is associated with, the smaller index number the LBP^2 quadruplet has[9] .

Then, the SSP starts the switching process with the LBP^2 quadruplet having the smallest index. Let the LBP^2 quadruplet be $(l_{ij}, b, q_{ij}^b, p_{ij}^b)$ on benchmark layer b. If $|\mathcal{Q}_{ij}| = 1$, then this LBP^2 quadruplet cannot be switched, and the SSP continues to check the next LBP^2 quadruplet. Otherwise, if $|\mathcal{Q}_{ij}| > 1$, the SSP needs to decide whether $(l_{ij}, b, q_{ij}^b, p_{ij}^b)$ can be switched into $(l_{ij}, k, q_{ij}^k, p_{ij}^k)$, where $(l_{ij}, k, q_{ij}^k, p_{ij}^k) \in \mathcal{Q}_{ij}$ and $k \neq b$. Let $\hat{T}_{\mathcal{P}}$ be the transmission time of local cliques on the benchmark layer b before quadruplet switching, $\hat{T}_{\mathcal{P}}^{''}$ be the largest transmission time of local cliques among all the layers after switching $(l_{ij}, b, q_{ij}^b, p_{ij}^b)$ to $(l_{ij}, k, q_{ij}^k, p_{ij}^k)$, and $\Pi_{\mathcal{P}}^{''}$ be the expense of $\mathcal{P}$ after switching $(l_{ij}, b, q_{ij}^b, p_{ij}^b)$ to $(l_{ij}, k, q_{ij}^k, p_{ij}^k)$. To make the decision of quadruplet switching, the SSP must consider the following two cases.

- If $\hat{T}_{\mathcal{P}}^{''} \leq \hat{T}_{\mathcal{P}}$ and $\Pi_{\mathcal{P}}^{''} \leq E$, the SSP will switch $(l_{ij}, b, q_{ij}^b, p_{ij}^b)$ to $(l_{ij}, k, q_{ij}^k, p_{ij}^k)$, eliminate *reducible edges* associated with LBP^2 quadruplet $(l_{ij}, b, q_{ij}^b, p_{ij}^b)$ on layer b, and add *reducible edges* associated with LBP^2 quadruplet $(l_{ij}, k, q_{ij}^k, p_{ij}^k)$ on layer k. In addition, the SSP will identify the layer with $\hat{T}_{\mathcal{P}}^{''}$, put $\hat{T}_{\mathcal{P}} = \hat{T}_{\mathcal{P}}^{''}$ and $\Pi_{\mathcal{P}} = \Pi_{\mathcal{P}}^{''}$, and set that layer as new benchmark layer. After that, the SSP will sort LBP^2 quadruplets on the new benchmark layer and continue switching process.
- If $\hat{T}_{\mathcal{P}}^{''} > \hat{T}_{\mathcal{P}}$ or $\Pi_{\mathcal{P}}^{''} > E$, the SSP cannot switch $(l_{ij}, b, q_{ij}^b, p_{ij}^b)$ to $(l_{ij}, k, q_{ij}^k, p_{ij}^k)$. The SSP will keep the benchmark layer and benchmark expense unchanged, and continue the process with the next LBP^2 quadruplet.

Iterations of quadruplet switching continue until $\hat{T}_{\mathcal{P}}$ cannot be decreased further under the CR source's budget E. Then, the SSP can estimate the throughput of $\mathcal{P}$ as $C_{\mathcal{P}}^* = \frac{1}{\hat{T}_{\mathcal{P}}^*}$ as shown in Alg. 3.

[9] If there are multiple LBP^2 quadruplets with the same number of *reducible edges*, the SSP will just index them in order according to their distance from the CR source.

Algorithm 3 Switching quadruplets for high throughput

Require: The benchmark layer is layer b and $\Pi_{\mathcal{P}} \leq E$.

1: Sort and index the LBP^2 quadruplets on the benchmark layer in a decreasing manner according to the number of *reducible edges* associated with these quadruplets.
2: Set $\alpha = 1$.
3: Start the switching-quadruplet process of the α-th quadruplet $(l_{ij}, b, q_{ij}^b, p_{ij}^b)$ on the benchmark layer.
4: **if** $|\mathcal{Q}_{ij}|$ == 1 **then**
5: $\quad\alpha = \alpha + 1$. Go to ***Line 3***.
6: **else if** $|\mathcal{Q}_{ij}| \geq 1$ **then**
7: $\quad$**for all** $(l_{ij}, k, q_{ij}^k, p_{ij}^k) \in \mathcal{Q}_{ij}$ **do**
8: $\quad\quad$Calculate $\hat{T}^{''}$ and $\Pi_{\mathcal{P}}^{''}$
9: $\quad\quad$**if** $\hat{T}_{\mathcal{P}}^{''} > \hat{T}_{\mathcal{P}}$ or $\Pi_{\mathcal{P}}^{''} > E$ **then**
10: $\quad\quad\quad$**continue**.
11: $\quad\quad$**else if** $\hat{T}_{\mathcal{P}}^{''} \leq \hat{T}_{\mathcal{P}}$ and $\Pi_{\mathcal{P}}^{''} \leq E$ **then**
12: $\quad\quad\quad$Switch $(l_{ij}, b, q_{ij}^b, p_{ij}^b)$ into $(l_{ij}, k, q_{ij}^k, p_{ij}^k)$.
13: $\quad\quad\quad$Delete the *reducible edges* associated with $(l_{ij}, b, q_{ij}^b, p_{ij}^b)$ on the benchmark layer.
14: $\quad\quad\quad$Identify the layer with $\hat{T}_{\mathcal{P}}^{''}$, and set that layer as new benchmark layer.
15: $\quad\quad\quad$$\hat{T}_{\mathcal{P}} = \hat{T}_{\mathcal{P}}^{''}$ and $\Pi_{\mathcal{P}} = \Pi_{\mathcal{P}}^{''}$. Go to ***Line 1***.
16: $\quad\quad$**end if**
17: $\quad$**end for**
18: $\quad\alpha = \alpha + 1$. Go to ***Line 3***.
19: **end if**
20: Output the throughput of $\mathcal{P}$: $C_{\mathcal{P}}^* = \frac{1}{\hat{T}_{\mathcal{P}}^*} = \frac{1}{\hat{T}_{\mathcal{P}}}$.

The heuristic algorithm provides a useful metric to the SSP for the path selection. Given possible paths of a CR session, the SSP can exploit the proposed algorithm above to calculate the throughput of these paths by using local cliques, and select the path with the highest path capacity.

4.6.3 Complexity Analysis

For a $\mathcal{G}_{\mathcal{P}}(\mathcal{V}_{\mathcal{P}}, \mathcal{E}_{\mathcal{P}})$ constructed from the candidate path $\mathcal{P}$, it is NP-hard to identify all the maximal independent sets. Given all the maximal independent sets and relaxed δ_{ij}-variables, the complexity of solving such an optimization problem by standard solvers such as CPLEX [79] is $\mathcal{O}(X^3 Y)$ [94], where X is the number of variables and Y is the number of bits required to store the data. By contrast, the proposed heuristic algorithm

can directly calculate the path capacity in each iteration. Thus, the complexity of the proposed algorithm mainly lies in the number of required iterations. Note that for a given candidate path, in each iteration, we determine the status of an additional link on an available band for the session under budget constraints. Let $|\mathcal{N}_{\mathcal{P}}|$ be the number of CR nodes along the path, and $|\mathcal{H}| = \max_{i \in \mathcal{N}_{\mathcal{P}}, b \in \mathcal{B}_i} |\mathcal{H}_i^b|$, where $|\mathcal{H}_i^b|$ is the number of CR nodes within the local clique of i over band b. Each link could be active at most $|\mathcal{B}|$ bands. So, for a path with $|\mathcal{N}_{\mathcal{P}}|$ CR nodes, the number of iterations for the proposed procedure is no more than the product $|\mathcal{N}_{\mathcal{P}}|^2 \cdot |\mathcal{H}| \cdot |\mathcal{B}|$, which indicates that the proposed algorithm has a polynomial-time complexity.

4.7 Performance Evaluation

4.7.1 Simulation Setup

We consider a multi-hop CRN consisting of $|\mathcal{N}| = 40$ CR nodes randomly distributed in a $800 * 800$ m^2 area. We assume each CR node has a fixed transmission range of 250 m and interference range of 500 m [96, 115]. Regarding the returning of primary services, the availability of a licensed band over a CR link at a certain location is with a random probability within $(0.5, 1]$, i.e., $q_{ij}^b \in (0.5, 1]$ ($\forall i, j \in \mathcal{N}$ and $\forall b \in \mathcal{B}$). Correspondingly, the price for opportunistic using a band for one time period is within $(50, 100]$. The price of a licensed band increases with the availability of that band, given the fact that all bands have the identical bandwidth. For illustrative purposes, we conduct simulations to study the path selection problem in CRNs with two different channel rates, i.e., 18 Mbps (802.11a) and 11 Mbps (802.11b), respectively.

We fix the CR node nearest to the upper left corner as the CR source and the CR node nearest to the lower right corner as the CR destination. We compare the path selection algorithms consisting of the optimal path selection, the proposed heuristic path selection and the single-band based path selection illustrated in [131]. The performance metric is the end-to-end throughput/path capacity. Note that the optimal path selection is the one obtained from the mixed integer-linear programming

problem formulated in Sec. 6.5.4. Given such a small network topology in simulations, we can find the independent sets [61, 131], relax the binary requirement on δ_{ij} and solve the optimization problem in a reasonable time by using CPLEX [79]. Besides, we demonstrate the impact of CR source's budget and the impact of the number of available licensed bands on the path capacity in CRNs, and present the results in Fig. 4-4 and 6-7. We also find the paths from the CR source to all the other CR nodes in this area, carry out simulations to evaluate the impact of distance from the CR source on the path capacity with different path selection algorithms, and show the results in Fig. 6-8.

4.7.2 Results and Analysis

In Fig. 4-4, we compare the optimal path selection with the proposed heuristic path selection at different CR source's budget levels, where the number of available licensed bands $|\mathcal{B}|$ is equal to 1, 2 and 3, respectively. Meanwhile, we set the path capacity obtained from the single-band based path selection algorithm in [131] as the baseline, where we assume the budget is large enough. From the results shown in Fig. 4-4A and Fig. 4-4B, four observations can be made in order. First, the single-band based path selection has the worst performance among all these algorithms. That is not surprising because the single-band based path selection algorithm in [131] is designed for SR-SC networks. It neither considers the CR capability of the CR relay nodes nor considers the possible returning of primary services at different CR links[10] in CRNs. Second, as the number of available bands increases, the end-to-end throughput increases as well. The reason is that more licensed bands available give more opportunities for CR users' accessing, so that more CR links along the selected

[10] In the simulations, we assume there exist perfect links, where the delivery ratio is equal to 1. The packet loss of CR transmissions is only caused by the returning of primary services.

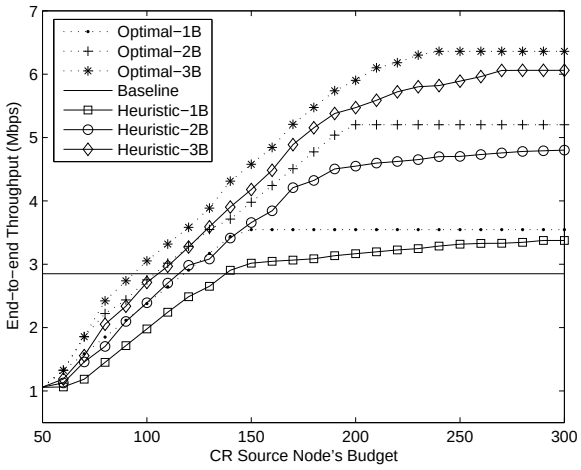

A Performance comparison among different path selection algorithms, where channel rate is 18M.

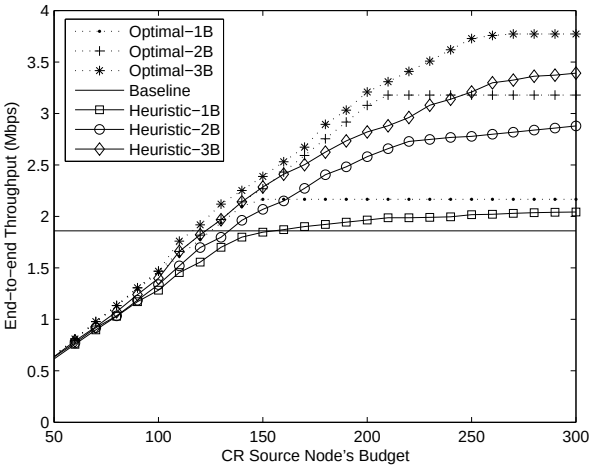

B Performance comparison among different path selection algorithms, where channel rate is 11M.

Figure 4-4. Impact of CR source's budget on path selection in multi-hop CRNs.

path can be activated for transmission simultaneously. Third, as the CR source's budget increases, the end-to-end throughput also increases. That is because the budget is one of the most important concerns of the SSP when it jointly conducts the flow routing and link scheduling for a CR session. However, when the budget of CR source node is large enough (e.g., beyond 250), it has no impact on the SSP's decision of path selection and the path capacity will not increase any more. Fourth, the performance of

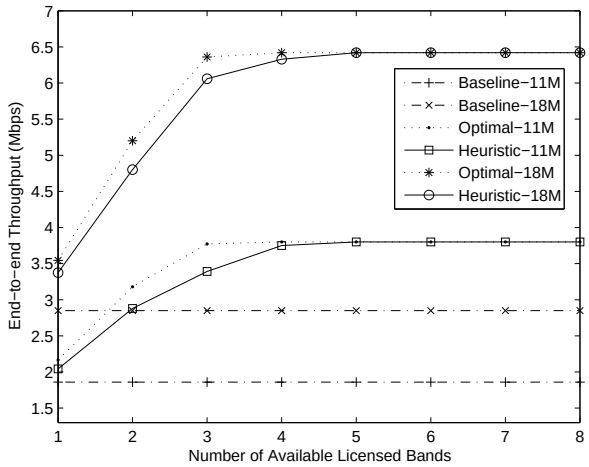

Figure 4-5. Impact of the number of available licensed bands on path selection in multi-hop CRNs.

the heuristic algorithm is close to that of the optimal one at different budget levels as shown in Fig. 4-4A and Fig. 4-4B.

Figure 6-7 presents the impact of the number of available bands on the path capacity in CRNs, where we can have the following two observations. i) The path capacity obtained from the heuristic path selection algorithm is close to that from the optimal one, especially when the number of available licensed bands is larger than 4. ii) The increment of path capacity basically stops when the number of available bands exceeds 4. As illustrated in Sec. 6.4.2 and Sec. 6.6, only the interference between LBP^2 quadruplets satisfying **Condition 2** can be reduced by switching LBP^2 quadruplets, due to the single radio constraint of CR devices. Given the network scale in the simulation, there are a limited number of LBP^2 quadruplets satisfying **Condition 2** in the maximal conflict cliques. Therefore, the maximum path capacity can be achieved by full exploitation of 4 licensed bands, even considering the potential interruption caused by primary services in multi-hop CRNs.

Figure 6-8 shows the impact of distance between the CR source and destination on the path capacity in CRNs. For the simplicity of computing independent sets [61], we assume there are 3 licensed bands available in the network. Except for the observations

we already have in Fig. 4-4 and Fig. 6-7, we find that the longer distance the path spans, the more likely the path capacity is affected by the budget of the CR source. It is obvious that a longer path may include more CR links along the path, which implies that more links could be scheduled to transmit at the same time. Thus, the end-to-end throughput of such a path depends more on the budget of the CR source.

4.8 Chapter Summary

In this chapter, we have studied the path selection problem in multi-hop CRNs under flow routing, link scheduling and CR source's budget constraints. We first introduce a novel service provider for CR users, SSP, and make the SSP help a given CR session to purchase the licensed spectrum and select the path for packet delivery. Then, considering the inherent single radio constraint of CR devices and the features of spectrum trading, we propose a 4-D conflict graph to describe the conflict relations among CR links. After that, we mathematically formulate the path selection problem under multiple constraints into an optimization problem with the objective of maximizing the end-to-end throughput for the CR session. Given all independent sets in 4-D conflict graph, we can relax the formulated optimization problem and solve it by linear programming. Regarding the NP-hardness of finding all independent sets, we provide a heuristic algorithm as well, which layers the 4-D conflict graph and exploits the maximal local cliques to approximately select the path with the highest throughput. By simulations, we demonstrate how the CR source's budget, the number of available bands and distance from CR source affect the performance of path selection in terms of path capacity. We also compare the heuristic path selection algorithm with the optimal one and show that the throughput obtained from the heuristic algorithm is close to that obtained from the optimal one in multi-hop CRNs.

As an initial step, in this chapter, we just consider a single-flow scenario and ignore the interference from the other flows as well as the competitive bidding for spectrum usage from the other flows. In a CRN with multi-flows, the CR source nodes need to

develop sophisticated bidding strategies considering the competition from the peer flows, and the SSP should jointly consider the cross-layer factors and the bidding values to determine the sharing of the harvested spectrum. Besides, the network performance improvement is still hindered by the inherent single-radio of CR devices. Another issue is the mobility of CR users, which may have negative impact on the scheduled transmissions. Similar to multi-hop cellular networks, a better CRN architecture involving some fixed multi-radio CR routers may further increase the network capacity and solve the mobility problem. The more complex design of path selection algorithms associated with multi-flows in mobile CRNs will be deferred for the next chapter.

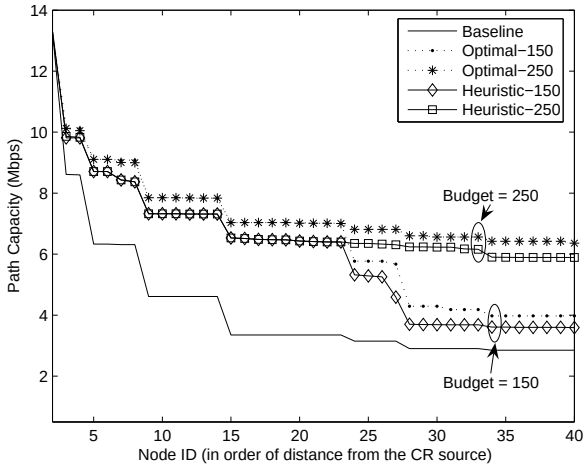

A Performance comparison among different path selection algorithms, where channel rate is 18M.

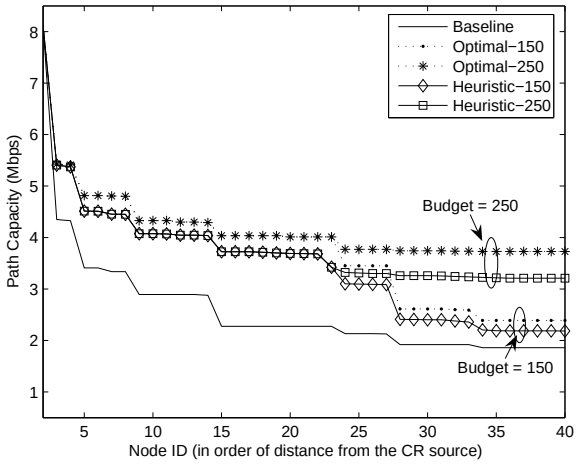

B Performance comparison among different path selection algorithms, where channel rate is 11M.

Figure 4-6. Path capacity for different path selection algorithms in CRNs.

CHAPTER 5
SPECTRUM CLOUDS: A SESSION BASED SPECTRUM TRADING SYSTEM FOR MULTI-HOP COGNITIVE RADIO NETWORKS

5.1 Chapter Overview

Nowadays, more and more people, families and companies rely on wireless services for their daily life and business, which leads to a booming growth of various wireless networks and a dramatic increase in the demand for radio spectrum. In parallel with that, current static spectrum allocation policy of Federal Communications Commission (FCC) [3, 20, 73] results in the exhaustion of available spectrum, while a lot of licensed spectrum bands are extremely under-utilized. Experimental tests in academia [9, 72] and measurements conducted in industries [70, 71] both show that even in the most crowed region of big cities (e.g., Washington, DC, Chicago, New York City, etc.), many licensed spectrum bands are not used in certain geographical areas and are idle most of the time. Those studies spur the FCC to open up licensed spectrum bands and pursue new innovative technologies to encourage dynamic use of the under-utilized spectrum [20]. As one of the most promising solutions, cognitive radio (CR) technology releases the spectrum from shackles of authorized licenses, and enables secondary users (SUs) to opportunistically access to the vacant licensed spectrum bands in either temporal or spatial domain.

The idea of opportunistic using licensed spectrum bands has initiated the spectrum trading in multi-hop cognitive radio networks (CRNs) and promoted a lot of interesting research on the design of spectrum trading systems [35, 48, 100, 124, 135, 136]. Through spectrum trading, primary users (PUs) can sell/lease/auction their vacant spectrum for monetary gains, and SUs can purchase/rent/bid the available licensed spectrum if they suffer from the lack of radio resources to support their traffic demands. However, to trade the licensed spectrum and opportunistically access to these bands, SUs' handsets have to be frequency-agile [73, 97]. It is imperative for the SUs' devices to have the CR capability such as exploring licensed spectrum bands, reconfiguring

RF, switching frequencies across a wide spectrum range (i.e., from 20 MHz to 2.5 GHz [14, 97, 110]), sending and receiving packets over non-contiguous spectrum bands, etc. Although some of the desired features may be realized in future, enormous amount of time and efforts must be spent in hardware designs and signal processing in order to implement these features in light weight radios [73, 97, 110]. In addition, to attract customers for any new technologies, there is no reason to enforce the users to replace their communication devices or to increase the complexity on the customers' side. For spectrum trading in CRNs, it is always appreciated to minimize the changes on the handsets of SUs while facilitating the spectrum trading to maximize the spectral efficiency.

Except for the harsh requirements on SUs' devices, another primary challenge for spectrum trading in multi-hop CRNs is how SUs conduct the multi-hop CR communications using the purchased spectrum. Most existing work focuses on per-user based spectrum trading [48, 124, 135, 136], i.e., each SU purchases available bands from PUs and uses the purchased spectrum for communications. Unfortunately, those spectrum trading designs are confronted with several critical problems when they are deployed in multi-hop CRNs. For instance, it is not clear whom a SU communicates with (i.e., the destination SU or the receiver is not explicitly specified); it is not clear how to find a common band between two SUs to establish communications; it is not clear what kind of quality of service (e.g., throughput, delay, rate or bandwidth requirement, etc.) can be supported. Besides, although some of prior spectrum trading systems consider the impact of frequency reuse [48, 84, 124, 135, 136], they ignore almost all the other factors, such as interference mitigation, link scheduling, flow routing, etc., which may significantly affect the performance of CR sessions in multi-hop CRNs.

To address the challenges above, in this chapter, we propose a session based spectrum trading system, *spectrum clouds*, for multi-hop CRNs. In order to facilitate the spectrum trading of SUs without CR capability, a novel network architecture and new

network entities are introduced in spectrum clouds. Under the proposed architecture of CRNs, we study the session based spectrum trading instead of per-user based spectrum trading. Given the rate requirements and bidding values[1] of candidate CR sessions, we endeavor to conduct the optimal spectrum trading under multiple constraints (e.g., the availability of spectrum bands, the competition among different CR sessions, link scheduling constraints, flow routing constraints, etc.) in multi-hop CRNs. We mathematically formulate these concerns into an optimization problem and provide both the near-optimal solution and the feasible solution in this work. Our salient contributions are listed as follows.

- Different from the architecture of traditional spectrum trading systems, we introduce a new emerging service provider, called *Secondary Service Provider* (SSP), in spectrum clouds, and assume the SSP has already established some partial infrastructure with CR mesh routers[2] at low cost to provide coverage in the area of interest. Suppose that the SSP has its own bands (i.e., basic bands) and can harvest the available licensed spectrum bands. To facilitate the accessing of SUs without CR devices, all the CR mesh routers are equipped with multiple CR radios. Under the guidance of the SSP, SUs access their nearby CR mesh routers using basic bands and deliver packets via CR mesh routers using both basic bands and harvested bands. Given rate requirements and bidding values of CR sessions with different source/destination SUs, the SSP seeks to optimally trade the spectrum with a objective of maximizing his revenue under multiple constraints in multi-hop CRNs, i.e., the spectrum availability, link scheduling and flow routing constraints.

- Similar to the multi-dimensional conflict graph illustrated in [61], we employ a 3-dimensional (3-D) conflict graph to characterize the conflict relations among CR links in spectrum clouds. Based on the 3-D conflict graph, we mathematically describe the competition among CR sessions for radio spectrum as well as the link scheduling and routing constraints. Furthermore, we formulate the optimal session based spectrum trading into the SSP's revenue maximization problem under those

[1] In this chapter, bidding values generally represent how much the SUs are willing to pay for purchasing/renting/bidding for the available spectrum, which can be used for the traffic delivery of corresponding CR sessions.

[2] In the rest of this chapter, we use the words CR router/CR mesh router/router interchangeably.

cross-layer constraints. Given all the independent sets in CRNs, we can relax the integer variables in the formulation, solve the optimization problem by linear programming, and find the upper bound of the SSP's revenue for session based spectrum trading in multi-hop CRNs.

- Since the competition relationship between any two sessions is represented by binary values, it is NP-hard to solve the formulated optimization, in which these integer constraints are involved [88, 94]. To pursue feasible solutions, we develop the heuristic *relax-and-fix* algorithms to determine the values of integer variables. Briefly speaking, we divide all the CR sessions into different sets and relax-and-fix the integer variables for CR sessions in one session set after another. If there exists a feasible solution, it yields a lower bound to the original optimization problem.

- By carrying out extensive simulations in both grid topology and random topology, we demonstrate that the proposed session based spectrum trading system has great advantages over the per-user based ones in multi-hop CRNs. We also compare the upper bound and lower bounds determined by the heuristic algorithms at different data sets, and show that the feasible solutions obtained by the proposed algorithms are really close to the optimal one in terms of the SSP's revenue.

The rest of this chapter is organized as follows. In Section 6.2, we review related work in CR community. In Section 6.3, we introduce the system architecture of spectrum clouds, corresponding network settings and related models in multi-hop CRNs. In Section 6.5, we mathematically describe link scheduling and routing constraints in spectrum clouds, formulate the session based spectrum trading under multiple constraints into an optimization problem and near-optimally solve it by linear programming. In Section 6.6, we develop the heuristic algorithms for feasible solutions. Finally, we conduct simulations and analyze the performance results in Section 6.7, and draw concluding remarks in Section 6.8.

5.2 Related Work

Prior work has investigated spectrum trading issues from different aspects. Specifically, in [35], Grandblaise et al. generally describe the potential scenarios and introduce some microeconomics inspired spectrum trading mechanisms, and in [100], Sengupta and Chatterjee propose an economic framework for opportunistic spectrum

accessing to guide the design of dynamic spectrum allocation algorithms as well as service pricing mechanisms. From the view of the PUs, Xing et al. in [125] and Niyato et al. in [75, 76] have well investigated the spectrum pricing issues in the spectrum market, where multiple PUs, whose goal is to maximize the monetary gains with their vacant spectrum, compete with each other to offer spectrum access to the SUs. From the view of the SUs, Pan et al. in [85, 87] have addressed how the SUs optimally distribute their traffic demands over the spectrum bands to reduce the risk for monetary loss, when there is more than one vacant licensed spectrum band. From the view of trading system design, models in game theory, by Wang et al. in [119, 120], Pan et al. in [84] and Zhang et al. in [132], and auction designs in microeconomics, by Zhou et al. in [135–137], Jia et al. in [48], Pan et al. in [86] and Wu et al. in [124], are exploited to construct spectrum trading systems with desired properties, such as power efficiency, allocation fairness, incentive compatibility, Pareto efficiency, collusion resistance and so on. Although these designs consider certain features of wireless transmissions, they are generally per-user based spectrum trading systems rather than session based ones.

The impact of multiple sessions on the performance of multi-hop wireless networks has been extensively investigated in existing literature. Jian et al. in [45] studied how the interference affects the performance of ad-hoc networks based on an NP-complete optimization problem. Zhai and Fang in [131] developed a high throughput routing metric under link scheduling and routing constraints in single-radio single-channel networks. In multi-radio multi-channel networks, Li et al. in [61] proposed a multi-dimensional conflict graph and exploited it to efficiently solve the optimal network throughput problem using linear programming. In CR research community, there have been some efforts devoted to cross-layer optimization as well. Tang et al. in [114] studied the joint spectrum allocation and link scheduling problems with the objectives of maximizing throughput and achieving certain fairness in CRNs. Hou et al. in [43, 108] investigated

the joint frequency scheduling[3] and routing problem with the objective of minimizing the network-wide spectrum usage in CRNs. Considering the uncertain spectrum supply, Pan et al. in [88] proposed to model the vacancy of licensed bands as a series of random variables, characterized the multi-hop CRNs with a pair of (α, β) parameters and minimized the usage of licensed spectrum to support CR sessions with rate requirements at certain confidence levels. However, there remains a lack of study to incorporate these multi-hop transmission concerns into the design of spectrum trading systems.

In this work, we are trying to bridge the gap between these two active research areas in multi-hop CRNs. With the proposed spectrum trading system, spectrum clouds, we have a comprehensive study on the optimal spectrum trading problem considering multiple factors including the competition among CR sessions, the availability of spectrum, link scheduling, flow routing, etc. Our work effectively extends the per-user based spectrum trading into the session based spectrum trading and makes those microeconomics inspired spectrum trading mechanisms practically applicable in multi-hop CRNs.

5.3 Network Model

5.3.1 System Architecture for Spectrum Clouds

We consider the proposed spectrum trading system in multi-hop CRNs, spectrum clouds, consisting of the SSP, a group of SUs, a set of CR mesh routers and a collection of available licensed spectrum bands[4] with unequal size of bandwidths as shown in

[3] In this chapter, frequency scheduling refers to the scheduling in frequency domain or means frequency band allocation, and link scheduling refers to the scheduling in time domain.

[4] Taking the least-utilized spectrum bands introduced in [43] for example, we found that the bandwidth between [1240, 1300] MHz (allocated to amateur radio) is 60 MHz, while bandwidth between [1525, 1710] MHz (allocated to mobile satellites, GPS systems, and meteorological applications) is 185 MHz.

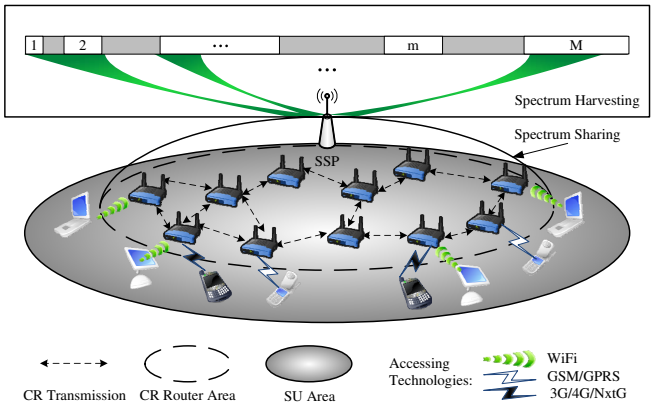

A System architecture for spectrum clouds.

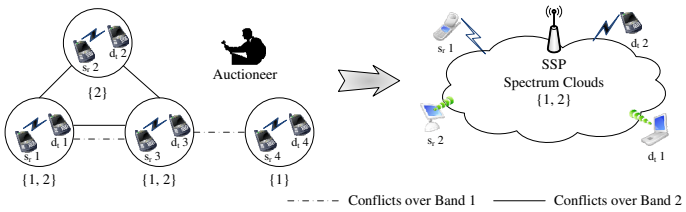

B A schematic for comparison between traditional spectrum trading mechanisms and spectrum clouds.

Figure 5-1. A novel architecture for spectrum trading in multi-hop CRNs.

Fig. 5-1A. The SSP is an independent wireless service provider (e.g., a base station or an access point) with its own spectrum, i.e., the SSP's basic bands (potentially congested already), and is able to collectively harvest the available licensed bands. The SSP has also deployed some CR mesh routers at low cost to facilitate the accessing of SUs. SUs are just end-users not subscribed to primary services. No specific requirements are imposed on the SUs' communication devices. They could be any devices using any accessing technologies (e.g. laptops or desktop computers using Wi-Fi, cell phones using GSM/GPRS, smart phones using 3G/4G/NxtG accessing technology, etc.). SUs can access to the basic bands owned by the SSP, but they cannot be tuned to the harvested licensed frequency. The CR mesh routers deployed by the SSP have CR capability and are equipped with multiple CR radios.

Under spectrum clouds' architecture, the mobile SUs report their online traffic requests, which include source/destination, rate requirements and corresponding

bidding values of the SUs' sessions, to their nearby CR mesh routers via basic bands. The fixed CR mesh routers collect these requests from different end-users and report them to the SSP. Depending on the bidding values, rate requirements and the available spectrum resources, the SSP makes decisions on the accessing/denial of the SUs' sessions, and jointly conducts link scheduling and flow routing among CR mesh routers for SUs' traffic delivery. Following the guidance of the SSP, the CR mesh routers form unicast CR communication sessions and deliver packets using both the leftover basic bands and harvested bands as shown in Fig. 5-1A.

In traditional spectrum trading systems, the spectrum bands to sell/lease/auction are known to every SU. Due to broadcasting nature of wireless transmissions, the SU may also know his potential competitors and overhear their bids, so that many schemes are proposed to ensure that the spectrum trading is not manipulated in multi-hop CRNs [124, 135]. By contrast, in spectrum clouds, the SU has no idea about the specific spectrum allocation across the whole session (i.e., from the source to the destination). Even if a SU overhears the bids of other SUs, it is not helpful since the SU is not sure who are his competitors for spectrum usage. Besides, spectrum clouds can support session based spectrum trading in multi-hop CRNs, whereas the other systems can only support single-hop spectrum trading as shown in Fig. 5-1B.

5.3.2 Network Configuration

Suppose there are $\mathcal{N} = \{1, 2, \cdots, n, \cdots, N\}$ CR mesh routers, each CR mesh router has $\mathcal{H} = \{1, 2, \cdots, h, \cdots, H\}$ radio interfaces, and these CR mesh routers form a set of $\mathcal{L}$ unicast communication sessions according to SUs' requests. Each session has a rate requirement and a corresponding bidding value. Denote the source/destination CR router of session $l \in \mathcal{L} = \{1, 2, \cdots, l, \cdots, L\}$ by $s_r(l)/d_t(l)$, and let $(r(l), b(l))$ be the rate requirement-bidding value pair for session $l \in \mathcal{L}$. Assume the SUs' usage of basic bands in the multi-hop CRNs is a *priori* information. The CR routers are able to use the rest of basic spectrum owned by the SSP. The CR routers are also allowed

to communicate with each other by opportunistically accessing to the licensed bands when the primary services are not active, but they must evacuate from these bands immediately when primary services become active. Considering the geographical location of the CR routers, the available spectrum bands at one CR router may be different from another one in the network. To put it in a mathematical way, let $\mathcal{M} = \{1, 2, \cdots, m \cdots, M\}$ be the band set including the available basic bands and licensed bands with different bandwidths $\mathcal{W} = \{W^1, W^2, \cdots, W^m, \cdots, W^M\}$ for communications, and $\mathcal{M}_i \subseteq \mathcal{M}$ represent the set of available bands at CR router $i \in \mathcal{N}$. $\mathcal{M}_i$ may be different from $\mathcal{M}_j$, where j is not equal to i, and $j \in \mathcal{N}$, i.e., possibly $\mathcal{M}_i \neq \mathcal{M}_j$.

5.3.3 Other Related Models in Multi-hop CRNs

5.3.3.1 Transmission range and interference range

Suppose all CR mesh routers use the same power P for transmission. The power propagation gain [23, 33, 43] is

$$g_{ij} = \gamma \cdot d_{ij}^{-\alpha}, \tag{5–1}$$

where α is the path loss factor, γ is an antenna related constant, and d_{ij} is the distance between CR routers i and j. We assume that the data transmission is successful only if the received power at the receiver exceeds the receiver sensitivity, i.e., a threshold P_T. Meanwhile, we assume interference becomes non-negligible only if it is over a threshold of P_I at the receiver. Thus, the transmission range for a CR router is $R_T = (\gamma P/P_T)^{1/\alpha}$, which comes from $\gamma \cdot (R_T)^{-\alpha} \cdot P = P_T$. Similarly, based on the interference threshold $P_I (P_I < P_T)$, the interference range for a CR router is $R_I = (\gamma P/P_I)^{1/\alpha}$. It is obvious that $R_I > R_T$ since $P_I < P_T$.

In the widely used protocol model [37, 43, 61, 88, 114, 131], the interference range is typically 2 or 3 times of the transmission range, i.e., $\frac{R_I}{R_T} = 2$ or 3. These two ranges may vary with frequency. The conflict relationship between two links over the same frequency band can be determined by the specified interference range. In addition, if the

interference range is properly set, the protocol model can be accurately transformed into the physical model as illustrated in [109].

5.3.3.2 Link capacity and achievable data rate

According to Shannon-Hartley theorem, if CR router i sends data to CR router j on link (i, j) with band m, the capacity of link (i, j) with band m is

$$c_{ij}^{m} = W^{m} \log_2 \left(1 + \frac{g_{ij} P}{\eta}\right), \tag{5–2}$$

where η is the ambient Gaussian noise power at CR mesh router j[5] . Depending on different modulation schemes, the achievable data rate is actually determined by the SNR at the receiver and receiver sensitivity [16, 131]. However, in most of existing literature [43, 61, 88, 103, 104], the achievable data rate is approximated by (5–2), even though this data rate can never be achieved in practical. In this chapter, we follow the same approximation. Note that this approximation will not affect the theoretical analysis or performance comparison in this work.

5.3.3.3 Uncertain spectrum supply

5.4 Optimal Spectrum Trading under Cross-layer Constraints in Multi-hop CRNs

We exploit binary value $\delta(l)$ to denote the success/failure of spectrum trading for session l, i.e.,

$$\delta(l) = \begin{cases} 1, & \text{session } l \text{ is accessed by the SSP;} \\ 0, & \text{session } l \text{ is denied by the SSP.} \end{cases} \tag{5–3}$$

[5] Note that the denominator inside the log function contains only η. This is because of one of our interference constraints, i.e., when CR router i is transmitting to CR router j on band m, then all the other neighbors of router j within its interference range are prohibited from using this band. We will address the interference constraints in details in the following section.

To make the decision of accessing/denying a session $l \in \mathcal{L}$, the SSP must consider both the rate requirement and bidding value of session l. Besides, to effectively utilize the leftover basic spectrum and the harvested licensed spectrum, it is necessary for the SSP to schedule data transmission among different CR mesh routers under joint spectrum assignment, link scheduling and flow routing constraints. In the rest of this section, we first extend the conflict graph [10, 131] to characterize the interference relationship among CR links in spectrum clouds. Then, based on the extended conflict graph, we mathematically describe link scheduling and flow routing constraints and formulate the spectrum trading into the revenue maximization problem of the SSP under multiple constraints. By relaxing the integral variables, we solve the optimization problem and provide an upper-bound of the SSP's revenue.

5.4.1 Extended Conflict Graph, Cliques and Independent Sets

5.4.1.1 Construction of 3-dimensional conflict graph

Regarding the availability of spectrum bands and radios at CR mesh routers, we introduce a 3-D conflict graph to characterize the interference relationship among CR links in spectrum clouds. Following the definitions in [61], we interpret a CRN as a three-dimensional resource space, with dimensions defined by links, the set of available bands and the set of available radios. In a 3-D conflict graph $\mathcal{G}(\mathcal{V}, \mathcal{E})$, each vertex corresponds to a link-band-radio (LBR) tuple, i.e.,

$$\text{link-band-radio:} \quad ((i, j), m, (u, v)),$$

where $i \in \mathcal{N}$, $m \in \mathcal{M}_i \bigcap \mathcal{M}_j$, $j \in \mathcal{T}_i^m$, $u \in \mathcal{H}_i$ and $v \in \mathcal{H}_j$. Here, $\mathcal{T}_i^m$ is the set of CR mesh routers within CR router i's transmission range. The LBR tuple indicates that the CR router i transmits data to CR router j on band m, where radio interfaces u and v are used at sending CR router and receiving CR router, respectively. Based on the definition of LBR tuples, we can enumerate all combinations of CR mesh routers, the

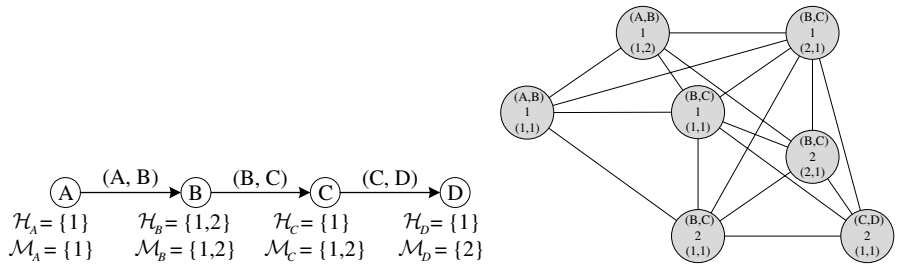

A Toy topology in spectrum clouds. B 3-D conflict graph.

Figure 5-2. Conflict relationship represented by 3-D conflict graph in CRNs.

vacant bands and the available radios, which can potentially enable CR communication links.

Different from multi-radio multi-channel networks [61], the availability of bands and radios (i.e., the leftover radios after collecting SUs' traffic) at each CR router in CRNs may be different, i.e., for $i, j \in \mathcal{N}$, maybe $\mathcal{M}_i \neq \mathcal{M}_j$ and $\mathcal{H}_i \neq \mathcal{H}_j$. Similar to the interference conditions in [43, 61, 88], two LBR tuples are defined to interfere with each other if either of the following conditions is true: (i) if two different LBR tuples are using the same band, the receiving CR router of one tuple is in the interference range of the transmitting CR router in the other tuple; (ii) two different LBR tuples have the same radios at one or two CR routers.

Note that the first condition not only represents co-band interference but also inherently covers the following two cases: any CR router cannot transmit to multiple routers on the same band; any CR router cannot use the same band for concurrent transmission and reception, due to "self-interference" at the physical layer. Meanwhile, the second condition represents the radio interface conflicts, i.e., a single radio cannot support multiple transmissions (either transmitting or receiving) simultaneously. According to these conditions, we connect two vertices in $\mathcal{V}$ with an undirected edge in $\mathcal{G}(\mathcal{V}, \mathcal{E})$, if their corresponding LBR tuples interfere with each other.

For illustrative purposes, we take a simple example to show how to construct a 3-D conflict graph. In this toy CRNs, we assume there are four CR routers with CR

transceivers, i.e., A, B, C and D, and two bands, i.e., band 1 and band 2. Depending on the geographic locations, the set of currently available bands and radios at one CR router may be different from that at another CR router. For example, the currently available band and radio sets for A are $\mathcal{M}_A = \{1\}$ and $\mathcal{H}_A = \{1\}$, and the band and radio sets for B are $\mathcal{M}_B = \{1, 2\}$ and $\mathcal{H}_B = \{1, 2\}$. Furthermore, we use $d(\cdot)$ to represent Euclidean distance and suppose that $d(A, B) = d(B, C) = d(C, D) = d(D, E) = R_T = 0.5R_I$. Given the above assumptions, we can establish the corresponding 3-D conflict graph as depicted in Fig. 5-2B. Here, each vertex corresponds to an LBR tuple, for example, vertex $((A, B), 1, (1, 1))$ corresponds to LBR tuple $((A, B), 1, (1, 1))$. Note that there is edge between vertices $((A, B), 1, (1, 1))$ and $((B, C), 1, (2, 1))$ because (A, B) is incident to (B, C) over band 1. There is an edge between vertices $((A, B), 1, (1, 1))$ and $((B, C), 2, (1, 1))$ because they share a radio in common at CR router B. Similar analysis applies to the other vertices in the conflict graph as well.

5.4.1.2 Three dimensional independent sets and conflict cliques

Given a 3-D conflict graph $\mathcal{G} = (\mathcal{V}, \mathcal{E})$ representing spectrum clouds, we describe the impact of vertex $i \in \mathcal{V}$ on vertex $j \in \mathcal{V}$ as follows,

$$w_{ij} = \begin{cases} 1, & \text{if there is an edge between vertex } i \text{ and } j \\ 0, & \text{if there is no edge between vertex } i \text{ and } j, \end{cases} \tag{5–4}$$

where two vertices correspond to two LBR tuples, respectively.

Provided that there is a vertex set $\mathcal{I} \subseteq \mathcal{V}$ and an LBR tuple $i \in \mathcal{I}$ satisfying $\sum_{j \in \mathcal{I}, i \neq j} w_{ij} < 1$, the transmission at LBR tuple i will be successful even if all the other LBR tuples in the set $\mathcal{I}$ are transmitting at the same time. If any $i \in \mathcal{I}$ satisfies the condition above, we can schedule the transmissions over all these LBR tuples in $\mathcal{I}$ to be active simultaneously. Such a vertex/LBR tuple set $\mathcal{I}$ is called a 3-D independent set. If adding any one more LBR tuple into a 3-D independent set $\mathcal{I}$ results in a non-independent one, $\mathcal{I}$ is defined as a maximal 3-D independent set. Besides, if

there exists a vertex/LBR tuple set $\mathcal{Z} \subseteq \mathcal{V}$ and any two vertexes i and j in $\mathcal{Z}$ satisfying $w_{ij} \neq 0$ (i.e., LBR tuples i and j cannot be scheduled to transmit successfully at the same time.), $\mathcal{Z}$ is called a 3-D conflict clique. If $\mathcal{Z}$ is no longer a 3-D conflict clique after adding any one more LBR tuple, $\mathcal{Z}$ is defined as a maximal 3-D conflict clique.

5.4.2 CR Link Scheduling and Flow Routing Constraints

5.4.2.1 CR link scheduling constraints

Link scheduling can be conducted in time domain, in frequency domain or in both of them [43, 88]. In this chapter, we only focus on time based link scheduling.

Given the 3-D conflict graph $\mathcal{G} = (\mathcal{V}, \mathcal{E})$ constructed from the spectrum clouds, suppose we can list all maximal 3-D independent sets[6] as $\mathfrak{I} = \{\mathcal{I}_1, \mathcal{I}_2, \cdots, \mathcal{I}_q, \cdots, \mathcal{I}_Q\}$, where Q is $|\mathfrak{I}|$, and $\mathcal{I}_q \subseteq \mathcal{V}$ for $1 \leq q \leq Q$. At any time, at most one maximal 3-D independent set can be active to transmit packets for all LBR tuples in that set. Let $\lambda_q \geq 0$ denote the time share scheduled to the maximal 3-D independent set $\mathcal{I}_q$, and

$$\sum_{1 \leq q \leq Q} \lambda_q \leq 1, \quad \lambda_q \geq 0 \, (1 \leq q \leq Q). \tag{5–5}$$

Let $r_{ij}^m(\mathcal{I}_q)$ be the data rate for CR link (i, j) over band m, where $r_{ij}^m(\mathcal{I}_q) = 0$ if LBR tuple $((i, j), m, (u, v)) \notin \mathcal{I}_q$; otherwise, $r_{ij}^m(\mathcal{I}_q)$ is the achievable data rate for CR link (i, j) over band m, which can be calculated from (5–2). Therefore, by exploiting the 3-D maximal independent set $\mathcal{I}_q$, the flow rate that link (i, j) can support over band m in the time share λ_q is $\lambda_q r_{ij}^m(\mathcal{I}_q)$. Let $f_{ij}(l)$ represent the flow rate of the session l over link (i, j), where $i \in \mathcal{N}$, $l \in \mathcal{L}$ and $j \in \bigcup_{m \in \mathcal{M}_i} \mathcal{T}_i^m$. Then, the trading CR sessions are feasible at link

[6] It is a NP-complete problem to find all maximal independent sets in $\mathcal{G}$ [15, 29, 61], which will be further addressed later in this chapter. In this subsection, we make the assumption we could find all the maximal independent sets just for the convenience of our theoretical analysis.

(i, j) if there exists a schedule of the maximal 3-D independent sets satisfying

$$\sum_{l \in \mathcal{L}}^{s_r(l) \neq j, d_t(l) \neq i} f_{ij}(l)\delta(l) \leq \sum_{q=1}^{|\mathfrak{I}|} \lambda_q \sum_{m \in \mathcal{M}_i \bigcap \mathcal{M}_j} r_{ij}^m(\mathcal{I}_q)\tau_{ij}^m. \tag{5–6}$$

5.4.2.2 Bandwidth required at α

Before we re-formulate the problem, we must quantify the bandwidth required for OSA when the vacancy of the licensed band is uncertain and modeled as a random variable. Thus, we leverage parameter α to define bandwidth required at α for OSA. Inspired by the mathematical expression of value at risk (VaR) in [39], we use $X_\alpha(w)$ to denote bandwidth required at α and define it as follows.

$$\begin{cases} H_W(\tau) = \int_{-\infty}^{\tau} h_W(w)dw, & \tau \in \mathcal{R} \\ X_\alpha(W) = \inf\{\tau : H_W(\tau) \geq \alpha\}, & \alpha \in [0, 1]. \end{cases} \tag{5–7}$$

From (5–7), we find that the available bandwidth of the licensed bandwidth integration for OSA is less than $X_\alpha(W)$ at confidence level α.

5.4.2.3 CR routing constraints

As for routing, the SSP will help the source CR mesh router to find the available paths and employ a number of relay CR mesh routers to forward the data packets toward its destination CR mesh router. It is obvious that there should be more than one path involved in data delivery since multi-path routing[7] is more flexible to route the traffic from a source router to its destination. Similar to the modeling in [43, 88], we mathematically present routing constraints as follows.

[7] The multiple radios of CR routers allow for multi-path routing.

To simplify the notation, let $\mathcal{T}_i = \bigcup_{m \in \mathcal{M}_i} \mathcal{T}_i^m$. If CR mesh router i is the source router of session l, i.e., $i = s_r(l)$, then

$$\sum_{j \in \mathcal{T}_i} f_{ji}(l) = 0. \tag{5–8}$$

$$\sum_{j \in \mathcal{T}_i} f_{ij}(l)\delta(l) = r(l)\delta(l), \tag{5–9}$$

where $\delta(l) \in \{0, 1\}$ indicates whether session l is accepted by the SSP (i.e., session l wins the opportunity for data transmission via spectrum trading) or not.

If CR mesh router i is an intermediate relay router of session l, i.e., $i \neq s_r(l)$ and $i \neq d_t(l)$, then

$$\sum_{j \in \mathcal{T}_i}^{j \neq s_r(l)} f_{ij}(l)\delta(l) = \sum_{p \in \mathcal{T}_i}^{p \neq d_t(l)} f_{pi}(l)\delta(l). \tag{5–10}$$

If CR mesh router i is the destination router of session l, i.e., $i = d_t(l)$, then

$$\sum_{j \in \mathcal{T}_i} f_{ji}(l)\delta(l) = r(l)\delta(l). \tag{5–11}$$

Note that if (6–11), (5–9) and (6–14) are satisfied, it can be easily verified that (6–15) must be satisfied. As a result, it is sufficient to list only (6–11), (5–9) and (6–14) as CR routing constraints in spectrum clouds.

5.4.3 Optimal Spectrum Trading under Multiple Constraints

In order to optimally trade spectrum resources and determine the access/denial of certain CR sessions, the SSP must consider the rate requirements and bidding values of CR sessions, the competition among different CR sessions, the availability of bands (including the SSP's leftover spectrum and the harvested spectrum) and the efficient utilization of spectrum resources. Thus, the SSP seeks for a feasible solution to trading the available frequency bands, assigning these bands to CR mesh routers, scheduling bands for CR transmission and reception and routing those CR flows so

that the revenue of the SSP is maximized and radio spectrum resources are efficiently utilized in multi-hop CRNs.

With the proposed trading system, spectrum clouds, the optimal spectrum trading problem under multiple constraints in multi-hop CRNs can be formulated as follows.

$$\text{Maximize} \sum_{l \in \mathcal{L}} b(l)\delta(l)$$

$$\text{s.t.:} \quad \sum_{j \in \mathcal{T}_i} f_{ji}(l) = 0 \qquad (l \in \mathcal{L}, i = s_r(l)) \tag{5–12}$$

$$\sum_{j \in \mathcal{T}_i} f_{ij}(l)\delta(l) = r(l)\delta(l) \qquad (l \in \mathcal{L}, i = s_r(l)) \tag{5–13}$$

$$\sum_{j \in \mathcal{T}_i}^{j \neq s_r(l)} f_{ij}(l)\delta(l) = \sum_{p \in \mathcal{T}_i}^{p \neq d_t(l)} f_{pi}(l)\delta(l)$$
$$(l \in \mathcal{L}, i \in \mathcal{N}, i \neq s_r(l), d_t(l)) \tag{5–14}$$

$$\sum_{l \in \mathcal{L}}^{s_r(l) \neq j, d_t(l) \neq i} f_{ij}(l)\delta(l) \leq \sum_{q=1}^{|\mathfrak{I}|} \lambda_q X_\alpha \Big(\sum_{m \in \mathcal{M}_i \bigcap \mathcal{M}_j} r_{ij}^m(\mathcal{I}_q)\tau_{ij}^m \Big)$$
$$(i \in \mathcal{N}, j \in \mathcal{T}_i, m \in \mathcal{M}_i \bigcap \mathcal{M}_j \text{ and } \mathcal{I}_q \in \mathfrak{I}) \tag{5–15}$$

$$\sum_{q=1}^{|\mathfrak{I}|} \lambda_q \leq 1, \;\; \lambda_q \geq 0 \qquad (\mathcal{I}_q \in \mathfrak{I}) \tag{5–16}$$

$$f_{ij}(l) \geq 0 \;\; (l \in \mathcal{L}, i \in \mathcal{N}, i \neq d_t(l), j \in \mathcal{T}_i, j \neq s_r(l)) \tag{5–17}$$

$$\delta(l) \in \{0, 1\} \qquad (l \in \mathcal{L}), \tag{5–18}$$

where $\delta(l)$, $f_{ij}(l)$ and λ_q are optimization variables, and $r(l)$ is deterministic value when session l is given. Here, (6–16), (6–17) and (6–18) specify the routing constraints in spectrum clouds. (6–20) and (6–21) indicate that the flow rates over link (i, j) cannot exceed the capacity of this CR link, which is obtained from the CR link scheduling as illustrated in Sec. 5.4.2. Note that $\mathfrak{I}$ includes all independent sets in CRNs. Given all the

maximal 3-D independent sets[8] in $\mathcal{G}(\mathcal{V}, \mathcal{E})$, we find that the formulated optimization is a mixed-integer linear programming (MILP) problem, which is NP-hard to solve as proved in [29, 94].

5.5 The Upper Bound for the Session Based Spectrum Trading Optimization

The complexity of the optimization above arises from two parts: (i) identifying all the maximal independent sets and (ii) fixing the binary $\delta(l)$ variables. To find all the maximal independent sets/cliques itself is NP-complete, but it is not a unique problem in spectrum clouds. It has been well investigated in prior multi-hop wireless networks and many approximation algorithms have been proposed in existing literature [61, 62, 131]. For example, one of the typical approaches is to employ K ($0 \leq K \leq |\mathfrak{I}|$) maximal independent sets (or a number of maximal conflict cliques) for approximation instead of finding out all the maximal independent sets in $\mathcal{G}(\mathcal{V}, \mathcal{E})$.

On the other hand, $\delta(l)$ variables will be involved as long as the SSP conducts the session based spectrum trading in multi-hop CRNs. Given all the maximal independent sets, we relax the binary requirement on $\delta(l)$ and replace it with $0 \leq \delta(l) \leq 1$ to reduce the complexity for the cross-layer optimization. Due to the enlarged optimization space (caused by relaxation on $\delta(l)$), the solution to this relaxed optimization problem yields an upper bound for the SSP's revenue maximization problem. Although the upper bound may not be achieved by a feasible solution, it can play as a benchmark to evaluate the quality of feasible solutions.

5.6 A Bidding Value-Rate Requirement Ratio Based Heuristic Algorithm for Spectrum Trading

In order to find feasible solutions, in this section, we propose a bidding value-rate requirement ratio (BVR[3]) based heuristic algorithm for the SSP's revenue maximization

[8] That is a general assumption used in existing literature [10, 61, 114, 115, 131] for obtaining throughput bounds or performance comparison.

problem. According to the bidding values and rate requirements of candidate trading sessions, we make the SSP classify those CR sessions into different categories in terms of decreasing access possibility. Then, we sequentially fix the $\delta(l)$-variables in different sets and give a heuristic solution, which is also a lower bound for the original MILP problem.

5.6.1 The BVR^3 Based Relax-and-Fix Algorithm

The key to simplifying the NP-hard optimization, fixing flow routing (i.e., $f_{ij}(l)$-variables) and link scheduling (i.e., λ_q-variables), and attaining a feasible solution is the determination of the binary values for the $\delta(l)$-variables [43, 88]. Although we can employ the classical branch-and-bound approach to determine $\delta(l)$-variables, the number of iterations involved in that algorithm grows exponentially with $|\mathcal{L}|$. To reduce the complexity, we propose a BVR^3 based *relax-and-fix* algorithm [94]. The intuition behind the proposed algorithm is that given the leftover basic spectrum and the harvested spectrum, the SSP would like to take the best use of spectrum resources to make as much revenue as possible. That can be roughly interpreted as the SSP prefers to access the CR session with large bidding value and small rate requirements in spectrum clouds. The detailed procedure of the heuristic algorithm for the SSP's revenue maximization is presented as follows.

Based on bidding values and rate requirements of candidate CR sessions, we first sort all the CR sessions in terms of $\frac{b(l)}{r(l)}$ and partition these sessions into S disjoint session sets $\mathcal{L}^1, \mathcal{L}^2, \cdots, \mathcal{L}^S$ in the order of decreasing BVR^3, where $\bigcup_{s\in\mathcal{S}} \mathcal{L}^s = \mathcal{L}$ and $\mathcal{S} = \{1, 2, \cdots, S\}$. The BVR^3 of the session in $\mathcal{L}^i$ is larger than that of the session in $\mathcal{L}^j$, if i is less than j ($\forall\, i, j \in \mathcal{S}$).

Then, we create auxiliary session sets by choosing subsets $\mathcal{A}^s$ with $\mathcal{A}^s \subseteq \bigcup_{u=s+1}^{S} \mathcal{L}^u$ for $s \in \{1, 2, \cdots, S-1\}$. For example, in the spectrum trading problem, $\mathcal{L}^1$ may include the $\delta(l)$-variables associated with candidate trading sessions in $\{1, 2, \cdots, l_1\}$, $\mathcal{L}^2$ may be

associated with sessions in $\{l_1+1, l_1+2, \cdots, l_2\}$, and so on, whereas $\mathcal{A}^1$ would include the $\delta(l)$-variables associated with sessions in $\{l_1+1, l_1+2, \cdots, a_1\}$, and so on.

By leveraging partitioned session sets (i.e., $\mathcal{L}^s$) and auxiliary session sets (i.e., $\mathcal{A}^s$), we sequentially solve $|\mathcal{S}|$ relaxed-MILPs (R-MILPs) (denoted by *R-MILP* ^{s} with $1 \leq s \leq |\mathcal{S}|$), determine the δ-variables in $\mathcal{L}^s$ ($s \in \mathcal{S}$) and find a heuristic solution to the original MILP problem. Specifically, in the first R-MILP, *R-MILP* ^{1}, we only impose the binary requirement on the $\delta(l)$-variables for session l in $\mathcal{L}^1 \cup \mathcal{A}^1$ and relax the integrality restriction on all the other $\delta(l)$-variables for session l in $\mathcal{L}$. Thus, we have

$$\textit{R-MILP}^1 \qquad \text{Maximize} \sum_{l \in \mathcal{L}} b(l)\delta(l)$$

$$\begin{aligned}
\text{s.t.:} \quad & (6--16),\ (6--17),\ (6--18),\ (6--20),\ (6--21),\ (5--17) \\
& \delta(l) \in \{0,1\} \qquad (\forall\, l \in \mathcal{L}^1 \cup \mathcal{A}^1) \\
& \delta(l) \in [0,1] \qquad (\forall\, l \in \mathcal{L} \backslash (\mathcal{L}^1 \cup \mathcal{A}^1))
\end{aligned}$$

Let $\{\hat{\delta}^1(1), \cdots, \hat{\delta}^1(l), \cdots, \hat{\delta}^1(L)\}$ be an optimal solution to *R-MILP*^{1}. We can fix the $\delta(l)$-variables in $\mathcal{L}^1$ at their corresponding binary values, i.e., $\delta(l) = \hat{\delta}^1(l) \in \{0,1\}$ for all $l \in \mathcal{L}^1$. Then, we move to *R-MILP*^{2}.

In the subsequent *R-MILP*^{s} (for $2 \leq s \leq S$), we sequentially fix the binary values of the $\delta(l)$-variables for sessions in $\mathcal{L}^{s-1}$ from the solution to *R-MILP*$^{s-1}$. After that, we further add the binary restriction for the $\delta(l)$-variables in $\mathcal{L}^s \cup \mathcal{A}^s$, and we have

$$\textit{R-MILP}^s \qquad \text{Maximize} \sum_{l \in \mathcal{L}} b(l)\delta(l)$$

$$
\begin{aligned}
\text{s.t.:} \quad & (6--16),\ (6--17),\ (6--18),\ (6--20),\ (6--21),\ (5--17) \\
& \delta(l) = \hat{\delta}^{s-1}(l) \qquad (\forall\, l \in \mathcal{L}^1 \cup \cdots \cup \mathcal{L}^{s-1}) \\
& \delta(l) \in \{0,1\} \qquad (\forall\, l \in \mathcal{L}^s \cup \mathcal{A}^s) \\
& \delta(l) \in [0,1] \qquad (\forall\, l \in \mathcal{L} \backslash (\mathcal{L}^1 \cup \cdots \cup \mathcal{L}^s \cup \mathcal{A}^s)).
\end{aligned}
$$

Either *R-MILP*^{s} is infeasible for certain $s \in \mathcal{S}$ and the heuristic algorithm has failed, or else the proposed BVR^3 based relax-and-fix algorithm provides a feasible solution (i.e., the solution to *R-MILP*$^{|\mathcal{S}|}$) to the original MILP problem. The procedure of the proposed heuristic algorithm is summarized in Alg. 4.

Algorithm 4 The BVR^3 based relax-and-fix algorithm

```
Sort all the CR sessions in terms of BVR^3, i.e., b(l)/r(l).
Partition all these sessions into S disjoint session sets, denoted by L^s (s ∈ S = {1, 2, ··· , S} and L^s ⊂ L).
Create auxiliary session sets A^s ⊆ ⋃_{u=s+1}^{S} L^u.
Set s = 1 and relax binary requirement on δ(l)-variables.
for all s ∈ S do
    Impose binary requirement on the δ(l)-variables for session l ∈ L^s ∪ A^s.
    Using L^s and A^s, solve the relaxed R-MILP^s.
    if R-MILP^s has a feasible solution then
        Determine the δ-variables in L^s.
        s = s + 1. continue
    else
        Return there is no feasible solution.
    end if
end for
Output the solution to R-MILP^|S| as a feasible solution to the original MILP.
```

For illustrative purposes, we take a multi-hop CRN consisting of 7 candidate trading CR sessions as an example. We sort these sessions by BVR^3 and divide them into 4 disjoint session sets, i.e., $|\mathcal{S}| = 4$. We conduct the BVR^3 based relax-and-fix algorithm with the following sets $\mathcal{L}^s$ and $\mathcal{A}^s$: $\mathcal{L}^1 = \{1,2\}$, $\mathcal{L}^2 = \mathcal{A}^1 = \{3,4\}$, $\mathcal{L}^3 = \mathcal{A}^2 = \{5,6\}$, and $\mathcal{L}^4 = \mathcal{A}^3 = \{7\}$. The iterations of the heuristic algorithm are as follows.

- In the first *R-MILP*^{1}, the $\delta(l)$-variables associated with sessions in $\{1, \cdots, 4\}$ (i.e., in $\mathcal{L}^1 \cup \mathcal{A}^1$) are restricted to be binary values, the other $\delta(l)$-variables being relaxed.

- From the solution to *R-MILP*^{1}, we can fix the $\delta(l)$-variables corresponding to the sessions in $\{1, 2\}$ (i.e., in $\mathcal{L}^1$). With the determined $\delta(l)$-variables for sessions in $\mathcal{L}^1$, we continue to solve *R-MILP*^{2} where the $\delta(l)$-variables associated with sessions in $\{3, \cdots, 6\}$ (i.e., in $\mathcal{L}^2 \cup \mathcal{A}^2$) are now integer and $\delta(l)$-variables in $\{7\}$ (i.e., in $\mathcal{L} \backslash (\mathcal{L}^1 \cup \mathcal{L}^2 \cup \mathcal{A}^2)$) are relaxed.

- From the solution to *R-MILP*^{2}, we can additionally fix the $\delta(l)$-variables corresponding to the sessions in $\{3, 4\}$ (i.e., in $\mathcal{L}^2$). Similarly, we can solve *R-MILP*^{3} where the $\delta(l)$-variables associated with sessions in $\{5, 6, 7\}$ (i.e., in $\mathcal{L}^3 \cup \mathcal{A}^3$) are now binary and there are no $\delta(l)$-variables to relax because $\mathcal{L} \backslash (\mathcal{L}^1 \cup \mathcal{L}^2 \cup \mathcal{L}^3 \cup \mathcal{A}^3) = \phi$.

- Based on the optimal solution to *R-MILP*^{3}, we can easily determine the value of $\delta(l)$ in $\{7\}$ and determine whether there is feasible solution to the original MILP.

The basic idea of the BVR^3 based relax-and-fix algorithm is explicitly explained in the example. At each iteration, we solve a *R-MILP*^{s} problem involving $\mathcal{L}^s \cup \mathcal{A}^s$ sessions and to avoid being too myopic we then only fix the $\delta(l)$-variables corresponding to sessions in $\mathcal{L}^s$. The auxiliary session sets $\mathcal{A}^s$ smooth the heuristic solution by creating some overlap between successive session sets.

Different from the upper bound obtained in Sec. 5.5, the proposed BVR^3 based relax-and-fix algorithm yields a lower bound to the optimal spectrum trading problem formulated in Sec. 5.4.3, provided that there exist feasible solutions.

5.6.2 A Coarse-Grained Relax-and-Fix Heuristic Algorithm

Following the same procedure in Sec. 5.5, we first relax the original MILP into LP and find the optimal solution to the relaxed LP, in which $\delta(l)$'s value is in $[0, 1]$. By employing a threshold $0.5 \leq \theta < 1$, we coarsely set the $\delta(l)$-variables exceeding θ to 1 and the other $\delta(l)$-variables to 0. Denote the value of $\delta(l)$ in this solution as $\tilde{\delta}(l) \in \{0, 1\}$. In addition, we keep the same decomposition of session sets as the BVR^3 based relax-and-fix algorithm, i.e., $\mathcal{L}^s$ and $\mathcal{A}^s$ for $s \in \mathcal{S}$.

Then, at each step s ($s \in \mathcal{S}$), all $\delta(l)$-variables are fixed at their $\tilde{\delta}(l)$ values in the best solution found so far (or in the last solution encountered), except the $\delta(l)$-variables

in the set $\mathcal{L}^s \cup \mathcal{A}^s$ which are restricted to binary values. Therefore, the problem solved at step s is

$$\textit{R-MILP}^s \qquad \text{Maximize} \sum_{l \in \mathcal{L}} b(l)\delta(l)$$

$$\begin{aligned}
\text{s.t.:} \quad & (6--16),\ (6--17),\ (6--18),\ (6--20),\ (6--21),\ (5--17) \\
& \delta(l) = \tilde{\delta}(l) \qquad (\forall\, l \in \mathcal{L} \backslash (\mathcal{L}^s \cup \mathcal{A}^s)) \\
& \delta(l) \in \{0, 1\} \qquad (\forall\, l \in \mathcal{L}^s \cup \mathcal{A}^s).
\end{aligned}$$

If a better solution is found, $\tilde{\delta}(l)$ is updated and the fixing procedure continues. Compared with the BVR[3] based relax-and-fix algorithm, different steps s ($s \in \mathcal{S}$) in coarse-grained relax-and-fix heuristic are independent of one another, and any subset of $\mathcal{S}$ can be performed in any order.

5.7 Performance Evaluation

5.7.1 Simulation Setup

We consider a spectrum clouds in multi-hop CRNs consisting of a SSP, $|\mathcal{N}| = 36$ CR mesh routers and $|\mathcal{L}| = 18$ candidate trading sessions, each of which has a random rate requirement within $[10, 30]$ Mb/s. The bidding values of these sessions are within $[100, 300]$. All CR mesh routers use the same power $P = 10$ W for transmission. Considering the AWGN channel, we assume the noise power η is 10^{-10} W at all routers. Moreover, suppose the path loss factor $\alpha = 4$, the antenna parameter $\gamma = 3.90625$, the receiver sensitivity $P_T = 100\eta = 10^{-8}$ W and the interference threshold $P_T = 6.25 \times 10^{-10}$ W. According to the illustration in Sec. 5.3.3, we can calculate the transmission range R_T and the interference range R_I, which are equal to 250 m and 500 m, respectively. For illustrative purposes, we assume all the bands have identical bandwidth, which is set to be 10 MHz, i.e., $W^m = 10$ MHz for all $m \in \mathcal{M}$. Besides, for the simplicity of computation, we set $K = 3 \times 10^4$, i.e., if the total number of the maximal independent sets in $\mathcal{G}(\mathcal{V}, \mathcal{E})$

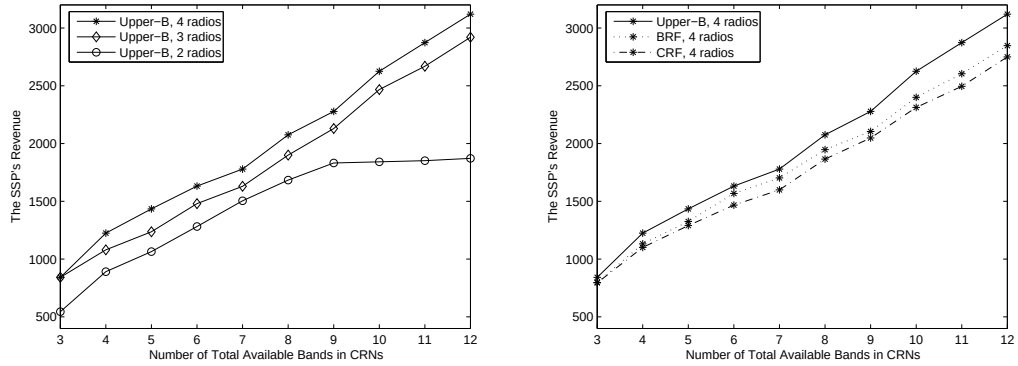

A Revenue upper bounds: $|\mathcal{H}|$ = 2, 3 and 4. B Revenue upper bound and lower bounds: $|\mathcal{H}|$ = 4.

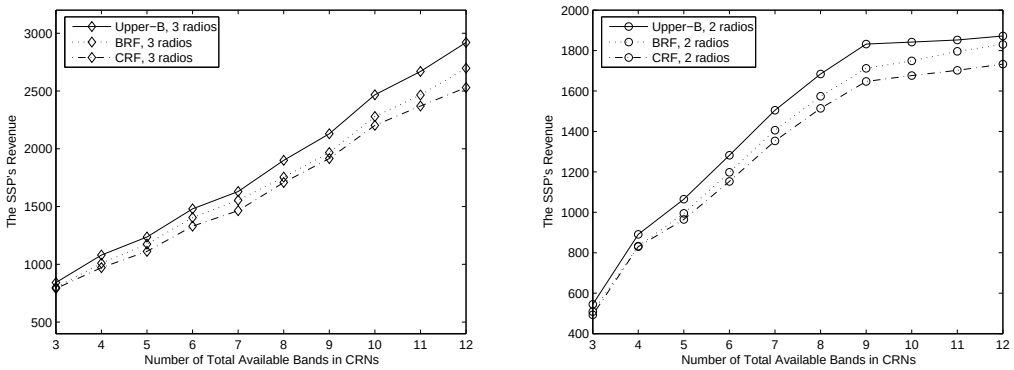

C Revenue upper bound and lower bounds: $|\mathcal{H}|$ = 3. D Revenue upper bound and lower bounds: $|\mathcal{H}|$ = 2.

Figure 5-3. Impact of the number of available bands $|\mathcal{M}|$ and radio interfaces $|\mathcal{H}|$ on spectrum trading in multi-hop CRNs: grid topology.

is less than or equal to 3×10^4, we employ all the maximal independent sets for the solution; otherwise, we employ 3×10^4 maximal independent sets for approximation.

Based on the simulation settings above, we conduct simulations to study the optimal spectrum trading problem in spectrum clouds with the following two topologies: i) a grid topology, where 36 CR mesh routers are distributed within 1000×1000 m^2 area and the area is divided into 25 square cells in 200×200 m^2; ii) a random topology, where 36 CR mesh routers are randomly deployed in a 1000×1000 m^2 area forming a connected network. Note that we employ CPLEX [79] to solve the relaxed optimization problems to obtain the upper bound and lower bounds of the SSP's revenue.

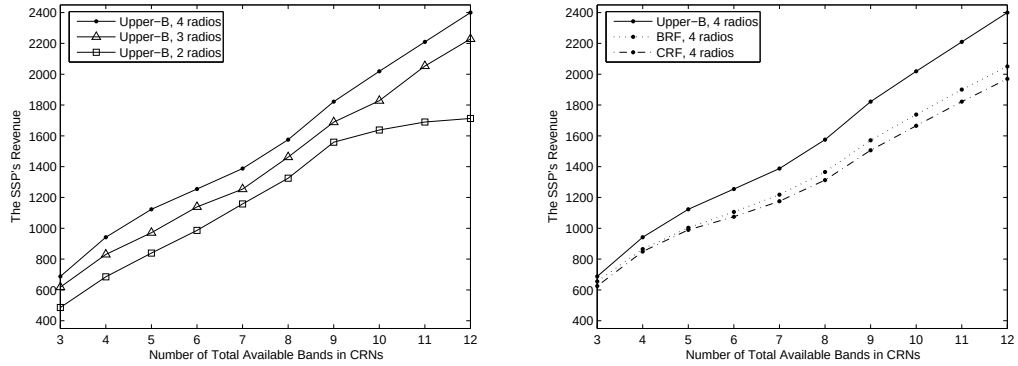

A Revenue upper bounds: $|\mathcal{H}|$ = 2, 3 and 4. B Revenue upper bound and lower bounds: $|\mathcal{H}|$ = 4.

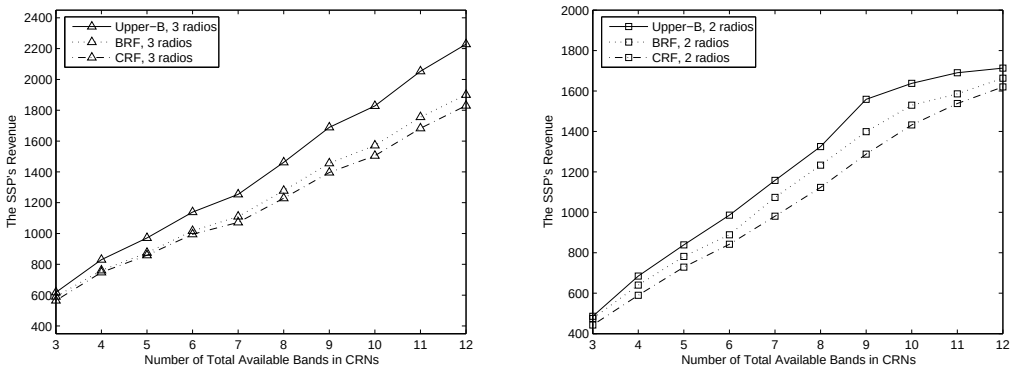

C Revenue upper bound and lower bounds: $|\mathcal{H}|$ = 3. D Revenue upper bound and lower bounds: $|\mathcal{H}|$ = 2.

Figure 5-4. Impact of the number of available bands $|\mathcal{M}|$ and radio interfaces $|\mathcal{H}|$ on spectrum trading in multi-hop CRNs: random topology.

5.7.2 Results and Analysis

In Fig. 5-3 and Fig. 5-4, we compare the upper bound of the SSP's revenue with the lower bounds determined by the heuristic BVR^3 based relax-and-fix algorithm (denoted by BRF in figures) and the coarse-grained relax-and-fix algorithm (denoted by CRF in figures) at different number of available bands (i.e., $|\mathcal{M}|$) and radios (i.e., $|\mathcal{H}|$) in multi-hop CRNs. We relax the $\delta(l)$-variables and employ $K = 3 \times 10^4$ maximal independent sets to solve the problem as illustrated in Sec. 5.5, which also yields the

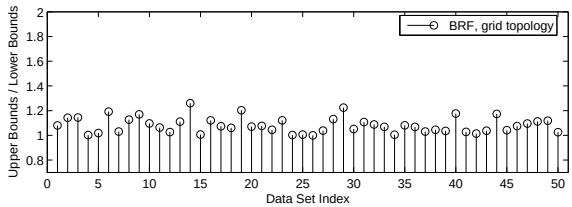

A Ratio of the upper bound to the lower bound determined by the BVR^3 based relax-and-fix algorithm: grid topology.

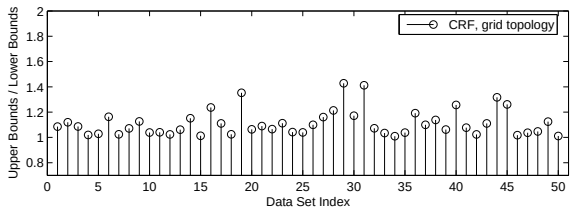

B Ratio of the upper bound to the lower bound determined by the coarse-grained relax-and-fix algorithm: grid topology.

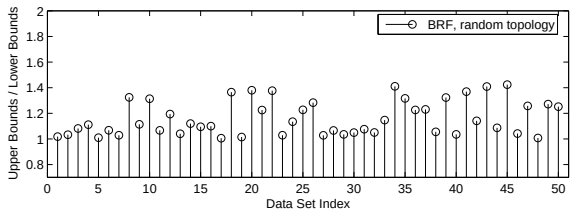

C Ratio of the upper bound to the lower bound determined by the BVR^3 based relax-and-fix algorithm: random topology.

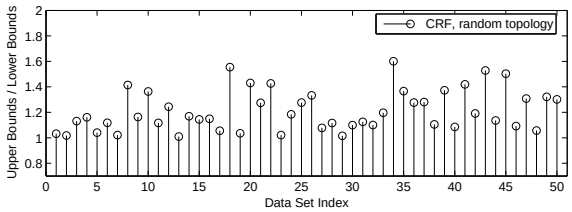

D Ratio of the upper bound to the lower bound determined by the coarse-grained relax-and-fix algorithm: random topology.

Figure 5-5. Ratio of the upper bound to lower bounds determined by the proposed algorithms at $|\mathcal{H}| = 3$ and $|\mathcal{M}| = 9$.

upper bound. To develop the lower bounds, we equally divide the 18 candidate trading sessions into 6 session sets (i.e., $|\mathcal{S}| = 6$ and each set has 3 sessions) for the BVR^3 based relax-and-fix algorithm, and set $\theta = 0.7$ for the coarse-grained relax-and-fix algorithm as shown in Sec. 6.6. Given the number of available bands $|\mathcal{M}|$ in CRNs and radios $|\mathcal{H}|$ at CR routers, we employ 50 data sets that can produce feasible solutions and take the average value as a result. For each data set, we re-generate available bands $\mathcal{M}_i$ at CR router i, $s_r(l)/d_t(l)$ and $(r(l), b(l))$ pair of session l, and the random network topology (we keep the same grid topology for each data set), which follows the guideline of simulation setup.

From the results shown in Fig. 5-3 and Fig. 5-4, four observations can be made in order. First, the upper bound is close to the lower bounds obtained from the proposed BVR^3 based relax-and-fix algorithm and the coarse-grained relax-and-fix algorithm, no matter how many available bands and radios are there in the spectrum clouds. We will further present the ratio of the upper bound to lower bounds with 50 data sets in Fig. 5-5, analyze the statistical results and show the closeness between those bounds. Second, as the number of available bands and the number of CR mesh router's radios increase, the SSP's revenue increases as well. The reason is that more bands and radios available create more LBR tuples, so that more CR links in spectrum clouds may be activated for transmission simultaneously and more opportunities can be leveraged for spectrum trading in CRNs. However, the increment of the SSP's revenue basically stops when $|\mathcal{M}|$ is over 9 for $|\mathcal{H}| = 2$ case in both grid topology and random topology, which leads to the third observation. That is, the CR mesh router has to equip a reasonable number of radios to utilize all the available bands efficiently (at least 3 radios for our simulation scenarios). This observation also gives a good suggestion on the design and deployment of CR mesh routers for spectrum clouds in practice. Fourth, the performance of the grid topology generally outperforms that of the random topology in terms of the SSP's revenue. The performance gap stems from the

differences in topological structure. For the grid topology, each CR link has the same topological information if we ignore the border effect. The performance improvement of spectrum trading is mainly determined by the number of radios and the available bands at different CR routers. By contrast, the random topology is non-uniformed topology. The performance improvement of spectrum trading is not only hindered by the number of bands and radios, but also bottlenecked by the critical cliques in the random topology.

Figure 5-5 presents the ratio of the upper bound to the lower bounds obtained from the proposed heuristic algorithms in both grid topology and random topology, where $|\mathcal{H}| = 3$ and $|\mathcal{M}| = 9$. As shown in Fig. 5-5A and Fig. 5-5B, the ratio of the upper bound to lower bound in the grid topology is near to 1 with 50 different data sets, where the lower bounds are determined by the BVR^3 based relax-and-fix algorithm and the coarse-grained relax-and-fix algorithm, respectively. Specifically, the average ratio of the upper bound to the BVR^3 based lower bound for all the data sets is 1.0826, and the standard deviation is 0.0632; the average ratio of the upper bound to the coarse-grained based lower bound for all the data sets is 1.1122, and the standard deviation is 0.1031. Similar analysis applies to the random topology as well. As shown in Fig. 5-5C and Fig. 5-5D, the average ratio of the upper bound to the BVR^3 based lower bound for all the data sets is 1.1611, and the standard deviation is 0.1387; the average ratio of the upper bound to the coarse-grained based lower bound for all the data sets is 1.2113, and the standard deviation is 0.1595. All these statistical results indicate that the solutions found by the heuristic algorithms must be close to the optimum, since the optimal solution lies between the upper bound and the lower bound.

Given the specific data set at $|\mathcal{H}| = 3$ and $|\mathcal{M}| = 9$, Table 5-1(a) and Table 5-1(b) present the trading status of the 18 candidate sessions w.r.t. BVR^3 values in the

grid topology and the random topology, respectively. The results[9] demonstrate that unlike per-user based spectrum trading in CRNs, it is not necessary for the SSP to accommodate the CR sessions with high BVR^3 values in order to maximize the SSP's revenue. Some other critical factors may also affect the results of the session based spectrum trading in multi-hop CRNs, e.g., the location of source/destination CR routers of a session, the interference a session incurs to the existing flows, etc. As shown in the formulation, the proposed spectrum clouds gives a comprehensive consideration on those factors. The data in Table 5-1 further verify this statement and explicitly show the advantages of our design over the per-user based spectrum trading systems in multi-hop CRNs.

5.8 Chapter Summary

In this chapter, we have proposed a novel spectrum trading system, i.e., spectrum clouds, and presented a theoretical study on the optimal session based spectrum trading problem under multiple cross-layer constraints in multi-hop CRNs. We introduce a new service provider, SSP, and let the SSP provide coverage in CRNs with low-cost CR mesh routers in order to facilitate the accessing of SUs without CR capability. Considering the special features of session based spectrum trading, we exploit the 3-D (link-band-radio) conflict graph to characterize the conflicts among CR links and mathematically describe the competitions among candidate trading sessions in spectrum clouds. Given the rate requirements and bidding values of candidate trading sessions, we formulate the optimal spectrum trading into the SSP's revenue maximization problem under the availability of spectrum, link scheduling and flow routing constraints in multi-hop CRNs. Since the formulated problem is NP-hard to solve, we derive an upper bound for the optimization by relaxing the integer variables.

[9] We exploit the proposed BVR^3 based relax-and-fix algorithm to derive these results in both the grid topology and the random topology.

Table 5-1. Spectrum trading status of the candidate sessions w.r.t. the descending BVR^3 values in multi-hop CRNs.

(a) Grid topology with 3 radios and 9 bands.

S-Index	BVR^3 Val.	Status	S-Index	BVR^3 Val.	Status
1	24.171	$\surd$	10	15.629	$\times$
2	23.222	$\surd$	11	14.878	$\surd$
3	22.411	$\surd$	12	14.627	$\times$
4	20.489	$\surd$	13	13.462	$\times$
5	20.014	$\surd$	14	12.239	$\times$
6	19.074	$\surd$	15	9.876	$\surd$
7	18.475	$\times$	16	8.358	$\times$
8	17.462	$\surd$	17	6.908	$\times$
9	16.081	$\times$	18	4.912	$\times$

(b) Random topology with 3 radios and 9 bands.

S-Index	BVR^3 Val.	Status	S-Index	BVR^3 Val.	Status
1	23.188	$\surd$	10	11.672	$\surd$
2	21.556	$\surd$	11	10.479	$\times$
3	20.139	$\surd$	12	9.002	$\times$
4	20.101	$\surd$	13	8.857	$\times$
5	18.525	$\surd$	14	6.971	$\times$
6	16.271	$\times$	15	5.223	$\times$
7	14.771	$\surd$	16	4.713	$\times$
8	14.365	$\times$	17	4.674	$\times$
9	13.213	$\times$	18	3.737	$\times$

Furthermore, we propose heuristic algorithms for feasible solutions (low bounds as well). Through simulations, we show that: i) the proposed session based spectrum trading has superior advantages over the per-user based one in multi-hop CRNs; ii) the solutions attained by the proposed heuristic algorithms are near-optimal under different data sets in both the grid topology and the random one.

CHAPTER 6
COOPERATIVE COMMUNICATION AWARE LINK SCHEDULING FOR COGNITIVE VEHICULAR AD-HOC NETWORKS

6.1 Chapter Overview

With the maturity of road infrastructure and the increasing number of motorists, highway traveling has become a part of life for people in US and many other countries. Various broadband vehicular communication applications in Vehicular Ad-hoc Networks (VANETs), which can entertain passengers and make long journeys enjoyable, are envisioned to be prevalent in the near future. However, proliferation of vehicular applications beyond safety requires additional radio resources to support, which makes the already crowed licensed spectrum even worse. Meanwhile, for all these passenger-oriented applications [44, 47, 116], no matter vehicle-to-vehicle (V2V) communication based applications (e.g., network gaming among passengers in different cars, file transfers, virtual meetings among coworkers, etc.) or vehicle-to-roadside (V2R) communication based ones (e.g., web browsing, cooperative downloading, online video, etc.), the most critical and essential requirement is the data transmission with high end-to-end throughput, which is also a challenging task in VANETs.

In view of the radio spectrum demands from VANETs, Federal Communications Commission (FCC) opens the under-utilized licensed TV spectrum (i.e., the UHF television frequency spanning over 470-806 MHz) [1] and allows the opportunistic accessing of unlicensed users. By exploiting cognitive radio (CR) technology, the vehicles/nodes (the words vehicles/nodes will be used in this chapter interchangeably) as well as the roadside unit (RSU) in VANETs can sense the vacant spectrum and opportunistically use these licensed bands temporally/geographically, when/where primary services are not active. We call such a VANET with CR capability [77, 116] as a cognitive VANET (C-VANET).

On the other hand, by employing multiple antennas, e.g., multiple-input and multiple-output (MIMO), spatial diversity has been shown to be effective in lowering bit

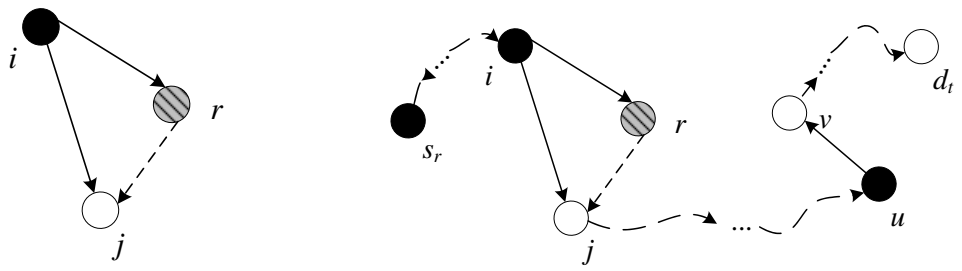

A A three-node schematic for cooperative communications.

B A schematic for the interference incurred by cooperative communications.

Figure 6-1. Illustrative toy topologies for cooperative communications.

error rate, enhancing power efficiency and improving throughput in VANETs. However, equipping a wireless node with multiple antennas may not always be practical. To achieve spatial diversity without requiring multiple transceiver antennas on the same node, the so-called cooperative communications has been introduced in [58, 59]. The idea of cooperative communications can be best illustrated by a three-node example [58, 59] shown in Fig. 6-1A. In this sub-figure, node i transmits to node j via one-hop, and node r acts as a cooperative relay node. Cooperative transmission from i to j is done on a frame-by-frame basis. Within each frame, there are two time slots [16, 17, 44, 59, 103]. In the first time slot (solid lines), i makes a transmission to destination j. Due to the broadcast nature of wireless transmissions, transmission by i is also overheard by relay node r. In the second time slot (dash lines), r forwards the data it overheard in the first time slot to j. Thus, under cooperative communications, each node is equipped with only a single antenna and relies on the antennas of neighboring cooperative nodes to achieve spatial diversity.

If the cooperative relay node is appropriately selected, cooperative communications can effectively increase the link capacity [103, 104]. However, if we take time-frame based link scheduling into consideration, cooperative communications is not necessarily helpful to improving the end-to-end throughput. Take the toy topology shown in Fig. 6-1B as an example. If node i directly transmits packets to node j, link (i, j) will have no

interference with link (u, v), so that they can be scheduled to transmit simultaneously. By contrast, if (i, j) employs r for cooperative communications, (i, j) will conflict with (u, v) since the transmissions of cooperative relay r cast interference on the receiving node v of (u, v). As a result, (i, j) and (u, v) cannot be scheduled to transmit simultaneously, which may decrease the end-to-end throughput from s_r to d_t. In terms of throughput, the benefit brought by cooperative communications may be offset, or even overwhelmed by the loss of opportunities for scheduling more links to transmit at the same time. Based on that observation, there appear several interesting questions for the throughput maximization problem in C-VANETs: When link scheduling is considered, does there exist an optimal approach to maximize the benefit brought by cooperative communications in terms of the end-to-end throughput? Does the availability of licensed bands have any impact on transmission mode selection (i.e., direct transmissions or cooperative communications) as well as the throughput? Can we find a simple and feasible way to solve this problem in practice?

To address these issues, in this chapter, we propose a cooperative communication aware link scheduling scheme, with the objective of maximizing the throughput for a session in C-VANETs. We let the RSU schedule the multi-hop data transmissions among vehicles on highways by sending small-size control messages. Jointly considering availability of licensed spectrum, transmission modes and link scheduling, we mathematically formulate the throughput maximization problem, near-optimally solve it by linear programming, and provide a simple heuristic algorithm to give feasible results. Our salient contributions are summarized as follows.

- Regarding the features of cooperative communications, we novelly extend a link using cooperative communications into a cooperative link. To keep notation consistent, we leverage a dummy cooperative relay and extend a link using direct transmissions into a general link.
- Inspired by the link conflict graph in prior work [10, 61, 114, 115, 131], we propose a 3-dimensional (3-D) cooperative conflict graph to describe the interference relationship among the extended links in C-VANETs. Similar to the methodology

used in [61, 114, 115], we interpret each vertex in the graph as a basic resource point for scheduling and represent each resource point with an *extended link-band pair*. Based on these extended link-band pairs, we establish the 3-D cooperative conflict graph and re-define the cooperative independent sets and conflict cliques.

- With the help of 3-D cooperative conflict graph, the RSU can mathematically formulate the throughput maximization problem under multiple constraints (i.e., availability of bands, selection of transmission modes and link scheduling). Given all cooperative independent sets in C-VANETs, the RSU can relax the integer variables in the formulation, solve the optimization problem by linear programming and obtain the optimal end-to-end throughput between the source and destination nodes.

- Since it is NP-complete to find all the cooperative independent sets in C-VANETs [30, 61, 114, 115, 131], we employ a number of maximal cooperative conflict cliques and develop a heuristic pruning algorithm to approximate the optimal end-to-end throughput. We let the RSU select the band and transmission mode for the extended link-band pairs in those cliques, prune the pairs not selected and update clique transmission time until the largest clique transmission time among all cliques cannot be further decreased. The throughput is estimated as the reciprocal of the largest clique transmission time.

- By carrying out numerical simulations, we demonstrate the impact of the number of available bands and the distance between source and destination nodes on the performance of throughput in C-VANETs. We also show that i) the CR capability creates more opportunities for using cooperative communications; ii) the performance of cooperative communication aware link scheduling is better than that purely relying on one transmission mode; iii) the proposed pruning algorithm is close to the optimal one in terms of end-to-end throughput in C-VANETs.

The rest of this chapter is organized as follows. We review related work on throughput maximization in Section 6.2. In Section 6.3, we introduce the settings and related models in C-VANETs. In Section 6.4, we describe the 3-D cooperative conflict graph and present the concept of cooperative independent sets and conflict cliques. In Section 6.5, we mathematically formulate the throughput maximization problem in C-VANETs and near-optimally solve it by linear programming. In Section 6.6, we develop a heuristic pruning algorithm for cooperative communication aware link scheduling. Finally, we conduct simulations and analyze the performance results in Section 6.7, and draw concluding remarks in Section 6.8.

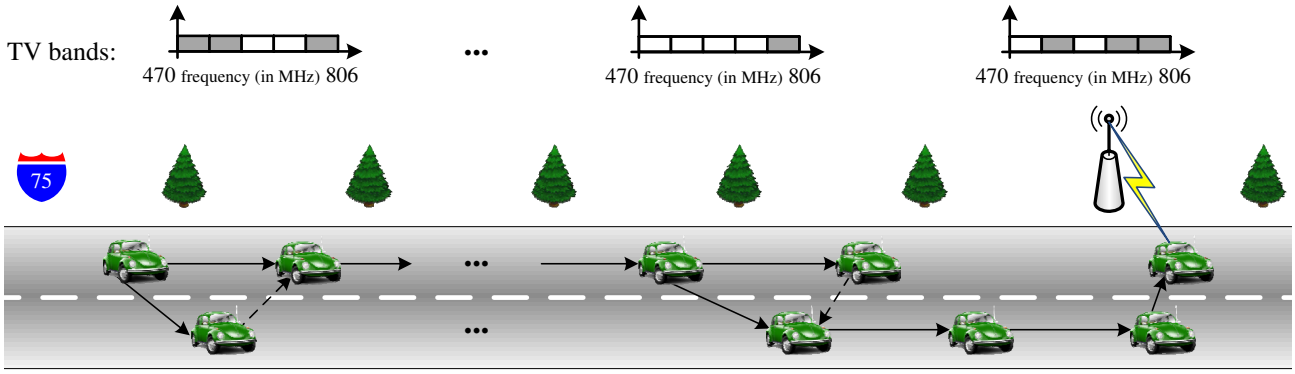

Figure 6-2. Network settings and the end-to-end traffic delivery with two different transmission modes in C-VANETs.

6.2 Related Work

Throughput maximization under cross-layer constraints (e.g., flow routing, link scheduling, etc.) has been extensively studied in existing literature. Jain et al. in [45] studied the impact of interference on performance of multi-hop wireless network based on an NP-complete optimization problem. Zhai and Fang in [131] investigated the path capacity of a given path considering link scheduling and leveraged the interference clique transmission time to design a routing metric for high throughput path selection in single-radio single-channel (SR-SC) networks. For multi-radio multi-channel (MR-MC) networks, Li et al. in [61] proposed a multi-dimensional (i.e., *radio-link-channel*) conflict graph and exploited it to solve the optimal path capacity problem by linear programming.

Different from the mobile device with a single radio in SR-SC networks or the one with multiple radios in MR-MC networks, the CR device has only one radio but the radio is a software defined one [1, 3, 73], which is supposed to switch frequencies across a wide spectrum range [14, 97, 110]. In CR research community, there have been some efforts devoted to cross-layer optimization as well. Tang et al. in [114] studied the joint spectrum allocation and link scheduling problems with the objectives of maximizing throughput and achieving certain fairness in multi-hop CR networks. Hou et al. in [43] investigated the joint frequency scheduling and routing problem with the

objective of minimizing the network-wide spectrum resource and presented a centralized algorithm for spectrum sharing in multi-hop CR networks. Considering the uncertain spectrum supply, Pan et al. in [88] proposed to model the vacancy of licensed bands as a series of random variables, characterized multi-hop CR networks with a pair of (α, β) parameters and minimized the usage of licensed spectrum to support CR sessions with rate requirements at certain confidence levels. Unfortunately, there is still a lack of cross-layer throughput maximization designs, which can effectively unify the CR capability of wireless devices and cooperative communications among those devices.

As for cooperative communications, research efforts mainly focus on information theoretic and communication theory problems. Liu et al. in [66] and Laneman in [58] provided an excellent survey of main results on related topics. The common theme for most research in this field is to optimize physical layer performance measures (i.e., bit error rate, power efficiency and link outage probability) from a general system perspective, without much concern about the impact of cooperative communications on network performance. For example, Host-Madsen and Zhang in [40] and Kramer et al. in [54] investigated the achievable rates and diversity gains of several cooperative schemes with a given source and destination pair. Based on cascaded Nakagami fading [121], which provides a realistic description of an intervehicular channel, Ilhan et al. in [44] studied cooperative diversity in VANETs, and proposed a relay-assisted scheme to optimize the power allocation for intervehicular communications. Some pioneering efforts on networking and cross-layer designs of cooperative communications include medium access control protocols to leverage cooperation [67], cooperative routing [16, 56, 104], optimal network-wide cooperative relay selection [103], network coded cooperative communications [105, 133] and cross-layer routing using cooperative communications in VANETs [17]. However, link scheduling with a joint consideration of cooperative communications and opportunistic spectrum accessing in VANETs is a substantially unexplored area.

Pagadarai et al. in [80] quantitatively and qualitatively measured and characterized the vacant TV spectrum (470-806 MHz) along interstate highway (I-90) in Massachusetts, which further paves the way for the research in C-VANETs. In this work, we are trying to give a comprehensive study on the end-to-end throughput maximization in C-VANETs, where transmission mode selection, availability of spectrum and link scheduling are all taken into consideration.

6.3 Network Model

6.3.1 Network Setting of C-VANETs

We consider a multi-hop C-VANETs [77, 116] consisting of multiple vehicles operating on different vacant licensed frequency bands and a RSU (e.g., a base station (BS), a gateway, an access point (AP), etc.) who serves this group of nodes $\mathcal{N} = \{1, 2, \cdots, n, \cdots, N\}$ on (one way) highways as shown in Fig. 6-2. Let s_r/d_t denote the source/destination node for a session in C-VANETs. Our objective is to maximize end-to-end throughput of this session. By exchanging small-size control messages with the vehicles, the RSU[1] can schedule the transmissions of large-size data packets for multi-hop V2V communications or V2R communications [77]. The scheduling period is set to τ considering the vehicles merging into/exiting from the highway as well as the availability of licensed bands. Suppose that the set of licensed spectrum bands $\mathcal{B} = \{1, 2, \cdots, b, \cdots, B\}$ have the identical bandwidth, where the size of the bandwidth is equal to W. Both direct transmissions and cooperative communications can be used for packets delivery. To distinguish two types of relay nodes [104] in C-VANETs, we call a relay node used for cooperative communications purpose as a cooperative relay and a relay node used for multi-hop relaying in the traditional sense as multi-hop

[1] The RSU can also be interpreted as a group of associated RSUs connected by the backbone network, if the length of the path is long.

relay[2] . Considering the concept of cooperative communications as well as the inherent hardware limitation of CR devices, we also assume that each node has only one radio, but the radio can be tuned into any available frequency band for packet delivery.

Each node $i \in \mathcal{N}$ employs certain spectrum sensing techniques (e.g., [51, 60]) to identify a set of available licensed bands, which are not occupied by primary services. Depending on the geographical locations of nodes, the available bands at one node may be different from another one in C-VANETs as shown in Fig. 6-2. To put it in a mathematical way, let $\mathcal{B}_i \subseteq \mathcal{B}$ represent the set of available licensed bands at CR node $i \in \mathcal{N}$. $\mathcal{B}_i$ may be different from $\mathcal{B}_j$, where j is not equal to i, and $j \in \mathcal{N}$, i.e., possibly $\mathcal{B}_i \neq \mathcal{B}_j$.

For a link (i, j) using cooperative relay r, we assume the transmission from i to j and the transmission from r to j use the same band. Thus, we have $\mathcal{B}_{(i,r,j)} = \mathcal{B}_{(i,j)} = \mathcal{B}_i \bigcap \mathcal{B}_j$. Besides, the time share[3] assigned by the RSU will be measured in time frames, and each time frame will be equally divided into two time slots for the transmission from i to j and that from r to j, if cooperative communications is employed.

6.3.2 Transmission Modes

In this subsection, we give expressions for achievable data rate under different transmission modes. For cooperative communications, we consider both AF and DF modes [59, 103].

[2] Note that a cooperative relay operates at the physical layer while a multi-hop relay operates at the network layer.

[3] In this chapter, time period refers to the scheduling period, i.e., τ; time share refers to the active time scheduled for an independent set, i.e., $\lambda_m \tau$, as illustrated in Sec. 6.5.2; time frame refers to the basic unit of time for link scheduling; time slot refers to the two time slots defined in cooperative communications [59, 103].

6.3.2.1 Amplify-and-forward (AF)

Under this transmission mode, cooperative relay r receives, amplifies and forwards the signal from node i to node j [59, 103, 104]. Let h_{ij}, h_{ir}, h_{rj} capture the effects of path-loss, shadowing and fading between nodes i and j, i and r, and r and j, respectively. Denote z_j and z_r the zero-mean background noise at nodes j and r, with variance σ_j^2 and σ_r^2, respectively. Besides, denote P_i and P_r the transmission powers at nodes i and r, respectively. Since the results are valid for all the bands, we omit the band notations in this subsection.

Following the same notations in [58, 59, 103, 104], the achievable data rate under AF can be expressed as[4]

$$C_{\mathrm{AF}}(i,r,j) = W \cdot I_{\mathrm{AF}}(i,r,j), \tag{6–1}$$

where $I_{\mathrm{AF}}(i,r,j) = \frac{1}{2}\log_2\left(1 + \mathrm{SNR}_{ij} + \frac{\mathrm{SNR}_{ir}\cdot\mathrm{SNR}_{rj}}{\mathrm{SNR}_{ir}+\mathrm{SNR}_{rj}+1}\right)$, $\mathrm{SNR}_{ij} = \frac{P_i}{\sigma_j^2}|h_{ij}|^2$, $\mathrm{SNR}_{ir} = \frac{P_i}{\sigma_r^2}|h_{ir}|^2$, $\mathrm{SNR}_{rj} = \frac{P_r}{\sigma_j^2}|h_{rj}|^2$, and W is the available bandwidth at nodes i and r.

6.3.2.2 Decode-and-forward (DF)

Under this transmission mode, relay node r decodes and estimates the received signal from node i in the first time slot, and then transmits the estimated data to node j in the second time slot [58, 59, 103]. As in [58, 59, 103, 104], the achievable data rate under DF transmission mode is given as

$$C_{\mathrm{DF}}(i,r,j) = W \cdot I_{\mathrm{DF}}(i,r,j), \tag{6–2}$$

[4] Depending on different modulation schemes, the achievable data rate is actually determined by the SNR at the receiver and receiver sensitivity [16, 131]. However, in most of existing literature [43, 61, 88, 103, 104], the achievable data rate is approximated by the link capacity obtained from Shannon-Hartley theorem, even though the capacity cannot be achieved in practice. Note that this approximation will not affect the theoretical analysis as well as performance comparison in this work.

where

$$I_{\mathrm{DF}}(i,r,j) = \frac{1}{2}\min\{\log_2(1+\mathrm{SNR}_{ir}),$$
$$\log_2(1+\mathrm{SNR}_{ij}+\mathrm{SNR}_{rj})\}.$$

Note that $I_{\mathrm{AF}}(\cdot)$ and $I_{\mathrm{DF}}(\cdot)$ are increasing functions of P_i and P_r, respectively. This suggests that, in order to achieve the maximal data rate under either mode, both node i and node r should transmit at the maximum power. In this chapter, we let $P_i = P_r = P$.

6.3.2.3 Direct transmission

When cooperative communications is not used, the achievable data rate from node i to node j is

$$C_{\mathrm{DTx}}(i,j) = W \cdot \log_2(1+\mathrm{SNR}_{ij}). \tag{6–3}$$

Based on the above results, we have two observations. First, comparing C_{AF} (or C_{DF}) to C_{DTx}, it is hard to say that cooperative communication is always better than the direct transmission. In fact, a poor choice of relay node could make the achievable data rate under cooperative communications be lower than that under direct transmissions [103]. Second, although AF and DF are different mechanisms, the capacities for both of them have the same form, i.e., a function of SNR_{ij}, SNR_{ir}, and SNR_{rj}. Therefore, a cooperative communication aware link scheduling algorithm designed for AF can be readily extended for DF. Therefore, it is sufficient to focus on one of them, where we choose AF in this chapter.

6.3.3 Transmission/Interference Range

The interference in wireless networks can be defined according to the protocol model or the physical model [37]. In protocol model [37, 131], there will be a fixed transmission range and a fixed interference range, where the interference range is typically 1.5 to 3 times of the transmission range. These two ranges may vary with the frequency bands. Let $\mathcal{T}_i^b$ denote the set of neighboring nodes within node i's

transmission range over licensed band $b \in \mathcal{B}_i$. For a link (i, j) using r for cooperative communications over band b, we have $r \neq j$ and $r \in \mathcal{T}^b_{(i,j)} = \mathcal{T}^b_i \bigcap \mathcal{T}^b_j$. On the other hand, the conflict relationship between two links over the same band can be determined by the specified interference range. The protocol model is adopted by most of the existing work [43, 61, 88, 114, 131], by which the interference over a network can be abstracted into a conflict graph. We also exploit the protocol model to characterize the interference relationship among the links in C-VANETs, and extend the conflict graph into 3-D cooperative conflict graph considering the features of cooperative communications. The details will be presented in the following section.

6.4 Cooperative Conflict Graph, Conflict Cliques and Independent Sets in C-VANETs

In this section, we first extend the links in C-VANETs into cooperative links/general links with respect to (w.r.t.) the special features of cooperative communications. Then, we establish a 3-D cooperative conflict graph to describe the interference relationship among these extended links. Besides, we also re-define independent sets and conflict cliques [10, 131] to show which links can be activated at the same time and which links cannot, when cooperative communications is involved in C-VANETs.

6.4.1 Extending Links into Cooperative/General Links

For a link (i, j), if node r is the best cooperative relay for it, we calculate the achievable data rate for cooperative communications (i.e., $C_{\mathsf{AF}}(i, r, j)$) as illustrated in (6–1). If $C_{\mathsf{AF}}(i, r, j) > C_{\mathsf{DTx}}(i, j)$, we can extend link (i, j) into (i, r, j) and define (i, r, j) as a cooperative link. To keep the link notation consistent, we exploit (i, ϕ, j) to denote a link using direct transmissions, where ϕ is a dummy cooperative relay, and define (i, ϕ, j) as a general link. The same procedure can be done for each link in the C-VANET. Define $\mathcal{R}^b_{(i,j)} = \{\phi\} \bigcup \mathcal{T}^b_{(i,j)}$. Then, we can extend each link (i, j) into the form of (i, r, j) over band b, where $r \in \mathcal{R}^b_{(i,j)}$. Note that for a link qualified to be a cooperative link, the RSU can choose to use it as a cooperative link or a general link, when the

RSU considers the interference relationship among different links and schedules the transmissions over these links.

6.4.2 Establishing the 3-D Cooperative Conflict Graph

Regarding the availability of licensed bands and the features of cooperative communications, we introduce a 3-D cooperative conflict graph to characterize the interference relationship among multiple links in C-VANETs.

Specifically, in a 3-D cooperative conflict graph $\mathcal{G}(\mathcal{V}, \mathcal{E})$, each vertex corresponds to an *extended link-band pair*, where a extended link-band pair is defined as $((i, r, j), b)$. The link-band pair indicates that the extended link (i, r, j) operates on available licensed band b. Note that it includes the general link when the cooperative relay $r = \phi$, and includes the cooperative link when the cooperative relay $r \neq \phi$. It also includes cooperative communications in single-radio single-channel networks as a special case when the number of available licensed bands $|\mathcal{B}| = 1$.

Two extended link-band pairs are defined to interfere with each other, if any of the following conditions is true:

- **Condition 1**: Two different extended link-band pairs have nodes in common.
- **Condition 2**: If the two extended link-band pairs are using the same band, their transmissions interfere with each other when either the receiving node or the cooperative relay node of one pair is in the interference range of either the transmitting node or the cooperative relay node in the other pair.

Based on these conditions, we connect two vertices in $\mathcal{V}$ with an undirected edge in $\mathcal{G}(\mathcal{V}, \mathcal{E})$, if their corresponding link-band pairs interfere with each other.

For illustrative purpose, we take a simple example to show how to construct a 3-D cooperative conflict graph. As the toy C-VANET shown in Fig. 6-3A, we assume there are six vehicles with CR transceivers, i.e., A, B, C, D, E and F, and two licensed bands, i.e., band 1 and band 2. There is a path with node A as the source and node E as the destination. For link (A, B), we assume $C_{\mathsf{AF}}(A, F, B) > C_{\mathsf{DTx}}(A, B)$. Thus, the RSU can employ node F as a cooperative relay and form a cooperative link (A, F, B).

For link (B, C), we assume $C_{\mathrm{AF}}(B, F, C) < C_{\mathrm{DTx}}(B, C)$, which means (B, C) cannot be extended to (B, F, C). For the other links, they can be extended into general links, e.g., $(C, D) \rightarrow (C, \phi, D)$. Depending on the geographic locations, the set of currently available frequency bands at one extended link may not be the same as that at another extended link as mentioned in Sec. 6.3.1. For example, the available licensed band set for $(A, \phi, B)/(A, F, B)$ is $\{1\}$ and the band set for (B, ϕ, C) is $\{1, 2\}$. Furthermore, we use $d(\cdot)$ to represent Euclidean distance, and suppose that $d(A, B) = d(A, F) = d(B, C) = d(C, D) = D_T = \frac{1}{2}D_I$, $d(F, B) < D_T$, $d(D, E) < D_T$ and $d(F, E) < D_I$, where D_T and D_I are the transmission range and interference range of the nodes, respectively.

Given the above assumptions and information about toy C-VANETs, we can construct the corresponding 3-D cooperative conflict graph, which are depicted in Fig. 6-3B. In this figure, each vertex corresponds to an extended link-band pair, e.g., vertex $((A, \phi, B), 1)$ in the 3-D cooperative conflict graph corresponds to general link-band pair $((A, \phi, B), 1)$. As shown in Fig. 6-3B, there are edges between vertices $((A, \phi, B), 1)$ and $((B, \phi, C), 1)$, and $((A, \phi, B), 1)$ and $((B, \phi, C), 2)$ because (A, ϕ, B) and (B, ϕ, C) have a node B in common, which satisfies **Condition 1**. There are edges between vertices $((A, \phi, B), 1)$ and $((C, \phi, D), 1)$ because (A, ϕ, B) is incident to (C, ϕ, D) over band 1, which satisfies **Condition 2**. Moreover, there is an edge between vertices $((B, \phi, C), 1)$ and $((B, \phi, C), 2)$ because any node has only one radio and can only work on one band at one time. There is an edge between vertices $((A, \phi, B), 1)$ and $((A, F, B), 1)$ because they are links with the same transmitting node and receiving node (which also satisfies **Condition 1**) but with different transmission modes. When the RSU schedules the transmissions, it can choose to use $((A, \phi, B), 1)$ or $((A, F, B), 1)$. Similar analysis applies to the other vertices in the 3-D cooperative conflict graph as well.

Note that cooperative communication may increase the achievable data rate of a link, but it also incurs additional interferences. As shown in Fig. 6-3B, if the cooperative link-band pair $((A, F, B), 1)$ is selected by the RSU, it will conflict with $((B, \phi, C), 1)$,

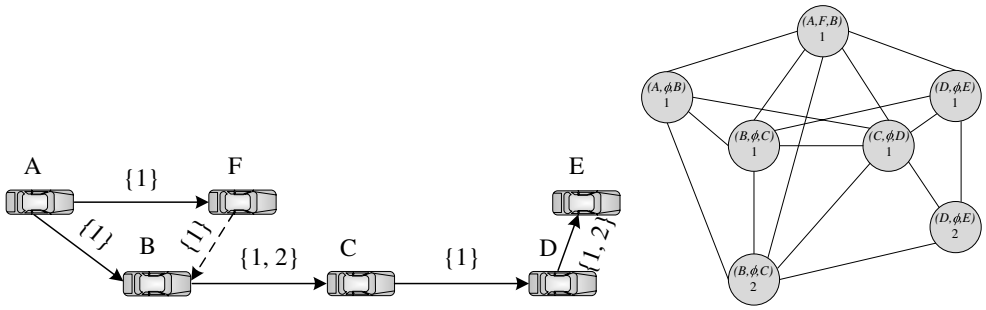

A Toy topology in C-VANETs. B 3-D cooperative conflict graph.

Figure 6-3. Conflict relationship represented by 3-D cooperative conflict graph.

$((B, \phi, C), 2)$, $((C, \phi, D), 1)$ and $((D, \phi, E), 1)$. By contrast, if the general link-band pair $((A, \phi, B), 1)$ is adopted, it will conflict with $((B, \phi, C), 1)$, $((B, \phi, C), 2)$ and $((C, \phi, D), 1)$. The reason is that we must consider both the nodes within the interference range of the transmitting node A and the nodes within the interference range of the cooperative relaying node F, when this cooperative link-band pair is scheduled for transmissions.

6.4.3 Cooperative Independent Sets and Conflict Cliques

Given a 3-D cooperative conflict graph $\mathcal{G} = (\mathcal{V}, \mathcal{E})$ representing C-VANETs, we describe the impact of vertex $u \in \mathcal{V}$ on vertex $v \in \mathcal{V}$ as follows,

$$w_{uv} = \begin{cases} 1, & \text{(if there is an edge between } u \text{ and } v\text{)} \\ 0, & \text{(if there is no edge between } u \text{ and } v\text{)}, \end{cases}$$

where the two vertices correspond to two link-band pairs.

Provided that there is a vertex/extended link-band set $\mathcal{I} \subseteq \mathcal{V}$ and an extended link-band $u \in \mathcal{I}$ satisfying $\sum_{v \in \mathcal{I}, u \neq v} w_{uv} < 1$, the transmission at link-band pair u will be successful even if all the other link-band pairs belonging to the set $\mathcal{I}$ are transmitting at the same time. If any $u \in \mathcal{I}$ satisfies the condition above, we can schedule the transmissions over all these extended link-band pairs in $\mathcal{I}$ to be active simultaneously. Such a vertex/extended link-band pair set $\mathcal{I}$ is called a cooperative independent set. If adding any one more extended link-band pair into a cooperative independent set $\mathcal{I}$

results in a non-independent one, $\mathcal{I}$ is defined as a maximal cooperative independent set. Besides, if there exists a vertex/extended link-band pair set $\mathcal{Z} \subseteq \mathcal{V}$ in $\mathcal{G}$ and any two extended link-band pairs u and v in $\mathcal{Z}$ satisfying $w_{uv} \neq 0$ (i.e., vertex u and v cannot be scheduled to transmit successfully at the same time.), $\mathcal{Z}$ is called a cooperative conflict clique. If $\mathcal{Z}$ is no longer a cooperative conflict clique after adding any one more extended link-band pair, $\mathcal{Z}$ is defined as a maximal cooperative conflict clique.

6.5 Optimal Cooperative Communication Aware Link Scheduling for High End-to-End Throughput

After we construct the 3-D cooperative conflict graph, in this section, we first discuss the possible collisions of relay selection w.r.t. link scheduling in C-VANETs. Then, we address how to calculate the path capacity and describe flow routing constraints for the single-radio based nodes. According to the cross-layer constraints, we mathematically formulate the throughput maximization problem in C-VANETs and near-optimally solve it by linear programming.

6.5.1 Collisions of Relay Selection w.r.t. Link Scheduling

Before we discuss cooperative communication aware link scheduling, we need to clarify two issues related to the collisions of relay selection w.r.t. link scheduling. As introduced in [104], two kinds of relay selection collisions may happen when cooperative communications is incorporated into multi-hop wireless networks. The first one is the collision between cooperative relay selection and multi-hop relay selection (i.e., a node is chosen both as a cooperative relay and a multi-hop relay), as shown in Case 1 and 2 in Fig. 6-4; the second one is the collision among different links for cooperative relay selection (i.e., different links choose the same node as cooperative relay), as shown in Case 3 in Fig. 6-4.

If there is only one band available in the network, it can easily be proved that the relay selection collisions can never happen w.r.t. link scheduling[5] . However, if there are multiple bands available in the network (e.g. in C-VANETs), both collisions exist as shown in Fig. 6-4. Fortunately, the 3-D cooperative conflict graph can perfectly describe all the relay selection collisions in C-VANETs (e.g., all three cases in Fig. 6-4 satisfying interference **Condition 1**), so that the RSU can exploit it to conduct the cooperative communication aware link scheduling. Note that a node in C-VANETs can alternate its role between cooperative relay and multi-hop relay at different time shares, which is different from the node's fixed role in [104].

6.5.2 Path Capacity with Link Scheduling Consideration

For a given path $\mathcal{P}$, we can establish the 3-D cooperative conflict graph $\mathcal{G}_{\mathcal{P}} = (\mathcal{V}_{\mathcal{P}}, \mathcal{E}_{\mathcal{P}})$ following the same approach illustrated in Sec. 6.4.2. Then, we can list all independent sets as $\mathfrak{I}_{\mathcal{P}} = \{\mathcal{I}_1, \mathcal{I}_2, \cdots, \mathcal{I}_m, \cdots, \mathcal{I}_M\}$, where M is $|\mathfrak{I}_{\mathcal{P}}|$, and $\mathcal{I}_m \subseteq \mathcal{V}_{\mathcal{P}}$ for $1 \leq m \leq M$. Although it is a NP-complete problem to find all independent sets [15, 30, 61], some brute-force algorithm can finish it in polynomial time if the number of extended link-band pairs in $\mathcal{V}_{\mathcal{P}}$ is not large [131].

At any time, at most one independent set can be activated to transmit packets for all link-band pairs in that set. Let $\lambda_m \geq 0$ denote the time share scheduled to independent set $\mathcal{I}_m$, and

$$\sum_{1 \leq m \leq M} \lambda_m \leq 1, \quad \lambda_m \geq 0 \ (1 \leq m \leq M). \tag{6–4}$$

Let $r^b_{(i,r,j)}(\mathcal{I}_m)$ be the data rate for the extended link (i, r, j) over band b, where $r^b_{(i,r,j)}(\mathcal{I}_m) = 0$ if link-band pair $((i, r, j), b) \notin \mathcal{I}_m$. Otherwise, if (i, r, j) is a cooperative link

[5] The hint is that for any two links having relay selection collision, these two links inherently interfere with each other if there is only one band available. They cannot be scheduled to transmit simultaneously.

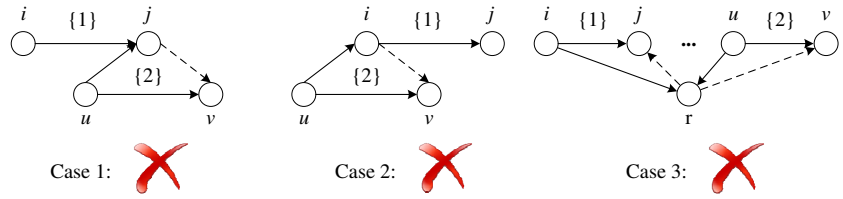

Figure 6-4. Possible cases for relay selection collisions w.r.t. link scheduling.

and $((i, r, j), b) \in \mathcal{I}_m$, $r^b_{(i,r,j)}(\mathcal{I}_m)$ is the achievable data rate for (i, r, j) over band b when cooperative communications is leveraged. Under AF transmission mode, $r^b_{(i,r,j)}(\mathcal{I}_m)$ can be calculated from (6–1); if (i, r, j) is a general link and $((i, r, j), b) \in \mathcal{I}_m$, $r^b_{(i,r,j)}(\mathcal{I}_m)$ is the achievable data rate for (i, r, j) over band b using direct transmissions, which can be calculated as illustrated in (6–3).

By exploiting the independent set $\mathcal{I}_m$, the flow rate that an extended link (i, r, j) can support over band b in the time share λ_m is $\lambda_m r^b_{(i,r,j)}(\mathcal{I}_m)$. Let s represent the aggregated traffic demands. Considering the availability of licensed bands in C-VANETs, the traffic is feasible at the extended link (i, r, j) if there exists a schedule of the independent sets satisfying

$$s \leq s_{(i,r,j)} = \sum_{m=1}^{|\mathfrak{I}_{\mathcal{P}}|} \lambda_m \sum_{b=1}^{|\mathcal{B}_{(i,r,j)}|} r^b_{(i,r,j)}(\mathcal{I}_m). \tag{6–5}$$

To maximize the end-to-end throughput of $\mathcal{P}$, we must consider the traffic traveling through all links along the given path from the source to the destination, i.e.,

$$C_{\mathcal{P}} = \max \min_{(i,r,j)\in\mathcal{P}} s_{(i,r,j)}. \tag{6–6}$$

Let s_e denote $\min_{(i,r,j)\in\mathcal{P}} s_{(i,r,j)}$, where e is the bottleneck extended link along $\mathcal{P}$ for the end-to-end throughput. Taking link scheduling into consideration, we can formulate the path capacity problem as follows,

$$\text{Maximize } s_e$$

$$\text{s.t.}: \sum_{m=1}^{|\mathfrak{I}_{\mathcal{P}}|} \lambda_m \leq 1 \tag{6–7}$$

$$s_e \leq \sum_{m=1}^{|\mathfrak{I}_{\mathcal{P}}|} \lambda_m \sum_{b=1}^{|\mathcal{B}_{(i,r,j)}|} r^b_{(i,r,j)}(\mathcal{I}_m) \tag{6–8}$$

$$\lambda_m \geq 0,\ 1 \leq m \leq |\mathfrak{I}_{\mathcal{P}}|,\ 1 \leq b \leq |\mathcal{B}_{(i,r,j)}|,\ s_e \geq 0. \tag{6–9}$$

As introduced in Sec. 6.3.1, the time is divided into time periods with the duration of τ. Each time period is further partitioned into a set of time slots indexed by m ($1 \leq m \leq M$), so that the m-th time slot has a length of $\lambda_m \tau$. In the m-th time slot, all the extended link-band pairs in the set $\mathcal{I}_m$ will be scheduled to transmit. The end-to-end throughput of $\mathcal{P}$ is determined by the throughput of the bottleneck extended link, i.e., s_e. So, during each time period of length τ, the path capacity of $\mathcal{P}$ is

$$s_e = \frac{1}{\tau} \sum_{m=1}^{|\mathfrak{I}_{\mathcal{P}}|} \lambda_m \tau \sum_{b=1}^{|\mathcal{B}_{(i,r,j)}|} r^b_e(\mathcal{I}_m) = \sum_{m=1}^{|\mathfrak{I}_{\mathcal{P}}|} \lambda_m \sum_{b=1}^{|\mathcal{B}_{(i,r,j)}|} r^b_e(\mathcal{I}_m). \tag{6–10}$$

6.5.3 Flow Routing Constraints in C-VANETs

As for routing, the RSU will help the source node to find the available paths to the destination node for data delivery. Similar to the modeling in [88], we mathematically present those routing constraints as follows.

Let $f^b_{(i,r,j)}$ represent the flow rate of the extended link (i, r, j) over band b, where $i \in \mathcal{N}$, $j \in \mathcal{T}^b_i$, $r \in \mathcal{R}^b_{(i,j)}$ and $r \neq j$. If node i is the source node, i.e., $i = s_r$, then

$$\sum_{b \in \mathcal{B}_{(j,r,i)}} \sum_{j \in \mathcal{T}^b_i}^{r \neq i, r \in \mathcal{R}^b_{(j,i)}} f^b_{(j,r,i)} = 0. \tag{6–11}$$

Regarding the single-radio requirement of cooperative communications and the inherent single-radio constraint of CR devices, we focus on the unicast and single-path routing problem. Thus, we have

$$\sum_{b \in \mathcal{B}_{(i,r,j)}} \sum_{j \in \mathcal{T}^b_i}^{r \neq j, r \in \mathcal{R}^b_{(i,j)}} f^b_{(i,r,j)}\, \delta^b_{(i,r,j)} = s, \tag{6–12}$$

where $\delta^b_{(i,r,j)}$ indicates that the extended link (i, r, j) can only have a nonzero flow at a time due to the single-radio constraint, i.e.,

$$\sum_{b\in\mathcal{B}_{(i,r,j)}} \sum_{j\in\mathcal{T}_i^b}^{r\neq j, r\in\mathcal{R}^b_{(i,j)}} \delta^b_{(i,r,j)} \leq 1, \quad \delta^b_{(i,r,j)} \in \{0, 1\}. \tag{6–13}$$

If node i is an intermediate multi-hop relay node (not a cooperative relay node), i.e., $i \neq s_r$ and $i \neq d_t$, then

$$\begin{aligned} &\sum_{b\in\mathcal{B}_{(i,r,j)}} \sum_{j\in\mathcal{T}_i^b}^{r\neq j, r\in\mathcal{R}^b_{(i,j)}} f^b_{(i,r,j)}\delta^b_{(i,r,j)} \\ &= \sum_{b\in\mathcal{B}_{(j,q,i)}} \sum_{j\in\mathcal{T}_i^b}^{q\neq i,\, q\in\mathcal{R}^b_{(j,i)}} f^b_{(j,q,i)}\delta^b_{(j,q,i)}. \end{aligned} \tag{6–14}$$

If node i is the destination node, i.e., $i = d_t$, then

$$\sum_{b\in\mathcal{B}_{(j,r,i)}} \sum_{j\in\mathcal{T}_i^b}^{r\neq i, r\in\mathcal{R}^b_{(j,i)}} f^b_{(j,r,i)}\delta^b_{(j,r,i)} = s. \tag{6–15}$$

Note that if (6–11), (6–12), (6–13) and (6–14) can be satisfied, (6–15) is automatically satisfied. Therefore, it is sufficient to list only (6–11), (6–12), (6–13) and (6–14) as single-radio based routing constraints.

6.5.4 Maximizing the Throughput under Multiple Constraints

To maximize the end-to-end throughput between the source node and the destination node, the RSU needs to find a feasible solution to jointly assigning the available frequency bands, conducting cooperative communication aware link scheduling bands, and routing the traffic for transmission and reception in multi-hop C-VANETs. Thus, the end-to-end throughput maximization problem under multiple constraints in C-VANETs can be formulated as follows.

$$\text{Maximize } s$$

$$\text{s.t.:} \quad \sum_{b\in\mathcal{B}_{(j,r,i)}} \sum_{j\in\mathcal{T}_i^b}^{r\neq i, r\in\mathcal{R}^b_{(j,i)}} f^b_{(j,r,i)} = 0 \quad (i = s_r) \tag{6–16}$$

$$\sum_{b\in\mathcal{B}_{(i,r,j)}} \sum_{j\in\mathcal{T}_i^b}^{r\neq j, r\in\mathcal{R}^b_{(i,j)}} f^b_{(i,r,j)}\, \delta^b_{(i,r,j)} = s \quad (i = s_r) \tag{6–17}$$

$$\sum_{b\in\mathcal{B}_{(i,r,j)}} \sum_{j\in\mathcal{T}_i^b}^{r\neq j, r\in\mathcal{R}^b_{(i,j)}} f^b_{(i,r,j)}\delta^b_{(i,r,j)} =$$

$$\sum_{b\in\mathcal{B}_{(j,q,i)}} \sum_{j\in\mathcal{T}_i^b}^{q\neq i,\, q\in\mathcal{R}^b_{(j,i)}} f^b_{(j,q,i)}\delta^b_{(j,q,i)} \;\; (i \in \mathcal{N}\backslash\{s_r, d_t\}) \tag{6–18}$$

$$\sum_{b\in\mathcal{B}_{(i,r,j)}} \sum_{j\in\mathcal{T}_i^b}^{r\neq j, r\in\mathcal{R}^b_{(i,j)}} \delta^b_{(i,r,j)} \leq 1, \;\; \delta^b_{(i,r,j)} \in \{0, 1\} \tag{6–19}$$

$$0 \leq \sum_{b=1}^{|\mathcal{B}_{(i,r,j)}|} f^b_{(i,r,j)} \leq \sum_{m=1}^{|\mathfrak{I}|} \lambda_m \sum_{b=1}^{|\mathcal{B}_{(i,r,j)}|} r^b_{(i,r,j)}(\mathcal{I}_m)$$

$$(i \in \mathcal{N}, j \in \mathcal{T}_i^b, r \in \mathcal{R}^b_{(i,j)}, b \in \mathcal{B}_{(i,r,j)} \text{ and } \mathcal{I}_m \in \mathfrak{I}) \tag{6–20}$$

$$\sum_{m=1}^{|\mathfrak{I}|} \lambda_m \leq 1, \;\; \lambda_m \geq 0 \;\; (1 \leq m \leq |\mathfrak{I}|), \tag{6–21}$$

where (6–16), (6–17), (6–18) and (6–19) specify that there is at most one outgoing link from each node with a nonzero flow, and that there is a path selected by the RSU between the source and the destination; (6–20) and (6–21) indicate that the flow rate of traffic over (i, r, j) cannot exceed the capacity of this extended link, which is obtained from the cooperative communication aware link scheduling as illustrated in Sec. 6.5.2.

Note that $\mathfrak{I}$ includes all independent sets in C-VANETs. Given all independent sets[6] in the network, we find that the formulated optimization is a mixed-integer linear

[6] That is a general assumption used in existing literature [10, 61, 114, 115, 131] for obtaining throughput bounds or performance comparison, where both link scheduling and flow routing are considered.

programming problem since δ_{ij} only has binary values. It can near-optimally be solved in polynomial time by some typical algorithms (e.g., sequential fixing algorithm [43, 88], branch and bound [94], etc.) or softwares (e.g., CPLEX [79, 131], LINDO, etc.), provided that all the cooperative independent sets can be found in $\mathcal{G}(\mathcal{V}, \mathcal{E})$.

6.6 A Heuristic Pruning Algorithm for Cooperative Communication Aware Scheduling

As we know, to find all cooperative independent sets in $\mathcal{G}(\mathcal{V}, \mathcal{E})$ is NP-complete [10, 45, 61, 115, 131]. Compared with complex path selection in other wireless networks, it is much more simple in C-VANETs because there are only a few paths between the source and destination nodes due to the limited spatial redundancy and fixed direction of highways[7] . However, even for a given path, it is too complex for the RSU to find all cooperative independent sets along the path, if the number of extended links or the number of available licensed bands along the path is large. Instead of using cooperative independent sets, in this section, we employ a number of maximal cooperative cliques and propose a 7-step pruning algorithm to approximate the maximal throughput for a session in C-VANETs.

6.6.1 An Iterative Link-band Pair Pruning Algorithm

The detailed procedure of the proposed pruning algorithm for cooperative communication aware link scheduling in C-VANETs is presented as follows.

Step 1: *Establishing the 3-D cooperative conflict graph*

Given a candidate path $\mathcal{P}$, we first set up a corresponding 3-D cooperative conflict graph $\mathcal{G}_{\mathcal{P}}(\mathcal{V}_{\mathcal{P}}, \mathcal{E}_{\mathcal{P}})$ as illustrated in Sec. 6.4.2.

Step 2: *Searching for the maximal conflict cliques*

[7] In [17], Ding and Leung even employ string topology to investigate the cross-layer routing problem in VANETs.

With the established 3-D cooperative conflict graph of the given path $\mathcal{P}$, we try to find all the maximal cooperative conflict cliques in $\mathcal{G}_{\mathcal{P}}(\mathcal{V}_{\mathcal{P}}, \mathcal{E}_{\mathcal{P}})$ and form the set $\mathfrak{Z}$ consisting of the maximal cooperative conflict cliques. If $\mathcal{P}$ involves with too many extended links or available bands, and it is impossible to find all the maximal cliques, we can employ K maximal cliques for approximation when K is large enough.

Step 3: *Calculating the conflict clique transmission time*

Then, we let the RSU employ the maximal cooperative conflict cliques to estimate the benchmark path capacity for the path $\mathcal{P}$. Similar to the illustration in [10, 131], we define the cooperative conflict clique transmission time $T_{\mathcal{Z}}$ for a cooperative conflict clique $\mathcal{Z}$ as

$$T_{\mathcal{Z}} = \sum_{((i,r,j),b)\in\mathcal{Z}} T_{((i,r,j),b)} \tag{6–22}$$

where $T_{((i,r,j),b)}$ is the transmission time for one unit of traffic over the extended link (i, r, j) using the available licensed band b. Specifically, $T_{((i,r,j),b)}$ can be written as

$$T_{((i,r,j),b)} = \frac{1}{r^b_{(i,r,j)}(\mathcal{Z})}, \tag{6–23}$$

where $r^b_{(i,r,j)}(\mathcal{Z})$ is equal to the achievable data rate of link (i, r, j) over band b, if $((i, r, j), b) \in \mathcal{Z})$. Otherwise, $r^b_{(i,r,j)}(\mathcal{Z}) = \infty$.

Step 4: *Sorting the maximal cooperative conflict cliques*

For $\mathcal{Z} \in \mathfrak{Z}$, we sort the maximal cooperative conflict cliques in terms of the cooperative conflict clique transmission time $T_{\mathcal{Z}}$. Let $T_{\mathcal{P}}$ be the maximum value of the transmission time for all cooperative conflict cliques. $T_{\mathcal{P}}$ can be written as

$$T_{\mathcal{P}} = \max_{\mathcal{Z}\in\mathfrak{Z}} T_{\mathcal{Z}}. \tag{6–24}$$

Considering an extended link-band pair $((i, r, j), b)$ in $\hat{\mathcal{Z}} = \underset{\mathcal{Z}\in\mathfrak{Z}}{\operatorname{argmax}}\,(T_{\mathcal{Z}})$ and one unit of traffic successfully delivered from the source to the destination, it takes time $T_{\mathcal{P}}$ to travel through all the extended link-band pairs in $\hat{\mathcal{Z}}$, and $((i, r, j), b)$ cannot be

scheduled to do any other transmission during $T_{\mathcal{P}}$. That indicates that the throughput at the extended link-band pair $((i, r, j), b)$ is less than or equal to $\frac{1}{T_{\mathcal{P}}}$. Since the end-to-end throughput cannot be larger than the throughput of any link along the path, the benchmark path capacity $C_{\mathcal{P}}$ can be estimated as[8]

$$C_{\mathcal{P}} = \frac{1}{T_{\mathcal{P}}} \tag{6–25}$$

Step 5: *Selecting the optimal band for the high throughput*

If there are multiple available licensed bands for an extended link to access, one of them must be chosen due to the single-radio constraint. On behalf of such an extended link, the RSU will select the optimal band for its accessing in order to improve the end-to-end throughput.

From (6–22), (6–24) and (6–25), we find that if the size of $\hat{\mathcal{Z}}$ shrinks, the throughput of the path may increase. It is obvious that if some of the co-band interference between the extended links can be mitigated, the size of $\hat{\mathcal{Z}}$ can be effectively reduced. As we know, the CR devices can be tuned into different frequencies and allow the extended links to operate on different bands. This special CR feature will help to reduce co-band interference between the extended links so that the end-to-end throughput may be improved. Following this thread, we conduct the optimal band selection as follows.

First, for an extended link (i, r, j) with multiple accessing bands, we randomly select an extended link-band pair $((i, r, j), b)$ in $\hat{\mathcal{Z}}$ and temporarily delete other $((i, r, j), \cdot)$ pairs as well as the conflict edges associated with $((i, r, j), \cdot)$. Then, we find the maximal cooperative conflict clique in the leftover graph cut from $\hat{\mathcal{Z}}$ and calculate the clique transmission time $T_{\hat{\mathcal{Z}}}^{((i,r,j),b)}$ as in (6–22). For $b \in \mathcal{B}_{(i,r,j)}$, the same process is conducted

[8] Actually, the benchmark path capacity $C_{\mathcal{P}}$ should be upper-bounded by $\frac{1}{T_{\mathcal{P}}}$, i.e., $C_{\mathcal{P}} \leq \frac{1}{T_{\mathcal{P}}}$. The equal sign holds if there are no odd cycles [15] in $\mathcal{G}_{\mathcal{P}}$ as illustrated in [131]. In this chapter, we just consider the general paths without odd cycles.

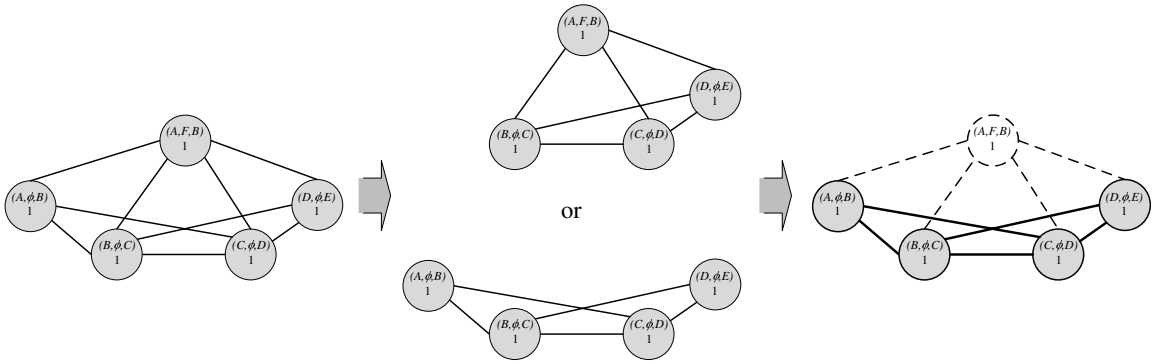

A Only one licensed band available in C-VANETs (without band selection).

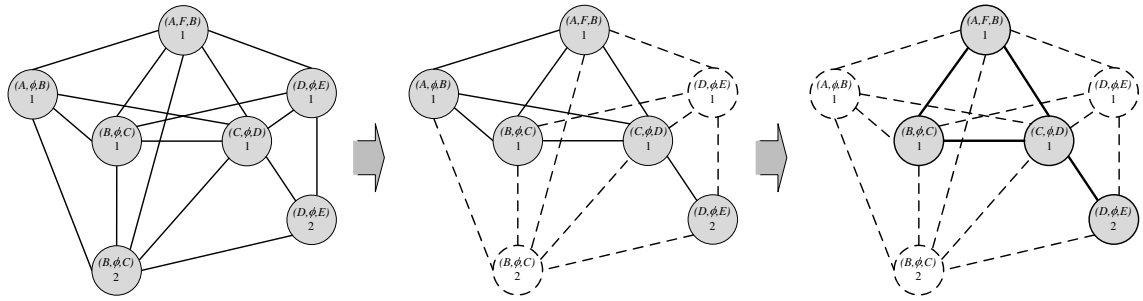

B Two licensed bands available in C-VANETs (with band selection).

Figure 6-5. Two illustrative examples for the proposed pruning algorithm with a given path: (a) one licensed band available; (b) two licensed bands available.

and the values of clique transmission time are stored. After that, we update $T_{\hat{\mathcal{Z}}}$ as

$$T_{\hat{\mathcal{Z}}} = \min\{ T_{\hat{\mathcal{Z}}}^{((i,r,j),1)}, T_{\hat{\mathcal{Z}}}^{((i,r,j),2)}, \cdots, T_{\hat{\mathcal{Z}}}^{((i,r,j),|\mathcal{B}_{(i,r,j)}|)} \}. \tag{6–26}$$

We identify the band reaching the value of $T_{\hat{\mathcal{Z}}}$, put that band into (i, r, j)'s usage and prune all the other $((i, r, j), \cdot)$ pairs as well as the conflict edges associated with $((i, r, j), \cdot)$.

The same procedure above is repeated by all the extended link-band pairs in $\hat{\mathcal{Z}}$ one after another, and the $T_{\hat{\mathcal{Z}}}$ is continuously updated.

If all the available licensed bands are identical to an extended link in terms of band condition (i.e., bandwidth, the propagation gain, etc.), it will be much more simple to select the optimal band for this extended link. As for such an extended link, we just need to keep the extended link-band pair with the least conflict edges and eliminate the

other link-band pairs associated with this extended link. Meanwhile, we also prune the corresponding conflict edges and update $T_{\hat{\mathcal{Z}}}$ based on the leftover graph cut from $\hat{\mathcal{Z}}$.

Step 6: *Pruning the cooperative/general link-band pairs*

After the band selection for an extended link, it is necessary to determine which type of transmission (i.e., cooperative communications or direct transmission) should be used by this extended link. In $\hat{\mathcal{Z}}$, there may be two coupled link-band pairs extended from the same link (i, j): a general link-band pair $((i, \phi, j), u)$ and a cooperative link-band pair $((i, r, j), v)$, ($r \in \mathcal{R}_{(i,j)}$ and $r \neq \phi$), where u and v are the available bands selected for (i, ϕ, j) and (i, r, j) in **Step 5**, respectively.

From (6–1), (6–2), (6–3), (6–23) and (6–22), we can easily calculate the transmission time for the clique $\hat{\mathcal{Z}}\backslash\{((i, \phi, j), u)\}$ and $\hat{\mathcal{Z}}\backslash\{((i, r, j), v)\}$, i.e., $T_{\hat{\mathcal{Z}}\backslash\{((i,\phi,j),u)\}}$ and $T_{\hat{\mathcal{Z}}\backslash\{((i,r,j),v)\}}$, respectively. We compare $T_{\hat{\mathcal{Z}}\backslash\{((i,\phi,j),u)\}}$ and $T_{\hat{\mathcal{Z}}\backslash\{((i,r,j),v)\}}$ and make the decision of pruning the cooperative/general link-band pairs as follows

- If $T_{\hat{\mathcal{Z}}\backslash\{((i,\phi,j),u)\}} > T_{\hat{\mathcal{Z}}\backslash\{((i,r,j),v)\}}$, the RSU will keep the general link-band pair $((i, \phi, j), u)$ and prune the cooperative link-band pair $((i, r, j), v)$ as well as the conflict edges associated with $((i, r, j), v)$. That is, the RSU chooses the direct transmission instead of cooperative communications for the link (i, j). In addition, the RSU will update $T_{\hat{\mathcal{Z}}}$ by setting $T_{\hat{\mathcal{Z}}} = T_{\hat{\mathcal{Z}}\backslash\{((i,r,j),u)\}}$.
- If $T_{\hat{\mathcal{Z}}\backslash\{((i,\phi,j),u)\}} \leq T_{\hat{\mathcal{Z}}\backslash\{((i,r,j),v)\}}$, the RSU will keep the cooperative link-band pair $((i, r, j), v)$ and prune the general link-band pair $((i, \phi, j), u)$ as well as the conflict edges associated with $((i, \phi, j), u)$. That is, the RSU chooses cooperative communications instead of the direct transmission for the link (i, j). In addition, the RSU will update $T_{\hat{\mathcal{Z}}}$ by setting $T_{\hat{\mathcal{Z}}} = T_{\hat{\mathcal{Z}}\backslash\{((i,\phi,j),u)\}}$.

The same procedure is repeated by any two coupled extended link-band pairs in $\hat{\mathcal{Z}}$ associated with the same link, and the $T_{\hat{\mathcal{Z}}}$ is continuously updated.

Step 7: *Iterating the procedure and estimating the throughput*

Jump back to **Step 4**, resort the maximal cooperative conflict cliques in terms of the cooperative conflict clique transmission time (with the updated $T_{\hat{\mathcal{Z}}}$), find new $\hat{\mathcal{Z}}$ and iterate the following steps with this clique. Iterations continue until $\hat{T}_{\mathcal{P}}$ cannot be decreased further. Then, the RSU can set $T^*_{\mathcal{P}} = T_{\mathcal{P}} = T_{\hat{\mathcal{Z}}}$ and estimate the throughput

of $\mathcal{P}$ as $C^*_{\mathcal{P}} = \frac{1}{T^*_{\mathcal{P}}}$. Similarly, the RSU can maximize the throughput of the other paths via cooperative communication aware link scheduling, and select the one with the highest end-to-end throughput.

6.6.2 Illustrative Examples for the Proposed Pruning Algorithm

We take two examples to further illustrate the proposed pruning algorithm. The network topologies of the two examples are the same as the one shown in Fig. 6-3A. The distance between nodes and the transmission/interference range assumptions are also the same, but the assumptions about band availability are different. For the first example, we assume there is only one licensed band available for each link in the network. For the second one, we assume the available band set for each link is the same as shown in Fig. 6-3A, and the two bands are identical to the extended links in terms of band condition. Besides, for both examples, we assume the cooperative relay F is optimally selected [103] and $r^1_{(A,F,B)} > r^1_{(A,\phi,B)}$, which indicates that $T_{((A,F,B),1)} < T_{((A,\phi,B),1)}$. Since $P_s = P_r = P$ as mentioned in Sec. 6.3.2, the cooperative conflict graphs of the two examples can be constructed as shown in Fig. 6-5A and 6-5B, respectively. Let $T_{((A,\phi,B),1)} = T$. According to the assumptions above, the transmission time over all the extended link-band pairs in Fig. 6-5 is equal to T except $((A, F, B), 1)$.

Then, in the first example, the RSU conducts the pruning algorithm as shown in Fig. 6-5A and finds that $T_{\hat{\mathcal{Z}}\setminus\{((A,\phi,B),1)\}} = 3T + T_{((A,F,B),1)}$ and $T_{\hat{\mathcal{Z}}\setminus\{((A,F,B),1)\}} = 3T$. Thus, the RSU will choose to use direct transmission instead of cooperative communications for link (A, B) and the end-to-end throughput is $\frac{1}{3T}$. In the second example, the RSU will first select the band for (B, ϕ, C) and (D, ϕ, E), whose available band set is $\{1, 2\}$. Band 2 is chosen for (D, ϕ, E) since $((D, \phi, E), 2)$ is associated with fewer conflict edges. As for (B, ϕ, C), there is no difference to use band 1 or band 2 based on the given assumptions. Thus, the RSU will keep $((B, \phi, C), 1)$ and $((D, \phi, E), 2)$, and prune $((B, \phi, C), 2)$ and $((D, \phi, E), 1)$ as well as the conflict edges associated with them as shown in Fig. 6-5B. After that, the RSU calculates the transmission time

over $T_{\hat{\mathcal{Z}}\setminus\{((A,\phi,B),1)\}} = 2T + T_{((A,F,B),1)}$ and that over $T_{\hat{\mathcal{Z}}\setminus\{((A,F,B),1)\}} = 3T$. Since $T_{((A,F,B),1)} < T_{((A,\phi,B),1)} = T$, the RSU will prune $((A,\phi,B),1)$ and use cooperative communications for link (A,B). The corresponding end-to-end throughput is $\frac{1}{2T+T_{((A,F,B),1)}}$.

6.7 Performance Evaluation

We consider a C-VANET consisting of $|\mathcal{N}| = 30$ vehicles randomly distributed along a 3 km two lane straight highway. All the vehicles are moving in the same direction. The bandwidth for each band W is set to be 8 MHz, schedule period τ is set to be 10 s, the maximum transmission power at each node is set to be 5 W, the transmission range is set to be 250 m, and the interference range[9] is set to be 400 m. For simplicity, we assume that h_{ij} only includes the propagation gain between node i and j and is given by $|h_{ij}|^2 = d(i,j)^{-4}$, where $d(i,j)$ is the distance (in meters) between nodes i and j and path loss index is 4. For the AWGN channel, we assume the variance of noise is 10^{-10} W at all nodes. Besides, we set $K = 200$, i.e., if the total number of maximal cooperative cliques in $\mathcal{G}_{\mathcal{P}}$ is less than or equal to 200, we employ all the maximal cooperative cliques; otherwise, we employ 200 maximal cooperative cliques for approximation. For illustrative purposes, we investigate the throughput maximization problem in C-VANETs with the following two scenarios: i) all the vehicles move at the speed of 75 mph (i.e., 120.7 km/h, the typical speed limit); ii) vehicle speed follows a Gaussian distribution with a mean of 75 mph and a standard deviation of 10 mph (i.e., 16.09 km/h).

By fixing the leftmost node as the source and the rightmost node as the destination, we compare the results of different throughput maximization algorithms. These results include the optimal throughput considering both transmission mode selection and band selection (i.e., "Optimal CC/Dtx w/ CR"), the throughput obtained from the proposed

[9] As illustrated in [43], the transmission range and interference range can be determined by the receiver sensitivity and the threshold of interference tolerance, respectively.

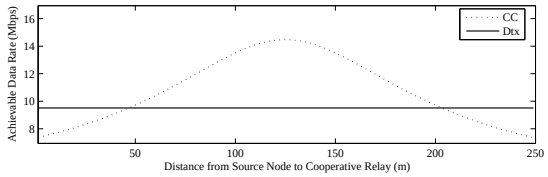

Figure 6-6. Comparison between cooperative communications and direct transmissions for a three-node schematic.

pruning algorithm (i.e., "Pruning CC/Dtx w/ CR"), the optimal throughput considering band selection under different transmission modes (i.e., "Optimal CC w/ CR" and "Optimal Dtx w/ CR") and the single-band based optimal throughput under different transmission modes (i.e., "Optimal CC w/o CR" and "Optimal Dtx w/o CR") [131]. Note that given the independent sets, we can employ CPLEX [79] to solve the optimization problems and obtain near-optimal results. Besides, we demonstrate the impact of the number of available licensed bands on the throughput in C-VANETs and present the results in Fig. 6-7. For the sessions from the source node to all the other nodes along the highway, we also conduct simulations to evaluate the impact of distance with different throughput maximization algorithms and show the corresponding results in Fig. 6-8.

In Fig. 6-6, we compare two transmission modes in terms of link capacity. Here, we assume the transmitter, the cooperative relay and the receiver are on the same lane, and the distance between the transmitter and the receiver is 250 m. We find that cooperative communications is not necessarily better than direct transmissions in terms of link capacity, and the benefit brought by cooperative communications highly depends on the location of the cooperative relay.

Figure 6-7 demonstrates the impact of the number of available licensed bands on the end-to-end throughput in C-VANETs. From the results shown in Fig. 6-7A and Fig. 6-7B, four observations can be made in order. First, "Optimal CC/Dtx w/ CR" and the heuristic pruning algorithm outperform the other algorithms in terms of end-to-end throughput. It is not surprising because both of them have a joint consideration of

transmission mode selection and the band selection, when the transmissions are scheduled. In addition, the throughput obtained from the proposed pruning algorithm is close to that from the optimal one. Second, considering link scheduling, cooperative communications may incur extra interference and hinder the end-to-end throughput, especially when the number of available bands is limited. Third, the CR capability of the nodes creates more opportunities to use cooperative communications and therefore improve the throughput. As for those algorithms considering the CR capability of nodes, the end-to-end throughput increases as the number of available bands increases. The reason is that more licensed bands available give more opportunities for nodes' accessing, so that more cooperative links can be utilized without incurring additional interference and more links can be activated for transmission simultaneously. The increment of throughput stops when the number of available bands is large enough, i.e., the throughput cannot be further increased since both cooperative communications and link scheduling are fully exploited. Fourth, the deviation of vehicle speed leads to performance degradation of link scheduling. That is because speeding up/slowing down may result in certain changes of network topology (e.g., overtaking) in C-VANETs.

Figure 6-8 shows the impact of distance between the source and destination nodes on the throughput in C-VANETs. For the simplicity of computing independent sets [61], we assume there are 2 licensed bands available in the network. Except for the observations we already have made in Fig. 6-7, we find that the longer distance the path spans, the more likely the throughput is affected by the band selection, transmission mode selection and link scheduling. For a short-distance path which includes only a few links, cooperative communications is always preferred since there is no link scheduling involved. By contrast, a long-distance path includes more links, which implies that more links could be scheduled to transmit at the same time. Thus, the end-to-end throughput maximization of such a path depends more on band selection, transmission mode selection and link scheduling.

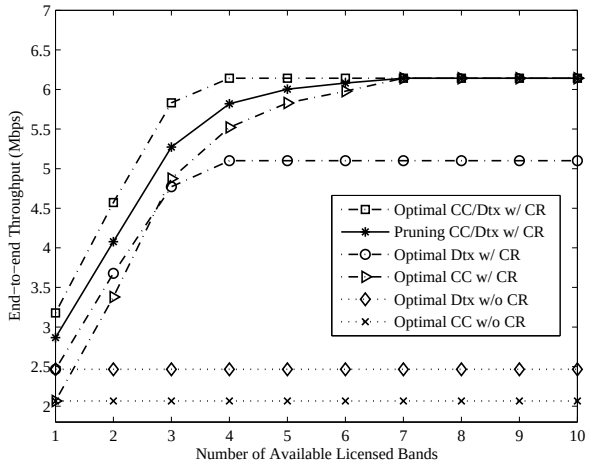

A Scenario 1: vehicle speed is 75 mph.

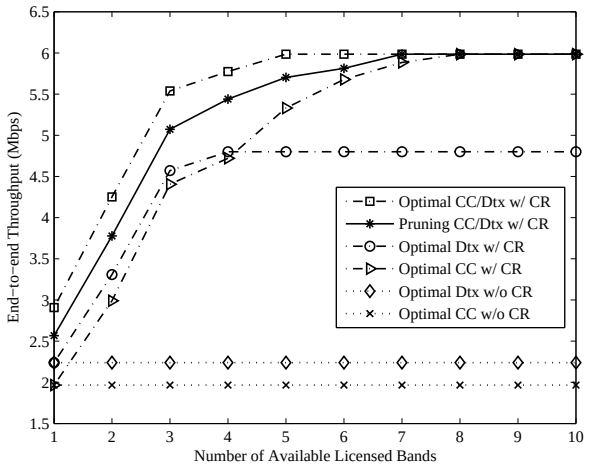

B Scenario 2: vehicle speed follows Gaussian distribution with a mean of 75 mph and a standard deviation of 10 mph.

Figure 6-7. Impact of the number of available licensed bands on the end-to-end throughput in C-VANETs.

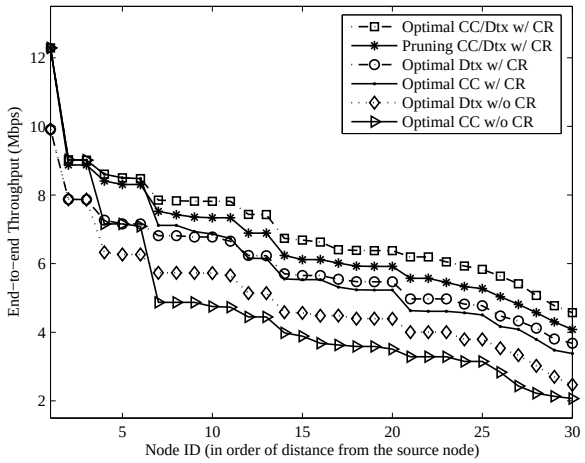

A Scenario 1: vehicle speed is 75 mph.

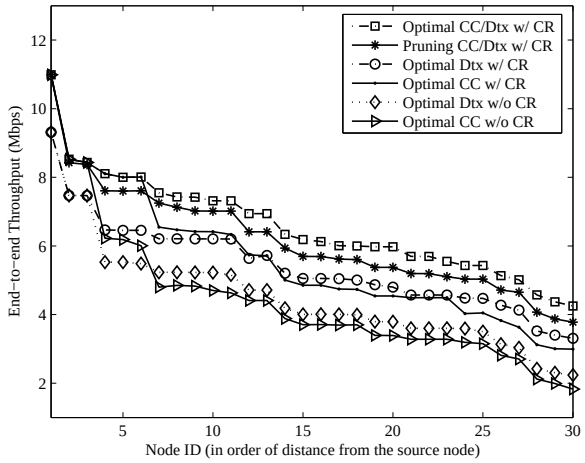

B Scenario 2: vehicle speed follows Gaussian distribution with a mean of 75 mph and a standard deviation of 10 mph.

Figure 6-8. Impact of distance between the source and destination nodes on the end-to-end throughput in C-VANETs.

6.8 Chapter Summary

In this chapter, we have studied the throughput maximization problem in C-VANETs under multiple constraints (i.e., CR devices' inherent single-radio constraint, the availability of licensed spectrum, transmission mode selection and link scheduling). Considering the special features of cooperative communications, we first extend the links and classify them into cooperative links/general links. Then, depending on the available bands at different extended links, we define extended link-band pairs and form a 3-D cooperative conflict graph to describe the conflict relationship among those pairs. After that, we mathematically formulate the end-to-end throughput maximization problem. Given all cooperative independent sets in C-VANETs, we can relax the formulated optimization problem and near-optimally solve it by linear programming. Due to the NP-completeness of finding all independent sets, we provide a heuristic pruning algorithm for the cooperative communication aware link scheduling as well. By numerical simulations, we demonstrate that: i) the CR capability creates more opportunities for using cooperative communications; ii) the performance of link scheduling with appropriately selected transmission mode is better than that purely relying on one transmission mode (either cooperative communications or direct transmissions).

CHAPTER 7
PURGING THE BACK-ROOM DEALING: SECURE SPECTRUM AUCTION LEVERAGING PAILLIER CRYPTOSYSTEM

7.1 Chapter Overview

During the last decade, the dilemma between the rapid growth of wireless services and the limited radio spectrum has shoved the fixed spectrum allocation of Federal Communications Commission (FCC) off the edge, and poured out numerous new techniques, which allow the opportunistic access to the under-utilized spectrum bands [1, 3, 20, 73]. Inspired by the mechanisms in microeconomics [84, 100, 132], auction seems to be one of the most promising solutions to the problem of vacant spectrum allocation to the potential unlicensed users [48, 124, 135, 136].

In general, conventional auctions can be classified into several categories by different criteria [52, 55], i.e., open or sealed auction by the bidding manner, first price auction, secondary price auction, Vickery auction [117], or Vickrey-Clarke-Groves (VCG) auction (also known as Generalized Vickrey Auction, i.e., GVA) by the pricing manner, and single item or combinatorial auction by the number of auctioned goods [13, 118]. According to the requirements, these auction mechanisms can be applied to different scenarios. For instance, the most widely used auctioneer-favored auction, English auction [52, 55], is an open first price auction, where the bidder with the highest bid wins the auction and pays at the price of his bid. This kind of open auction enables the auctioneer to maximize his monetary gains, but it is not strategy-proof. In English auction, each bidder has to strategize delicately to win, which inevitably leads to great complexity and a long auction time. On the contrary, the sealed secondary price auction can make sure the bidders submit their bids with true evaluation values and save the auction time. However, it often results in unsatisfactory revenue for the auctioneer. Equivalent to sealed secondary price auction for single item auction, VCG auction has been proved to be incentive compatible, Pareto efficient, and individual rational [55]. Under certain assumptions, VCG auction is the only mechanism that can satisfy all the

above three properties while maximizing the expected revenue of the auctioneer [36]. With respect to the security issues, there has been considerable work on designing electronic auction with different features, such as fairness [92, 123], confidentiality, anonymity and so on [7].

Despite the desirable characteristics, traditional auction cannot be hammered into the spectrum auction design directly. Unlike common goods in conventional auctions, spectrum is reusable among bidders subject to the spatial interference constraints, i.e., bidders geographically far apart can use the same frequency simultaneously while bidders in close proximity cannot. Even though interference is only a local effect, the spatial reuse of frequency makes the problem of finding the optimal spectrum allocation NP-complete [25, 45], which fails all the optimal allocation based conventional auction mechanisms [135]. Besides, these unique properties of spectrum *butterfly* the effect of the local back-room dealing (i.e., untruthful bidding, collusion among the bidders, frauds of the auctioneer, and bid-rigging between bidders and auctioneer) to the whole network within the coverage of the auctioneer. Therefore, the task of designing a secure spectrum auction is highly challenging but imperative.

To deal with the mutual interference between neighboring bidders, Gandhi et al. [25] has proposed the conflict graph and a general framework for wireless spectrum auctions. Based on these concepts, a truthfully bidding spectrum auction, *VERITAS*, is addressed by Zhou et al. in [135]. The notion of critical neighbor/value is proposed and employed to guarantee the auction strategy-proof. However, the bidders in *VERITAS* must be risk-seeking [99]. Otherwise, if the bidders are only greedy, but still rational and risk neutral, bidders do not have incentive to bid arbitrarily high or low with the concern of overpayment or losing in an auction [36]. In the sealed secondary price/VCG auction, if a risk neutral bidder has no information about the bids of the other bidders, the dominant strategy for him is to bid with his true evaluation values [50, 55]. Zhou et al. [135] also provide an efficient allocation algorithm, which assigns bidders with

spectrum bands sequentially from the bidder with the highest bid to the one with the lowest bid by considering the complex heterogeneous interference constraints. However, the validity of this algorithm is challenged by a special scenario in [124]. Wu et al. in [124] show that it is not always right to allocate the spectrum bands to the bidder with the highest bid in case that the sum of the neighboring bids is much higher than the highest bid. In addition, the collusion among the bidders is described in [124]. As a possible solution, they group the nodes with negligible interference together as virtual bidders, trim the multi-winner spectrum auction [124] into a traditional single-winner auction, and then split the payment or revenue among the participating bidders using game theory. However, it should be noted that the issue of group partition itself is NP-complete in terms of the spatial reuse [45].

Aside from truthfully bidding and collusion among the bidders, a secure spectrum auction design should also take the frauds of the insincere auctioneer (i.e., the auctioneer overcharges the winning bidders with the forged price) and the bid-rigging between the bidders and the auctioneer (i.e., the auctioneer colludes with greedy bidders to manipulate the auction) into consideration[1] . A combination of interference consideration and cryptographic techniques allows us to provide a novel secure spectrum auction scheme, *THEMIS*[2] , to purge these possible back-room dealing. The major contributions of the proposed auction are listed as follows:

[1] In this chapter, greedy bidders and insincere auctioneer are different from malicious attackers, though all of them may impair the performance of the spectrum auction. Greedy bidders and insincere auctioneer are rational because they do not attempt to attack others on sacrificing their own profits. Malicious attackers always try to degrade the performance of the auction even with huge cost. In addition, the fraud and big-rigging are formally defined in Sec. 7.2.2.

[2] *THEMIS* is an ancient Greek goddess who is a blind-folded lady holding a sword and a set of scales as shown in Fig. 7-1. *THEMIS* is world-widely referred as the symbol of truth and justice.

1. *THEMIS* supports spectrum bands with diverse characteristics other than the bands only with uniform characteristics in previous works [25, 124, 135].

2. *THEMIS* provides an effective procedure to auction the spectrum bands with consideration of the interference constraints. To counter the NP-completeness of spectrum allocation in view of the frequency reuse, *THEMIS* divides the whole network into small subnetworks according to the number of bidders and auctions the spectrum bands in subnetworks one by one. Meanwhile, each bidder maintains a local conflict-table, and a bidder is able to update his conflict-table and broadcast the spectrum occupancy information to his neighbors when detecting changes of the environment.

3. *THEMIS* leverages Paillier cryptosystem [81–83] to mask the bidding values of each bidder with a vector of ciphertexts, which enables the auctioneer to find the maximum value, randomize the bids, and charge the bidders securely. In this way, the auctioneer could compute and reveal the results of spectrum auction, while the actual bidding values of the bidders are kept secret from the other bidders and even from the auctioneer himself.

4. *THEMIS* secures the spectrum auction effectively against the back-room dealing with limited communication and computational complexity. Our simulation results show that *THEMIS* achieves similar performance compared with existing insecure auction designs in terms of spectrum utilization, the revenue of the auctioneer, and bidders' satisfactory degree.

The remainder of the chapter is organized as follows. In Section 7.2, system model is outlined and design challenges are described. VCG auction and Paillier cryptosystem are introduced as the fundamentals in Section 7.3. In Section 7.4, the procedure and encryption design of *THEMIS* are illustrated. The performance analysis is presented in Section 7.5. Finally, concluding remarks are drawn in Section 7.6.

7.2 System Model

7.2.1 Overview

We consider a typical spectrum auction setting, where one auctioneer auctions his unutilized spectrum bands $\mathcal{S} = \{1, 2, ..., s\}$ to $\mathcal{N} = \{1, 2, ..., n\}$ nodes/bidders located in the geographic region. The available $\mathcal{S}$ spectrum bands are supposed to have different characteristics to different nodes (in the sequel, we use the words nodes and bidders interchangeably) in terms of the frequency of the available band, the segment type of

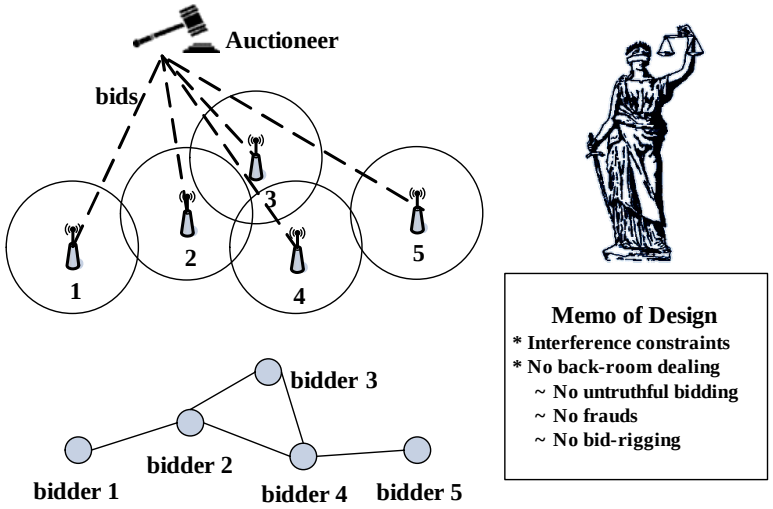

Figure 7-1. System architecture, conflict graph, and secure spectrum auction memo.

the band (i.e., contiguous segment or discontinuous one), the location of the bidders, etc. [75, 76, 125], so that bidders may submit different bids for different combinations of the spectrum bands. Considering the frequency reuse [25, 45], i.e., adjacent nodes must not use the same bands simultaneously while geographically well-separated ones can, we represent the interference relationship among bidders by a conflict graph, which can be constructed from either physical model [8] or protocol model [37] as described in [25, 124, 135, 136]. As shown in Fig. 7-1, the edges stand for mutual interference between corresponding nodes. Moreover, we assume that spectrum auctions take place periodically[3] , the bidders are static in each period, and there is a common channel[4] for necessary information exchanges between the auctioneer and bidders.

[3] The auction period should not be too long (e.g., months or years) to make dynamic spectrum allocation infeasible, and it should not be too short (e.g., seconds or minutes) to incur overwhelming overhead in spectrum trading. The typical duration is hours or days as shown in [31]. In the rest of chapter, we assume that all the spectrum auctions are of fixed duration, so that the time parameter is not included, and we only need to focus on a specific period for the design of secure spectrum auction.

[4] It is like the common control channel (CCC) proposed in [1], or the common pilot channel (CPC) in [93]

The main notations and definitions related to the spectrum auction are summarized as follows.

- *Bidder Set* ($\mathcal{N}$) – $\mathcal{N} = \{1, 2, ..., n\}$ represents the set of n bidders.
- *Spectrum Band Set* ($\mathcal{S}$) – $\mathcal{S} = \{1, 2, ..., s\}$ is the set of s available spectrum bands.
- *Allocation Set* ($\mathcal{N}^{\mathcal{S}}$) – $\mathcal{N}^{\mathcal{S}} = \{\lambda : \mathcal{S} \rightarrow \mathcal{N}\}$ denotes the set of allocations of spectrum bands $\mathcal{S}$ to bidders $\mathcal{N}$. For instance, for $\mathcal{N} = \{1, 2\}$ and $\mathcal{S} = \{1\}$, $\mathcal{N}^{\mathcal{S}} = \{\lambda_1 = (\{1\}, \{\}), \lambda_2 = (\{\}, \{1\})\}$, e.g., $(\{1\}, \{\})$ denotes that spectrum band 1 is allocated to bidder 1 and nothing to bidder 2.
- *Bidding Values* (b_i) – b_i indicates the bidding values of node i for certain allocation set, e.g., for $\mathcal{N}^{\mathcal{S}} = \{\lambda_1 = (\{1\}, \{\}), \lambda_2 = (\{\}, \{1\})\}$, $b_1 = (1, 0)$ and $b_2 = (0, 2)$ indicate that node 1 bids 1 for the allocation λ_1 and 0 for λ_2, and node 2 bids 2 for the allocation λ_2 and 0 for λ_1.
- *Evaluation Values* (v_i) – v_i represents the true evaluation values of node i for certain allocation set. In case that the auction is incentive compatible, v_i equals to b_i.
- *Charging Price* (p_i) – p_i is the price charged by the auctioneer for allocating the spectrum bands to winning bidder i. This charging price might be different among bidders, and the charging mechanisms are different over various allocations as well.
- *Bidder's Utility* (u_i) – u_i stands for the budget balance of bidder i. It is defined as $u_i(\lambda) = v_i(\lambda) - p_i$ for the specific allocation λ.
- *Auctioneer's Revenue* (R) – R denotes the monetary gains of the auctioneer. It is simply expressed as $R = \sum_1^n p_i$.

7.2.2 Design Challenges

To preclude the threats from untruthful spectrum auction bidders, sealed secondary price auction or VCG auction seems to be the most favorite choice, as mentioned in the introduction. However, based on trustable auctioneer, this type of auction is vulnerable to the frauds of the auctioneer and not bid-rigging resistant.

Definition 7.1. A fraud is a deception made by the insincere auctioneer. The auctioneer commits frauds by overcharging the winning bidders with the forged price for his

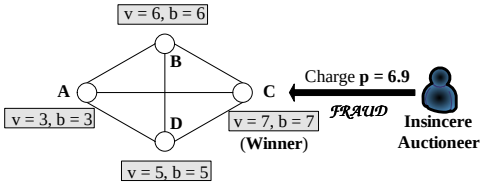

A Frauds of the insincere auctioneer

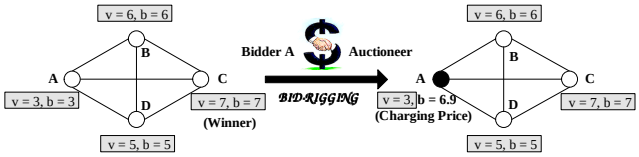

B Bid-rigging between the auctioneer and the bidders

Figure 7-2. Challenges to secure spectrum auction design

personal monetary gain, which damages the utility of the corresponding winners in the spectrum auction.

Definition 7.2. Bid-rigging in the spectrum auction is a form of collusion between the auctioneer and the bidders, where insincere auctioneer conspires with greedy bidders to illegally fix the price, share the spoils, and manipulate the auctions.

To be specific, we take the scenario shown in Fig.7-2 for example, where only one spectrum band is available for auction[5] . In Fig.7-2(a), the winning bid (i.e., the highest bid) is 7 and the charging price (i.e. the second highest bid) should be 6 for the winner C. However, by fabricating a dummy bid close to the highest bid at 6.9, the insincere auctioneer can obtain higher revenue. Since the auction is sealed and no bidders are able to check the bids of others during the auction, the auctioneer may abuse his unsupervised authority by carrying out frauds, which would not be exposed by the bidders unless the winning bidders can verify each bid from their interfering neighbors later after the spectrum auction.

[5] VCG is equivalent to the sealed secondary price auction in the sense of single spectrum band auction.

In Fig.7-2(b), we show an example of bid-rigging between the auctioneer and the bidders. Suppose node A is a greedy bidder who can collude with the auctioneer. Since all the bidding values are open to the auctioneer for appropriately sorting the bids and allocating the bands, the auctioneer can conspire with A by revealing the winning bid of C to A. Node A may bid far more than his true evaluation value so that the auctioneer is able to charge more from winner C, and shares the spoils with A. In this way, no flaws can be found by the winners, even if they take the trouble in verifying each bid after the auction.

Therefore, to purge these potential back-room dealing, an ideal spectrum auction should allow the auctioneer to make the appropriate decision of allocating spectrum bands and publish only the results of the auction, i.e., winners and their payments, while the bidding values must be kept secret even from the auctioneer.

7.3 Preliminaries

In this section, we introduce VCG auction and describe the properties of Paillier cryptosystem as the fundamentals for our proposed *THEMIS* auction.

7.3.1 VCG Auction

As one of the most widely used auction schemes, VCG auction is proved to be individual rational, Pareto efficient, and incentive compatible [117]. In VCG, the dominant strategy for a bidder to win the auction and maximize his utility is to declare his true evaluation values regardless of the bidding actions of the other bidders. Details of VCG auction are as follows. To distinguish from the notations in *THEMIS*, we substitute $\mathcal{S} = \{1, 2, 3, ..., s\}$ with $\mathcal{G} = \{1, 2, 3, ..., g\}$ for illustrative purposes in this subsection.

Bidding :

Each bidder i submits his sealed bidding vector b_i for all the possible allocations $\lambda \in \mathcal{N}^{\mathcal{G}}$.

Allocation :

The auctioneer selects a Pareto efficient allocation $\lambda^* \in \mathcal{N}^{\mathcal{G}}$ based on the truthful bidding values. That is

$$\lambda^* = \underset{\lambda \in \mathcal{N}^{\mathcal{G}}}{\operatorname{argmax}} \Big(\sum_i b_i(\lambda) \Big). \tag{7–1}$$

Then, the goods are assigned according to λ^*.

Charging :

Assume $\lambda^*_{\sim i}$ is an allocation without node i satisfying the following inequality

$$\sum_{j \neq i} b_j(\lambda^*_{\sim i}) \geq \sum_{j \neq i} b_j(\lambda). \tag{7–2}$$

Then, the payment of bidder i is defined as

$$p_i = \sum_{j \neq i} b_j(\lambda^*_{\sim i}) - \sum_{j \neq i} b_j(\lambda^*). \tag{7–3}$$

So, the utility of bidder i is $u_i(\lambda^*) = v_i(\lambda^*) - p_i$. It can also be expressed as

$$\begin{aligned} u_i(\lambda^*) &= v_i(\lambda^*) - \big(\sum_{j \neq i} b_j(\lambda^*_{\sim i}) - \sum_{j \neq i} b_j(\lambda^*) \big) \\ &= \big[v_i(\lambda^*) + \sum_{j \neq i} b_j(\lambda^*) \big] - \sum_{j \neq i} b_j(\lambda^*_{\sim i}), \end{aligned} \tag{7–4}$$

where the last term is determined independently of bidder i's bidding values, so that bidder i can maximize his utility by maximizing the two terms within the square bracket. Since

$$\sum_i b_i(\lambda^*) \geq \sum_i b_i(\lambda), \quad \forall \lambda \in \mathcal{N}^{\mathcal{G}}, \tag{7–5}$$

to maximize his utility, the dominant strategy of bidder i is to submit $b_i(\lambda^*) = v_i(\lambda^*)$, i.e., to bid with his true evaluation values.

Even though VCG auction has several good properties, it cannot be directly extended to spectrum auction because of the following two issues:

1. VCG requires the solution to the optimal allocation, which is NP-complete in spectrum auction w.r.t. the spatial reuse.

2. VCG is vulnerable to the frauds of the insincere auctioneer and the bid-rigging between the bidders and the auctioneer.

7.3.2 Paillier Cryptosystem

In order to thwart the back-room dealing and allocate the spectrum bands, bidding values should be kept secret. On the other hand, the auctioneer has to find the maximum bid and charge the corresponding bidder. Therefore, a cryptosystem is in need for spectrum auction, which enables the auctioneer to properly execute the auction and reveal nothing more than the resultant payments and allocation of spectrum bands.

Paillier cryptosystem is such a probabilistic[6] asymmetric public key encryption system that satisfies these requirements. The special features of Paillier cryptosystem includes homomorphic addition, indistinguishability, and self-blinding [32, 81, 82]:

- **Homomorphic addition.** Given $\mathbb{E}$ is the Paillier's encryption of a message M, $\mathbb{E}(\cdot)$ is additive homomorphic, i.e., $\mathbb{E}(M_1 + M_2) = \mathbb{E}(M_1)\mathbb{E}(M_2)$.

- **Indistinguishability.** $\mathbb{E}(\cdot)$ is considered indistinguishable if the same plaintext M is encrypted twice, these two ciphertexts are totally different, and no one can succeed in distinguishing the corresponding original plaintexts with a probability significantly greater than $1/2$ (i.e., random guessing) unless he decrypts the ciphertexts.

- **Self-blinding.** Any ciphertext can be publicly changed into another one without affecting the plaintext, which means a different randomized ciphertext $\mathbb{E}^{''}(M)$ can be computed from the ciphertext $\mathbb{E}(M)$ without knowing either the decryption key or the original plaintext.

These desired properties of Paillier cryptosystem are essential for our secure spectrum auction design as described in Section 7.4.2.

[6] The term "probabilistic encryption" is typically used in reference to public key encryption algorithms. Probabilistic encryption uses the randomness in an encryption algorithm, so that when encrypting the same plaintext for several times, it will yield different ciphertexts.

7.4 Auction Design of THEMIS

Since spatial reuse of spectrum bands makes finding the optimal spectrum allocation NP-complete [45, 135], researchers resort to greedy algorithms for possible solutions [124, 135]. In order to sort the bidders for the allocation of spectrum bands, the auctioneer has to know the global information of bids in these schemes, rendering them vulnerable to frauds and bid-rigging.

In order to deal with the back-room dealing, the proposed *THEMIS* leverages Paillier cryptosystem to encrypt the bidding values and enable the auctioneer to charge the winners without leaking any information about the bidding values. In parallel with the encryption design, *THEMIS* also provides a supporting conflict-table-driven auction procedure to implement the spectrum auction. Thus, in this section, we first describe the implementation procedure of *THEMIS* to give an overall impression. Then, we dwell on the encryption design details of the proposed auction.

7.4.1 THEMIS: Spectrum Auction Procedure

Similar to the table-driven routing algorithms, we allow each bidder to maintain a local conflict-table reflecting the interference constraints. The local conflict-table can be constructed based on the conflict-matrix derived from the conflict graph as demonstrated in [124]. A bidder needs to update his bids if any of his neighboring nodes in the conflict-table wins spectrum bands or the number of available bands for auction with his interference range has changed.

Considering spatial reuse, the whole network is divided into small subnetworks based on the interference range and the location of the bidders, i.e., subnetwork i consists of all the nodes within the circle area centered at the location of bidder i with the radius of bidder i's interference range. Auction is executed in one subnetwork after another until each node has been the center. The spectrum band allocation and price charged for the winning bidders depend both on the results of the subnetwork auctions

and on the location of the winning bidders (especially for the nodes in the crossing area of different subnetworks) when taking the interference constraints into account.

The detailed procedure of *THEMIS* is presented as follows.

Step 1. Preparation:

Let $\mathcal{N} = \{1, 2, \cdots, i, \cdots, n\}$ be the set of n bidders, $\mathcal{S} = \{1, 2, \cdots, j, \cdots, s\}$ be the set of s spectrum bands, and $\mathcal{N}^{\mathcal{S}} = \{\lambda : \mathcal{S} \rightarrow \mathcal{N}\}$ be the set of possible allocations of spectrum bands to bidders. Each bidder sets up two tables, a conflict-table for storing the nodes causing mutual interference and a price-charged table for storing a series of charging prices for the spectrum bands he won. Bidders fill in the conflict-table with current interfering neighbors and initialize the price-charged table with zeros. For any bidder i, he encloses his identity, location information and his own bidding values b_i for $\mathcal{N}^{\mathcal{S}}$ allocations into his bid, where the identity and location information of bidder i are public to the auctioneer for subnetwork division, allocating spectrum bands and charging prices, but b_i is encrypted using Paillier cryptosystem (How to encrypt b_i is elaborated in the next subsection). Then, bidders submit their bids to the auctioneer.

Step 2. Start-up:

Due to the NP-completeness of spectrum allocation, there is no optimal choice for the auctioneer to start the subnetwork spectrum auctions with a designated bidder in order to maximize his revenue. Therefore, the auctioneer can initiate the subnetwork auctions with a randomly chosen bidder, say node i, where bidder i is regarded as the center of the current subnetwork, and his interference range is set to be the radius of the subnetwork.

Step 3. Bidder Indexing:

The auctioneer sorts the bidders within the subnetwork according to their Euclidean distances from the center i. The closer to the center, the smaller index the bidder is labeled. The auctioneer stores the index information in a distance vector $\mathcal{D}$, whose element d_j denotes the j-th node away from the center i in terms of distance.

Step 4. Subnetwork Auction:

After indexing the bidders, the auctioneer collects the bids and carries out the secure spectrum auction within the subnetwork using Paillier cryptosystem. The results of the subnetwork auction, i.e., the set of winners and the set of corresponding charging prices, are published. Details of encryption design for the secure subnetwork spectrum auction are elaborated in Section 7.4.2.

Step 5. Allocation & Payment:

Determined by both subnetwork auction results and location of the winners, the allocation of spectrum bands and the payment are different in the following three cases:

- *Case 1:* If the current center, bidder i, is not one of the winners, the auctioneer needs to check the elements in the winner set $\mathcal{W}$, choose the winning bidder with the smallest index to be the next center, and set his interference range as the radius of the next subnetwork. According to the results of current subnetwork auction, all the winning bidders store the spectrum bands they won and the corresponding charging prices into their price-charged tables. After that, current center, bidder i, is deleted from the conflict-tables of his neighbors. The subnetwork spectrum auction centered at node i ends, and the auction goes to ***Bidder Indexing*** of the next center for the next subnetwork auction.

- *Case 2:* If the center, bidder i, is the only winner of the auction, and he is charged at p_i for the allocation λ, he will compare the current charging price p_i with the previous charging prices, $\mathcal{P}_\lambda$, stored in his price-charged table and pay the highest one of all the prices for the allocation λ. That is to say, the payment for the center node i is $\max(\mathcal{P}_\lambda)$[7] . Then, the center node updates his spectrum occupancy information and his neighbors eliminate him from their conflict-tables. After that, the auctioneer sets the node with the smallest index as the next center. The auction goes to ***Bidder Indexing*** for the next subnetwork auction.

- *Case 3:* Provided that there are more winners than the current center i, the process is the same as in *Case 2*, except that the auctioneer would rather take the node with the smallest index in the winning set $\mathcal{W}$ as the next center for the consideration of computational efficiency.

The overall spectrum auction procedure of *THEMIS* is summarized in Alg. 5.

[7] Paying $\max(\mathcal{P}_\lambda)$ is to guarantee the center, bidder i, to beat other competitors in the previous subnetwork auctions, where i is not the center.

Algorithm 5 THEMIS - *Spectrum Allocation Procedure*

```
i = randomch(𝒩)
while 𝒩 != ϕ do
    set up the subnetwork centered at i
    𝒟 = sorted 𝒩 by distance to i
    auction 𝒮 securely within the subnetwork
    if i ∉ 𝒲 then
        𝒩 = 𝒩 \ {i}
        i = min(𝒟)
        continue
    else
        allocate(i, λ, max(𝒫_λ))
        𝒩 = 𝒩 \ {i}
        𝒲 = 𝒲 \ {i}
        if 𝒲 == ϕ then
            i = min(𝒟)
            continue
        else
            i = min(𝒟 ∩ 𝒲)
        end if
    end if
end while
```

7.4.2 THEMIS : Secure Spectrum Auction Design

Now, the only problem left is how to securely carry out the spectrum auction in each subnetwork. Since VCG auction has been proved to be incentive-compatible from the bidder side, we can modify it with cryptographic tools to prevent the insincere behaviors from the auctioneer side and apply it into spectrum auctions of the subnetworks. Assuming the only information that the auctioneer can exploit is the subnetwork auction winners and their corresponding payments, there is no way for him to conduct any frauds or bid-rigging to manipulate the market. So, in the encryption design part of *THEMIS*, we elaborate on how to represent the bidding values, how to entitle the auctioneer to select the maximum from the encrypted bids, how to reveal the charging prices for the winners, and how to establish the subnetwork auction resistant to back-room dealing.

7.4.2.1 Representation of bidding values

Bidding Value Encryption.

We use Paillier cryptosystem [81, 83] to mask the bidding values. Assuming k ($1 \leq k \leq q$) is the bidding value for the spectrum allocation λ (i.e., $k = b(\lambda)$), k can be represented by a vector $\mathbf{e}(k)$ of ciphertexts

$$\mathbf{e}(k) = (e^1, \cdots, e^q) = (\underbrace{\mathbb{E}(x), \cdots, \mathbb{E}(x)}_{k}, \underbrace{\mathbb{E}(0), \cdots, \mathbb{E}(0)}_{q-k}), \tag{7–6}$$

where $\mathbb{E}(0)$ and $\mathbb{E}(x)$ account for the Paillier encryption of 0 and the common public element x ($x \neq 0$), respectively. Here, q is a number large enough to cover all the possible bidding values for the allocation of available spectrum bands. For instance, assuming $q = 3$ and $k = 2$ for given spectrum allocation λ, $\mathbf{e}(k) = \mathbf{e}(2) = \big(\mathbb{E}(x), \mathbb{E}(x), \mathbb{E}(0)\big)$.

Because of the self-blinding property of $\mathbb{E}$, k cannot be determined without decrypting each element in the vector $\mathbf{e}(k)$.

Maximum Bid Selection.

The maximum of encrypted bidding value, $\mathbf{e}(k_i) = (e_i^1, ..., e_i^q)$, can be found without leaking information about any other bidding value, $\mathbf{e}(k_j) = (e_j^1, ..., e_j^q), j \neq i$, as follows. Let us consider the product of all the bidding vectors for certain spectrum allocation λ,

$$\prod_i \mathbf{e}(k_i) = (\prod_i e_i^1, \cdots, \prod_i e_i^q). \tag{7–7}$$

Due to the homomorphic addition of Paillier cryptosystem, the j-th component of the vector above can be denoted as

$$y_j = \prod_i e_i^j = \mathbb{E}^{c(j)}(x) = \mathbb{E}(c(j)x), \tag{7–8}$$

where $c(j) = |\{i | j \leq k_i\}|$ indicates the number of values that are equal to or greater than j.

It is obvious that $c(j)$ monotonically decreases when j increases, which gives us some hints to solving the maximum value selection problem. To find the maximum of these bidding values, we decrypt y_j and check whether decryption $\mathbb{E}^{-1}(y_j)$ is equal to 0 or not from $j = q$ down to $j = 1$ until we find the largest j subject to $\mathbb{E}^{-1}(y_j) \neq 0$. This j is equal to $\max\{k_i\}$, i.e., the maximum of the bidding value for the spectrum allocation λ.

Bid Randomization.

We can make the auctioneer randomize the elements in the bidding value vector or add constants to encrypted vector $\mathbf{e}(k) = (e^1, ..., e^q)$ without decrypting $\mathbf{e}(k)$ nor learning k. Shifting $\mathbf{e}(k)$ by a constant r and randomizing the rest of elements, we have

$$\mathbf{e}^{''}(k+r) = (\underbrace{\mathbb{E}(x), \cdots, \mathbb{E}(x)}_{r}, e_1^{''}, \cdots, e_{q-r}^{''}), \tag{7–9}$$

where $e_j^{''}$ is a randomized version of ciphertext e_j. No information about the constant r can be obtained from $\mathbf{e}(k)$ as well as $\mathbf{e}^{''}(k+r)$ w.r.t. self-blinding property of Paillier cryptosystem. Moreover, it should be noted that during randomizing and constant adding operations, neither $\mathbf{e}(k)$ is decrypted nor k is exposed. That is to say, if we compare $\mathbf{e}(k)$ and $\mathbf{e}(k+r)$, we cannot figure out the amount of the shift without decrypting both of them.

7.4.2.2 Secure subnetwork spectrum auction

Representing bids by encrypted vectors based on Paillier cryptosystem, we can easily find the maximum of the given bids and randomize the bidding values without knowing these values themselves, which paves the way to the secure computation of the VCG based spectrum auction in the subnetwork.

For the simplicity of description, we use $\mathbf{E}(f)$ to denote the encrypted vector of bidding values, where f is a function from $\mathcal{N}^{\mathcal{S}}$ to the vector of bidding values. The proposed secure subnetwork spectrum auction is as follows.

Initial Phase :

The auctioneer[8] generates his private and public key of Paillier cryptosystem, and publishes the public key and public element $x(x \neq 0)$ over the common channel.

Bidding Phase :

Step 1 : Each bidder z decides his vector of bidding values b_z for $\mathcal{N}^{\mathcal{S}}$. Since the subnetwork spectrum auction is VCG based, $b_z(\lambda)$, $\forall \lambda \in \mathcal{N}^{\mathcal{S}}$, is also the true evaluation value of bidder z for the allocation λ.

Step 2 : The auctioneer creates $(n+1)$ representing vectors $\mathbf{E}_\xi = \mathbf{E}(O), \mathbf{E}_1 = \mathbf{E}(O), \cdots, \mathbf{E}_n = \mathbf{E}(O)$, where the size of vector $\mathbf{E}$ is equal to $|\mathcal{N}^{\mathcal{S}}|$, and the initial $O(\lambda)$ is always equal to 0.

Step 3 : Each bidder z adds his encrypted bidding value vector b_z to the representing vectors $\mathbf{E}_\xi, \mathbf{E}_1, \cdots, \mathbf{E}_{z-1}, \mathbf{E}_{z+1}, \cdots, \mathbf{E}_n$ except the z-th representing vector $\mathbf{E}_z$ to keep b_z secret. When all bidders have finished this process, the auctioneer obtains

$$\mathbf{E}_\xi = \Big(\prod_i \mathbf{e}\big(b_i(\lambda_1)\big), \prod_i \mathbf{e}\big(b_i(\lambda_2)\big), \cdots, \prod_i \mathbf{e}\big(b_i(\lambda_{|\mathcal{N}^{\mathcal{S}}|})\big) \Big). \tag{7–10}$$

According to the homomorphic addition property of Paillier cryptosystem, the equation above can be rewritten as

$$\begin{aligned} \mathbf{E}_\xi &= \Big(\mathbf{e}\big(\sum_i b_i(\lambda_1)\big), \mathbf{e}\big(\sum_i b_i(\lambda_2)\big), \cdots, \mathbf{e}\big(\sum_i b_i(\lambda_{|\mathcal{N}^{\mathcal{S}}|})\big) \Big) \\ &= \mathbf{E}(\sum_i b_i). \end{aligned} \tag{7–11}$$

Similarly, the auctioneer also has

$$\mathbf{E}_z = \mathbf{E}(\sum_{i \neq z} b_i) \quad z = 1, 2, \cdots, n. \tag{7–12}$$

[8] In fact, the auctioneer should be implemented by plural servers to prevent the auctioneer from learning the bidding values. Indeed, the decryption to find the maximum combination of the bids and the addition of random mask constant r in the following design are performed in a distributed manner by these servers. For the details of how to share the secret information among these servers, please refer to [90, 128].

Opening Phase:

The 5-step opening phase of subnetwork auction consists of two parts: allocation selection and charging price calculation.

I. Allocation Selection

Step 1 : The auctioneer derives $\mathbf{E}(\sum_i b_i + R)$ from $\mathbf{E}_\xi$ by adding a random constant function $R(\lambda) = r$ to mask the values. With $\mathbf{E}(\sum_i b_i + R)$, the auctioneer can find masked maximum sum value of the bids

$$m = \max_{\lambda \in \mathcal{N}^{\mathcal{S}}}(\sum_i b_i(\lambda) + R(\lambda)) = \max_{\lambda \in \mathcal{N}^{\mathcal{S}}}(\sum_i b_i(\lambda)) + r. \tag{7–13}$$

To be more specific, the auctioneer takes the product of the encrypted elements in $\mathbf{E}_\xi$ to obtain $\prod_{j=1}^{|\mathcal{N}^{\mathcal{S}}|} \mathbf{e}(\sum_{i=1}^{n} b_i(\lambda_j) + r)$, and makes use of **Maximum Bid Selection** to determine the maximum element of $\prod_{j=1}^{|\mathcal{N}^{\mathcal{S}}|} \mathbf{e}(\sum_{i=1}^{n} b_i(\lambda_j) + r)$, whose value is $m = \max_{\lambda \in \mathcal{N}^{\mathcal{S}}}(\sum_i b_i(\lambda) + R(\lambda))$.

Step 2 : The auctioneer then decrypts the m-th element of every vector $\mathbf{e}(\sum_i b_i(\lambda) + R(\lambda))$ in $\mathbf{E}_\xi$, i.e., for any allocation $\lambda \in \mathcal{N}^{\mathcal{S}}$, and finds out whether the decryption is equal to x or equal to 0. If it is equal to x at allocation $\lambda^* \in \mathcal{N}^{\mathcal{S}}$, the auctioneer regards λ^* as the allocation that maximizes $\sum_i b_i$, the sum of all bidding values. The allocation λ^* is the result of the subnetwork auction. Correspondingly, the winner set is determined by λ^*.

II. Charging Price Calculation

The auctioneer then computes the charging price p_z of bidder z as shown in Step 3 to Step 5.

Step 3 : The auctioneer derives $\mathbf{e}(\sum_{i \neq z} b_i(\lambda^*) + r^{''})$ from the element $\mathbf{e}(\sum_{i \neq z} b_i(\lambda^*))$ of $\mathbf{E}_z$ by adding a random constant $r^{''}$ to mask the value. Then, the auctioneer decrypts and finds out the masked value of $(\sum_{i \neq z} b_i(\lambda^*) + r^{''})$.

Step 4 : The auctioneer derives $\mathbf{E}(\sum_{i \neq z} b_i + R^{''})$ from $\mathbf{E}_z$ by adding random constant function $R^{''}(\lambda) = r^{''}$ to mask the values. Similar to ***Step 1***, the auctioneer

takes the product of the Paillier encrypted elements in $\mathbf{E}(\sum_{i\neq z} b_i + R^{''})$, and employs **Maximum Bid Selection** to find out the masked maximum, $\max_{\lambda\in\mathcal{N}^{\mathcal{S}}}(\sum_{i\neq z} b_i(\lambda) + r^{''})$. By the definition of $\lambda^*_{\sim x}$, $\max_{\lambda\in\mathcal{N}^{\mathcal{S}}}(\sum_{i\neq z} b_i(\lambda) + r^{''})$ is equal to $(\sum_{i\neq z} b_i(\lambda^*_{\sim z}) + r^{''})$.

Step 5 : After that, the auctioneer calculates the charging price by subtracting these masked values.

$$p_z = \Big(\sum_{i\neq z} b_i(\lambda^*_{\sim z}) + r^{''}\Big) - \Big(\sum_{i\neq z} b_i(\lambda^*) + r^{''}\Big). \tag{7–14}$$

In consistent with the allocation λ^*, bidder z should be charged with p_z for spectrum bands he won in this subnetwork auction.

7.4.3 THEMIS: An Example

To make better understanding of the proposed *THEMIS*, we illustrate it with an example, where $\mathcal{S} = \{1, 2\}$ and $\mathcal{N} = \{1, 2, 3, 4\}$, in a simplified topology reflecting the typical interference constraints as depicted in Fig.7-3(a).

In *THEMIS*, the overall network in Fig.7-3(a) can be substituted with four subnetworks based on the number of the nodes and their mutual interference. Since Subnetwork $\underline{3}$ and Subnetwork $\underline{4}$ are symmetric with the same bidding nodes and available spectrum resource, they can be combined into one subnetwork. Hence, the network can be decomposed into three subnetworks and the spectrum auction is executed in these subnetworks consecutively like the abstract state machine as shown in Fig.7-3(b).

As for Subnetwork $\underline{1}$, node 1 has no conflicts with node 3 and 4 but node 2. The competition for spectrum bands is between node 1 and 2. Therefore, the set of bidders is $\mathcal{N} = \{1, 2\}$, and the set of available spectrum bands is $\mathcal{S} = \{1, 2\}$. So,

$$\begin{aligned}\mathcal{N}^{\mathcal{S}}_{\underline{1}} = \{&\lambda_1 = (\{1, 2\}, \{\}), \lambda_2 = (\{1\}, \{2\}), \lambda_3 = (\{2\}, \{1\}),\\ &\lambda_4 = (\{\}, \{1, 2\})\},\end{aligned}$$

where, e.g., $\lambda_2 = (\{1\}, \{2\})$ indicates that spectrum band 1 is allocated to bidder 1 and band 2 to bidder 2. Assume the truthful bidding values b_1 and b_2 of bidder 1 and 2 are

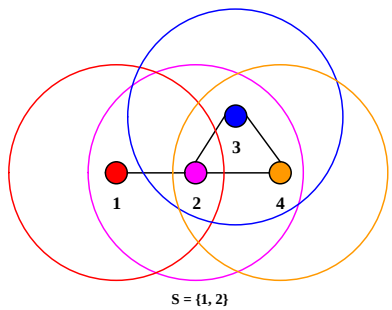

A The topology of the example.

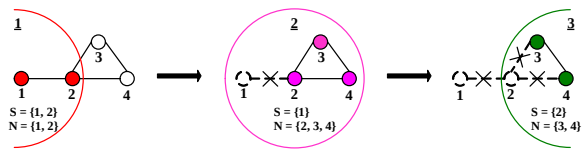

B Subnetwork decomposition for spectrum auctions.

Figure 7-3. An illustrative example for THEMIS.

$b_1 = (3, 2, 2, 0)$ and $b_2 = (0, 0, 2, 3)$, respectively. Then, we obtain

$$b_1 + b_2 = (3, 2, 4, 3).$$

The auctioneer creates $\mathbf{E}_\xi$, $\mathbf{E}_1$, and $\mathbf{E}_2$ = $\mathbf{E}(O)$ = $(\mathbf{e}(0), \mathbf{e}(0), \mathbf{e}(0), \mathbf{e}(0))$. Then, bidders use Paillier cryptosystem to encrypt their bids. Bidder 1 adds his bidding values to $\mathbf{E}_\xi$, $\mathbf{E}_2$ and bidder 2 adds his values to $\mathbf{E}_\xi$, $\mathbf{E}_1$, i.e.,

$$\mathbf{E}_\xi = (\mathbf{e}(3), \mathbf{e}(2), \mathbf{e}(4), \mathbf{e}(3)),$$

$$\mathbf{E}_1 = (\mathbf{e}(0), \mathbf{e}(0), \mathbf{e}(2), \mathbf{e}(3)),$$

$$\mathbf{E}_2 = (\mathbf{e}(3), \mathbf{e}(2), \mathbf{e}(2), \mathbf{e}(0)).$$

First, the auctioneer should find the allocation of spectrum bands in Subnetwork $\underline{1}$.

The auctioneer adds random constant function $R(\lambda) = r = 2$ to $\mathbf{E}_\xi$, which leads to

$$\mathbf{E}(\sum_i b_i + R) = (\mathbf{e}(3+2), \mathbf{e}(2+2), \mathbf{e}(4+2), \mathbf{e}(3+2)).$$

The auctioneer takes the product of all elements in $\mathbf{E}(\sum_i b_i + R)$, $\big(\mathbf{e}(3+2)\cdot\mathbf{e}(4+2)\cdot\mathbf{e}(2+2)\cdot\mathbf{e}(3+2)\big)$, which can also be interpreted as

$$\big(\mathbb{E}(4x), \mathbb{E}(4x), \mathbb{E}(4x), \mathbb{E}(4x), \mathbb{E}(3x), \mathbb{E}(x), \underbrace{\mathbb{E}(0), \cdots, \mathbb{E}(0)}_{q-(4+2)}\big).$$

Then, the auctioneer decrypts this vector to find

$\max_{\lambda\in\mathcal{N}_{\underline{1}}^{S}}(\sum_{i=1,2} b_i(\lambda) + r) = 4+2$. After that, the auctioneer decrypts the $(4+2)$-th element of $\mathbf{e}(3+2), \mathbf{e}(2+2), \mathbf{e}(4+2), \mathbf{e}(3+2)$ to determine $\lambda^* = \lambda_3$.

Next, the auctioneer should calculate the charging prices for the winners in Subnetwork $\underline{1}$.

The auctioneer adds random constant $r^{''} = 1$ to the 3-rd element $\mathbf{e}(2)$ of $\mathbf{E}_1$ to yield

$$\mathbf{e}(\sum_{i\neq 1} b_i(\lambda^*) + r^{''}) = \mathbf{e}(2+1),$$

and decrypts $\mathbf{e}(2+1)$ to find $\big(\sum_{i\neq 1} b_i(\lambda^*) + r^{''}\big) = b_2(\lambda_3) + r^{''} = 2+1$.

Then, the auctioneer adds random constant function $R^{''}(\lambda) = r^{''} = 1$ to $\mathbf{E}_1$ to yield

$$\mathbf{E}(\sum_{i\neq 1}(b_i) + R^{''}) = (\mathbf{e}(0+1), \mathbf{e}(0+1), \mathbf{e}(2+1), \mathbf{e}(3+1)),$$

takes the product of $\big(\mathbf{e}(0+1)\cdot\mathbf{e}(2+1)\cdot\mathbf{e}(0+1)\cdot\mathbf{e}(3+1)\big)$, and then decrypts this to find $\max\big(\sum_{i\neq 1}(b_i) + R^{''}\big) = \big(\sum_{i\neq 1} b_i(\lambda^*_{\sim 1}) + r^{''}\big) = b_2(\lambda_4) + r^{''} = 3+1$.

According to ***Step 5*** in opening phase of the subnetwork spectrum auction, $p_1 = b_2(\lambda_4) - b_2(\lambda_3)$. Thus, the auctioneer calculates $p_1 = (b_2(\lambda_4) + r^{''}) - (b_2(\lambda_3) + r^{''}) = (3+1) - (2+1) = 3-2 = 1$. The auctioneer can also compute $p_2 = 3-2 = 1$ in the same way. Consequently, in terms of spectrum auction in Subnetwork $\underline{1}$, spectrum band 2 is allocated to bidder 1 at the price of 1, and spectrum band 1 is allocated to bidder 2 at the price of 1.

However, the spectrum allocation of bidder 2 is determined not only by the interference between node 2 and 1, but also by the interference between node 2

and node 3, as well as node 4. So, whether available spectrum band 1 should be allocated to bidder 2 and how much the charging price is cannot be determined until the auctioneer finishes the auction in Subnetwork $\underline{2}$ centered at node 2. Before the auction in Subnetwork $\underline{2}$ starts, bidder 1 should update his bid information, i.e., broadcasting his spectrum occupancy and location information to his neighbors to notify them which bands are taken within his interference range.

As a result, the nodes within Subnetwork $\underline{2}$ are only able to bid for the left spectrum band 1 subject to the interference constraints. In this way, bidder 1 and his interference to bidder 2 can be ignored, so that node 1 can be deleted both from the conflict-table of bidder 2 and from the bidder list of auction in Subnetwork $\underline{2}$ as shown in Fig.7-3(b).

Meanwhile, nodes in Subnetwork $\underline{2}$ have to renew their bids for the available spectrum band 1. Hence, the set of the bidders in Subnetwork $\underline{2}$ is $\mathcal{N} = \{2, 3, 4\}$, the spectrum band set is $\mathcal{S} = \{1\}$, and the allocation set can be represented as

$$\mathcal{N}_{\underline{2}}^{\mathcal{S}} = \{\lambda_1 = (\{1\}, \{\}, \{\}), \lambda_2 = (\{\}, \{1\}, \{\}), \lambda_3 = (\{\}, \{\}, \{1\})\}.$$

Similar to auction in Subnetwork $\underline{1}$, e.g., $\lambda_2 = (\{\}, \{1\}, \{\})$ stands for allocating available spectrum band 1 to bidder 3 and no spectrum bands to bidder 2 or bidder 4. Suppose the bidding values b_2, b_3 and b_4 of bidder 2, 3, and 4 are $b_2 = (3, 0, 0)$, $b_3 = (0, 2, 0)$, and $b_4 = (0, 0, 1)$, respectively. The sum of the bidders is $(b_2 + b_3 + b_4) = (3, 2, 1)$.

First, the auctioneer makes $\mathbf{E}_\xi$, $\mathbf{E}_2$, $\mathbf{E}_3$, and $\mathbf{E}_4$ = $(\mathbf{e}(0), \mathbf{e}(0), \mathbf{e}(0))$. Bidder 2 adds his bids to $\mathbf{E}_\xi$, $\mathbf{E}_3$, and $\mathbf{E}_4$, bidder 3 adds his bid to $\mathbf{E}_\xi$, $\mathbf{E}_2$, and $\mathbf{E}_4$, and bidder 4 adds his bid to $\mathbf{E}_\xi$, $\mathbf{E}_2$ and $\mathbf{E}_3$, which leads to

$$\mathbf{E}_\xi = (\mathbf{e}(3), \mathbf{e}(2), \mathbf{e}(1)),$$

$$\mathbf{E}_2 = (\mathbf{e}(0), \mathbf{e}(2), \mathbf{e}(1)),$$

$$\mathbf{E}_3 = (\mathbf{e}(3), \mathbf{e}(0), \mathbf{e}(1)),$$

$$\mathbf{E}_4 = (\mathbf{e}(3), \mathbf{e}(2), \mathbf{e}(0)).$$

Table 7-1. The comparison of different spectrum auction designs.

S-Auction Designs	Spatial Reuse	R-Neutral Attraction	Truthful bidding	Bid-rigging Resistant	Frauds Resistant
VERITAS	✓	×	✓	×	×
M–W	✓	✓	✓	×	×
THEMIS	✓	✓	✓	✓	✓

Then, the auctioneer adds random constant function $R(\lambda)$ to $\mathbf{E}_\xi$, takes the product of elements in $\mathbf{E}_\xi$ and decrypts this to find $\max_{\lambda \in \mathcal{N}_{\underline{2}}^{\mathcal{S}}}(\sum_{i=2,3,4} b_i(\lambda) + R(\lambda))$. After that, the auctioneer decrypts the corresponding max-th element of $\big(\mathbf{e}(3+R(\lambda)), \mathbf{e}(2+R(\lambda)), \mathbf{e}(1+R(\lambda))\big)$ to find $\lambda^* = \lambda_1$.

Then, the auctioneer adds random constant $R^{''}(\lambda) = r^{''} = 2$ to the 1-st component $\mathbf{e}(0)$ of $\mathbf{E}_2$ to obtain $\mathbf{e}(\sum_{i=3,4} b_i(\lambda^*) + r^{''}) = \mathbf{e}(0+2)$, and decrypts $\mathbf{e}(0+2)$ to find $\big(\sum_{i=3,4} b_i(\lambda^*) + r^{''}\big) = b_3(\lambda_1) + b_4(\lambda_1) + r^{''} = 0 + 2$.

The auctioneer adds random constant function $R^{''}(\lambda) = r^{''} = 2$ to $\mathbf{E}_2$ to yield

$$\mathbf{E}(\sum_{i=3,4} b_i + R^{''}) = (\mathbf{e}(0+2), \mathbf{e}(2+2), \mathbf{e}(1+2)).$$

The auctioneer takes the product of $\big(\mathbf{e}(0+2) \cdot \mathbf{e}(2+2) \cdot \mathbf{e}(1+2)\big)$, and decrypts this vector to find $\max(\sum_{i=3,4} b_i + R^{''}) = \sum_{i \neq 2} b_i(\lambda^*_{\sim 2}) + r^{''} = b_3(\lambda_2) + b_4(\lambda_2) + r^{''} = 2 + 2$.

Finally, the auctioneer calculates $p_2 = [b_3(\lambda_2) + b_4(\lambda_2) + r^{''}] - [b_3(\lambda_1) + b_4(\lambda_1) + r^{''}] = (2+2) - (0+2) = 2 - 0 = 2$. For Subnetwork $\underline{2}$, spectrum band 1 is allocated to bidder 2, and spectrum band 2 is not vacant. Furthermore, since node 2 lies in the crossing area of Subnetwork $\underline{1}$ and Subnetwork $\underline{2}$, his payment for the spectrum band 1 should be $p_2 = \max\{p_{(2,\underline{1})}, p_{(2,\underline{2})}\} = \max\{1, 2\} = 2$.

In Subnetwork $\underline{3}$, all these processes are repeated, and node 3 and 4 are charged in the same manners.

7.5 Simulation and Analysis

Compared with two existing spectrum auction schemes, *VERITAS* [135] and the Multi-Winner spectrum auction (*M-W*) [124], *THEMIS* beats two unsolved challenges

of secure spectrum auction design, i.e., the frauds of the insincere auctioneer and the bid-rigging between bidders and auctioneer. Leveraging subnetwork division and Paillier cryptosystem encrypted subnetwork auction, the proposed *THEMIS* is resistant to these two back-room dealing, while it supports spatial reuse, attracts risk neutral bidders, and guarantees strategy-proof bidding as listed in Table I.

In this section, we also show that *THEMIS* achieves similar performance to *VERITAS* and *M-W* in terms of spectrum utilization, auctioneer's revenue, and bidders' satisfactory degree. Besides, we carry out the security analysis of *THEMIS* and demonstrate the efficiency of the proposed spectrum auction by evaluating its communication and computational complexity.

7.5.1 Performance Comparison

7.5.1.1 Simulation setup

We assume the spectrum auction hosted by the auctioneer is deployed in a 1*1 square area, where nodes are uniformly distributed and connected [6, 112, 127]. Suppose the wireless mutual interference is simply distance-based, and any two bidders within 0.1 distance conflict with each other and cannot be allocated with the same spectrum bands. The bidding values of different bidders over different bands are supposed to be i.i.d random variables uniformly distributed over $(0, 10]$. To be simple, we let each bidder request only one spectrum band.

We use the following three performance metrics to compare *THEMIS* with *VERITAS* and *M-W*.

- *Spectrum Utilization :* It is the sum of allocated spectrum bands of all the winning bidders, which is the same as the definition in [135].
- *Auctioneer's Revenue :* It is the sum of payments of all the winning bidders, as defined in Section 7.2.
- *Bidders' Satisfaction :* It is defined as the ratio of $\sum_{i \in \mathcal{W}} u_i$ to $\sum_{i \in \mathcal{N}} v_i$, which denotes the percentage of bidders' potential monetary gains realized.

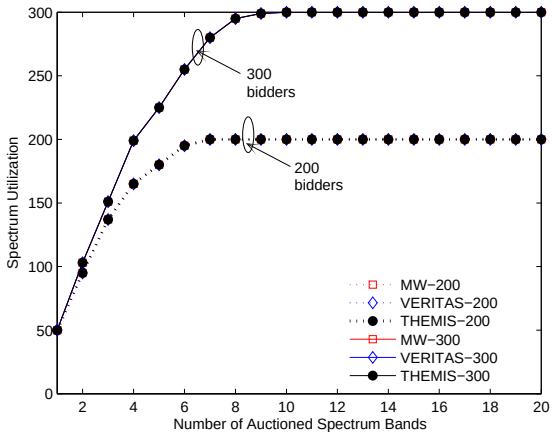

A Spectrum Utilization

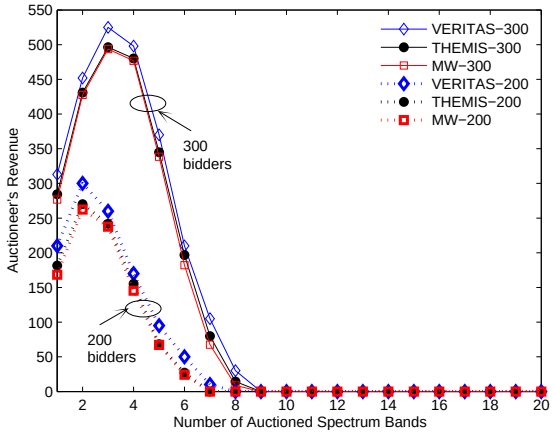

B Revenue of the Auctioneer

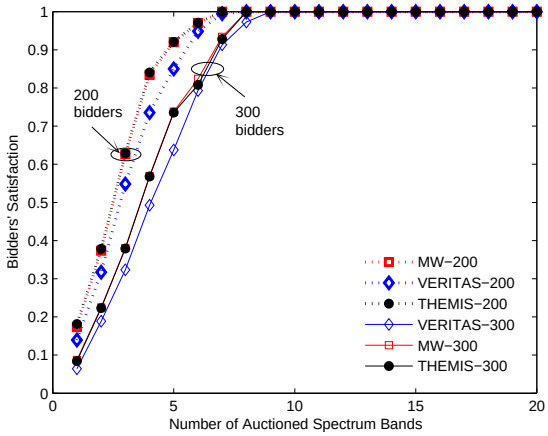

C Bidders' Satisfaction

Figure 7-4. Performance comparison of *THEMIS*, *VERITAS* and *M-W*

7.5.1.2 Results and analysis

When we compare the performance of *THEMIS* with that of *VERITAS* or *M-W*, we assume all the auctions are collusion-free, and there are not any frauds or bid-rigging. In Fig.7-4, we plot the spectrum utilization, auctioneer's revenue, and bidder's satisfaction of the three auction designs with 200 bidders and 300 bidders, respectively.

In Fig.7-4(a), as the number of spectrum bands increases, the spectrum utilization also increases until it saturates (i.e., every bidder is allocated a band) in all these three auctions. It is not surprising that the performance results of *THEMIS*, *VERITAS* and *M-W* are the same in terms of spectrum utilization, because they mainly differ in their price charging designs if all the possible back-room dealing could be neglected.

In Fig.7-4(b), we find that *THEMIS* and *M-W* are almost the same in terms of the auctioneer's revenue, and *THEMIS* is slightly higher than *M-W* at only a few points. It makes sense because *THEMIS* originates from the VCG auction and *M-W* is based on secondary price auction, while VCG is equivalent to secondary price auction provided that the good is a single item [55]. Therefore, the performance results of *THEMIS* and *M-W* are quite similar in our simulations. The bump of *THEMIS* over *M-W* is from the payments for the winning bidders located in the crossing area, as we illustrated in Section 7.4.1. In addition, *VERITAS* is characterized by charging the winners with their *critical neighbor* prices [135], which make it perform a little bit better than the other two schemes in the auctioneer's revenue.

On the other hand, in Fig.7-4(c), *VERITAS* loses his advantages correspondingly, and *THEMIS* and *M-W* outperform it in bidders' satisfactory degree. Actually, the auctioneer's revenue and bidders' satisfactory degree are just two complementary evaluation metrics.

From the comparison and analysis above, we show that *THEMIS* sacrifices nothing in performance when guaranteeing the spectrum auction secure.

Table 7-2. The communication complexity

pattern	round	volume
the bidder $\leftrightarrow$ the auctioneer	$\mathcal{O}(n \log n)$	$\mathcal{O}\big(n \log n \times (\log n)^s \times q \log n\big)$
the bidder $\leftrightarrow$ neighbor bidders	$\mathcal{O}(\log n)$	$\mathcal{O}(\log n)$

Table 7-3. The computational complexity

	computational complexity
the bidder	$\mathcal{O}\big(n \log n \times (\log n)^s \times q \log n\big)$
the auctioneer	$\mathcal{O}\big(a \times n \log n \times (\log n)^s \times q \log n\big)$

7.5.2 Security Analysis

Before presenting our security analysis of *THEMIS*, we must re-emphasize and clarify two properties of Paillier cryptosystem. First, due to the indistinguishability of this encryption, no information about the value k can be leaked out from its representation $\mathbf{e}(k)$ without decrypting each element. Second, self-blinding property makes it impossible to find a mapping function from $\mathbf{e}(k)$ to $\mathbf{e}^{''}(k + r)$, where r is a random number.

To prevent an insincere auctioneer from learning the bids and manipulating the auction by frauds, we embodies the auctioneer by multiple servers[9] in *THEMIS*. The decryption to determine the maximum of truthful bidding values and the addition of random mask constant r are both performed in a distributed manner by these servers, so that no insincere auctioneer can decrypt to learn about the bids or learn random mask constant r illegally. Hence, *THEMIS* can keep bids confidential except the results of the auction, i.e., the winners and their corresponding payments.

Asides from the frauds, the bid-rigging between the bidders and the auctioneer becomes meaningless because the auctioneer himself knows nothing more than the

[9] The keys for decrypting bidding values are shared by the plural servers by using secret sharing technique. A lot of secret sharing or group decription mechanisms can be employed to effectively prevent the distributed servers from colluding with each other to reveal the bids. Please refer to [91, 101] for the details about secret sharing designs.

winners and their payments in *THEMIS*. Even if a certain bidder colludes with each of servers composing the auctioneer, he is not able to find out any information about the bids if the auction is carried out in a distributed manner by these servers.

Obviously, *THEMIS* satisfies the fairness requirements of the spectrum auction because it treats all the bidders equally, selects the bidder with the highest bid to win the spectrum band in each subnetwork, and makes the multiple winning bidders pay by predefined rule. Besides, *THEMIS* also guarantees the confidentiality and anonymity of the spectrum auction in the sense that it leaks out no more information than the winning bidders and corresponding price charged during both the bidding phase and opening phase.

7.5.3 Efficiency Analysis

The communication and computational complexity of *THEMIS* are determined by several factors, namely, the number of bidders n, the number of available spectrum bands s, the number of possible bidding values q, and the number of servers a composing the auctioneer. Here, we assume the network in the auction area is connected, which implies that the node density of the subnetworks is on the order of $\mathcal{O}(\log n)$ [127].

Table 7-2 shows the communication pattern, the order of communication rounds and the communication volume per bidder in *THEMIS*. The communication complexity from the bidder to the auctioneer is linear in terms of the number of possible bidding values q, so it may incur a heavy cost for a large range of bidding values. However, this is inevitable cost for purging the back-room dealing. Meanwhile, the communication complexity are closely related to s. Since spectrum is scare resource and the available bands cannot be arbitrarily large, s may only impose limited communication cost. Compared with conventional secure auction designs [113, 129, 130], there is also additional communication complexity incurred by the subnetwork decomposition. But

this overhead is avoidable when we take frequency reuse into consideration in spectrum auctions.

Table 7-3 shows the computational complexity for the auctioneer and a bidder in *THEMIS*. Similar to the communication cost, the complexity of each bidder and the auctioneer is related to the subnetwork composition, linear in terms of the number of possible bidding values q and exponential in terms of available spectrum bands s, which are inevitable but limited.

7.6 Chapter Summary

In this chapter, we have incorporated cryptographic technique into the spectrum auction design and proposed *THEMIS*, a secure spectrum auction scheme leveraging Paillier cryptosystem to purge the back-room dealing. Considering spectrum reuse, we have divided the whole network into small subnetworks and allowed the bidders to maintain and update their conflict-tables, which facilitate the spectrum allocation. *THEMIS* masks the bidding values of a bidder with a vector of Paillier ciphertexts, whose additive homomorphic property enables the auctioneer to find the maximum bid and calculate the charging prices securely in the subnetwork auction, while the actual bidding values are kept secret. In this case, frauds and bid-rigging becomes impossible, and manipulation of the auction is implausible. We have also shown that *THEMIS* is a secure spectrum auction with limited communication and computational complexity, and is as good as other insecure spectrum auction schemes in terms of spectrum utilization, the auctioneer's revenue, and bidders' satisfaction.

CHAPTER 8
CONCLUSION

In this dissertation, we have studied several challenging and fundamental issues related to the architecture, modeling and design of multi-hop CRNs. The main contributions of this dissertation can be summarized as follows.

Considering the uncertain spectrum supply from the PSPs, we first introduce an intuitive method, the X loss, to quantify the risk for SUs at a given confident level. Since the X loss theoretically underestimates the potential risk for OSA and mathematically lacks of subadditivity, we further propose the expected X loss, a more suitable risk measurement for OSA with desired properties. Based on the simplified expected X loss, we formulate the SSP's band-mix selection for traffic splitting into an optimization problem and solve it by linear programming. By numerical simulations, we show that compared with the X loss based band-mix selection for OSA, the expected X loss based selection not only provides much more accurate efficient OSA curves at different confidence levels, but also gives much better performance in terms of spectrum utilization, SUs' satisfaction and the SSP's profit, especially when the distribution of the primary services has a fat tail.

With those metrics, we have proposed a novel architecture of CRNs for spectrum harvesting and sharing, and presented a theoretical study on the joint frequency scheduling and routing problem in multi-hop CRNs under uncertain spectrum supply. We first introduce a new service provider, SSP, and let the SSP provide coverage in CRNs with low-cost CR mesh routers in order to facilitate the accessing of SUs without CR capability. Enlightened by the statistics of spectrum utilization, we then model the vacancy of an available band with a random variable satisfying certain statistical distribution. After that, we elaborate on scheduling and interference constraints as well as routing constraints w.r.t. the unpredictable activities of primary services. Furthermore, we characterize the network with a pair of (α, β) parameters, and present

a mathematical formulation with the goal of minimizing the required network-wide spectrum resource at a (α, β) level for a set of CR sessions with rate requirements. Since the formulated optimization problem is NP-hard, we derive a lower bound for the objective by relaxing the integer variables. Furthermore, we propose a coarse-grained fixing algorithm for a feasible solution. Through simulations, we show that the solution attained by the proposed algorithm is near-optimal to the formulated NP-hard problem at any (α, β) level; meanwhile, the (α, β) based solution is better than expected bandwidth based one in terms of blocking ratio and spectrum utilization.

Under the proposed network architecture, we have studied the path selection problem in multi-hop CRNs under flow routing, link scheduling and CR source's budget constraints. Considering the inherent single radio constraint of CR devices and the features of spectrum trading, we propose a 4-D conflict graph to describe the conflict relations among CR links. After that, we mathematically formulate the path selection problem under multiple constraints into an optimization problem with the objective of maximizing the end-to-end throughput for the CR session. Given all independent sets in 4-D conflict graph, we can relax the formulated optimization problem and solve it by linear programming. Regarding the NP-hardness of finding all independent sets, we provide a heuristic algorithm as well, which layers the 4-D conflict graph and exploits the maximum local cliques to approximately select the path with the highest throughput. By simulations, we demonstrate how the CR source's budget, the number of available bands and distance from CR source affect the performance of path selection in terms of path capacity. We also compare the heuristic path selection algorithm with the optimal one and show that the throughput obtained from the heuristic algorithm is close to that obtained from the optimal one in multi-hop CRNs.

As an extension of path selection in multi-hop CRNs, we have proposed a novel spectrum trading system, i.e., spectrum clouds, and presented a theoretical study on the optimal session based spectrum trading problem under multiple cross-layer constraints

in multi-hop CRNs. Considering the special features of session based spectrum trading, we exploit the 3-D (link-band-radio) conflict graph to characterize the conflicts among CR links and mathematically describe the competitions among candidate trading sessions in spectrum clouds. Given the rate requirements and bidding values of candidate trading sessions, we formulate the optimal spectrum trading into the SSP's revenue maximization problem under the availability of spectrum, link scheduling and flow routing constraints in multi-hop CRNs. Since the formulated problem is NP-hard to solve, we derive an upper bound for the optimization by relaxing the integer variables. Furthermore, we propose heuristic algorithms for feasible solutions (low bounds as well). Through simulations, we show that: i) the proposed session based spectrum trading has superior advantages over the per-user based one in multi-hop CRNs; ii) the solutions attained by the proposed heuristic algorithms are near-optimal under different data sets in both the grid topology and the random one.

We have also studied the throughput maximization problem in C-VANETs under multiple constraints (i.e., CR devices' inherent single-radio constraint, the availability of licensed spectrum, transmission mode selection and link scheduling). Considering the special features of cooperative communications, we first extend the links and classify them into cooperative links/general links. Then, depending on the available bands at different extended links, we define extended link-band pairs and form a 3-D cooperative conflict graph to describe the conflict relationship among those pairs. After that, we mathematically formulate the end-to-end throughput maximization problem. Given all cooperative independent sets in C-VANETs, we can relax the formulated optimization problem and near-optimally solve it by linear programming. Due to the NP-completeness of finding all independent sets, we provide a heuristic pruning algorithm for the cooperative communication aware link scheduling as well. By numerical simulations, we demonstrate that: i) the CR capability creates more opportunities for using cooperative communications; ii) the performance of link scheduling with

appropriately selected transmission mode is better than that purely relying on one transmission mode (either cooperative communications or direct transmissions).

As for the security issues in multi-hop CRNs, we have incorporated cryptographic technique into the spectrum auction design and proposed *THEMIS*, a secure spectrum auction scheme leveraging Paillier cryptosystem to purge the back-room dealing. Considering spectrum reuse, we have divided the whole network into small subnetworks and allowed the bidders to maintain and update their conflict-tables, which facilitate the spectrum allocation. *THEMIS* masks the bidding values of a bidder with a vector of Paillier ciphertexts, whose additive homomorphic property enables the auctioneer to find the maximum bid and calculate the charging prices securely in the subnetwork auction, while the actual bidding values are kept secret. In this case, frauds and bid-rigging becomes impossible, and manipulation of the auction is implausible. We have also shown that *THEMIS* is a secure spectrum auction with limited communication and computational complexity, and is as good as other insecure spectrum auction schemes in terms of spectrum utilization, the auctioneer's revenue, and bidders' satisfaction.

REFERENCES

[1] IEEE P802.22/D0.1 Draft Standard for Wireless Regional Area Networks Part 22: Cognitive Wireless RAN Medium Access Control (MAC) and Physical Layer (PHY) specifications: Policies and procedures for operation in the TV Bands, IEEE 802.22 Working Group on Wireless Regional Area Networks, IEEE doc: 22-06-0067-00-0000_P802-22_D0.1, May 2006.

[2] R. Agusti, O. Sallent, J. Perez-Romero, and L. Giupponi. A fuzzy-neural based approach for joint radio resource management in a beyond 3g framework. In *Proc. of the International Conference on Quality of Service in Heterogeneous Wired/Wireless Networks, QSHINE 2004*, Dallas, TX, October 2004.

[3] I.F. Akyildiz, W. Lee, M. Vuran, and M. Shantidev. Next generation/ dynamic spectrum access/ cognitive radio wireless networks: a survey. *Computer Networks (Elsevier) Journal*, 50(4):2127–2159, September 2006.

[4] Mansoor Alicherry, Randeep Bhatia, and Li (Erran) Li. Joint channel assignment and routing for throughput optimization in multi-radio wireless mesh networks. In *Proc. of international conference on Mobile computing and networking, ACM Mobicom 2005*, Cologne, Germany, August 2005.

[5] Soren Asmussen. *Applied probability and queues*. John Wiley & Sons Ltd., West Sussex, UK, 1987.

[6] C. Bettstetter. On the minimum node degree and connectivity of a wireless multihop network. In *Proc. of ACM international symposium on Mobile ad hoc networking and computing, Mobihoc '02*, Lausanne, Switzerland, June 2002.

[7] Colin Boyd and Wenbo Mao. Security issues for electronic auctions. In *Proc. of the Financial Cryptography Conference FC '03*, Guadeloupe, French West Indies, Jan. 2003.

[8] Chun-Chia Chen and Duan-Shin Lee. A joint design of distributed qos scheduling and power control for wireless networks. In *Proc. of IEEE Conference on Computer Communications, INFOCOM '06*, Barcelona, Catalunya, Spain, April 2006.

[9] D. Chen, S. Yin, Q. Zhang, M. Liu, and S. Li. Mining spectrum usage data: a large-scale spectrum measurement study. In *Proc. of international conference on Mobile computing and networking, ACM Mobicom, 2009*, Beijing, China, September 2009.

[10] Feng Chen, Hongqiang Zhai, and Yuguang Fang. Available bandwidth in multirate and multihop wireless ad hoc networks. *IEEE Journal on Selected Areas in Communications*, 28(3):299–307, April 2010.

[11] R. Chen, J.-M. Park, and J. H. Reed. Defense against primary user emulation attacks in cognitive radio networks. *IEEE Journal on Selected Areas in Communications*, 26(1), January 2008.

[12] Y. Chen, Q. Zhao, and A. Swami. Joint design and separation principle for opportunistic spectrum access in the presence of sensing errors. *IEEE Transactions on Information Theory*, 54(5):2053–2071, May 2008.

[13] P. Cramton, Y. Shoham, and R. Steinberg. *Combinatorial auctions*. MIT Press, 2006.

[14] Defense Advanced Research Projects Agency (DARPA). The neXt generation program (XG) official website.

[15] Reinhard Diestel. *Graph Theory*. Springer, 2005.

[16] Lei Ding, Tommaso Melodia, Stella Batalama, and John Matyjas. Distributed routing, relay selection, and spectrum allocation in cognitive and cooperative ad hoc networks. In *Proc. of IEEE Communications Society Conference on Sensor and Ad Hoc Communications and Networks, SECON, 2010*, Boston, MA, June 2010.

[17] Zhiguo Ding and Kin K. Leung. Cross-layer routing using cooperative transmission in vehicular ad-hoc networks. *IEEE Journal on Selected Areas in Communications*, 29(3):571–581, March 2011.

[18] Richard Draves, Jitendra Padhye, and Brian Zill. Routing in multi-radio, multi-hop wireless mesh networks. In *Proc. of international conference on Mobile computing and networking, ACM Mobicom 2004*, Philadelphia, PA, September 2004.

[19] Lingjie Duan, Jianwei Huang, and Biying Shou. Cognitive mobile virtual network operator: Investment and pricing with supply uncertainty. In *Proc. of IEEE Conference on Computer Communications, INFOCOM 2010*, San Diego, CA, March 2010.

[20] FCC. Spectrum policy task force report. Report of Federal Communications Commission, Et docket No. 02-135, November 2002.

[21] FCC. Unlicensed operation in the tv broadcast bands and additional spectrum for unlicensed devices below 900 mhz and in the 3 ghz band. Report of Federal Communications Commission, ET Docket No. 04-186 and ET Docket No. 02-380, September 2010.

[22] W. Feller. *An Introduction to Probability Theory and its Applications*. John Wiley Sons Inc., New York, NY, 1971.

[23] Zhenhua Feng and Yaling Yang. Joint transport, routing and spectrum sharing optimization for wireless networks with frequency-agile radios. In *Proc. of IEEE*

Conference on Computer Communications, INFOCOM 2009, Rio de Janeiro, Brazil, April 2009.

[24] Serguei Foss, Takis Konstantopoulos, and Stan Zachary. Discrete and continuous time modulated random walks with heavy-tailed increments. *Journal of Theoretical Probability*, 20(3):581ł612, 2007.

[25] S. Gandhi, C. Buragohain, L. Cao, H. Zheng, and S. Suri. A general framework for wireless spectrum auctions. In *Proc. of IEEE International Symposium on New Frontiers in Dynamic Spectrum Access Networks, DySPAN 2007*, Dublin, Ireland, April 2007.

[26] G. Ganesan and Y. (G.) Li. Cooperative spectrum sensing in cognitive radio: Part i: two user networks. *IEEE Transactions on Wireless Communications*, 6:2204–2213, June 2007.

[27] G. Ganesan and Y. (G.) Li. Cooperative spectrum sensing in cognitive radio: Part ii: Multiuser networks. *IEEE Transactions on Wireless Communications*, 6(6):2214 – 2222, June 2007.

[28] Cunhao Gao, Yi Shi, Y. Thomas Hou, Hanif D. Sherali, and Huaibei Zhou. Multicast communications in multi-hop cognitive radio networks. *to appear in IEEE Journal on Selected Areas in Communications*, 2011.

[29] Michael R. Garey and David S. Johnson. *Computers and Intractability: A Guide to the Theory of NP-Completeness*. W. H. Freeman and Company, New York, NY, 1979.

[30] Michael R. Garey and David S. Johnson. *Computers and Intractability; A Guide to the Theory of NP-Completeness*. W. H. Freeman & Co., New York, NY, 1990.

[31] L. Giupponi, R. Agusti, J. Perez-Romero, and O. Sallent Roig. A novel approach for joint radio resource management based on fuzzy neural methodology. *IEEE Transactions on Vehicular Technology*, 57(3):1789–1805, May 2008.

[32] E. Goh. Encryption schemes from bilinear maps. Ph.D. Thesis, Stanford University, USA, September 2007.

[33] Andrea Goldsmith. *Wireless Communications*. Cambridge University Press, Cambridge, NY, 2005.

[34] Google. Proposal by google inc. to provide a tv band device database management solution. Proposals from Entities Seeking to Be Designated TV Band Device Database Managers, DA 09-2479, January 2010.

[35] D. Grandblaise, P. Bag, P. Levine, K. Moessner, and M. Pan. Microeconomics inspired mechanisms to manage dynamic spectrum allocation. In *Proc. of IEEE International Symposium on New Frontiers in Dynamic Spectrum Access Networks, DySPAN 2007*, Dublin, Ireland, April 2007.

[36] T. Groves. Incentives in teams. *Econometrica*, 41:617–631, 1973.

[37] P. Gupta and P. R. Kumar. The capacity of wireless networks. *IEEE Transactions on Information Theory*, 46(2):388–404, March 2000.

[38] W.V. Harlow. Asset allocation in a downside risk framework. *Financial Analysts Journal*, 47(5):28 – 40, September 1991.

[39] Glyn Holton. *Value-at-Risk: Theory and Practice*. Academic Press, 2003.

[40] A. Host-Madsen and J. Zhang. Capacity bounds and power allocation for wireless relay channels. *IEEE Transactions on Information Theory*, 51(6):2020–2040, June 2005.

[41] Y. Thomas Hou, Yi Shi, and Hanif D. Sherali. Optimal spectrum sharing for multi-hop software defined radio networks. In *Proc. of IEEE Conference on Computer Communications, INFOCOM '07*, Anchorage, AK, May 2007.

[42] Y. Thomas Hou, Yi Shi, and Hanif D. Sherali. Optimal spectrum sharing for multi-hop software defined radio networks. In *Proc. of IEEE Conference on Computer Communications, INFOCOM 2007*, Anchorage, AL, May 2007.

[43] Y. Thomas Hou, Yi Shi, and Hanif D. Sherali. Spectrum sharing for multi-hop networking with cognitive radios. *IEEE Journal on Selected Areas in Communications*, 26(1):146–155, January 2008.

[44] H. Ilhan, M. Uysal, and I. Altunbas. Cooperative diversity for intervehicular communication: Performance analysis and optimization. *IEEE Transactions on Vehicular Technology*, 58(7):3301–3310, Februrary 2009.

[45] K. Jain, J. Padhye, V. N. Padmanabhan, and L. Qiu. Impact of interference on multi-hop wireless network performance. In *Proc. of Mobile Computing and Networking, Mobicom '03*, San Diego, CA, September 2003.

[46] A. Jamalipour. *The Wireless Mobile Internet: Architectures, Protocols, and Services*. John Wiley & Sons Ltd., West Sussex, UK, 2003.

[47] Boangoat Jarupan and Eylem Ekici. A survey of cross-layer design for VANETs. *Ad Hoc Networks*, 9(5):966–983, July 2011.

[48] J. Jia, Q. Zhang, Q. Zhang, and M. Liu. Revenue generation for truthful spectrum auction in dynamic spectrum access. In *Proc. of ACM International Symposium on Mobile Ad Hoc Networking and Computing, ACM MobiHoc, 2009*, New Orleans, LA, May 2009.

[49] J. R. Key. Routing in probabilistic networks. Master's Thesis, Massachusetts Institute of Technology, USA, June 2004.

[50] H. Kikuchi. (m+1)st-price auction protocol. In *Proc. of Financial Cryptography, FC '01*, Grand Cayman, British West Indies, February 2001.

[51] H. Kim and K. G. Shin. Efficient discovery of spectrum opportunities with mac-layer sensing in cognitive radio networks. *IEEE Transactions on Mobile Computing*, 7(5):533–545, May 2008.

[52] P. Klemperer. Auction theory: a guide to the literature. *Economics Surveys*, 13(3):227–286, 1999.

[53] M. Kodialam and T. Nandagopal. Characterizing the capacity region in multi-radio multi-channel wireless mesh networks. In *Proc. of international conference on Mobile computing and networking, ACM Mobicom 2005*, Cologne, Germany, August 2005.

[54] G. Kramer, M. Gastpar, and P. Gupta. Cooperative strategies and capacity theorems for relay networks. *IEEE Transactions on Information Theory*, 51(9):3037–3063, September 2005.

[55] V. Krishna. *Auction Theory*. Academic Press, 2002.

[56] M. Kurth, A. Zubow, and J.-P. Redlich. Cooperative opportunistic routing using transmit diversity in wireless mesh networks. In *Proc. of IEEE Conference on Computer Communications, INFOCOM 2008*, Phoenix, AZ, April 2008.

[57] Pradeep Kyasanur and Nitin H. Vaidya. Capacity of multi-channel wireless networks: impact of number of channels and interfaces. In *Proc. of international conference on Mobile computing and networking, ACM Mobicom 2005*, Cologne, Germany, August 2005.

[58] J. Nicholas Laneman. Cooperative diversity in wireless networks: Algorithms and architectures. PhD's Thesis, Massachusetts Institute of Technology, USA, September 2002.

[59] J. Nicholas Laneman, David N. C. Tse, and Gregory W. Wornell. Cooperative diversity in wireless networks: efficient protocols and outage behavior. *IEEE Transactions on Information Theory*, 50(12):3062–3080, December 2004.

[60] Won-Yeol Lee and I. F. Akyildiz. Optimal spectrum sensing framework for cognitive radio networks. *IEEE Transactions on Wireless Communications*, 7(10):3845–3857, October 2008.

[61] H. Li, Y. Cheng, C. Zhou, and P. Wan. Multi-dimensional conflict graph based computing for optimal capacity in MR-MC wireless networks. In *Proc. of International Conference on Distributed Computing Systems, ICDCS 2010*, Genoa, Italy, June 2010.

[62] Hongkun Li, Yu Cheng, Pengjun Wan, and Jiannong Cao. Local sufficient rate constraints for guaranteed capacity region in multi-radio multi-channel wireless

networks. In *Proc. of IEEE Conference on Computer Communications, INFOCOM 2011*, Shanghai, China, April 2011.

[63] Xiaojun Lin and Ness B. Shroff. Joint rate control and scheduling in multihop wireless networks. In *Proc. of IEEE Conference on Decision and Control*, Paradise Island, Bahamas, December 2004.

[64] Xiaojun Lin and Ness B. Shroff. The impact of imperfect scheduling on cross-layer congestion control in wireless networks. *IEEE/ACM Transactions on Networking*, 14(2):302–315, April 2006.

[65] K. Liu and Q. Zhao. Indexability of restless bandit problems and optimality of whittle index for dynamic multichannel access. *IEEE Transactions on Information Theory*, 56(11):5547–5567, November 2010.

[66] K. J. Ray Liu, Ahmed K. Sadek, Weifeng Su, and Andres Kwasinski. *Cooperative Communications and Networking*. Cambridge University Press, Cambridge, NY, 2008.

[67] Pei Liu, Zhifeng Tao, Sathya Narayanan, Thanasis Korakis, and Shivendra S. Panwar. Coopmac: A cooperative mac for wireless lans. *IEEE Journal on Selected Areas in Communications*, 25(2):340–354, February 2007.

[68] Xin Liu and Wei Wang. On the characteristics of spectrum-agile communication networks. In *Proc. of IEEE International Symposium on New Frontiers in Dynamic Spectrum Access Networks, DySPAN 2005*, Baltimore, MD, November 2005.

[69] Harry Markowitz. Portfolio selection. *The Journal of Finance*, 7(1):77–91, Mar. 1952.

[70] M. McHenry. Spectrum white space measurements. New america foundation broadband forum, June 20, 2003.

[71] M. A. McHenry, P. A. Tenhula, D. McCloskey, D. A. Roberson, and C. S. Hood. Chicago spectrum occupancy measurements and analysis and a long-term studies proposal. In *Proc. of TAPAS 2006*, Boston, MA, August 2006.

[72] Shridhar Mubaraq Mishra, Danijela Cabric, Chen Chang, Daniel Willkomm, Barbara Van Schewick, Adam Wolisz, and Robert W. Brodersen. A real time cognitive radio testbed for physical and link layer experiments. In *Proc. of IEEE International Symposium on New Frontiers in Dynamic Spectrum Access Networks, DySPAN 2005*, Baltimore, MD, November 2005.

[73] J. Mitola. Cognitive radio: An integrated agent architecture for software defined radio. Ph.D. Thesis, Royal Institute of Technology, Sweden, May 2000.

[74] Ali Motamedi and Ahmad Bahai. Optimal channel selection for spectrum-agile low-power wireless packet switched networks in unlicensed band. *EURASIP J. Wirel. Commun. Netw.*, 2008:1–10, 2008.

[75] D. Niyato and E. Hossain. Competitive pricing for spectrum sharing in cognitive radio networks: Dynamic game, inefficiency of nash equilibrium, and collusion. *IEEE Journal on Selected Areas in Communications*, 26(1):192–202, January 2008.

[76] D. Niyato, E. Hossain, and Z. Han. Dynamics of multiple-seller and multiple-buyer spectrum trading in cognitive radio networks: A game theoretic modeling approach. *IEEE Transactions on Mobile Computing*, 8(8):1009–1022, Aug. 2009.

[77] D. Niyato, E. Hossain, and P. Wang. Optimal channel access management with QoS support for cognitive vehicular networks. *to appear in IEEE Transactions on Mobile Computing*.

[78] Alan V. Oppenheim and Ronald W. Schafer. *Discrete-Time Signal Processing*. Prentice Hall, New York, 3rd edition, 2009.

[79] IBM ILOG CPLEX Optimizer. http://www-01.ibm.com/software/integration/optimization/cplex-optimizer/.

[80] Srikanth Pagadarai, Alexander M. Wyglinski, and Rama Vuyyuru. Characterization of vacant uhf tv channels for vehicular dynamic spectrum access. In *Proc. of IEEE Vehicular Networking Conference*, Tokyo, Japan, October 2009.

[81] P. Paillier. Public-key cryptosystems based on composite degree residuosity classes. In *Proc. of IEEE International Conference on Computational Intelligence for Modelling, Control, and Automation, EUROCRYPT '99*, Prague, Czech Republic, May 1999.

[82] P. Paillier and D. Pointcheval. Efficient public-key cryptosystems provably secure against active adversaries. In *In proceedings of Advances in Cryptology, ASIACRYPT '99, LNCS series*, pages 165–179. SpringerVerlag, 1999.

[83] Pascal Paillier. Cryptographie à clé publique basée sur la résiduosité de degré composite. Ph.D. Thesis, École Nationale Supérieure des Télécommunications, Paris, France, Sep. 1999.

[84] Miao Pan, Feng Chen, Xiaoyan Yin, and Yuguang Fang. Fair profit allocation in the spectrum auction using the shapley value. In *Proc. of IEEE Global telecommunications conference, Globecom 2009*, Honolulu, HI, USA, December 2009.

[85] Miao Pan, Yang Song, Pan Li, and Yuguang Fang. Reward and risk for opportunistic spectrum accessing in cognitive radio networks. In *Proc. of IEEE Global telecommunications conference, Globecom 2010*, Miami, FL, December 2010.

[86] Miao Pan, Jinyuan Sun, and Yuguang Fang. Purging the back-room dealing: Secure spectrum auction leveraging paillier cryptosystem. *IEEE Journal on Selected Areas in Communications*, 29(4):866–876, April 2011.

[87] Miao Pan, Hao Yue, Yuguang Fang, and Hongyan Li. The X loss: Band-mix selection with uncertain supply for opportunistic spectrum accessing. In *Proc. of IEEE Global telecommunications conference, Globecom 2010*, Miami, FL, December 2010.

[88] Miao Pan, Chi Zhang, Pan Li, and Yuguang Fang. Joint routing and scheduling for cognitive radio networks under uncertain spectrum supply. In *Proc. of IEEE Conference on Computer Communications, INFOCOM 2011*, Shanghai, China, April 2011.

[89] Athanasios Papoulis and S. Unnikrishna Pillai. *Probability, Random Variables, and Stochastic Processes*. McGraw-Hill, New York, 2002.

[90] T. P. Pedersen. Non-interactive and information-theoretic secure verifiable secret sharing. In *Proc. of the International Cryptology Conference on Advances in Cryptology, CRYPTO '91*, London, UK, 1991.

[91] Torben P. Pedersen. Non-interactive and information-theoretic secure verifiable secret sharing. In *Proc. of Advances in Cryptology CRYPTO '91*, Santa Barbara, CA, US, Aug. 1991.

[92] Kun Peng, Colin Boyd, and Ed Dawson. Batch verification of validity of bids in homomorphic e-auction. *Computer Communications*, 29(15):2798–2805, Sep. 2006.

[93] J. Perez-Romero, O. Salient, R. Agusti, and L. Giupponi. A novel on-demand cognitive pilot channel enabling dynamic spectrum allocation. In *Proc. of IEEE International Symposium on New Frontiers in Dynamic Spectrum Access Networks, DySPAN 2007*, Dublin, Ireland, April 2007.

[94] Yves Pochet and Laurence A. Wolsey. *Production Planning by Mixed Integer Programming*. Springer-Verlag New York, Inc., Secaucus, NJ, USA, 2006.

[95] B.N. Pshenichnyi. *Necessary Conditions for an Extremum*. Dekker, New York.

[96] A. Raniwala and Tzi cker Chiueh. Architecture and algorithms for an ieee 802.11-based multi-channel wireless mesh network. In *Proc. of IEEE Conference on Computer Communications, INFOCOM 2005*, Miami, FL, March 2005.

[97] Jeffrey H. Reed. *Software Radio: A Modern Approach to Radio Engineering*. Prentice Hall, New York, May 2002.

[98] R.T. Rockafellar. *Convex Analysis*, volume 28. Princeton Mathematics, Princeton Univ. Press, 1970.

[99] S. Sawa, H. Itoh, and K. Nakamura. An evolutionary basis for preference behavior in decision making under risk. In *Proc. of IEEE International Conference on Computational Intelligence for Modelling, Control, and Automation, CIMCA '06*, Sydney, Australia, November 2006.

[100] Shamik Sengupta and Mainak Chatterjee. An economic framework for dynamic spectrum access and service pricing. *IEEE/ACM Transactions on Networking*, 17(4):1200–1213, Aug. 2009.

[101] Adi Shamir. How to share a secret. *Communications of the ACM*, 22(11):612–613, Nov. 1979.

[102] A. Shapiro and Y. Wardi. Nondifferentiability of the steady-state function in discrete event dynamic systems. *IEEE Transactions on Automatic Control*, 39, 1994.

[103] Sushant Sharma, Yi Shi, Y. Thomas Hou, and Sastry Kompella. An optimal algorithm for relay node assignment in cooperative communications. *to appear in IEEE/ACM Transactions on Networking*.

[104] Sushant Sharma, Yi Shi, Y. Thomas Hou, Hanif D. Sherali, and Sastry Kompella. Cooperative communications in multi-hop wireless networks: Joint flow routing and relay node assignment. In *Proc. of IEEE Conference on Computer Communications, INFOCOM 2010*, San Diego, CA, March 2010.

[105] Sushant Sharma, Yi Shi, Y. Thomas Hou, Hanif D. Sherali, and Sastry Kompella. Optimizing network-coded cooperative communications via joint session grouping and relay node selection. In *Proc. of IEEE Conference on Computer Communications, INFOCOM 2011*, Shanghai, China, April 2011.

[106] William F. Sharpe. Risk, market sensitivity and diversification. *Financial Analysts Journal*, 28(1):74–79, Feb. 1972.

[107] William F. Sharpe. Macro-investment analysis. Investments text (partial), Stanford University, 2009.

[108] Yi Shi and Y. Thomas Hou. A distributed optimization algorithm for multi-hop cognitive radio networks. In *Proc. of IEEE Conference on Computer Communications, INFOCOM 2008*, Phoenix, AZ, April 2008.

[109] Yi Shi, Y. Thomas Hou, and Sastry Kompella. How to correctly use the protocol interference model for multi-hop wireless networks. In *Proc. of ACM International Symposium on Mobile Ad Hoc Networking and Computing, ACM MobiHoc, 2009*, New Orleans, LA, May 2009.

[110] H. So, A. Tkachenko, and R. W. Brodersen. A unified hardware/software runtime environment for FPGA based reconfigurable computers using borph. In *Proc. of*

International Conference on Hardware-Software Codesign and System Synthesis, Seoul, Korea, October 2006.

[111] Yang Song, Chi Zhang, and Yuguang Fang. Stochastic traffic engineering in multi-hop cognitive wireless mesh networks. *IEEE Transactions on Mobile Computing*, 9(3):305–316, March 2010.

[112] F. Sun and M. Shayman. On the average pairwise connectivity of wireless multihop networks. In *Proc. of IEEE Global telecommunications conference, Globecom '05*, St. Louis, MO, USA, November 2005.

[113] K. Suzuki and M. Yokoo. Secure generalized vickrey auction using homomorphic encryption. In *Proc. of the Financial Cryptography Conference, FC '03*, Guadeloupe, French West Indies, Jan. 2003.

[114] J. Tang, S. Misra, and G. Xue. Joint spectrum allocation and scheduling for fair spectrum sharing in cognitive radio wireless networks. *Computer Networks (Elsevier) Journal*, 52(11):2148–2158, August 2008.

[115] J. Tang, G. Xue, and W. Zhang. Interference-aware topology control and qos routing in multi-channel wireless mesh networks. In *Proc. of ACM International Symposium on Mobile Ad Hoc Networking and Computing, ACM MobiHoc, 2005*, Urbana-Champaign, IL, May 2005.

[116] Kazuya Tsukamoto, Shinya Matsuoka, Masato Tsuru, Yuji Oie, and Onur Altintas. Distributed channel coordination in cognitive wireless vehicle-to vehicle communications. In *Proc. of International Conference on Wireless Access in Vehicular Environments*, Dearborn, MI, December 2008.

[117] W. Vickrey. Counter speculation, auctions, and competitive sealed tenders. *Finance*, 16(1):8–37, 1961.

[118] S. Vries and R. Vohra. Combinatorial auctions: A survey. *INFORMS Journal on Computing*, 15(3):284–309, 2003.

[119] Beibei Wang, Zhu Han, and K. J. Ray Liu. Distributed relay selection and power control for multiuser cooperative communication networks using buyer/seller game. In *Proc. of IEEE Conference on Computer Communications, INFOCOM 2007*, Anchorage, AK, May 2007.

[120] Beibei Wang, Zhu Ji, and K. J. Ray Liu. Primary-prioritized markov approach for dynamic spectrum access. In *Proc. of IEEE International Symposium on New Frontiers in Dynamic Spectrum Access Networks, DySPAN 2007*, Dublin, Ireland, April 2007.

[121] Jiangzhou Wang and Jun Chen. Performance of wideband cdma systems with complex spreading and imperfect channel estimation. *IEEE Journal on Selected Areas in Communications*, 19(4):152–163, January 2001.

[122] B. Wild and K. Ramchandran. Detecting primary receivers for cognitive radio applications. In *Proc. of IEEE International Symposium on New Frontiers in Dynamic Spectrum Access Networks, DySPAN 2005*, Baltimore, MD, November 2005.

[123] Chia-Chi Wu, Chin-Chen Chang, and Iuon-Chang Lin. New sealed-bid electronic auction with fairness, security and efficiency. *Journal of Computer Science and Technology*, 23(2):253–264, Apr. 2008.

[124] Y. Wu, B. Wang, K. J. Liu, and T. Clancy. A multi-winner cognitive spectrum auction framework with collusion-resistant mechanisms. In *Proc. of IEEE International Symposium on New Frontiers in Dynamic Spectrum Access Networks, DySPAN '08*, Chicago, IL, October 2008.

[125] Yiping Xing, R. Chandramouli, and C. Cordeiro. Price dynamics in competitive agile spectrum access markets. *IEEE Journal on Selected Areas in Communications*, 25(3):613–621, April 2007.

[126] Dongyue Xue and Eylem Ekici. Guaranteed opportunistic scheduling in multi-hop cognitive radio networks. In *Proc. of IEEE Conference on Computer Communications, INFOCOM 2011*, Shanghai, China, April 2011.

[127] F. Xue and P.R. Kumar. The number of neighbors needed for connectivity of wireless networks. *Wireless Networks*, 10(2):169–181, 2004.

[128] A. Yao. Protocols for secure computations. In *In proceedings of the 23rd Annual Symposium on Foundations of Computer Science, SFCS '82*, pages 160–164, Washington, DC, USA, 1982. IEEE Computer Society.

[129] M. Yokoo and K. Suzuki. Secure multi-agent dynamic programming based on homomorphic encryption and its application to combinatorial auctions. In *Proceedings of the first international joint conference on Autonomous agents and multiagent systems, AAMAS '02*, 2002.

[130] M. Yokoo and K. Suzuki. Secure generalized vickrey auction without third-party servers. In *Proc. of the Financial Cryptography Conference, FC '04*, Key West, FL, February 2004.

[131] Hongqiang Zhai and Yuguang Fang. Impact of routing metrics on path capacity in multirate and multihop wireless ad hoc networks. In *Proc. of the IEEE International Conference on Network Protocols, ICNP 2006*, Santa Barbara, CA, November 2006.

[132] J. Zhang and Q. Zhang. Stackelberg game for utility-based cooperative cognitive radio networks. In *Proc. of ACM International Symposium on Mobile Ad Hoc Networking and Computing, ACM MobiHoc, 2009*, New Orleans, LA, May 2009.

[133] Jin Zhang and Qian Zhang. Cooperative network coding-aware routing for multi-rate wireless networks. In *Proc. of IEEE Conference on Computer Communications, INFOCOM 2009*, Rio de Janeiro, Brazil, April 2009.

[134] Q. Zhao, L. Tong, A. Swami, and Y. Chen. Decentralized cognitive mac for opportunistic spectrum access in ad hoc networks: A pomdp framework. *IEEE Journal on Selected Areas in Communications*, 25(3):589–600, April 2007.

[135] X. Zhou, S. Gandhi, S. Suri, and H. Zheng. ebay in the sky: strategy-proof wireless spectrum auctions. In *Proc. of Mobile Computing and Networking, Mobicom '08*, San Francisco, CA, September 2008.

[136] X. Zhou and H. Zheng. Trust: A general framework for truthful double spectrum auctions. In *Proc. of INFOCOM 2009*, Rio de Janeiro, Brazil, April 2009.

[137] Xia Zhou and Haitao Zheng. Breaking bidder collusion in large-scale spectrum auctions. In *Proc. of ACM International Symposium on Mobile Ad Hoc Networking and Computing, ACM MobiHoc, 2010*, Chicago, IL, September 2010.

BIOGRAPHICAL SKETCH

Miao Pan was born in 1981 in Dalian, Liaoning, China. Miao grew up in Dalian and graduated from the NO.8 Middle School in the summer of 1999. Following high school, Miao enrolled at Dalian University of Technology (DUT) in Dalian, China in the fall of 1999. He received his B.E. in electrical and information engineering and B.A. in English from DUT in 2004. After that, Miao enrolled at Beijing University of Posts and Telecommunications (BUPT) in Beijing, China in the fall of 2004, and received his M.E. degrees in electrical and computer engineering from BUPT in 2007. Miao enrolled in the Ph.D. program in the Department of Electrical and Computer Engineering at the University of Florida in the fall of 2007, as a recipient of the University of Florida's Alumni Fellowship. He received his Ph.D. degree in electrical and computer engineering from the University of Florida in the summer of 2012. His research interests are in the areas of network protocol design, network performance analysis, and network security guarantee, particularly for cognitive radio networks. He has published over 30 papers in prestigious journals including IEEE/ACM Transactions on Networking, IEEE Journal on Selected Areas in Communications, and IEEE Transactions on Mobile Computing, or in top networking conferences such as IEEE INFOCOM, and IEEE IPDPS. He also has been selected several times as a recipient of the travel grant from the National Science Foundation (NSF). Miao is a student member of IEEE.